NUREG/CR-3761
EGG-2310

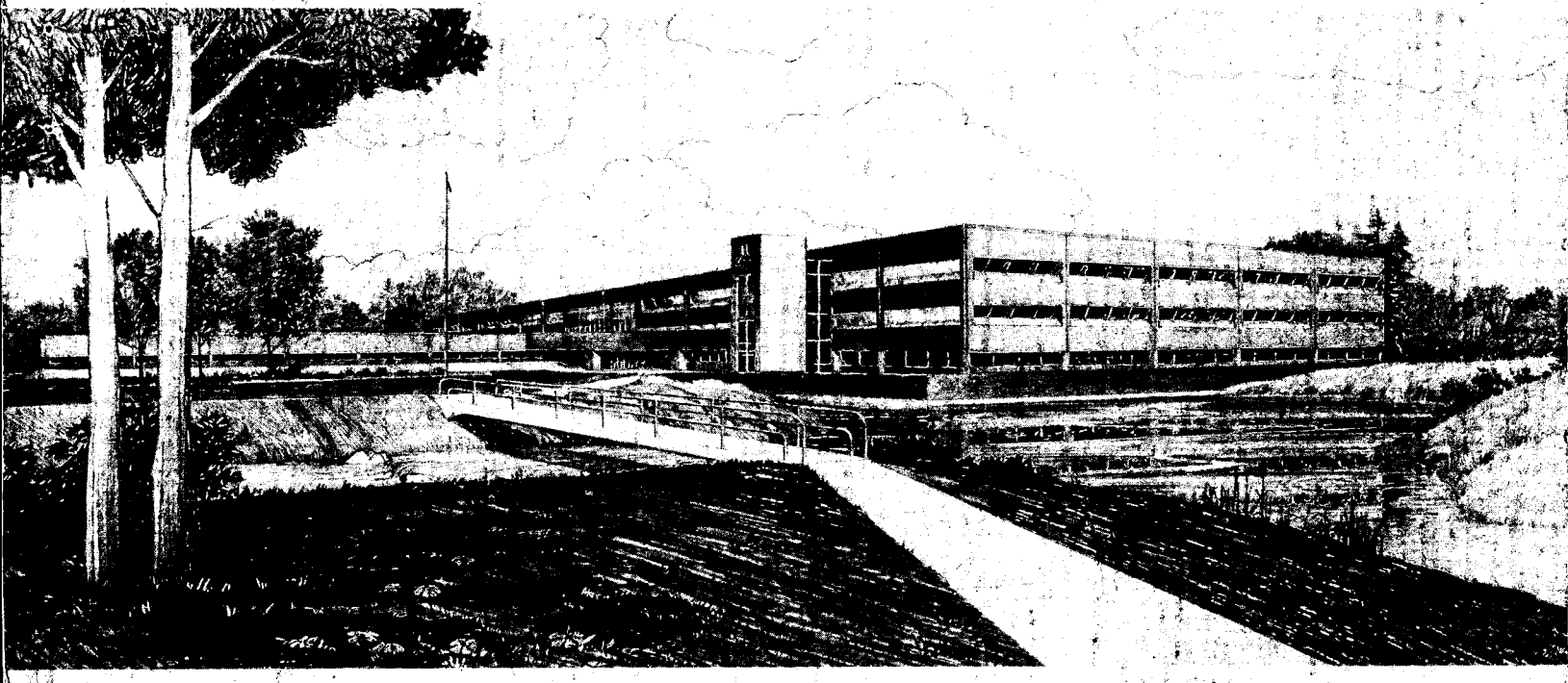

Idaho National Engineering Laboratory
Operated by the U.S. Department of Energy

50-269

RELAP5 Thermal-Hydraulic Analyses of Pressurized Thermal Shock Sequences for the Oconee-1 Pressurized Water Reactor

Ltr dtd 7/31/84

C. Don Fletcher
Mark A. Bolander
Benjamin D. Stitt
Michael E. Waterman

June 1984

8408160248

Prepared for the
U.S. Nuclear Regulatory Commission
Under DOE Contract No. DE-AC07-76IDO1570

EG&G Idaho

Available from

GPO Sales Program
Division of Technical Information and Document Control
U.S. Nuclear Regulatory Commission
Washington, D.C. 20555

and

National Technical Information Service
Springfield, Virginia 22161

NUREG/CR-3761
EGG-2310
Distribution Category: R4

RELAP5 THERMAL-HYDRAULIC ANALYSES OF PRESSURIZED THERMAL SHOCK SEQUENCES FOR THE OCONEE-1 PRESSURIZED WATER REACTOR

C. Don Fletcher
Mark A. Bolander
Benjamin D. Stitt
Michael E. Waterman

Published June 1984

EG&G Idaho, Inc.
Idaho Falls, Idaho 83415

Prepared for the
U.S. Nuclear Regulatory Commission
Washington, D.C. 20555
Under DOE Contract No. DE-AC07-76IDO1570
FIN No. A6047

ABSTRACT

Using the RELAP5 computer code, engineers at the Idaho National Engineering Laboratory (INEL) performed thermal-hydraulic analyses of pressurized thermal shock sequences for the Oconee-1 pressurized water reactor. This report summarizes the results of previously reported calculations and presents the results of more recently completed calculations. Comparisons of two counterpart calculations performed, using the RELAP5 code at the INEL and the TRAC code at Los Alamos National Laboratory (LANL), are included as appendices. The results of these thermal-hydraulic analyses will serve as boundary conditions for fracture-mechanics calculations which are to be performed at Oak Ridge National Laboratory.

SUMMARY

In support of the U.S. Nuclear Regulatory Commission's investigation of the pressurized thermal shock (PTS) unresolved safety issue, the Idaho National Engineering Laboratory (INEL) performed thermal-hydraulic analyses, using RELAP5 computer code calculations.

The ten event sequences to be investigated were defined at Oak Ridge National laboratory (ORNL), the integrator of the PTS study.

Four of the ten sequences analyzed have been reported in Reference 1. These sequences were: (a) main steam line break, (b) steam generator overfeed, (c) hot leg small break (stuck-open power-operated relief valve), and (d) Oconee-3 turbine trip plant transient. For each of these, we provide in this report a sequence description and summary of analysis results.

The remaining six sequences were: (a) revised main steam line break, (b) maximum sustainable steam generator overfeed, (c) failure open of four turbine bypass valves at reactor hot standby, (d) pressurizer surge line small break, (e) reactor coolant pump suction small break, and (f) steam generator tube rupture. This report provides a detailed description and a discussion of the specific model changes for each of these sequences. Also provided are details and analyses of calculation results and limited estimates of uncertainty for the reactor vessel downcomer fluid temperature and pressure.

For the revised main steam line break and pressurizer surge line break, counterpart calculations were performed at Los Alamos National Laboratory, using the TRAC computer code. These calculations were compared with those performed at INEL using the RELAP5 code. The results appear as appendices to this report. These comparisons proved invaluable in the estimating of uncertainties in the RELAP5 calculations.

An extensive computer model of the Oconee-1 pressurized water reactor (PWR) was developed specifically to perform these calculations. The model contained detailed representations of the pertinent PWR primary and secondary system components, including the feedwater train. Control system models were also included for the turbine bypass, emergency feedwater, and main feedwater functions of the Babcock & Wilcox integrated control system.

A table summarizing the lowest fluid temperatures and highest subsequent pressures in the reactor vessel downcomer for each sequence is presented in the conclusions section. The maximum estimated effect of uncertainty on both fluid temperatures and subsequent pressures is also shown for the most severe sequences.

The results of the thermal-hydraulic analyses presented in this report will be used as boundary conditions in PTS fracture mechanics analyses to be performed at ORNL.

CONTENTS

RELAP5 THERMAL-HYDRAULIC ANALYSES OF PRESSURIZED THERMAL SHOCK SEQUENCES FOR THE OCONEE-1 PRESSURIZED WATER REACTOR

1. INTRODUCTION

The U.S. Nuclear Regulatory Commission (NRC) is investigating the pressurized thermal shock (PTS) unresolved safety issue (Number A49). PTS refers to plant transients in which the welded reactor vessel walls of a pressurized water reactor (PWR) are subjected to rapid cooldown at interior surfaces and coincident (or subsequent) high pressures. The concern centers on reactors which have been operating for long periods of time and have reactor vessels that were welded with high-copper-content weld rod. Transients of interest must include the potential for the cold reactor vessel downcomer fluid temperatures with high primary system pressures.

The NRC has identified a group of PWRs for which PTS is of near-term concern. The Oconee-1 PWR was selected as the first plant in this group for detailed investigation. The Oconee-1 PWR is a Babcock & Wilcox, low-loop design reactor, operated by Duke Power Company since 1973.

The NRC has contracted with Oak Ridge National Laboratory (ORNL) to integrate the investigation into the PTS unresolved safety issue. The NRC has also contracted with the Idaho National Engineering Laboratory (INEL) and Los Alamos National Laboratory (LANL) to support ORNL's activities by performing thermal-hydraulic analyses, using state-of-the-art computer codes and plant-specific models of the PWRs under investigation. The NRC has contracted with Brookhaven National Laboratory (BNL) to provide a quality-assurance audit function on the work performed at INEL and LANL. The functions ORNL will retain include: (a) probabilistic risk assessment, which is used to define potential PTS transients, (b) definition of specific sequences to be analyzed by INEL and LANL, (c) fracture mechanics analyses of the vessel wall, and (d) integration of the overall study.

This report documents the Oconee-1 thermal-hydraulic analyses performed by INEL in support of the PTS study.

Section 2 describes the RELAP5 model of the Oconee-1 PWR. Analyses of ten transient sequences were performed. Detailed analysis results for the first four of these sequences appear in Reference 1; a summary of the results of these is presented in Section 3. The first four sequences were: (a) main steam line break, (b) steam generator overfeed, (c) hot leg small break, and (d) the turbine trip plant transient that occurred in the Oconee-3 PWR and for which calculated and measured data are compared.

Sections 4 through 9 contain the detailed analysis results for the remaining six transients: (a) revised main steam line break sequence (Section 4), (b) maximum sustainable steam generator overfeed (Section 5), (c) turbine bypass valve failure at reactor hot standby (Section 6), (d) pressurizer surge line small break (Section 7), (e) reactor coolant pump suction small break (Section 8), and (f) steam generator tube rupture (Section 9).

An overview and conclusions for all ten analyzed sequences are presented in Section 10; references are listed in Section 11. Appendix A presents computer run time statistics for the calculations. A comparison between the two calculations performed, the one at INEL using the RELAP5 code, and the other at LANL using the TRAC-PF1 code, are presented in Appendix B for the revised main steam line break sequence and Appendix C for the pressurizer surge line small break sequence.

2. MODEL DESCRIPTION

This section describes the RELAP5 Oconee-1 PWR model, which was used for the pressurized thermal shock (PTS) calculations. Transient models were modifications to the steady state model. Specific model changes (required to perform the transient calculations) are described under the "Model Changes" headings in Sections 4 through 9.

Full Power Steady State Model

The RELAP5 Oconee-1 PWR steady state model is a detailed model of the Oconee-1 PWR power plant and describes all major flow paths for both primary and secondary systems, including the main feedwater train. Also modeled are power-operated relief valves (PORV), safety valves, and the emergency core cooling system (ECCS). Secondary system features include turbine bypass and turbine stop valves, safety valves, and the emergency feedwater (EFW) system. Another feature modeled was the integrated control system (ICS), shown schematically in Figures 1 to 8. The model contained 220 volumes, 232 junctions, and 208 heat structures. A description of the primary system, secondary system, feedwater train and the control system is presented in the following sections. Table 1 shows comparisons of full-power steady state conditions calculated by the model with nominal plant conditions.

Primary System

The Oconee-1 PWR plant is a 2 by 4 configuration, i.e., two loops, each containing one hot leg and two cold legs. The loops are designated loop A and loop B. Each loop contains one hot leg, one steam generator, two pump suction legs, two reactor coolant pumps, and two cold legs (refer to Figures 1 and 2). The pressurizer and pressurizer surge line (Figure 3) are attached to the hot leg in loop A. Each cold leg contains a high pressure injection (HPI) port. Table 2 summarizes the relationship between the physical components of the Oconee-1 A and B primary loops and the corresponding mathematical components of the RELAP5 model. RELAP5 components were numbered between 100 and 199 for the A loop, 200 and 299 for the B loop, and 600 and 630 for the pressurizer.

The RELAP5 vessel model, shown in Figure 4, consisted of several components describing the various vessel flow paths. The RELAP5 vessel included an inlet annulus, downcomer, lower plenum, core, core bypass, upper plenum, upper head, and a vent valve.

The eight reactor vessel internal vent valves between the upper plenum and downcomer inlet annulus were modeled with a single RELAP5 servo valve. A servo valve uses the output of a RELAP5 control variable to determine the open area of the valve. The control variable was designed to calculate a valve flow area as a function of the differential pressure across the valve. Differential pressures at which the valves start to open and are full open were obtained from Reference 2.

Because the range of differential pressure over which the valve position changes is small, it was found necessary to smooth the calculated differential pressure to prevent valve chattering. Without smoothing, the valve position responded instantaneously to the differential pressure across it. With smoothing, the change in valve position in a time step was limited, thus preventing excessively rapid opening and closing of the valve and qualitatively simulating the response time of the flapper valves. The model of the vent valve used in the RELAP5 model is the best usable representation of the Oconee-1 reactor vessel vent valve available at present. Discussions of vent valve behavior, and possible uncertainties involved, are addressed in the transient results in Sections 4 through 9.

The RELAP5 component numbers for the vessel were between 500 and 599. Table 3 summarizes the relationship between the physical components of the Oconee-1 vessel and the corresponding mathematical components of the RELAP5 model.

Also included in the primary system were the low pressure injection (LPI) system, the core flood system, PORV, and the safety valves. The LPI and core flood systems were connected to the vessel inlet annulus. The PORV and safety valves were connected to the top of the pressurizer. Table 2 summarizes the relationship between the physical components of the Oconee-1 LPI, core flood systems, PORV, and safety valves and the corresponding mathematical components of the RELAP5 model.

The RELAP5 nonequilibrium model was applied to all volumes in the primary system, except to the accumulator, where the accumulator model was applied. The wall friction model was applied in all primary volumes. Centrally located junctions for horizontal stratification were applied to all horizontal junctions. The choking and two-velocity models and an inertial solution were calculated at all junctions. The smooth area change model was applied at all junctions except those listed in Table 4.

Heat structures were used to represent heat transfer and stored energy from fuel rods, steam generator tubes, loop piping, vessel wall, vessel internals, pressurizer wall, pressurizer surge line, and pressurizer heaters.

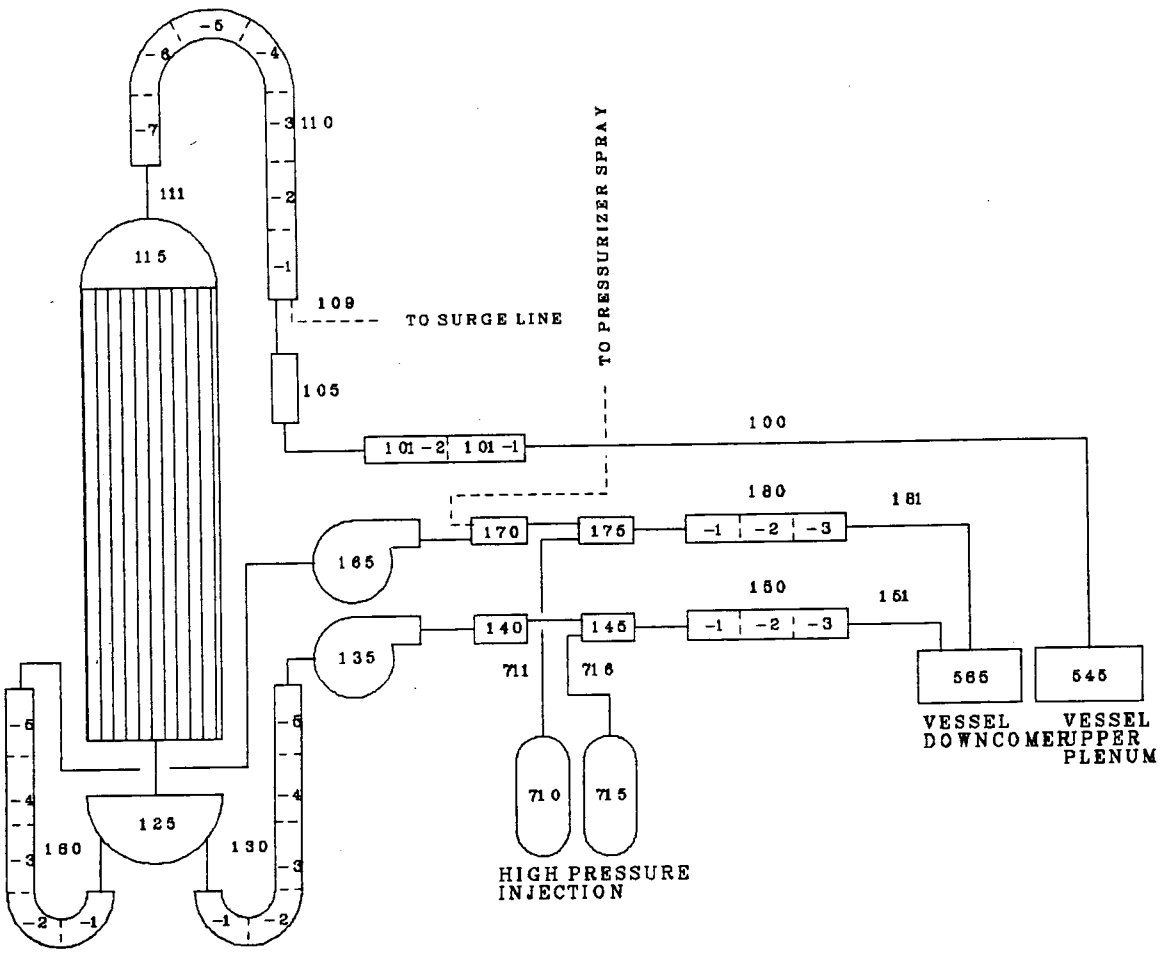

Figure 1. RELAP5 Oconee-1 model; primary loop A.

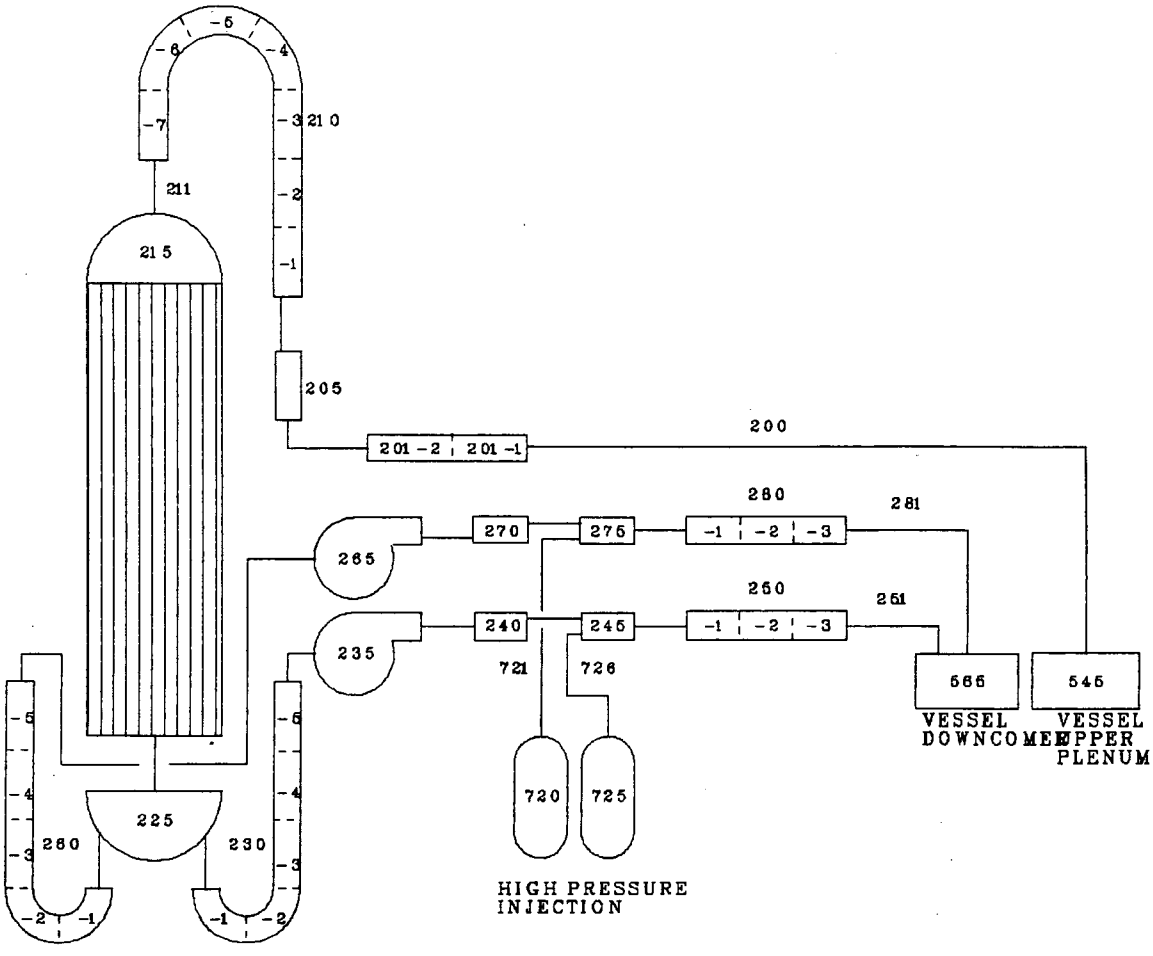

Figure 2. RELAP5 Oconee-1 model; primary loop B.

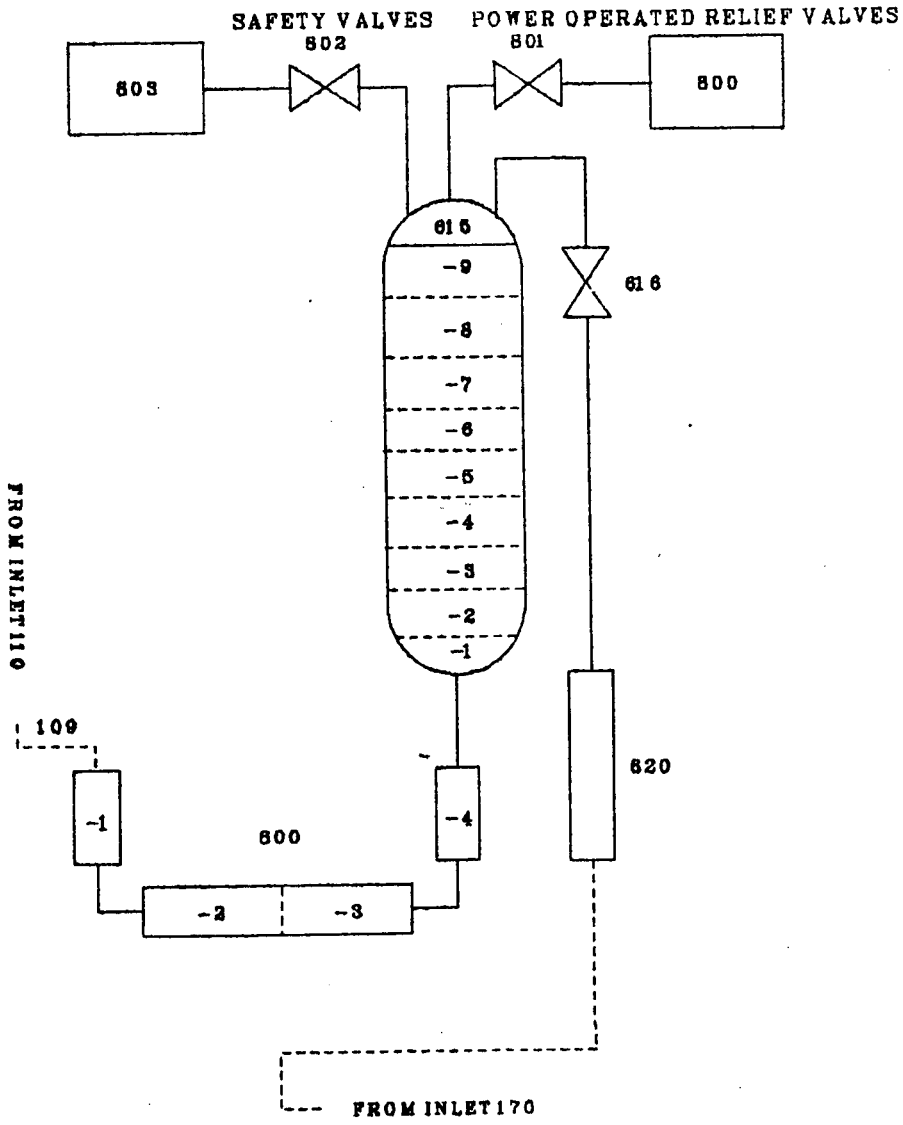

Figure 3. RELAP5 Oconee-1 model; pressurizer system.

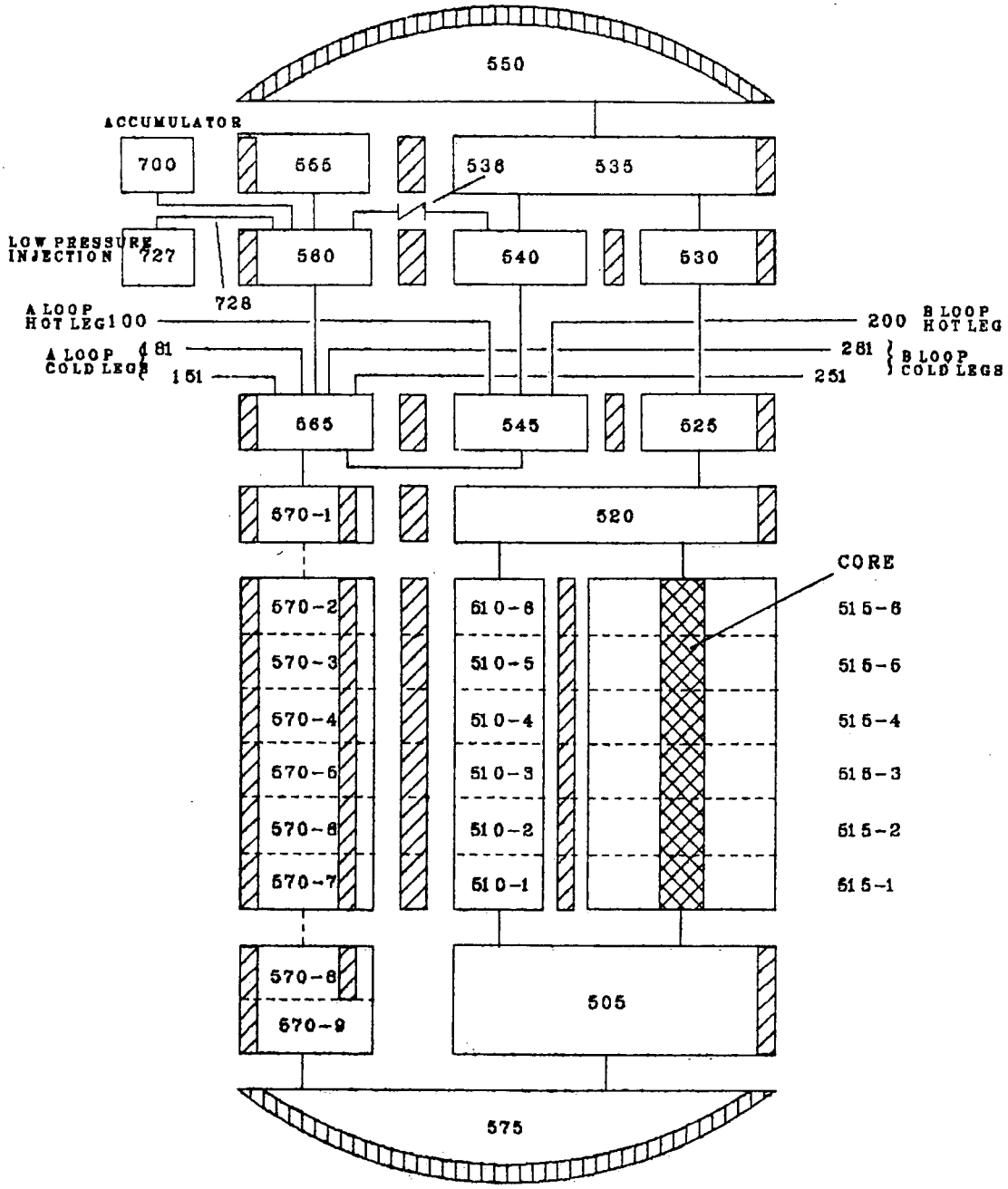

Figure 4. RELAP5 Oconee-1 model; vessel, core flood tank and LPI system.

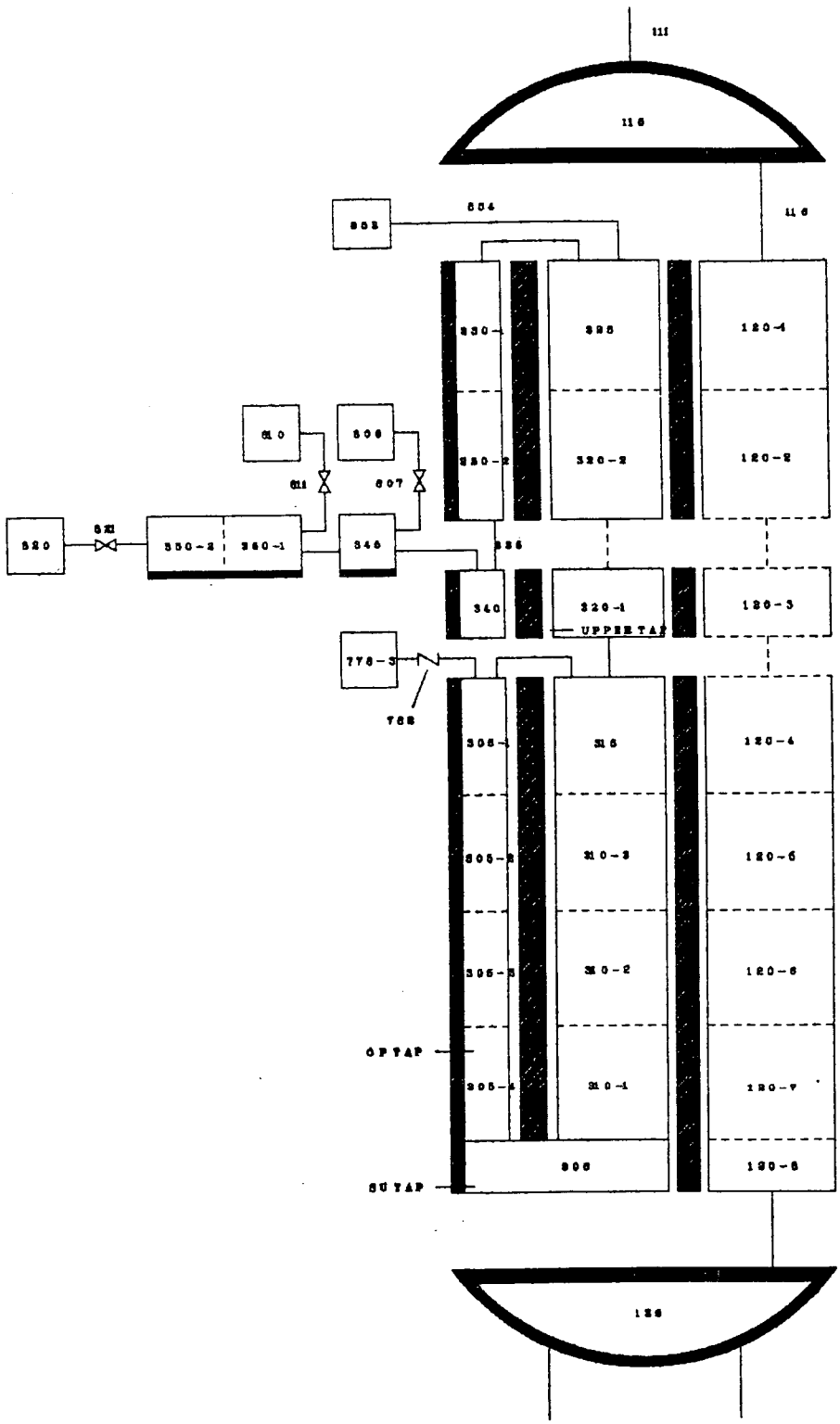

Figure 5. RELAP5 Oconee-1 model; loop A steam generator secondary side, and main steam line.

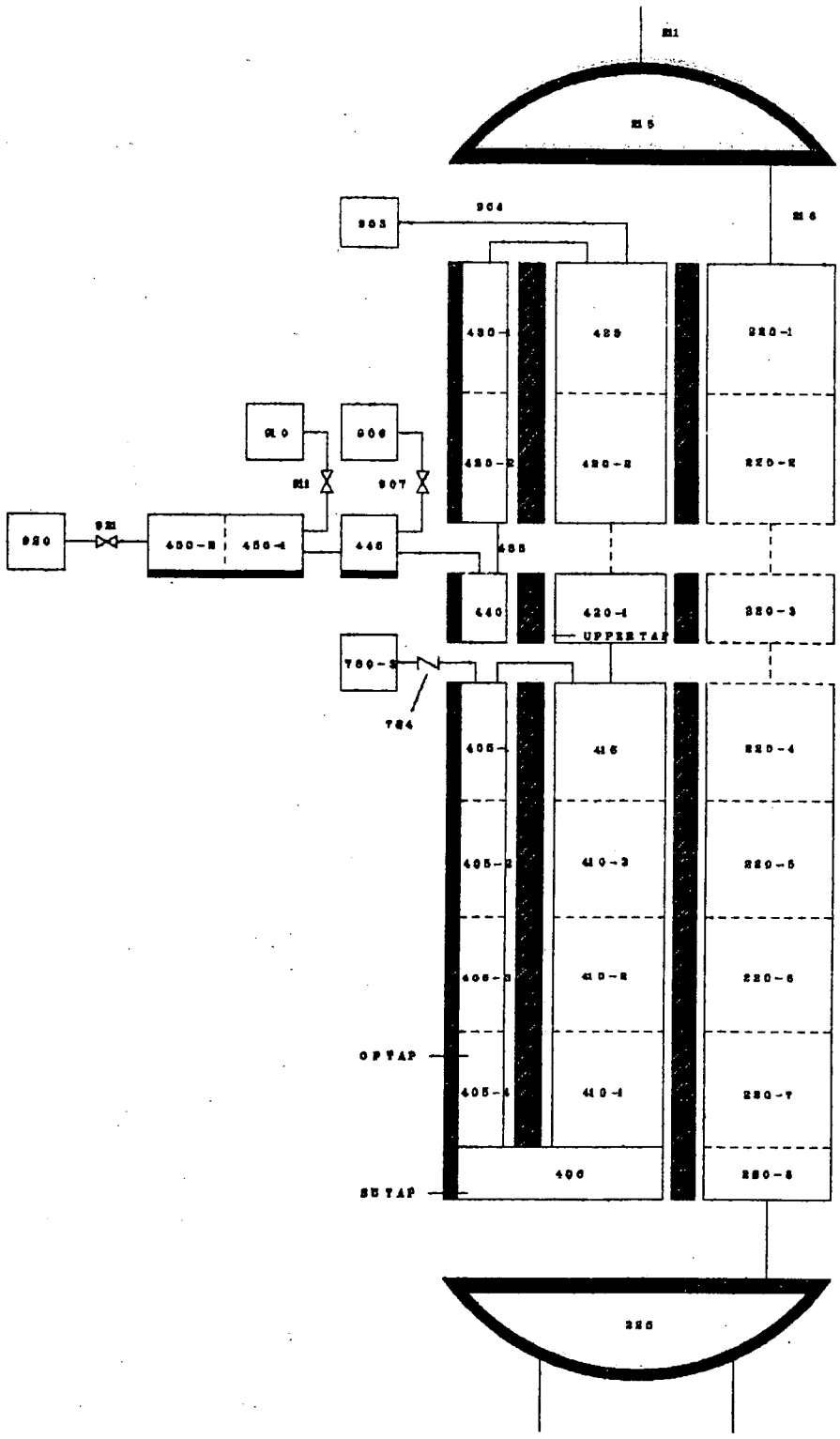

Figure 6. RELAP5 Oconee-1 model; loop B steam generator secondary side, and main steam line.

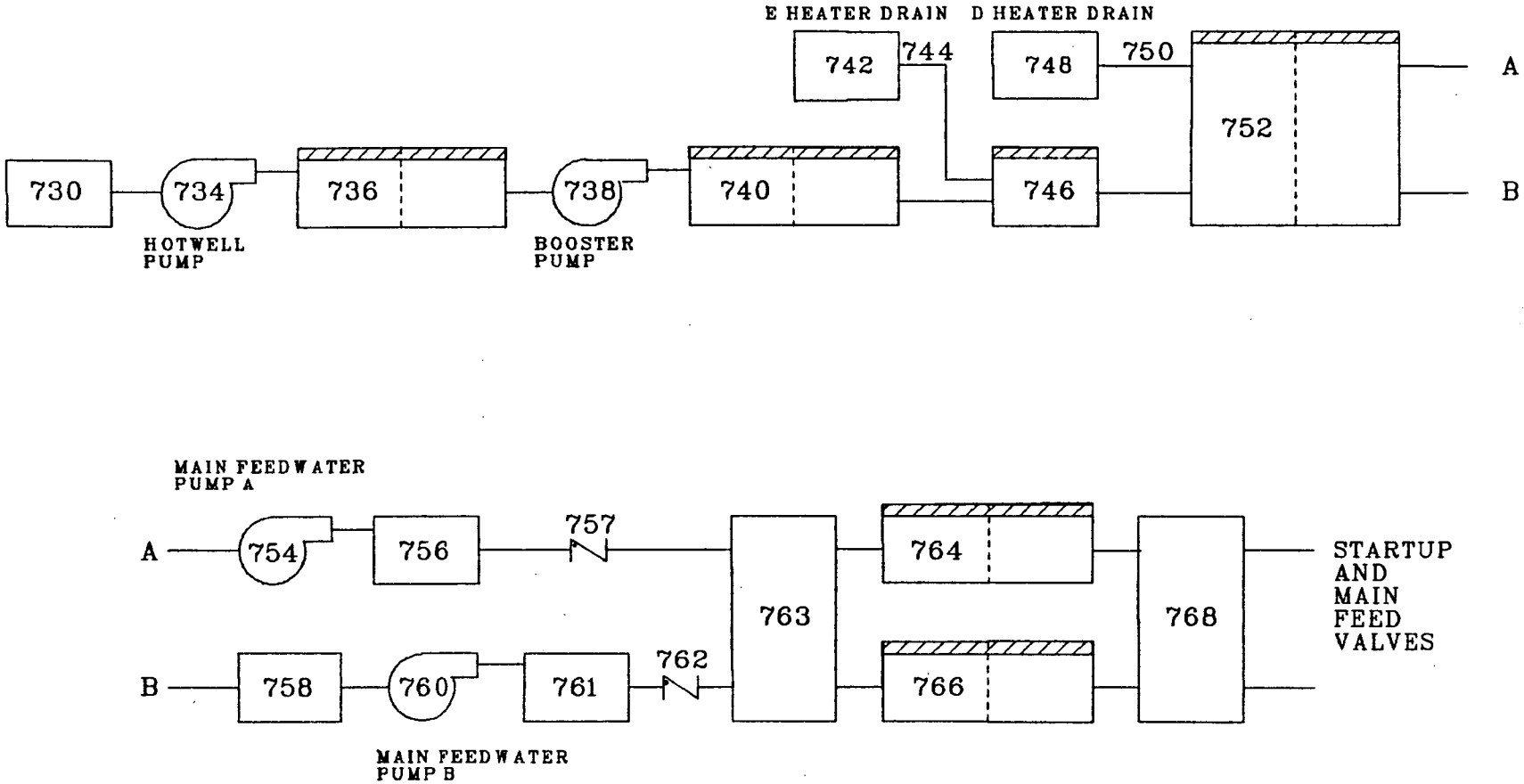

Figure 7. RELAP5 Oconee-1 model; feed train from hotwell to start-up and main feed valves.

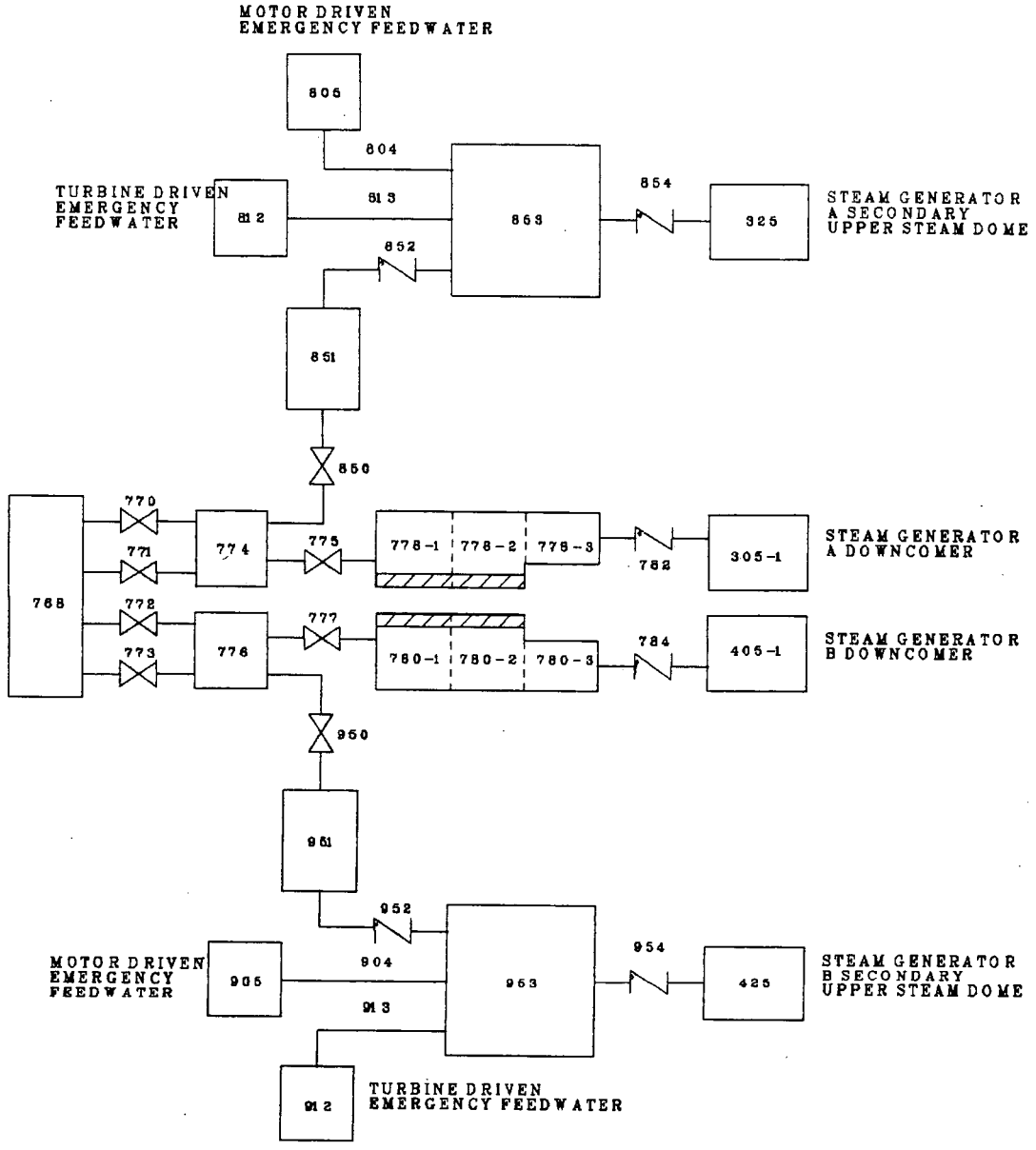

Figure 8. RELAP5 Oconee-1 model; feed train from start-up and main feed valves to steam generator, crossover, and emergency feedwater system.

Table 1. Full power steady state conditions calculated by RELAP5 compared with plant nominal conditions

Parameter	Plant	RELAP5
Core power (MW)	2568	2546
Average of hot and cold leg temperatures (K)	577	577
Hot leg pressure (MPa)	14.96	14.93
Steam generator secondary system pressure (MPa)	6.377	6.380
Mass per steam generator secondary (kg)	17700	17100
Feedwater temperature (K)	511	511
Steam exit superheat (K)	33.3	32.8
Mass flow per hot leg (kg/s)	8820	8819
Feedwater flow per steam generator (kg/s)	680.4	689.9
Pressurizer level (m)	5.59	5.71

Table 2. Correspondence between the physical and mathematical components in primary loops

Physical Component	RELAP5 Component(s)
Loop A	
Hot leg	100, 101, 105, 110, 111
Steam generator inlet plenum	115, 116
Steam generator tube bundle	120
Steam generator outlet plenum	125
A-1 pump suction leg	160
A-2 pump suction leg	130
A-1 reactor coolant pump	165
A-2 reactor coolant pump	135
A-1 cold leg	170, 175, 180, 181
A-2 cold leg	140, 145, 150, 151
A-1 HPI	710, 711
A-2 HPI	715, 716
Loop B	
Hot leg	200, 201, 205, 210, 211
Steam generator inlet plenum	215, 216
Steam generator tube bundle	220
Steam generator outlet plenum	225
B-1 pump suction leg	260
B-2 pump suction leg	230
B-1 reactor coolant pump	265
B-2 reactor coolant pump	235
B-1 cold leg	270, 275, 280, 281
B-2 cold leg	240, 245, 250, 251
B-1 HPI	720, 721
B-2 HPI	725, 726

Table 2. (continued)

Physical Component	RELAP5 Component(s)
Pressurizer	
Surge line	600, 605
Pressurizer	610
Pressurizer dome	615
Spray line	620
Spray valve	616
PORV	800, 801
Safety valve	800, 803
Low pressure injection system	727, 728
Core flood system	700

Table 3. Correspondence between physical and mathematical components in the vessel

Physical Component	RELAP5 Component(s)
Inlet annulus	555, 560, 565
Downcomer	570
Lower plenum	505, 575
Core	515
Core bypass	510
Upper plenum	520, 525, 530, 535, 540, 542, 545
Upper head	550
Vent valve	536

Table 4. Junctions using the abrupt area change model

Junction Number[a]	Description
116	Steam Generator A inlet plenum to tube bundle
12501	Steam Generator A tube bundle to outlet plenum
216	Steam Generator B inlet plenum to tube bundle
22501	Steam Generator B tube bundle to outlet plenum
34501	Steam Generator A outlet to main steam line
44501	Steam Generator B outlet to main steam line
536	Reactor vessel vent valve
811	Steam Generator A turbine bypass valve
821	Steam Generator A turbine stop valve
911	Steam Generator B turbine bypass valve
921	Steam Generator B turbine stop valve

a. Junctions with three-digit numbers represent RELAP5 components and are either valves or single junctions. Junctions with five-digit numbers are internal junctions of either a branch or pipe component. The first three digits of the internal junction number specify which component the junction is associated with. The last two digits are sequence numbers which uniquely define the internal junction.

Secondary System

The Oconee-1 steam generators are once-through type steam generators and are oriented vertically. Between the outer shell and the heat exchanger tube bundle is a cylindrical baffle, forming a downcomer section. A gap in the baffle allows steam to be drawn from the boiler region into the downcomer to heat the incoming feedwater. After falling through the downcomer, the feedwater enters the tube bundle and flows upward, vaporizing to saturated steam in the nucleate boiling region. Dry saturated steam is produced in the film boiling region and raised to the final steam temperature in the superheat region. The steam flow then enters the steam outlet section, which is between the outer shell and the cylindrical baffle and above the feedwater inlet port. The superheated steam then exits the steam generator via the main steam line.

The RELAP5 model of the steam generator secondary is shown schematically in Figures 5 and 6. Table 5 summarizes the relationship between the physical components of the Oconee-1 loop A and B steam generator secondaries and the corresponding mathematical components of the RELAP5 model. RELAP5 component numbers between 300 and 399 were used to represent the loop A steam generator secondary. Numbers between 400 and 499 were used for the loop B steam generator secondary. Also described in Table 5 are the emergency feedwater system and the main steam line components for each loop out to the turbine stop valves, including the turbine bypass and safety valves.

After the initial calculations were performed using this model (Reference 1), the manner in which secondary levels were calculated in the model was revised in order to better represent the actual method used in the plant. The startup and operating levels were originally calculated based on the collapsed downcomer liquid level. For calculations presented in this report, the levels were based on calculated static pressures and fluid temperatures at the locations corresponding to pressure and temperature taps in the Oconee-1 steam generators. The calculated temperatures and differential pressures were smoothed in a manner consistent with the actual instrumentation system. The improved method of level calculation significantly affected the sequence of events in the revised main steam line break transient (discussed further in Section 4). In general, this method improved the calculated response of emergency feedwater injection, which was controlled on steam generator level.

The RELAP5 nonequilibrium option was applied to all volumes in the secondary system. This was a change from the equilibrium option used to perform the initial calculations with this model. Difficulties encountered with secondary behavior during the initial portion of the main steam line break calculation were overcome, allowing the nonequilibrium option to be used. As will be described later, this change resulted in a more satisfactory calculated response of the secondary system during periods of emergency feedwater injection. The wall friction model was applied to all secondary volumes. Centrally located junctions for horizontal stratification were applied to all horizontal junctions. The choking and two-velocity models and an inertial solution were calculated at all junctions. The smooth area change model was applied at all junctions, except those listed in Table 4.

Heat structures were used to simulate the stored energy contained in the secondary shell wall, piping, and internals.

Feedwater System

This section describes the Oconee-1 feedwater system. This portion of the Oconee-1 model was originally supplied by SAI-Oak Ridge (Reference 3) and has been extensively revised. The various components of the feedwater system model are shown in Figures 7 and 8. Table 6 summarizes the relationship between the physical components of the Oconee-1 feedwater system and the corresponding mathematical components of the RELAP5 model.

The purpose of the feedwater system is to supply demineralized/de-aerated subcooled water to the A and B steam generator secondary inlets. The water is heated and pressurized from 305 K (90°F) and 0.01 MPa (1.50 psia) to 511 K (460°F) and 6.55 MPa (950 psia).

The RELAP5 options used in describing the feedwater system include the nonequilibrium and wall friction models. Centrally located junctions were applied to all horizontal junctions. Choking and two-velocity models were also applied at all junctions.

Heat structures were used to represent the high and low pressure heaters and the piping wall metal

Table 5. Correspondence between the physical and mathematical components in the A and B steam generator secondaries

Physical Component	RELAP5 Component
Steam Generator A	
Downcomer	305
Tube bundle	
Nucleate boiling region	306, 310
Film boiling region	315, 320
Superheat region	320, 325
Aspirator region	315
Superheat steam outlet region	330, 335, 340
Main steam line	345, 350
Turbine stop valve	820, 821
Turbine bypass valve	810, 811
Safety valves	806, 807
Emergency feedwater system	
Turbine-driven	812, 813
Motor-driven	803, 804
Steam Generator B	
Downcomer	405
Tube bundle	
Nucleate boiling region	406, 410
Film boiling region	415, 420
Superheat region	420, 425
Aspirator region	415
Super heat steam outlet region	430, 435, 440
Main steam line	445, 450
Turbine stop valve	920, 921
Turbine bypass valve	910, 911
Safety valves	906, 907
Emergency feedwater system	
Turbine-driven	912, 913
Motor-driven	903, 904

Table 6. Correspondence between the physical and mathematical components in the feed train

Physical Component	RELAP5 Component
Hotwell	730
Hotwell pump	734
Demineralizer and de-aerator system	736
Booster pump	738
Low pressure F and E heaters	740
E heater drain	742, 744
Low pressure D heaters	746
D heater drain	748, 750
Low pressure C heaters	752
A main feedwater pump	754
A main feedwater pump discharge line	756, 757
B main feedwater pump inlet line	758
B main feedwater pump	760
B main feedwater pump discharge line	761, 762
Main feedwater pump header	763
A and B heater train number 1	764
A and B heater train number 2	766
High pressure heater header	768
A and B startup and main feedwater control valves	770, 771, 772, 773
Steam Generator A control valve header	774, 775
Steam Generator B control valve header	776, 777
Steam Generator A feedwater header	778, 782
Steam Generator B feedwater header	780, 784
Steam Generator A feedwater crossover	850, 851, 852, 853, 854
Steam Generator B feedwater crossover	950, 951, 952, 953, 954

masses. The feedwater heaters were modeled using the appropriate tube bundle surface areas. The energy contributed to the feedwater from the heater secondaries was modeled using the heat structure energy source option. The piping was modeled by first calculating the applicable metal volume and then adding the equivalent metal thickness to the appropriate heat structure. Heat structures representing several components were combined and added to selected components in order to reduce the computer storage requirements.

Integrated Control System

The Babcock & Wilcox Integrated Control System (ICS) is a comprehensive system which controls all major portions of the Oconee-1 plant. A schematic of the system is shown in Figure 9. The models developed for the Pressurized Thermal Shock program study of the Oconee-1 plant comprise only the following three portions of the overall control system: (a) turbine bypass control, (b) feedwater control, and (c) emergency feedwater control.

The model of the ICS was developed by SAI-Oak Ridge with some modifications supplied by INEL (Reference 4). The unit load demand and reactor control subsystems have not been modeled, except to provide the demand signal for the feedwater control subsystem and the reactor control demand signal. The reactor demand signal was required for the neutron power error cross-limit signal from reactor control to feedwater control.

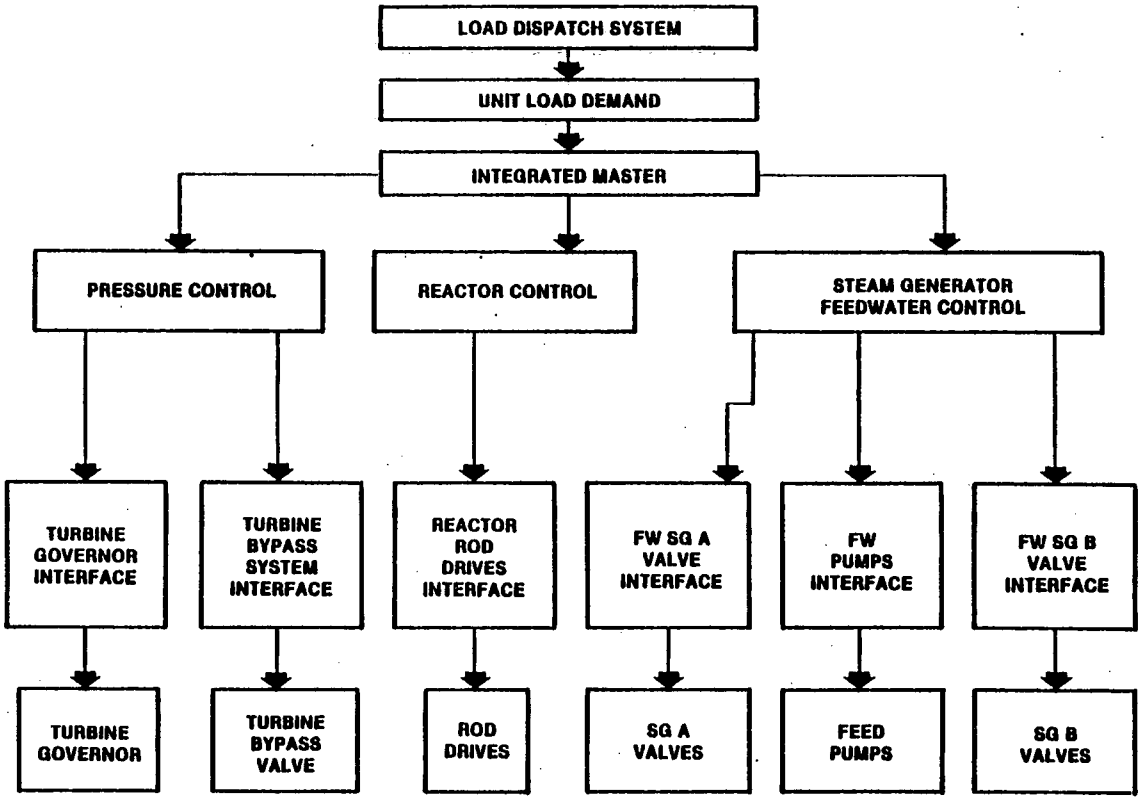

Figure 9. Organization B&W integrated control system.

The integrated master was not modeled, except for the turbine bypass valve control. Specific limitations of the model were:

1. Operator hand-control stations were not modeled. The sequences modeled did not require hand-control actions.

2. The turbine header pressure was assumed to be a boundary condition. Consequently, turbine control was not modeled in the integrated master. This was not a significant limitation because, in the sequences evaluated, turbine trips occurred early in the transients.

3. It was assumed that unit load demand transfers to "track generated megawatts" upon reactor/turbine trip. This initiated a -20% full power (FP)/min runback. (If a reactor coolant pump or a main feedwater pump is tripped before the unit load demand has reached its lower limit of 10% FP, the ramp rate should be switched to -50% FP/min.) Since either the Btu limits or the neutron cross-limit were the dominant controls in the transients that were simulated, this was not a significant limitation.

4. Small subsystems within the feedwater control block were not modeled. These include:

   a. Ratio Controller. This subsystem is designed to split the total feedwater demand between the two steam generators so as to maintain equal reactor coolant cold leg temperatures and total feedwater demand. This system was not modeled because it is blocked during transients, or when either steam generator is on level control. Since these conditions existed throughout the transients calculated, it was unnecessary to model this effect.

   b. Total Feedwater Controller. This subsystem is designed to aid in quick recovery of large feedwater/demand mismatches, which are possible during operational upsets such as loss of a reactor coolant pump. This controller is blocked if the primary loop flow

mismatch is <10%. Since no transient specified asymmetric reactor coolant pump status during periods of main feedwater delivery, this system was not simulated.

5. Calibrating integrals were not modeled. These integrating controllers are provided for long-term control of system mismatches and are consequently blocked during transients.

All other portions of the feedwater control and the turbine bypass control were faithful implementations of the ICS control logic. Gains for proportional and proportional-plus-integral control modules were taken from generic Bailey Meter Company Integrated Control System manuals (Reference 5) where available. Proportional gains for the manual control of feedwater were adjusted so that 1% flow error provided approximately 1/2% main feedwater valve motion, and 1-in. water level error provided approximately 2% startup feedwater valve movement. These sensitivities were provided by Mr. Luther Joiner of Babcock & Wilcox.

Mr. Joiner also provided ranges of integral controller gains which are typical of operating plants. The midrange values of these gains were selected, or values from Bailey literature were used, if they were available and consistent with Mr. Joiner's recommendations. The Btu limits were provided by Duke Power Company for Oconee-1. These curves indicated a design flow of 2.4×10^6 kg/h (5.3×10^6 lb/h) for each steam generator. The nominal feedwater flow specified for the simulation model was 2.45×10^6 kg/h (5.4×10^6 lb/h). The Btu curves were adjusted upward to provide the same margin at the higher flow.

In summary, the model was an accurate representation of the ICS functions necessary to model the specified transients. For the long response time transients under consideration, the controller gains were sufficiently accurate to provide reasonable response.

Documentation Control of Codes and Models

Input decks and the code versions used to perform the Oconee-1 pressurized thermal shock RELAP5 calculations are documented in Table 7. Input decks are controlled on tape at INEL under configuration control number F01216.

Table 7. Documentation control of code versions and models

Calculation	RELAP5/MOD1.5 Cycle Used	Record Number on Configuration Control Tape F01216	Steady State From which Transient Was Initiated
Steady state number 1 (hot standby)	27	1	—
Steady state number 2 (full power)	16	2	—
Steady state number 3 (full power)	27	3	—
Steady state number 4 (full power)	30	4	—
Main steam line break[a]	23	5	2
Steam generator overfeed[a]	23	6	2
Hot leg small break (PORV)[a]	23	7	2
Oconee-3 plant transient[a]	23	8	2
Revised main steam line break	27	9	3
Maximum sustainable steam generator overfeed	25	10	2
Turbine bypass valve failure at hot standby	27	11	1
Pressurizer surge line small break	30	12	4
RC pump suction small break	30	13	4
Steam generator tube rupture	31	14	4

a. Results of these calculations are detailed in Reference 1.

3. OVERVIEW OF PREVIOUSLY REPORTED ANALYSES

Detailed results of the first four sequences analyzed were presented in Reference 1. A brief overview of the results for these sequences is presented in the following subsections along with plotted results of key parameters to be used as boundary conditions in fracture mechanics calculations.

Main Steam Line Break Transient

A description of the transient, as defined by ORNL, appears in Table 8. The sequence is identical to that of the revised main steam line break presented in Section 4, excepting the reactor coolant pump (RCP) restart and high pressure injection (HPI) throttling criteria. For this sequence, one RCP per loop was restarted 10 min after attainment of 28 K (50°F) subcooling in both hot legs. HPI was not throttled. In the revised sequence, the RCP restart was immediate upon attaining 42 K (75°F) subcooling, and HPI was throttled in order to maintain 28 to 56 K (50° to 100°F) subcooling.

Results of the calculation, and extrapolations to 2 h, are shown in Figures 10 through 12. Figure 10 shows the reactor vessel downcomer pressure response. The minimum pressure calculated was 5.02 MPa (728 psia) and the maximum was 17.0 MPa (2465 psia), the opening setpoint of the power-operated relief valve. Figure 11 shows the reactor vessel downcomer fluid temperature. The minimum temperature calculated was 482 K (408°F). The heat transfer coefficient on the reactor vessel wall inside surface is shown in Figure 12. The low values (at 500 s, for example) correspond to periods of low loop flow; high values correspond to periods when the reactor coolant pumps are operating.

Table 8. Main steam line break transient scenario

1. Reactor trips, coincident with break of 0.86 m (34 in.) steam line.
2. Turbine trips; TSVs close.
3. ICS functions as designed.
4. Protection systems on hotwell, condensate booster, and MFW pumps function as designed.
5. HPI actuates at setpoint of 10.45 MPa (1515 psia).
6. Operator trips RC pumps 30 s after HPI actuation.
7. EFW pumps start when low MFW pump discharge pressure is sensed.[a]
8. MFW/EFW system attempts to maintain 6.1 m (240 in.) steam generator level.[a]
9. Core flood tanks actuate at setpoint.[a]
10. LPI actuates at setpoint.[a]
11. Operator isolates feedwater to affected steam generator 10 min[b] into the transient.
12. Operator restarts one RC pump in each loop 10 min[c] after attaining 28 K (50°F) subcooling in the hot legs.
13. PORV opens at setpoint of 17.0 MPa (2465 psia).
14. SRVs open at setpoint of 17.34 MPa (2515 psia).[a]
15. PORV/SRVs reseat at their setpoints 16.65 MPa (2415 psia).
16. Pressurizer becomes water-solid.
17. EFW surge tank capacity of 272544 liters (72,00 gal) is exhausted; the two motor-driven EFW pumps trip.[a]
18. Turbine-driven EFW continues to draw from hotwell.[a]

a. Event is dependent upon phenomena encountered.

b. Five times a typical time for operator action, based on simulator experience.

c. Two times a typical time for operator action, based on simulator experience.

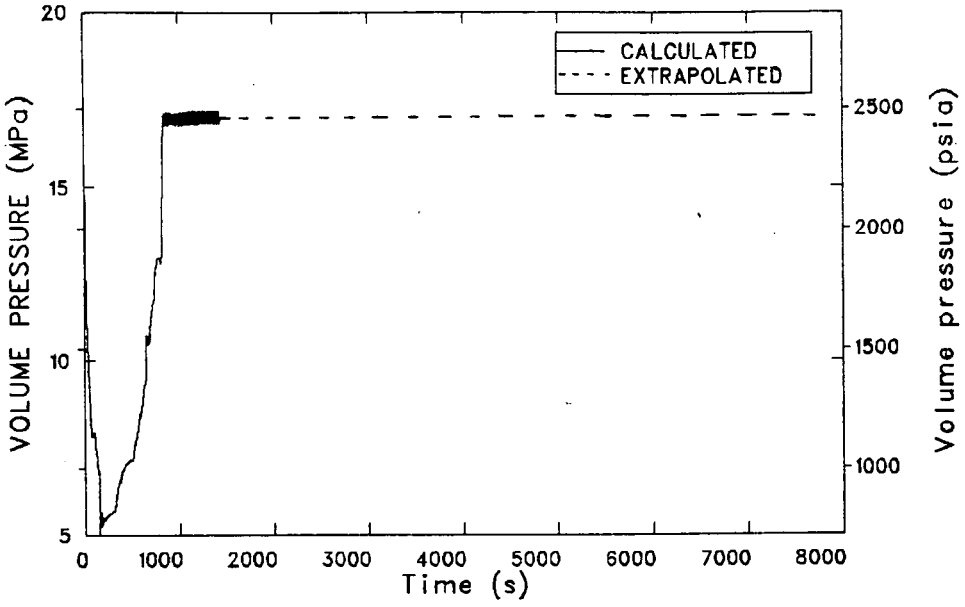

Figure 10. Main steam line break, RV downcomer pressure.

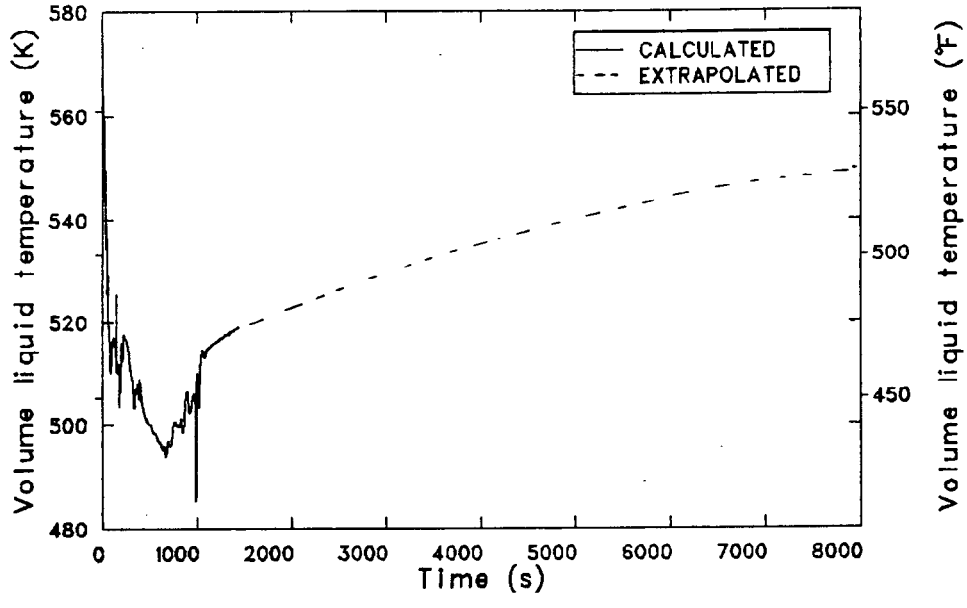

Figure 11. Main steam line break, RV downcomer fluid temperature.

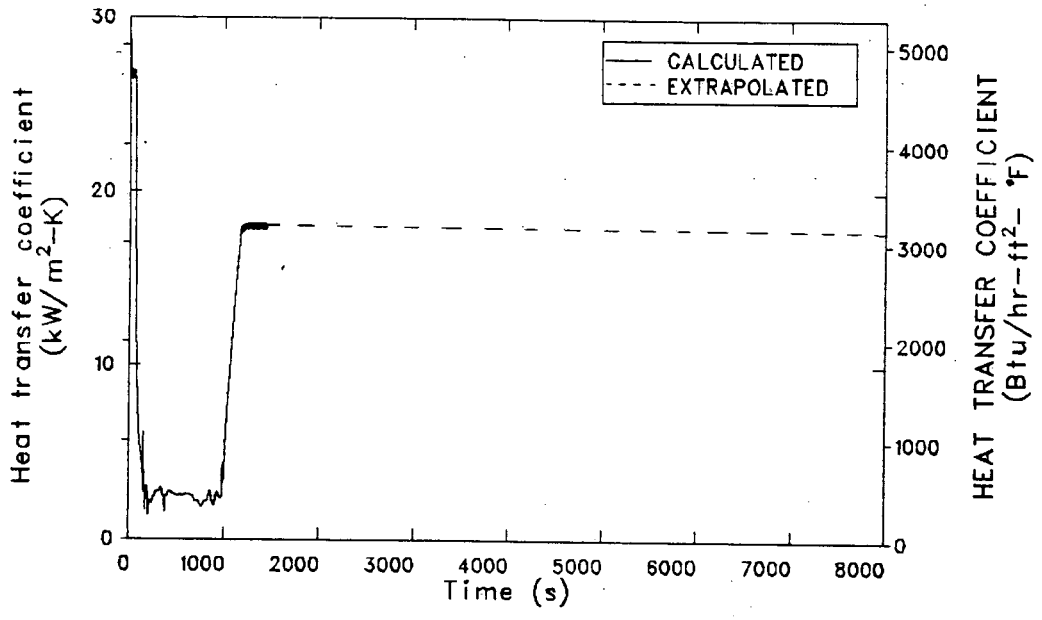

Figure 12. Main steam line break, heat transfer coefficient of RV downcomer inside surface.

Steam Generator Overfeed Transient

A description of the transient, as defined by ORNL, appears in Table 9. The scenario differs from that of the maximum sustainable overfeed transient, presented in Section 5, in the availability of feed train protection functions. In this sequence, the protection functions (primarily low suction pressure trips on the feed train pumps) were available. As a result, the main feedwater pumps were tripped shortly after the transient was initiated. This sequence differs further from the sequence in Section 5 in that reactor coolant pump power was not tripped off by the operator.

Results of the calculation, and extrapolations to 2 h, are shown in Figures 13 through 15. Figure 13 shows the reactor vessel downcomer fluid pressure response. The minimum pressure calculated was 8.92 MPa (1294 psia). The maximum pressure calculated was 17.0 MPa (2465 psia), which corresponds to the power-operated relief valve opening setpoint pressure. The minimum calculated downcomer fluid temperature was 505 K (449°F), as shown in Figure 14. The heat transfer coefficient on the reactor vessel wall inside surface, shown in Figure 15, represents forced convection conditions throughout the calculation. The variations observed in the coefficient were due primarily to changing fluid densities and pressures as the transient proceeded.

Hot Leg Small Break Transient

The sequence was initiated by a stuck open power-operated relief valve. It was assumed that the operator did not trip power to the reactor coolant pumps. A description of the transient, as defined by ORNL, is described in Table 10.

Results of the calculation, and an extrapolation to 2 h, are shown in Figures 16 through 18. Figure 16 shows the reactor vessel downcomer fluid pressure response. The minimum calculated pressure was 8.68 MPa (1259 psia). As shown in Figure 17, the minimum downcomer fluid temperature was 545 K (521°F) and occurred at 2 h, the end of the extrapolation. The extrapolated primary pressure at 2 h was 11.38 MPa (1650 psia). The heat transfer coefficient on the inside surface of the reactor vessel downcomer wall was estimated to drift downward as fluid properties changed, as shown in Figure 18. The coefficient represents forced-convection conditions throughout the calculation.

Oconee-3 Plant Transient

On March 14, 1980 the Oconee-3 PWR experienced a transient from full power. This was initiated by a turbine trip and followed by a partial steam generator overfeed. The Oconee-3 PWR is a virtually identical sister plant to the Oconee-1 PWR.

Table 9. Steam generator overfeed transient scenario

1. Reactor trip, turbine trip, TSVs close.
2. TBVs open; safety valves open and reseat at setpoints.
3. Full MFW flow continues.
4. HPI actuates at setpoint of 10.45 MPa (1515 psia); operator does not trip RCPs.
5. MFW pump trip due to steam generator high level fails to occur.
6. Steam generators fill.
7. Core flood tanks actuate at setpoint.[a]
8. LPI actuates at setpoint.[a]
9. Protection systems on hotwell, condensate booster, and MFW/EFW pumps function as designed.
10. Main steam lines fill with water.
11. TBV closes, due to loss of condenser vacuum.
12. EFW pumps start, due to low MFW pump discharge pressure setpoint.
13. EFW flow is controlled at steam generator level setpoint of 0.61 m (24 in.).
14. PORV opens at setpoint of 17.0 MPa (2465 psia).
15. SRVs open at setpoint of 17.34 MPa (2515 psia).[a]
16. Pressurizer relief valves reseat at setpoint of 16.65 MPa (2415 psia).
17. Pressurizer goes water-solid.

a. Event is dependent upon phenomena encountered.

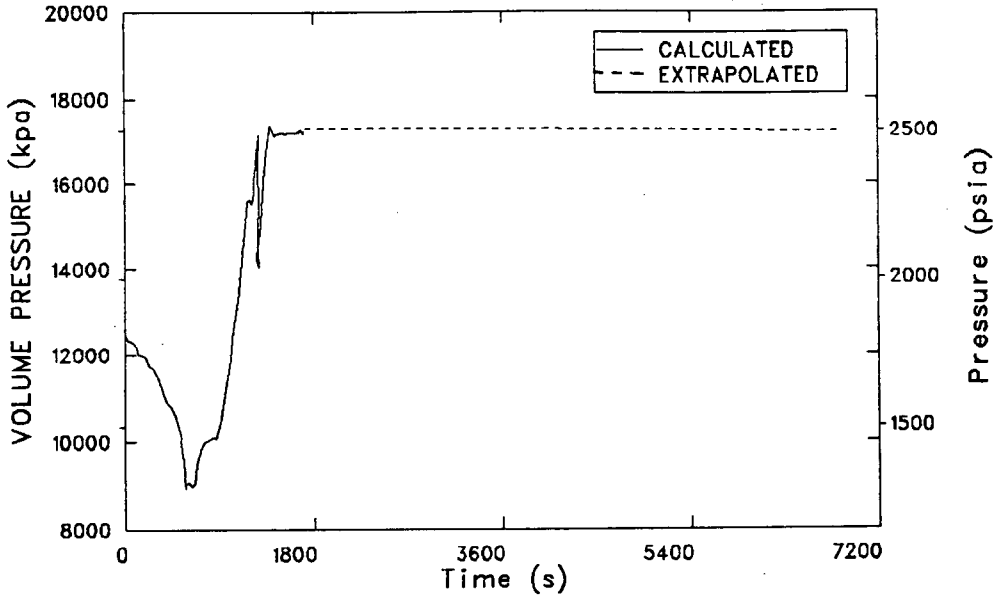

Figure 13. SG overfeed, RV downcomer pressure.

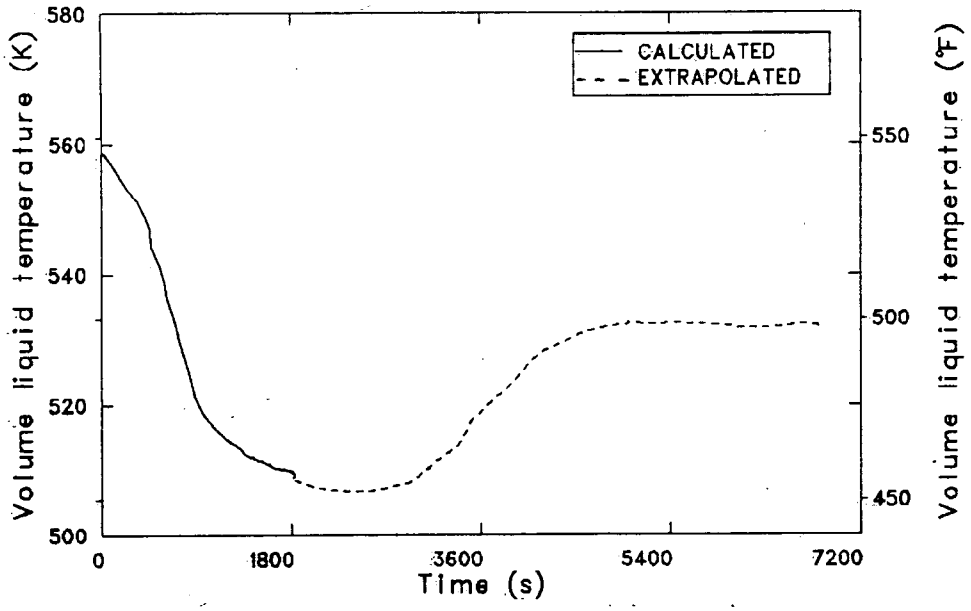

Figure 14. SG overfeed, RV downcomer fluid temperature.

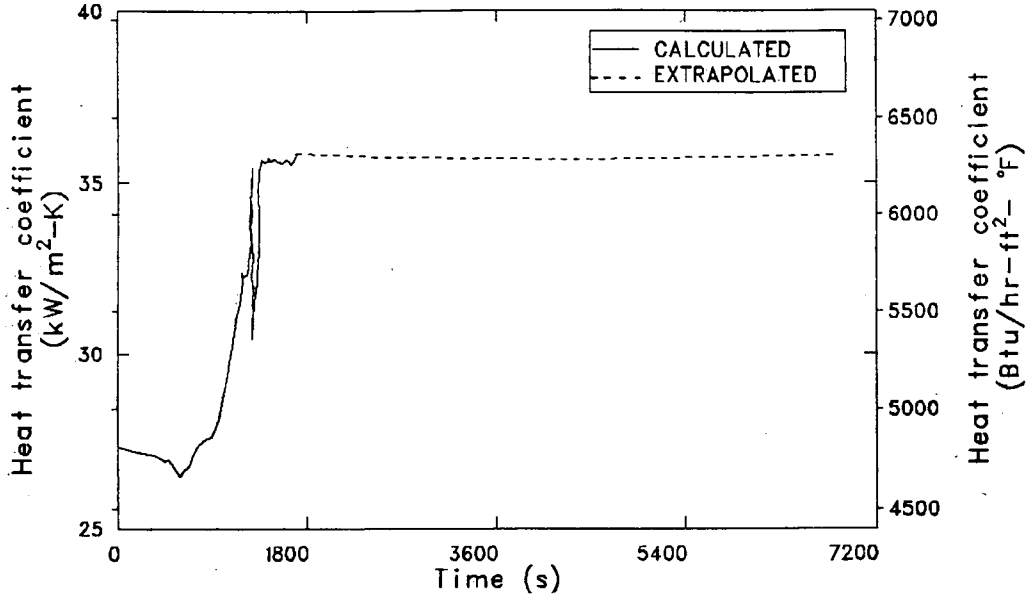

Figure 15. SG overfeed, heat transfer coefficient of RV downcomer inside surface.

By performing a RELAP5 calculation duplicating the transient sequence and comparing calculated data with that measured in the plant, a limited assessment of the computer model was formed.

The plant data measured during the transient are proprietary to Duke Power Company. Specific comparisons between computed and measured data are not presented here, since their inclusion would necessitate the same classification of this report. These comparisons, presented in Reference 1, generally indicate good agreement between calculated and measured data. Differences, where noted, were found to be caused by minor modeling problems or suspect plant data.

Table 10. Hot leg small break transient scenario

1. Small break loss-of-coolant accident.[a]
2. Reactor trips, turbine trips, TSVs close.
3. HPI actuates at setpoint of 10.45 MPa (1515 psia).
4. TBVs/SRVs in secondary function as designed.
5. ICS fails to run back MFW.
6. MFW pumps trip due to high steam generator level.
7. EFW system functions as designed.
8. Core flood tanks dump; LPI system actuates.[b]

a. Size: 2.1368×10^{-3} m^2 (0.023 ft^2); location: pressurizer relief valve.

b. Event is contingent on size of break.

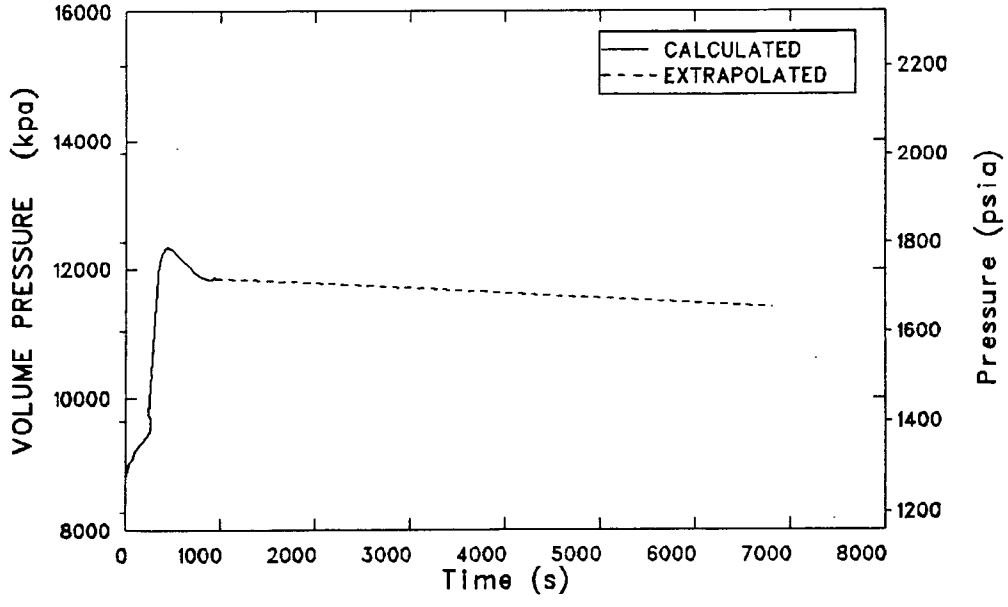

Figure 16. Hot leg small break, RV downcomer pressure.

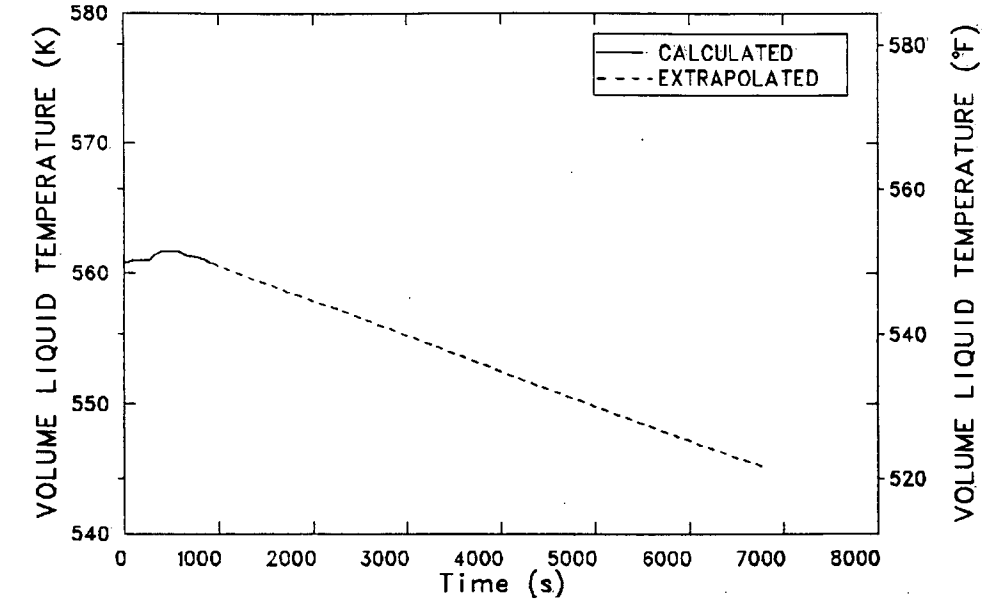

Figure 17. Hot leg small break, RV downcomer fluid temperature.

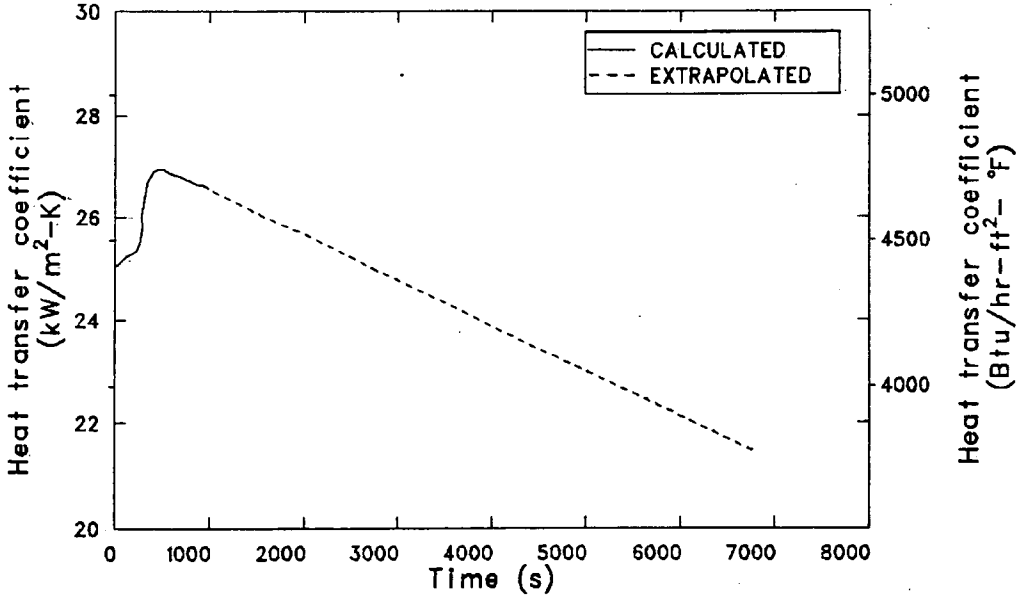

Figure 18. Hot leg small break, heat transfer coefficient of RV downcomer inside surface.

4. MAIN STEAM LINE BREAK REVISED TRANSIENT

The following subsections contain the scenario description of the main steam line break revised transient, modeling changes effected in order to perform the transient calculation, detailed analysis of the transient results, and conclusions drawn from the analysis.

Transient Scenario Description

A description of the revised main steam line break scenario appears in Table 11. This scenario definition was developed at Oak Ridge National Laboratory (ORNL).

The transient was initiated by a 200% double-ended rupture of the main steam line on one steam generator. All automatic plant functions were assumed to be operative. It was assumed that operator actions would trip reactor-coolant pump power 30 s after initiation of high pressure injection, terminate all feedwater and turbine bypass on both steam generators at 10 min, and reactivate emergency feedwater and turbine bypass to the unaffected steam generator at 15 min.

Model Changes

The RELAP5 model used to perform the main steam line break transient calculation was described in Section 2.

The double-ended rupture of the steam line on loop A was simulated by simultaneously inserting the break flow path (at the downstream end of Component 345) into an atmospheric pressure sink and isolating downstream steam line volumes (Components 350, 820, and 821). Component numbers correspond to those shown on the nodalization diagram in Figure 5. The unaffected loop steam generator was assumed to be immediately isolated from the effects of the break, due to the very rapid closure time of the turbine stop valves.

For this transient, where the secondary pressure in the unaffected steam generator far exceeds that in the affected steam generator, all of the turbine-driven emergency feedwater (EFW) capacity was assumed to be available for the affected loop steam generator. Motor-driven EFW continued to be split evenly between the two steam generators, since one motor-driven EFW pump is specifically dedicated to each steam generator.

Transient Results

A sequence of events for this calculation is summarized in Table 12.

At the start of the transient, a 0.864-m (34 in.) diameter break opened in the steam line. Turbine and reactor trips were also assumed to occur at the start. As a result, the turbine stop valves were closed over a period of 0.5 s; the feedwater heater power and feedwater heater drain flows were terminated at 5 s, and an instantaneous reactor shutdown to the ANS decay heat was modeled.

The primary and secondary system pressure responses are shown in Figure 19. The affected secondary system depressurized rapidly, and the resulting cooling depressurized the primary system. The unaffected secondary system was initially pressurized to the secondary relief valve opening setpoint at 3 s, and the valves remained open until 13 s. Depressurization in the affected secondary, due to the break, caused the secondary liquid inventory to flash rapidly. The resulting vapor velocities were sufficient to entrain liquid and sweep it out of the generator to the break. Figures 20 and 21 show the void fraction and the mass flow rate at the break, respectively.

Because the flow in the affected loop secondary was accelerated as a result of the break, the indicated operating level increased dramatically during the initial phase of the transient, as shown in Figure 22. This increase was observed because the operating level indication is based on the differential pressure between the lower-downcomer and midboiler regions. When the flow was accelerated and liquid was entrained, both the differential pressure sensed and the operating level dramatically increased at the start of the transient. The affected loop secondary operating level remained above its initial, steady state value for the first 5 s of the transient. At 0.3 s, the level exceeded the 90% of range limit, causing a main feedwater pump trip.

Emergency feedwater was initiated to both steam generators at 4.4 s, as a result of the main feedwater

Table 11. Revised main steam line break scenario

Summary Description:

The accident sequence begins with the simultaneous break of a 34-in. steam line and the reactor and turbine trips. The forcing function for the accident is the delay by the operator in isolating the FW flow to the affected steam generator, combined with the delay in throttling the HPI flow and in restarting one RC pump in each loop after 50°F subcooling is attained.

Initial Conditions:

1. Reactor at full power.
2. Temperatures and pressures in primary/secondary are nominal.
3. Decay heat is at the ANS standard.
4. Pressurizer spray and heaters operate as designed.

Sequence of Events:

1. Reactor trips, simultaneous break of 0.864 m (34 in.) steam line.
2. Turbine trips; TSVs close.
3. ICS functions as designed.
4. Protection systems on hotwell, condensate booster, and MFW/EFW pumps function as designed.
5. HPI actuates at setpoint (1500 psig).
6. Operator trips RC pumps 30 s after HPI actuation.
7. EFW pumps start when low MFW pump discharge pressure is sensed.[a]
8. MFW/EFW system attempts to maintain 6.1 m (240 in.) steam generator level.[a]
9. Core flood tanks actuate at setpoint.[a]
10. LPI actuates at setpoint.[a]
11. a. Operator isolates feedwater to both steam generators 10 min into transient (close MFW, start-up-FW, EFW, and TBV systems).
    b. Operator begins refilling unaffected steam generator to 6.1 m (240 in.) level with EFW at maximum rate 15 min. into transient.
    c. Turbine bypass system on unaffected steam line opens at 15 min. and maintains 7.0 MPa (1015 psia) pressure.
12. Operator restarts one RC pump in each loop, after attaining 42 K (75°F) subcooling, and throttles HPI to maintain 42 ± 14 K (75 ± 25°F) subcooling.
13. PORV opens at setpoint (17.0 MPa, 2465 psia).
14. SRVs open at setpoint (17.34 MPa, 2515 psia).[a]
15. PORV/SRVs reseat at their setpoints (2400 psig).
16. Pressurizer becomes water-solid.
17. EFW surge tank capacity 272544 L (72,000 gal) is exhausted, and the two motor-driven EFW pumps trip.[a]
18. Turbine-driven EFW continues to draw from hotwell.[a]

a. Event is dependent upon phenomena encountered.

Table 12. Revised MSLB sequence of events

Event	Time from Start of Transient (s)
Reactor trip, turbine trip breaker opens.	0
Main feedwater pumps trips due to high level in affected steam generator.	0.3
Emergency feedwater trips on, based on low main feedwater pump discharge pressure.	4.4
HPI trips on, based on low hot leg pressure.	5.3
RC pumps trip (30 s after HPI initiation); main feedwater rerouted to emergency feedwater header.	35.3
75°F subcooling attained in both hot legs; 2 RC pumps restarted and HPI throttled to maintain 50—100°F subcooling.	300
Unaffected steam generator level recovers to 240 in.; main feedwater to this steam generator is terminated; emergency feedwater is throttled to maintain 240 in. level.	320
Restarted RC pumps are up to full speed.	360
Hotwell surge tank is empty; motor-driven emergency feedwater is terminated to both steam generators.	513
As anticipated, all main and emergency feedwater and the turbine bypass capability are terminated.	600
HPI injection ends due to 100°F subcooling.	1992
Pressurizer level reaches 100%.	2354
PORV opening setpoint pressure reached.	2432
Calculation terminated.	2697

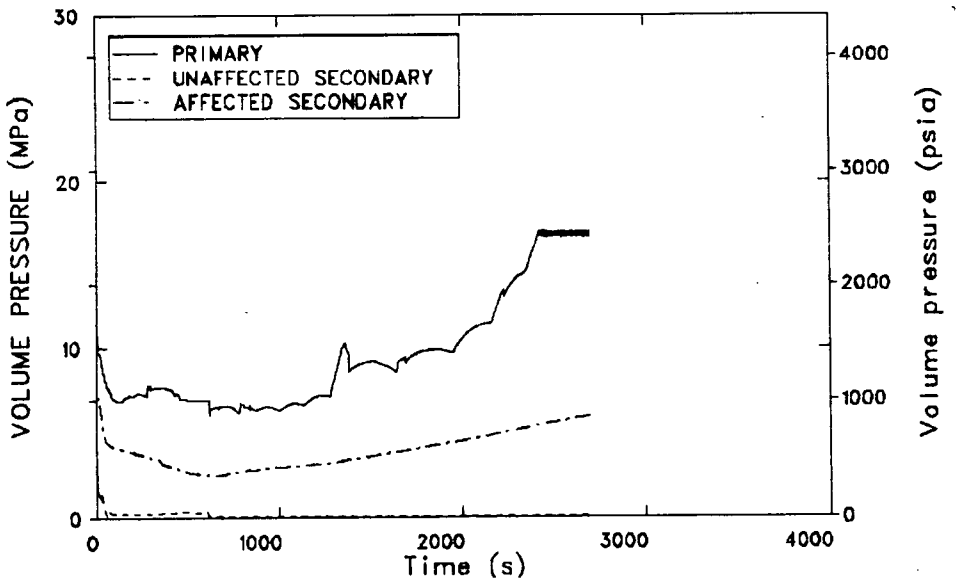

Figure 19. Revised MSLB, primary and secondary system pressures.

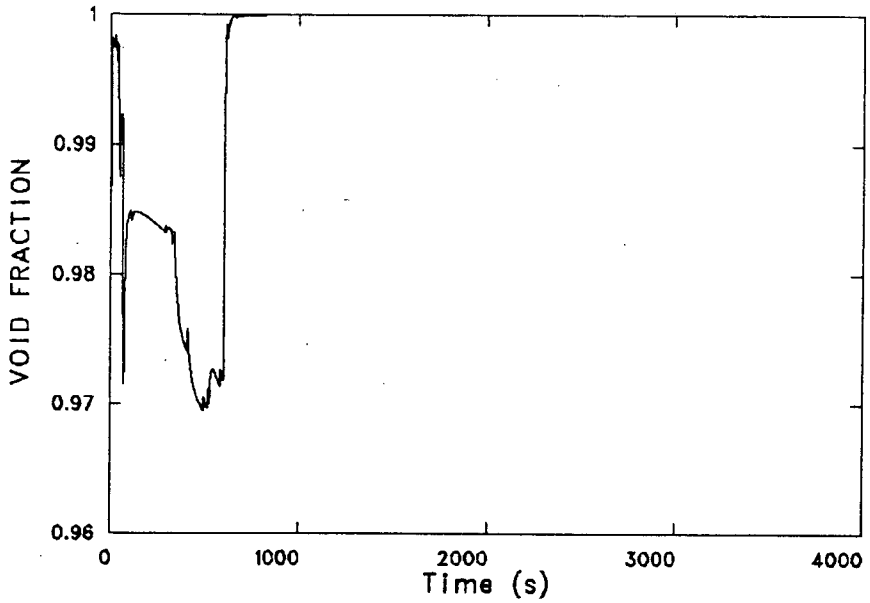

Figure 20. Revised MSLB, void fraction at the break junction.

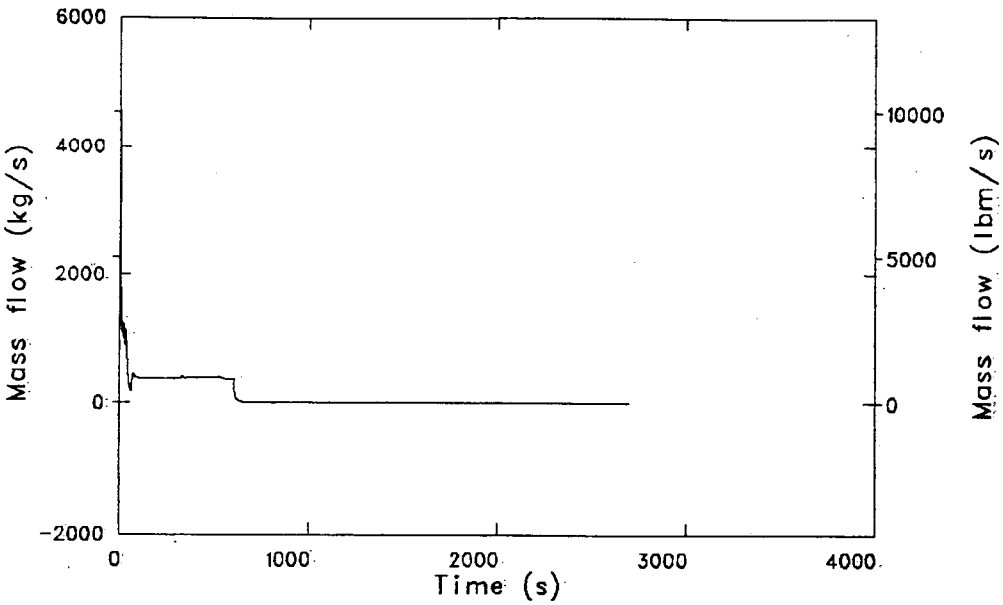

Figure 21. Revised MSLB, break mass flow rate.

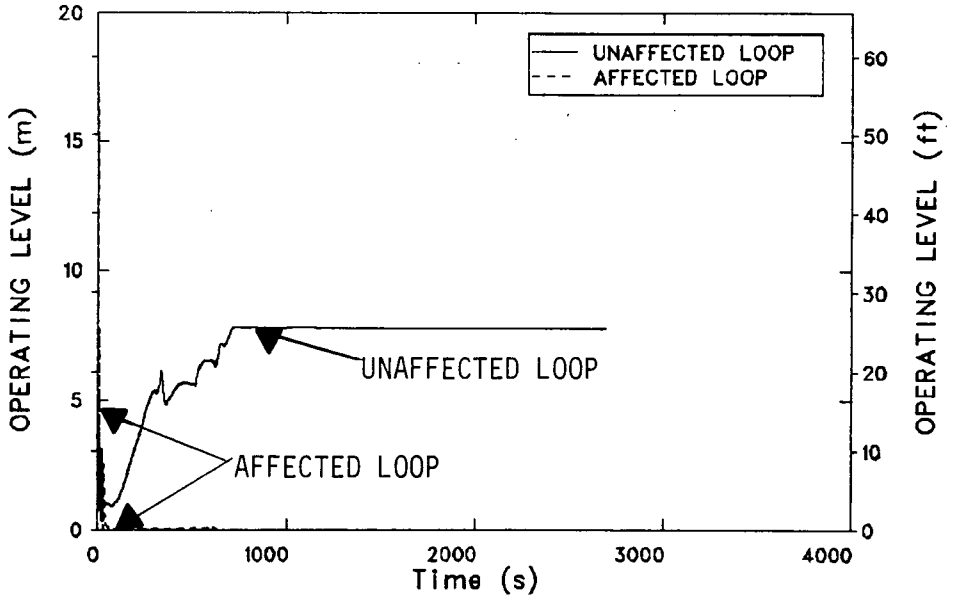

Figure 22. Revised MSLB, steam generator operating levels.

pump discharge pressure's falling below 5.27 MPa (765 psia). This was an error in the calculation, in that emergency feedwater initiation should have been delayed until the startup levels fell below 0.61 m (24 in.) when reactor coolant pumps were powered, or 6.1 m (240 in.) when reactor coolant pumps were tripped. If this error had not occurred, emergency feedwater would have been initiated at 8 s to the affected steam generator and 15 s to the unaffected steam generator. The effect on the overall calculation results of this early initiation of emergency feedwater was minor.

At 5.3 s, high pressure injection (HPI) was initiated when the hot leg pressure fell below 10.4 MPa (1515 psia). As defined by the sequence description, 30 s after HPI initiation, power to the reactor coolant pumps was tripped off, and main feedwater was rerouted to the emergency feedwater headers. Mass flow rates in the cold legs, between the HPI injection nozzles and the vessel, are shown in Figures 23 through 26. The increased flow rates during the initial portion of the transient reflect the increased densities associated with the decreasing fluid temperatures calculated following the break of the main steam line. After the reactor coolant pumps were tripped, the cold leg flow rates decreased in conjunction with the coastdown of the pumps. Due to natural loop circulation set up by core heat addition and heat removal to the steam generator secondaries, loop flow in all four cold legs continued following pump coastdown. Flow rates during this period were slightly higher in the affected loop cold legs than in those of the unaffected loop. This was due to a higher heat transfer rate to the affected loop steam generator and to the higher HPI injection rates in the A loop than in the B loop.

Due to the primary liquid volume shrinkage resulting from the cooldown, the pressurizer collapsed liquid level, shown in Figure 27, initially decreased to zero. HPI injection, however, added liquid volume to the primary, and the pressurizer level began to recover. The shrinkage also caused the formation of a large void in the upper head of the reactor vessel, as shown in Figure 28, and smaller voids in the hot legs, as shown in Figures 29 and 30.

The first repressurization of the primary system, shown in Figure 19, resulted when the upper head and hot leg voids collapsed and continuing HPI flow started to compress the steam inside the pressurizer. Due to one-dimensional modeling limitations, the calculated collapse rate of reactor vessel upper head voids was probably overpredicted. Due to the accumulated effects of addition of cold HPI fluid and cooling to the steam generators, when the upper head started to refill, the liquid entering was cooler than that which was already there . As a result, steam in the upper head was condensed, causing a localized depressurization which accelerated the refilling, causing more condensation. The process continued at a nonphysical,

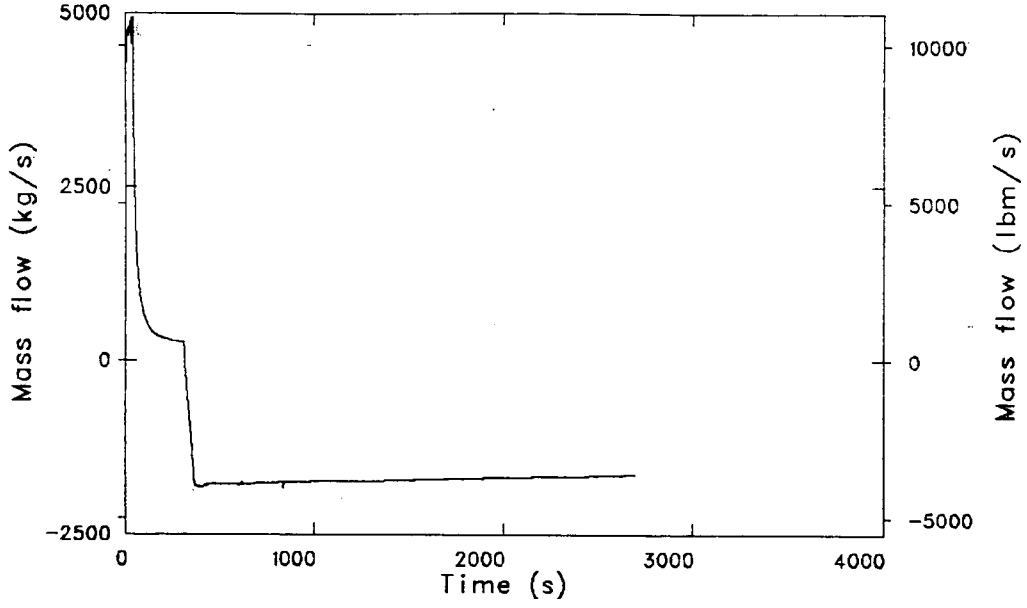

Figure 23. Revised MSLB, cold leg A-2 mass flow rate at RV.

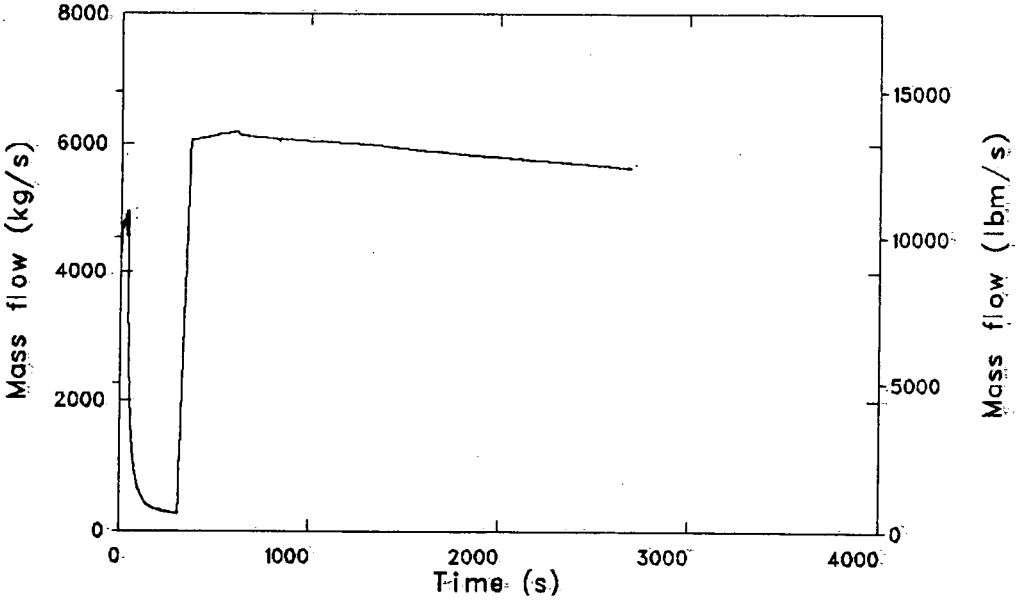

Figure 24. Revised MSLB, cold leg A-1 mass flow rate at RV.

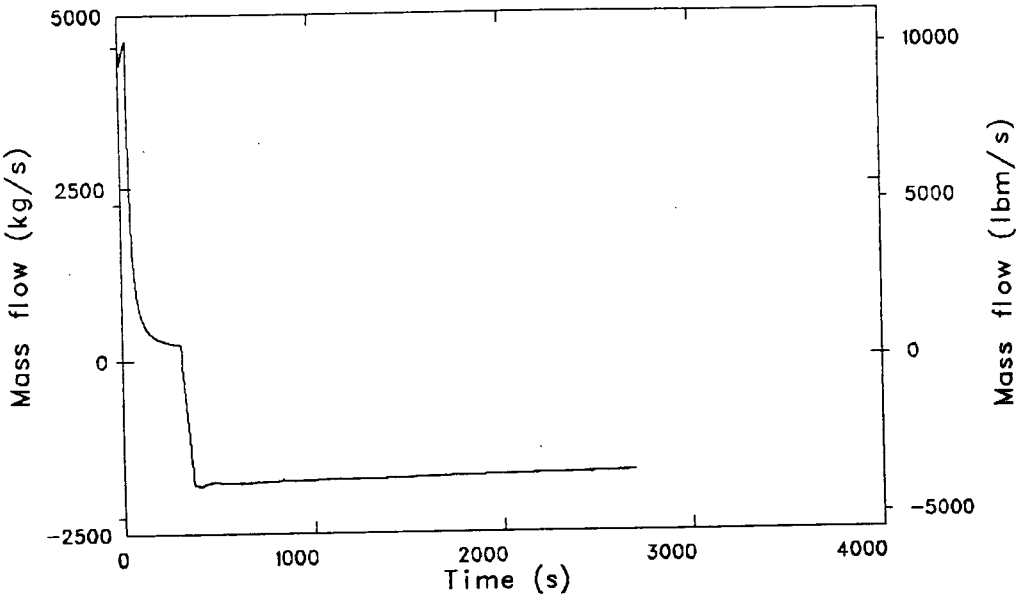

Figure 25. Revised MSLB, cold leg B-2 mass flow rate at RV.

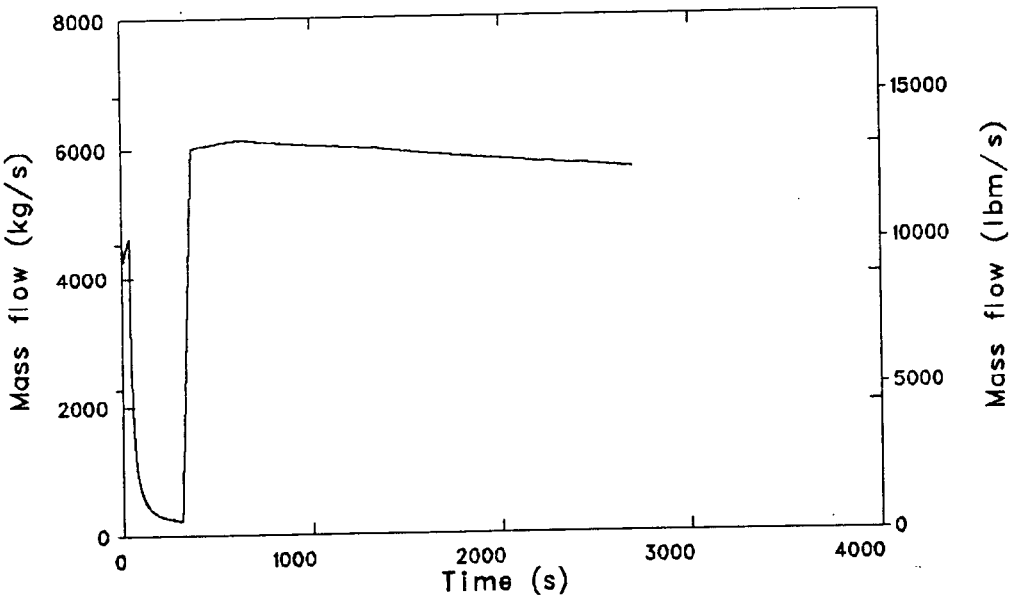

Figure 26. Revised MSLB, cold leg B-1 mass flow rate at RV.

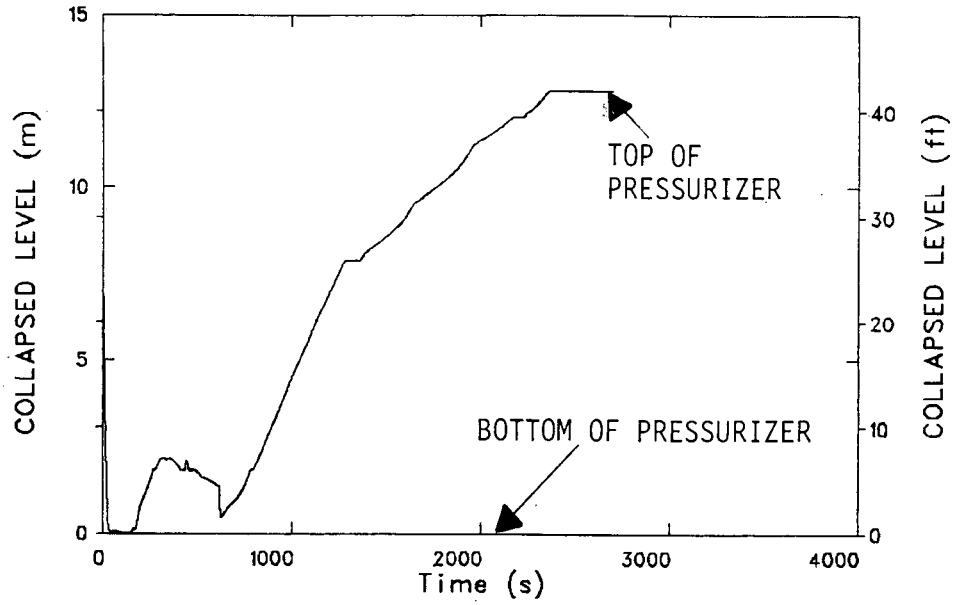

Figure 27. Revised MSLB, pressurizer collapsed liquid level.

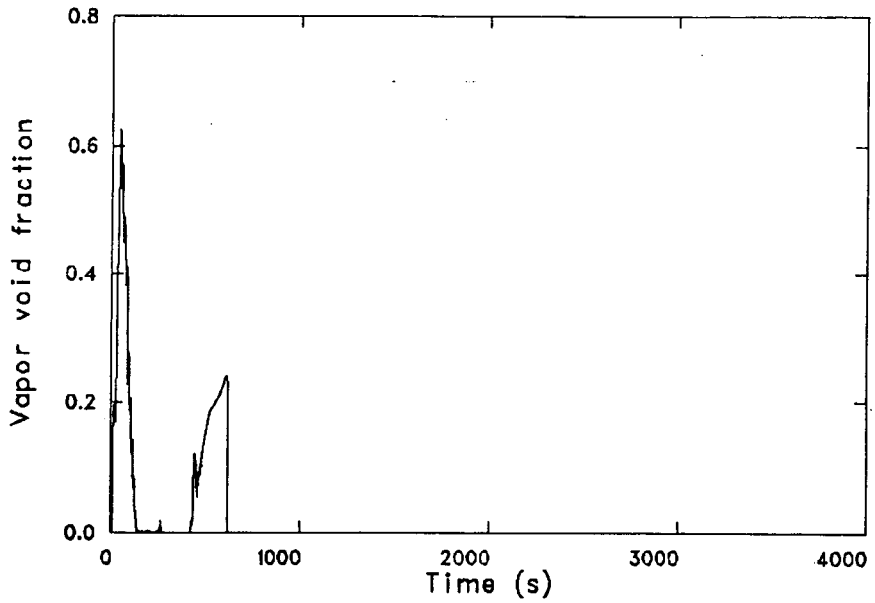

Figure 28. Revised MSLB, RV upper head void fraction.

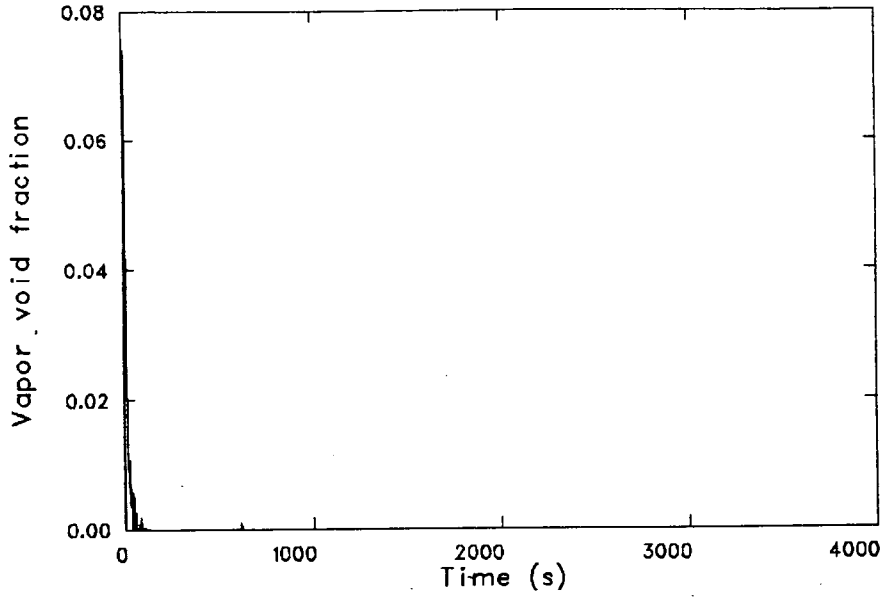

Figure 29. Revised MSLB, void fraction at top of affected loop hot leg.

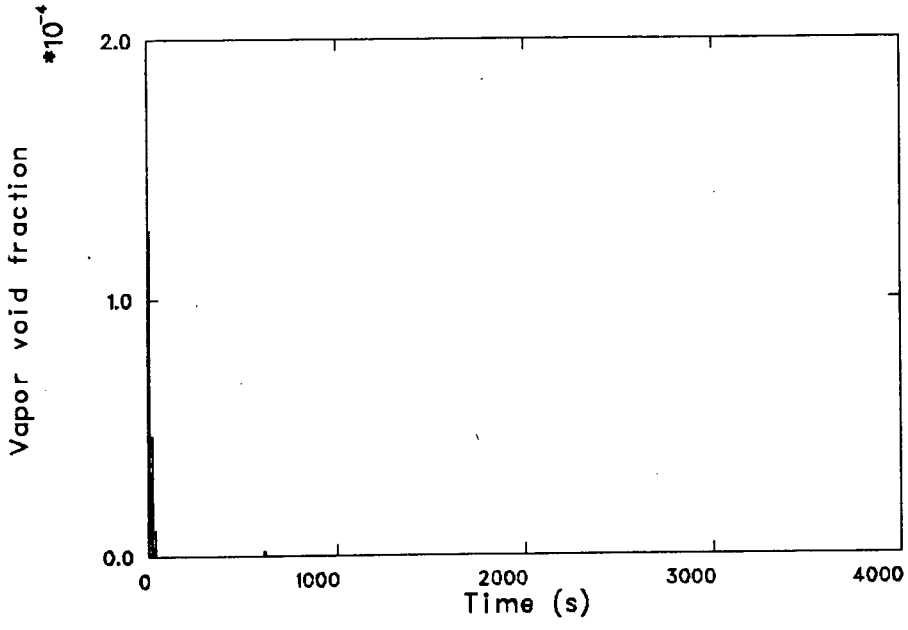

Figure 30. Revised MSLB, void fraction at top of unaffected loop hot leg.

ever-increasing rate until the upper head was completely refilled. The upper head void thus collapsed too quickly and was accompanied by a rapid drop in primary system pressure, as indicated in Figure 19 at 600 s. Since the magnitude of the primary system pressure decrease was small, the poorly calculated upper head refill behavior had only a minor effect on the overall results of this calculation.

The main feedwater flow rates at the entrances to the steam generators are shown on an expanded scale plot in Figure 31. In the unaffected loop, main feedwater delivery decreased smoothly over the first 3 s because the pressure in the steam generator secondary quickly exceeded that at the main feedwater pump discharge header. The flow decrease shown represents only the blowdown of fluid between the discharge header and the unaffected steam generator. In the affected loop, the main feedwater flow decreased during the first second because the main feedwater valves initially closed in response to the previously discussed high secondary level indication. As the effects of the break were propagated back to the feed train, however, the affected loop main feedwater flow increased dramatically, with flashing occurring in the main feed lines until main feedwater realignment to the emergency feedwater headers at 35.3 s.

The calculated flow rate responses in the emergency feedwater headers at the entrances to the steam generators are shown in Figure 32. After 35.3 s, these curves represent the combined flow rates due to emergency feedwater and main feedwater, the latter being fed through the startup valves to the emergency feedwater headers. Before 35.3 s, the curves represent only the emergency feedwater flow rates. Figure 33 shows the temperatures of the fluids entering the steam generators through the emergency feedwater headers. In the unaffected loop, only emergency feedwater was delivered until about 80 s, when the pressure in the unaffected secondary fell below the head of the condensate booster pump, allowing main feedwater to be injected. At 320 s, the main feedwater to the unaffected loop was terminated when the level had recovered to 6.1 m (240 in.). Motor-driven emergency feedwater to the unaffected secondary was terminated at 513 s, when the hotwell surge tank was calculated to be empty. In the affected loop, the secondary pressure was much lower than in the unaffected loop. This resulted in a greater flow to the affected loop steam generator, as shown in Figure 32. At 513 s the motor-driven emergency feedwater was also terminated to the affected loop steam generator; however, full turbine-driven emergency feedwater flow continued until all feedwater was terminated at 600 s.

After the performance of this calculation, new information, which indicated that the emergency feedwater was improperly modeled in two ways, was obtained. First, emergency feedwater control should have been based on startup level rather than operating level. Secondly, the hotwell and hotwell surge tanks are isolated from each other by a closed valve so that the only fluid removed from the surge tank is due to motor-driven emergency feedwater flow. The effect of using operating level instead of startup level was minor for this calculation since the levels closely tracked each other. Because the calculation assumed the hotwell-to-tank valve was open during the transient, an early surge tank emptying time was calculated. This resulted in termination of motor-driven emergency feedwater at 513 s. Had this been modeled differently, motor-driven emergency feedwater flow termination would have occurred at 600 s. This would have resulted in an estimated mixed downcomer fluid temperature about 5 K (9°F) lower than that which was calculated.

Figure 34 shows the loop A-1 high pressure injection (HPI) rate. The rate for loop A-2 was identical. The trends were the same for loops B-1 and B-2 but the rates were lower, due to a lower HPI capacity available to loop B. The figure shows that from 5.3 s, when low hot leg pressure tripped the HPI on, until 300 s, when 42 K (75°F) hot leg subcooling was obtained, full HPI flow, based on cold leg pressures, was injected. After 300 s, HPI was throttled by applying a multiplier based on subcooling in the hot legs, so that no HPI flow was allowed when subcooling exceeded 55 K (100°F). Full HPI was allowed when subcooling was less than 28 K (50°F).

Between these extremes, 40% of full flow was allowed at 50 K (90°F) subcooling; 60% of full flow was allowed at 33 K (60°F) subcooling. By controlling HPI flow in this way, the operator action associated with throttling was approximated by assuming only minor throttling, as long as subcooling remained well within range (33 to 50 K). Major throttling occurred only when subcooling approached either extreme (28 or 55 K).

An initial calculation of an Oconee-1 main steam line break sequence was reported in Reference 1.

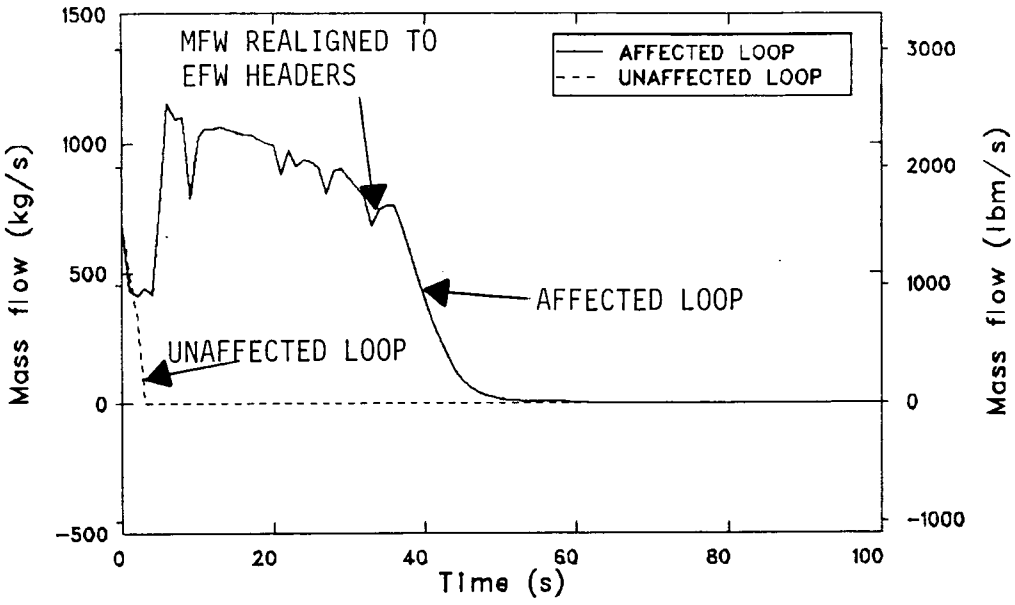

Figure 31. Revised MSLB, main feedwater flow rates at SG entrances.

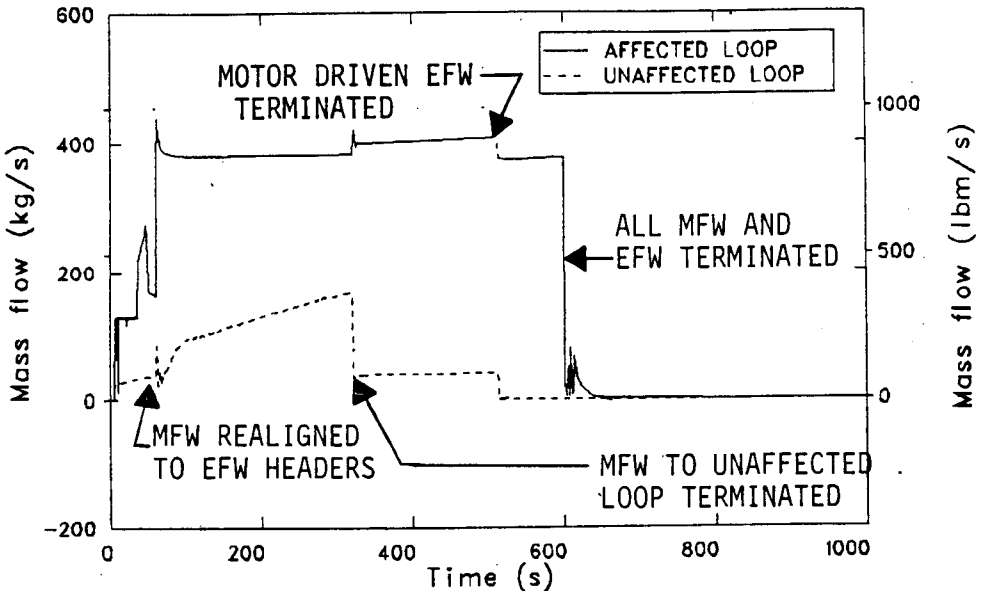

Figure 32. Revised MSLB, flow rates at emergency feedwater header.

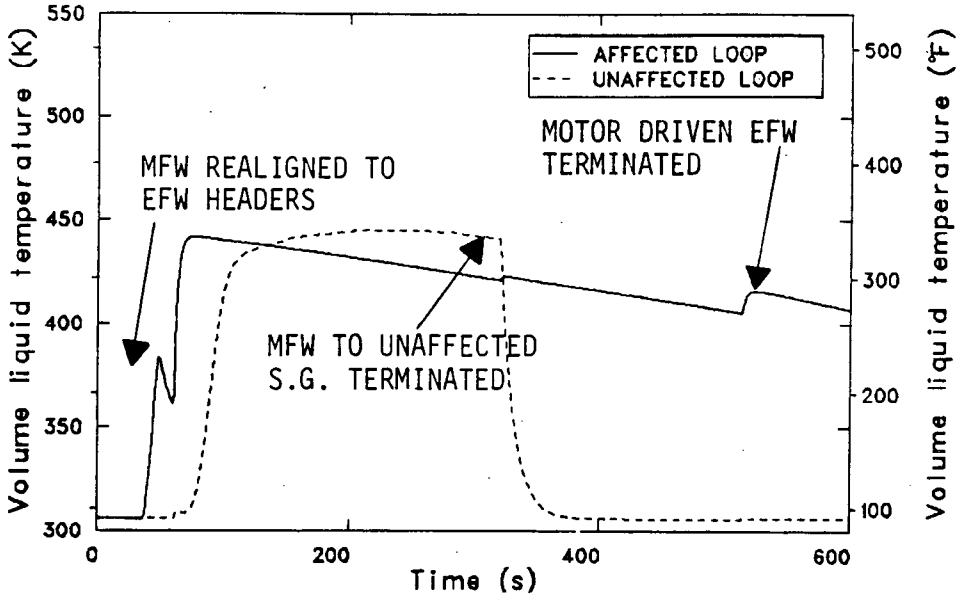

Figure 33. Revised MSLB, fluid temperatures in emergency feed headers.

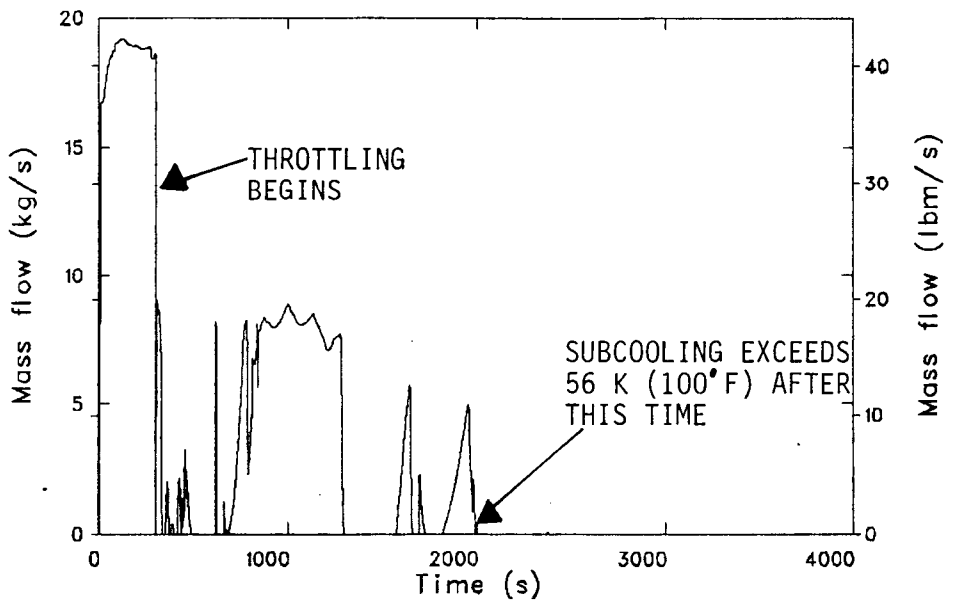

Figure 34. Revised MSLB, loop A-1 high pressure injection flow rate.

Following that calculation, the sequence description was modified by changing the reactor coolant pump restart criteria. An analysis of the affected steam generator heat removal rate was also performed. This indicated that the calculated rate was probably underpredicted. The primary purposes of recalculating the main steam line break were to update the sequence description and to obtain a more representative heat removal rate to the affected steam generator secondary.

In the original main steam line break calculation, the combination of main and emergency feedwater injected at the top of the affected steam generator boiler was totally bypassed to the break. As a result, heat was removed from the primary system only in the uppermost volume of the boiler. As reported in Reference 6, the heat removal rate was about 40 MW. Based on one-dimensional countercurrent flow limiting (CCFL) phenomena at the uppermost tube support plate (reported in Reference 6), upward steam velocities associated with a 68 MW heat removal rate below the plate would allow an equal amount of liquid mass downflow as vapor mass upflow. Therefore, an 88 MW heat removal rate (including 20 MW above the plate) represented a steady state operating condition. The conclusion was that, in the original calculation, the heat removal rate was less than that expected, based on one-dimensional CCFL phenomena. Furthermore, if three-dimensional effects are considered, such as liquid downflow at the perimeter and vapor upflow at the center of the boiler, then the underprediction of the heat removal rate would be even more severe.

In the second main steam line break sequence, when feedwater was injected at the emergency feedwater header, a downflow of liquid was calculated throughout the boiler section of the affected steam generator. Figure 35 shows qualities at five locations in the affected steam generator secondary. From 35 to 600 s, feedwater enters only through the emergency feedwater header at the top of the boiler section. The injection rate during this period was about 400 kg/s (882 lbm/s), as shown in Figure 32. The temperature of the injected fluid decreased during this period from about 440 K (332°F) to 405 K (269°F), as shown in Figure 33. At the operating pressure of the affected steam generator secondary, about 0.35 MPa (50 psia), the injected fluid temperature is about 28 K (50°F) superheated at the beginning of the period and 6 K (10°F) subcooled at the end. The uppermost cell of the boiler operated at about 8% quality during the injection period as shown by Curve 1 in Figure 35. Vapor in this cell was produced by boiling the injected fluid on the tubes and by flashing during periods when the injected fluid was superheated. At a pressure of 0.35 MPa (50 psia), an 8% quality corresponds to a void fraction of about 98%. Thus, the void fractions in the affected steam generator boiler were very high during the injection period, as opposed to the lower void fractions calculated in the first main steam line break sequence.

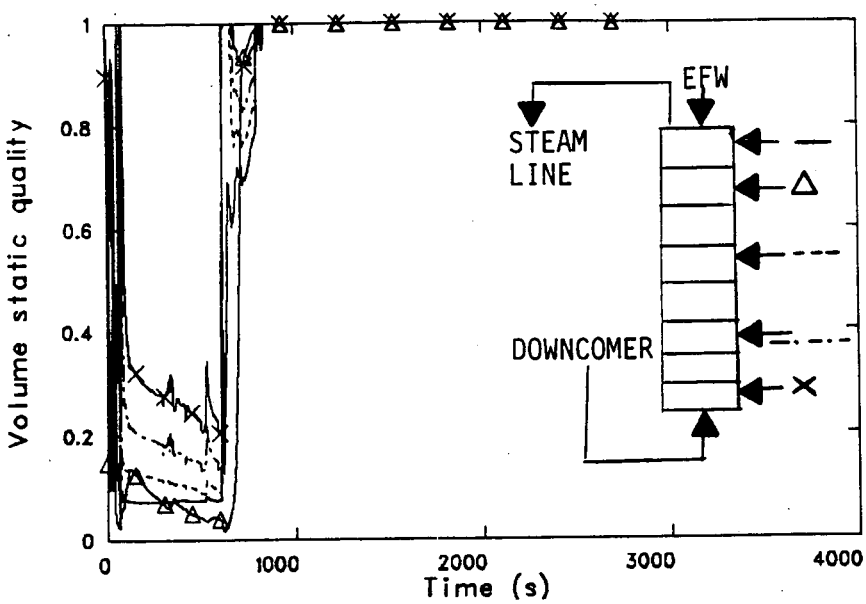

Figure 35. Revised MSLB, qualities in affected SG secondary boiler.

Figure 36 shows the vapor and liquid velocities at the uppermost tube support plate. This junction is between cells 1 and 2 on Figure 35. A vapor upflow velocity of about 15 m/s (50 ft/s) and a liquid downflow velocity of about 1 m/s (3 ft/s) are shown. The corresponding vapor mass upflow rate is about 43 kg/s (95 lbm/s); liquid downflow rate is about 48 kg/s (105 lbm/s). As the liquid fell below this junction, some of it is vaporized on tubes located in the lower cells. This caused an increase in quality with a decrease in elevation, as shown in Figure 35. The net mass downflow of about 4.5 kg/s (10 lbm/s) resulted in a pooling of liquid in the bottom cell of the boiler, as indicated in Figure 35 by the decreasing quality in the lower cell. This pooling of liquid was also indicated by an increasing affected steam generator secondary mass during the injection period, as shown in Figure 37.

As a result of the thermal-hydraulic processes just described, heat was removed from the primary system to the affected steam generator secondary at rates significantly higher than in the original main steam line break calculation. This heat removal rate is shown in Figure 38. Note that the spike in heat transfer, shortly after termination of all feedwater at 600 s, was due to a blowout of the liquid pooled at the bottom of the boiler. This blowout was also observed in the tube support plate velocities in Figure 36 and in the boiler qualities in Figure 35.

The range of the calculated affected steam generator heat removal rate was 80 to 180 MW during the injection period. Reference 6 indicated that a heat removal rate of 68 MW below the plate, and 88 MW total, is predicted for a steady state downflow of liquid and upflow of vapor through the uppermost tube support plate. This heat removal rate was based on the one-dimensional Kutateladze CCFL correlation. The RELAP5-calculated heat removal rate generally exceeded that predicted using the CCFL correlation. This represents an improvement over the original main steam line break calculation, in which the opposite was true.

Fluid temperatures in the four cold legs are shown in Figures 39 and 40. Before 300 s, when the reactor coolant pumps were restarted in the A-1 and B-1 cold legs, the greater cooling by the affected steam generator caused the affected cold leg temperatures to decrease at a rate faster than those in the unaffected cold leg. After reactor coolant pump restart, the cooldown rates of the two loops were nearly the same, due to the better fluid mixing associated with higher loop flows. After all feedwater was terminated at 600 s, fluid temperatures in all cold legs increased, because the heat sink for the primary system was lost.

The fluid temperature in the reactor vessel downcomer, at the elevation of the first circumferential weld below the cold leg nozzles, is shown in Figure 41. In this calculation the reactor coolant pumps were restarted before loop natural circulation was lost. As a result, vent valve opening was not calculated, and the reactor vessel downcomer fluid temperature was simply a mass-flow-weighted average of the cold leg fluid temperatures shown in Figures 39 and 40. The minimum calculated downcomer fluid temperature was 494 K (430°F). This minimum temperature occurred at 600 s, the time at which all feedwater was terminated.

As shown in Figure 41, uncertainty bars and a shifted mean have been added to the RELAP5-calculated reactor vessel downcomer fluid temperature curve. A comprehensive study of the uncertainties in the calculation is beyond the scope of this work. However, an estimate of uncertainty in the calculation was required by the fracture mechanics calculations analysts, who will use the downcomer temperature-time history, shown in Figure 41, as a boundary condition. Therefore, a limited-uncertainty estimate has been made, based primarily on insights gained from the comparison of TRAC and RELAP5 calculations of the main steam line break sequence presented in Appendix B.

The uncertainty was addressed first by shifting the calculated data to account for the known deficiencies in the RELAP5 calculation, as detailed here and in Appendix B. This shifted mean appears as the dashed line on Figure 41 and represents a best estimate response, which (a) compensates directly for known deficiencies, and (b) uses an arithmetic average of extremes where uncertainties in phenomena have been identified. The upper and lower ends of the uncertainty bars were then constructed by (a) again compensating for the known deficiencies, but (b) using the upper or lower extreme of uncertain phenomena behavior.

Different phenomena are observed early in the transient between the TRAC and RELAP5 calculations, as detailed in Appendix B. It was observed that the TRAC cooldown rate exceeded that for RELAP5 up to the time of reactor coolant pump (RCP) trip. The time of RCP trip was at 51.2 s with TRAC and 35.3 s with RELAP5. The conclusion

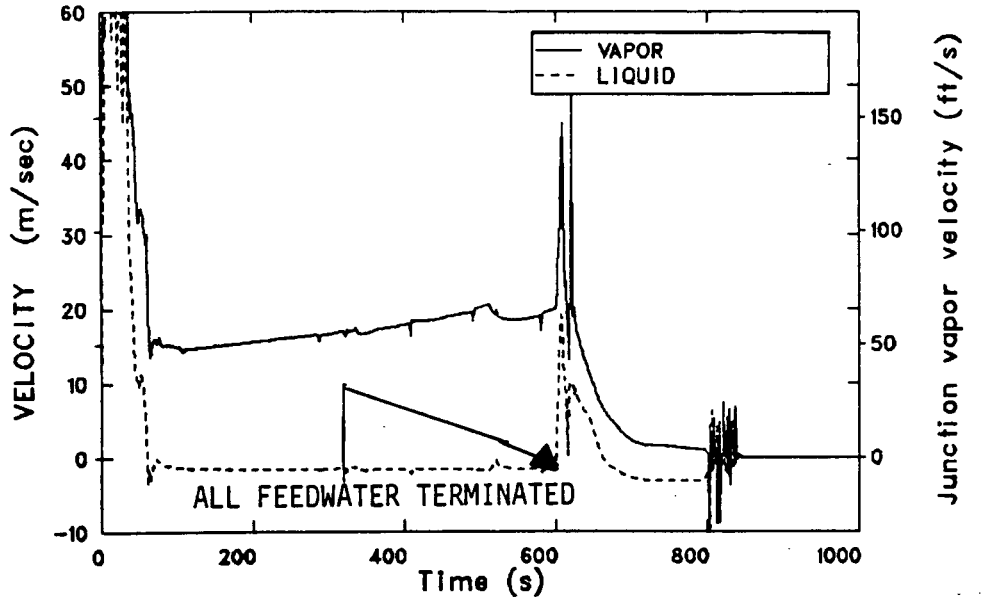

Figure 36. Revised MSLB, phasic velocities through uppermost tube support plate of affected SG.

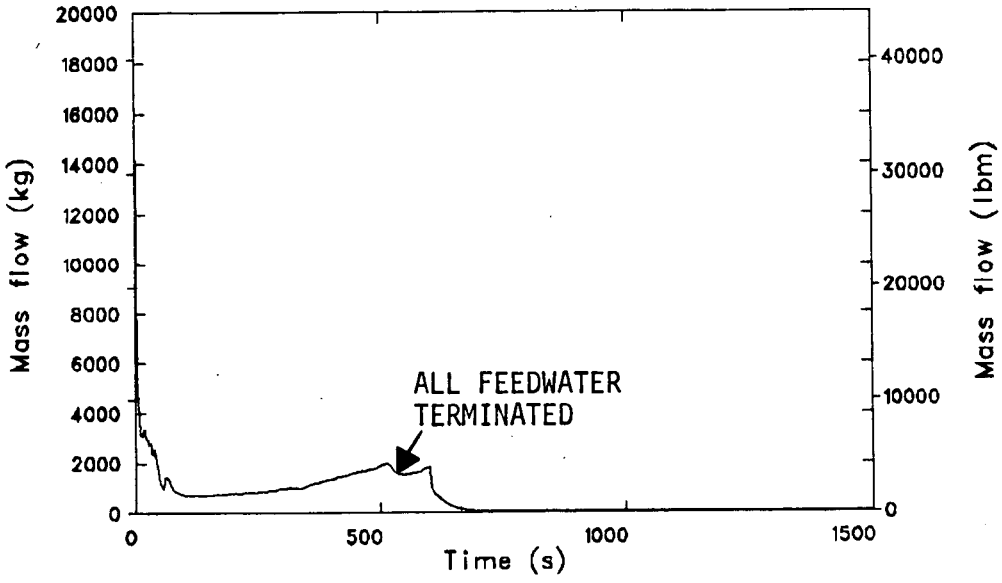

Figure 37. Revised MSLB, affected SG secondary water mass.

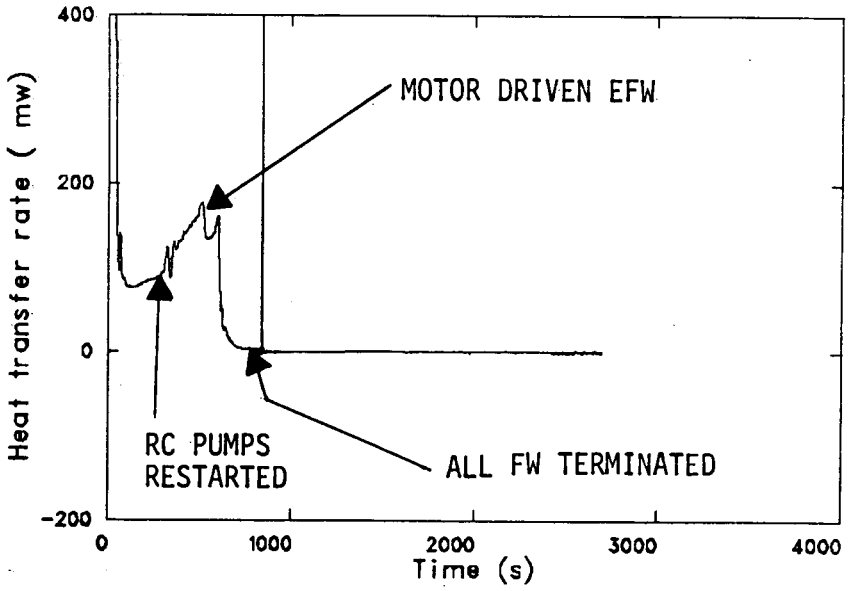

Figure 38. Revised MSLB, affected SG heat removal rate.

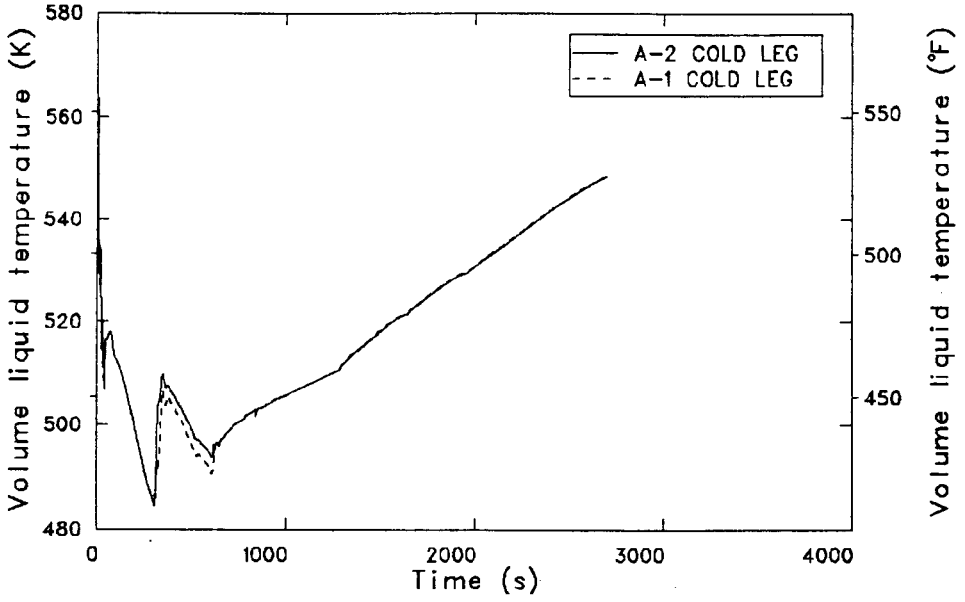

Figure 39. Revised MSLB, affected loop cold leg fluid temperatures at RV.

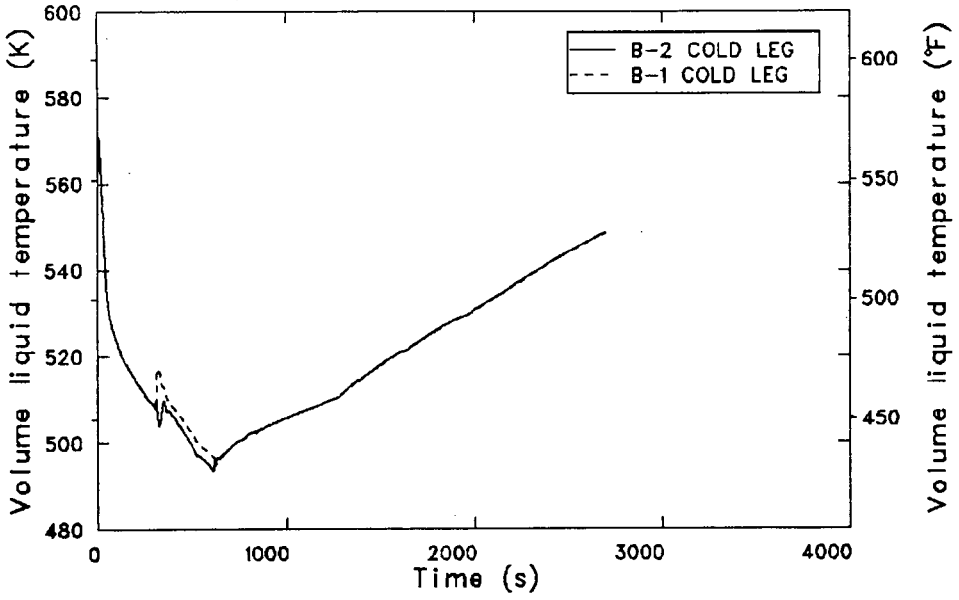

Figure 40. Revised MSLB, unaffected loop cold leg fluid temperatures at RV.

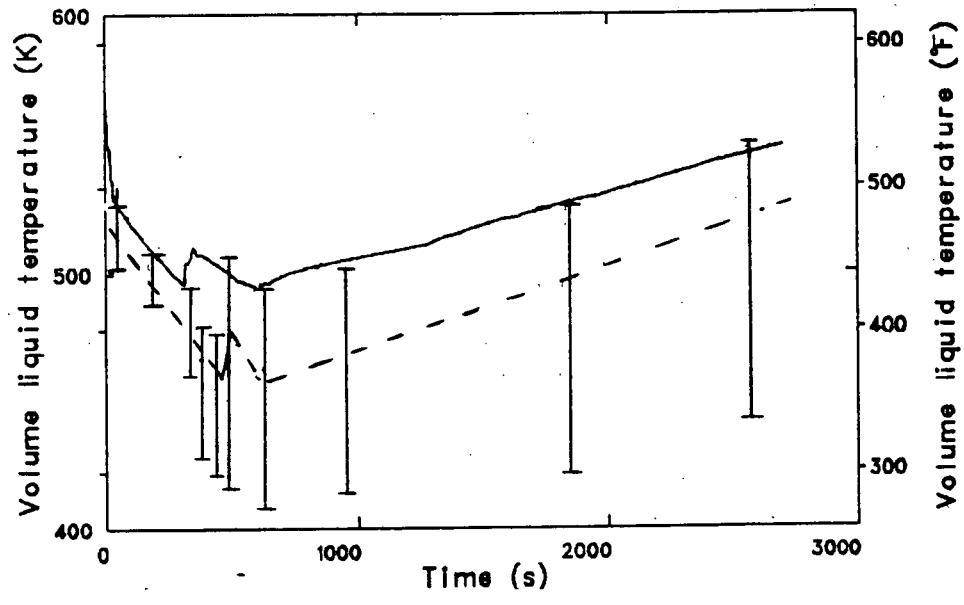

Figure 41. Revised MSLB, fluid temperature in RV downcomer.

was that the RELAP5 calculation, with its prototypical main feedwater (MFW) pump trip, better represented the cooldown rate up to the time of RCP trip. However, there is an unresolved uncertainty in the RCP trip time. The shifted mean (dashed line on Figure 41) assumes an RCP trip time of 43.25 s, the average of the TRAC and RELAP5 trip times. The uncertainty bar upper and lower extremes during this period assume RCP trip times of 35.3 and 51.2 s, respectively. Both the mean and the extremes were generated using the RELAP5 cooldown rate.

Another difference between the TRAC and RELAP5 calculations was the time of RCP restart. With TRAC this occurred at 526 s and with RELAP5 at 300 s. This difference was caused by a combination of asymmetric hot leg fluid temperatures, calculated with TRAC but not with RELAP5, and different reactor vessel upper head flashing behavior. The conclusion of the comparison was that the asymmetric hot leg behavior calculated with TRAC better represents the plant behavior than the calculation with RELAP5. However, it is likely the RELAP5 calculation better represents the upper head behavior. For the shifted mean (dashed line on Figure 41), it was assumed the RCP restart occurs at 450 s, which is the average of the RELAP5 calculated time (300 s) and the latest time at which the minimum downcomer temperature is sensitive to the RCP restart (600 s). The uncertainty bar upper extreme assumes the RCP restart is at 300 s; the lower extreme assumes it at 600 s.

Appendix B identifies different affected steam generator heat removal rates between TRAC and RELAP5 between the times of RCP trip and restart. While some of the difference could be explained, most of it was found to be due to uncertainty in the heat transfer processes calculated above the uppermost tube support plate during periods when combined MFW and EFW were injected through the EFW header. Furthermore, a sensitivity to the modeling of the height of the uppermost boiler section calculational cell was identified; this affected both calculations. To account for these differences, an average of adjusted TRAC-related and adjusted RELAP5-related heat removal rates was used to generate the shifted mean between the times of RCP trip and restart. The TRAC and RELAP5 heat removal rates above the plate were adjusted to compensate for the discrepancies between calculational cell heights and the distance from the lower surface of the upper tubesheet and the upper tube support plate. The RELAP5 rate was further adjusted for the RELAP5 vapor superheat problem discussed in Appendix B. The adjusted heat removal rates above the plate were calculated as 95 MW for TRAC and 10 MW for RELAP5, for a 53 MW average. To these amounts were added the best-estimate below-the-plate heat removal rate of 70 MW, based on Reference 6. The shifted mean thus assumes a total affected steam generator heat removal rate of 123 MW, while the upper uncertainty bar limits assume 80 MW and the lower uncertainty bar limits assume 165 MW. It is noted that the uncertainty bars include the effects of different above-the-plate heat removal rates between the two code calculations. The bars do not, however, account for possible multidimensional effects of liquid downflow and vapor upflow at the uppermost tube support plate. Multidimensional effects would probably increase the affected steam generator heat removal rate over that which was predicted using one-dimensional correlations such as used in Reference 6.

The minimum temperature reached by the shifted mean, best estimate dashed line on Figure 41 is 462 K (372°F). The lowest temperature included within the uncertainty bars is 415 K (287°F).

Figure 42 shows the calculated fluid pressure response in the reactor vessel downcomer at the elevation of the first circumferential weld below the cold leg nozzles. Uncertainty bars and a shifted mean have been added to this figure in a manner similar to those in Figure 41. The primary uncertainty just discussed for the downcomer temperature response, which also affects the pressure response, is the reactor vessel upper head flashing phenomenon. The shifted mean, which appears as the dashed line in Figure 42, represents the pressure response expected if the upper head flashing phenomenon were the average of those calculated with TRAC and RELAP5. The extremes of the uncertainty bars represent the results of the calculations themselves.

Figures 43, 44 and 45 provide extrapolations of reactor vessel downcomer pressure, fluid temperature, and inside surface heat transfer coefficient, from the end of the calculation at 2697, to 7200 s. It was estimated that the downcomer pressure would continue to be controlled by the power-operated relief valve throughout the extrapolated period. It was also estimated that fluid temperature would continue increasing until it

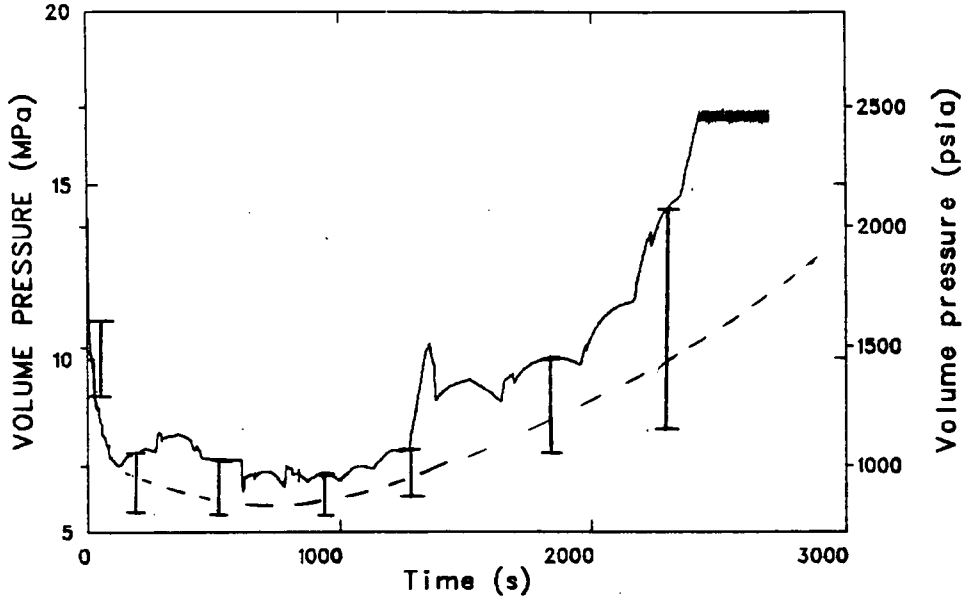

Figure 42. Revised MSLB, fluid pressure in RV downcomer.

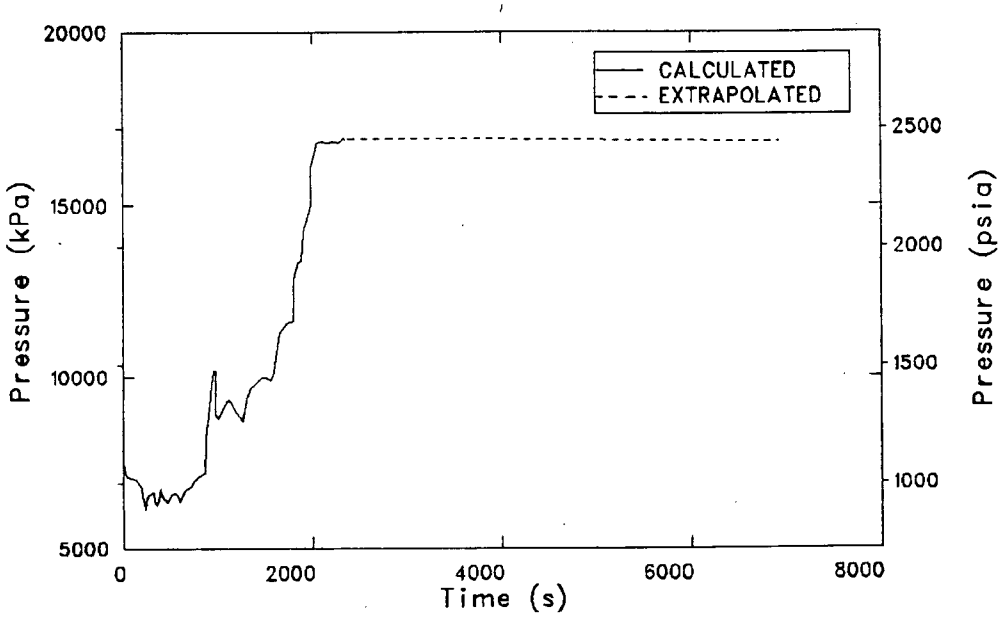

Figure 43. Revised MSLB, extrapolated pressure in RV downcomer.

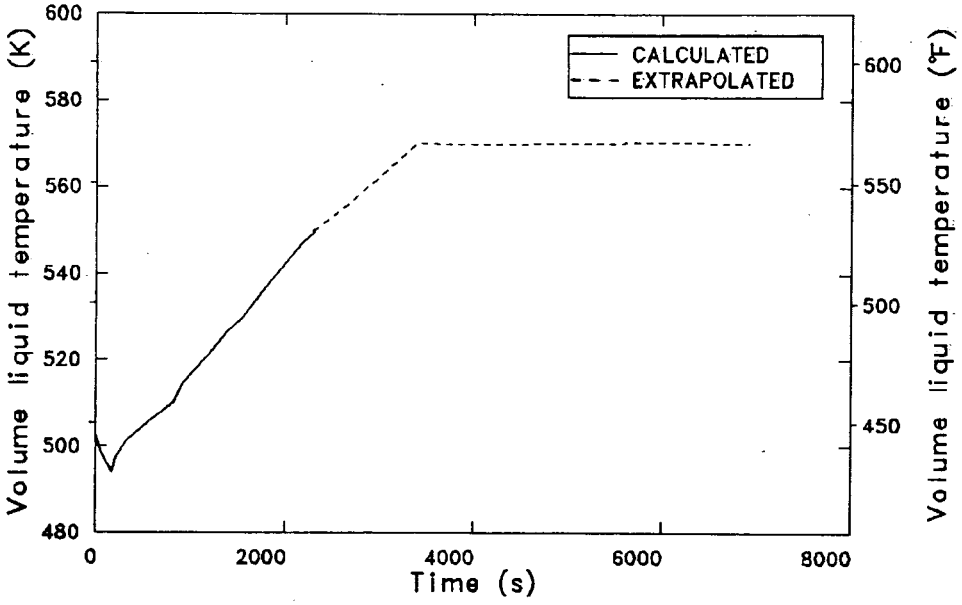

Figure 44. Revised MSLB, extrapolated fluid temperature in RV downcomer.

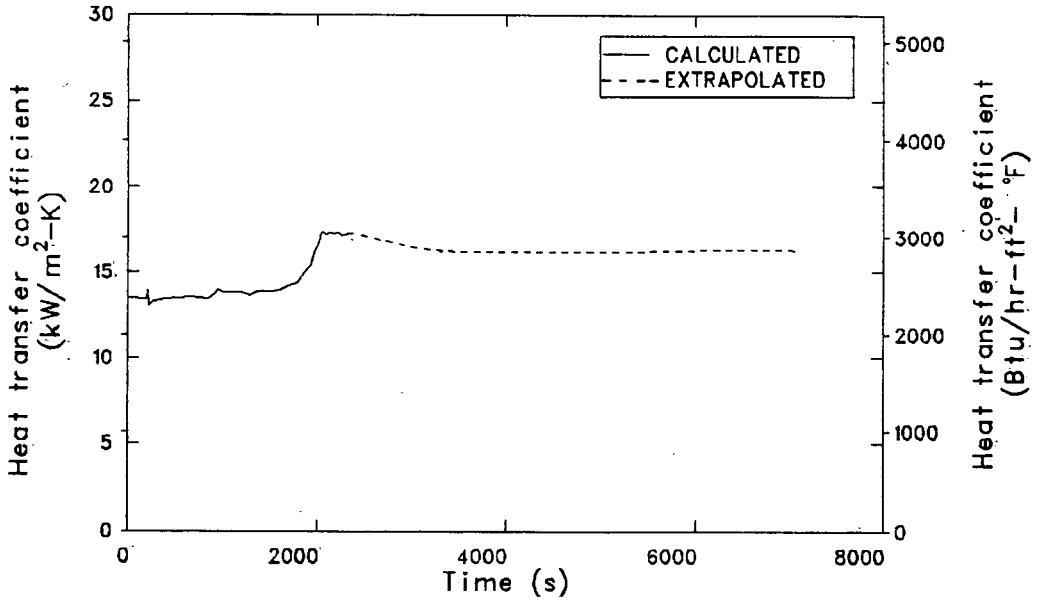

Figure 45. Revised MSLB, extrapolated heat transfer coefficient of inside surface of RV downcomer wall.

reached 571 K (568°F) and would remain near that temperature for the remainder of the extrapolated period. Above this temperature, the subcooling margin would be less than 56 K (100°F), and the injection of cold HPI fluid would resume, thereby preventing the primary fluid temperature from increasing further. It was assumed that the heat transfer coefficient would continue drifting lower until the fluid temperature stabilized but would remain constant thereafter.

Conclusions

The calculated minimum reactor vessel downcomer mixed fluid temperature was 494 K (429°F). The calculated maximum subsequent fluid pressure was 17.0 MPa (2465 psia).

The calculation of downcomer fluid temperature was particularly sensitive to the scenario requirement that reactor coolant pumps be restarted upon attaining 42 K (75°F) subcooling in both hot legs. This requirement was met at 300 s. Restarting of the pumps caused the minimum downcomer temperature to be much warmer than if the pumps had not been restarted. Since the attainment of subcooling is sensitive to hot leg asymmetry, and because a one-dimensional computer model will not predict this asymmetry, the timing of the pump restart is uncertain. The effect of this and other specific uncertainties on minimum downcomer fluid temperature is estimated to reduce the best estimate minimum downcomer fluid temperature to 462 K (372°F), with a lower uncertainty bound of 415 K (287°F).

5. MAXIMUM SUSTAINABLE OVERFEED TRANSIENT

The following subsections contain a description of the maximum sustainable overfeed transient scenario, modeling changes effected in order to perform the transient calculation, detailed analysis of the transient results, and conclusions drawn from the analysis.

Transient Scenario Description

A description of the maximum sustainable overfeed sequence which was analyzed appears in Table 13. This sequence definition was developed at Oak Ridge National Laboratory.

The transient was initiated from full power, steady state conditions (nominal temperature and pressure). The pressurizer heaters and spray operate as designed. The transient was initiated by a turbine trip, which tripped the reactor and closed the turbine stop valves. Decay heat was assumed to be at the ANS standard rate. Instead of decreasing flow, the main feedwater system continued to supply the maximum sustainable flow to both steam generators, without tripping the main feedwater pumps. It was assumed the main feedwater pump trip on steam generator high level failed to occur, allowing both steam generators to completely fill.

Model Changes

The RELAP5 model used to perform the maximum sustainable overfeed transient calculation was described in Section 2. In order to initiate the transient, the following changes were made to the integrated control system model: (a) the steam generator high level signal to trip main feedwater pumps was disengaged, and (b) the steam generator low level signal controller was set at a maximum.

Table 13. Maximum sustainable overfeed transient scenario

1. Reactor trip, turbine trip, turbine stop valves close.
2. Turbine bypass valves and safety relief valves open and reseat at setpoints.
3. Instead of running back, main feedwater system continues to supply maximum sustainable flow to both steam generators.[a]
4. High pressure injection actuates at setpoint, and operator trips all 4 reactor coolant pumps 30 s after high pressure injection actuation (according to procedures).[b]
5. Main feedwater pump trip due to steam generator high level fails to occur; both steam generators fill completely.
6. Core flood tanks and low pressure injection system function as designed.[b]
7. Turbine bypass valves close due to loss of condenser vacuum, at TBV setpoint.[b]
8. Main feedwater and turbine-driven emergency feedwater pumps trip due to low steam quality.
9. Emergency feeudwater system functions as designed.

a. To be determined by trial and error or by an automated search for maximum main feedwater flow which will not result in trip of main feedwater pumps due to exceeding of suction pressure or high discharge pressure limits.

b. Event may or may not occur, depending on phenomena encountered.

This maximum signal overrode the Btu cross-limit and neutron power cross-limit signal thereby controlling the start up and main feed valves in the feed train. The signal held these valves full open to provide the maximum possible flow through the feed train.

Following reactor trip, the Btu cross-limit and neutron cross-limit signal normally run back the main feedwater pump speed to a minimum value of 447 rad/s (4270 rpm). In the RELAP5 analysis, that minimum value was increased to 490 rad/s (4675 rpm). This was done to obtain the maximum sustainable main feedwater flow without tripping the main feedwater pumps due to low suction or high discharge pressure. At this pump speed, the suction pressure steadily decreased toward the low suction pressure trip setpoint. The main feedwater pumps tripped due to low void fraction in the steam line, following complete refill of the steam generator secondaries.

Transient Results

This section presents the results of the steam generator overfeed transient with maximum sustainable feed flow. A sequence of events for the transient is presented in Table 14.

The initiating event was a turbine trip, which tripped the reactor and closed the turbine stop valves over a period of 1 s. Upon closure of the turbine stop valves, the secondary pressure, shown in Figure 46, rapidly increased to the turbine bypass and safety relief valve setpoints, which stabilized the pressure. The rapid secondary system depressurization resulted in a cooldown and a consequent depressurization of the primary system, as shown in Figure 47. At approximately 25 and 28 s, the secondary side pressure for steam generators B and A, respectively, dropped below the safety relief and turbine bypass setpoints, closing the valves, as shown by the mass flow rates in Figures 48 and 49. Also at this time, the primary liquid temperature approached the secondary system saturation temperature, and primary-to-secondary heat transfer was reduced to a minimum, resulting in the decrease of the primary system depressurization rate shown in Figure 47.

Between 28 and 300 s, primary and secondary pressures were strongly influenced by the turbine bypass valve flow. As the generators filled, primary-to-secondary heat transfer was enhanced, as shown in Figure 50, causing steam generation and steam flow out through the bypass valve. At 150 s, the boiler region of the steam generator secondaries had become liquid-full, and the steam lines began filling. At 180 s, the volumetric liquid inflows to the steam generators from the feed line exceeded the volumetric outflow through the turbine bypass valves, and the secondary pressures increased, as shown in Figure 46. Shortly thereafter, low quality steam began exiting the turbine bypass valves; valve mass flow rates increased significantly, as shown in Figure 49, and secondary pressures stabilized. This higher mass flow rate enhanced primary-to-secondary heat transfer, further cooling the primary system, as shown in Figures 51 and 52. The increased cooling of the primary side caused the liquid inventory to shrink, as illustrated by the decrease in pressurizer liquid level shown in Figure 53, and increased the depressurization rate as shown in Figure 47.

At 269 s, the primary pressure had dropped below the high pressure injection (HPI) initiation setpoint, and cold HPI liquid flow to the cold legs was initiated, as shown in Figures 54 and 55. The introduction of the cold HPI fluid further increased the depressurization rate in the primary system, as shown in Figure 47. At 275 s, the primary pressure had dropped below the saturation temperature in the vessel upper head, and voiding of the upper head began. The primary depressurization rate decreased, due to the volumetric expansion of the steam generated in the upper head.

According to the scenario description, the reactor coolant pumps were tripped at 299 s, 30 s after the initiation of HPI. Realignment of the main feedwater flow to the emergency feedwater headers was coincident with the reactor coolant pump trip. When the realignment occurred, cold fluid which had been in the crossover lines was pushed into the steam generators, resulting in a momentary increase in the primary-to-secondary heat transfer rate, shown in Figure 50, and in a sharp local decrease in liquid temperature at the point of injection into the secondary system, shown in Figure 56. The increased primary-to-secondary heat transfer rate, coupled with the establishment of natural circulation in the primary system (see Figure 57), resulted in better cooling of the primary liquid as it passed through the steam generator, as shown in Figures 51 and 52. Also, as a result of injecting the cold liquid into the secondary, the secondary pressure decreased, as shown in Figure 46.

Table 14. Maximum sustainable overfeed transient sequence of events

Event	Time (s)
Turbine trip, reactor trip, turbine stop valves close, main feedwater pumps run back to 490 rad/s (4675 rpm); secondary pressure increases to turbine bypass and safety relief valve setpoints; feed train heater drains begin to close; pressurizer begins to drain.	0.0
Heater drains close.	5.0
Steam generator B secondary pressure drops below safety relief valve setpoint; valves close.	25.0
Steam generator A secondary pressure drops below safety relief valve setpoint; valves close.	28.0
Pressurizer liquid level drops below heater cutoff setpoint; heaters latch off.	35.0
Steam generator B secondary completely liquid-full; steam line begins to fill.	240.0
Steam generator A secondary completely liquid full; steam line begins to fill.	250.0
Primary pressure drops below high pressure injection setpoint; high pressure injection flow initiated.	269.0
Vessel upper head begins to void.	275.0
Reactor coolant pumps trip; feed flow realigns to EFW header; main feed valves close.	299.0
Steam generator B turbine bypass valves close.	341.0
Steam generator A turbine bypass valves close.	350.0
Void in steam line B drops below 20%; main feedwater pumps trip off.	417.0
Void in vessel upper head collapses.	434.0
Pressurizer begins to refill.	448.0
Primary system begins to repressurize.	524.0
Steam generator A secondary pressure reaches turbine bypass valve setpoint; valves open.	930.0
Primary pressure reaches power-operated relief valve opening setpoint and cycles around setpoint.	1054.0
Pressurizer becomes liquid-full.	1079.0
Steam generator B secondary pressure reaches turbine bypass valve setpoint; valves open.	1424.0
Transient terminated; system pressure stabilized at power-operated relief valve opening setpoint. Primary temperature slowly increasing.	1695.0

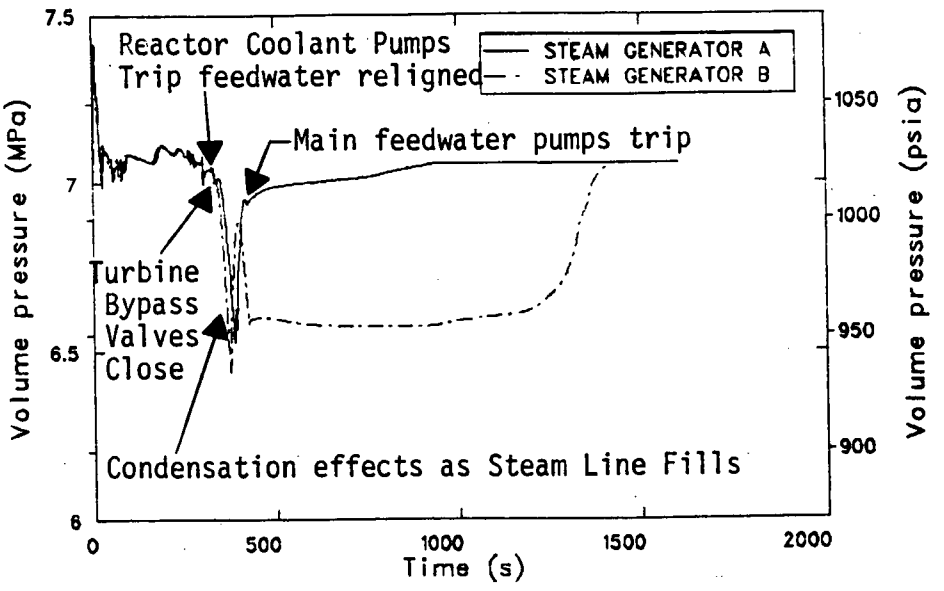

Figure 46. Maximum sustainable overfeed, SG secondary pressures.

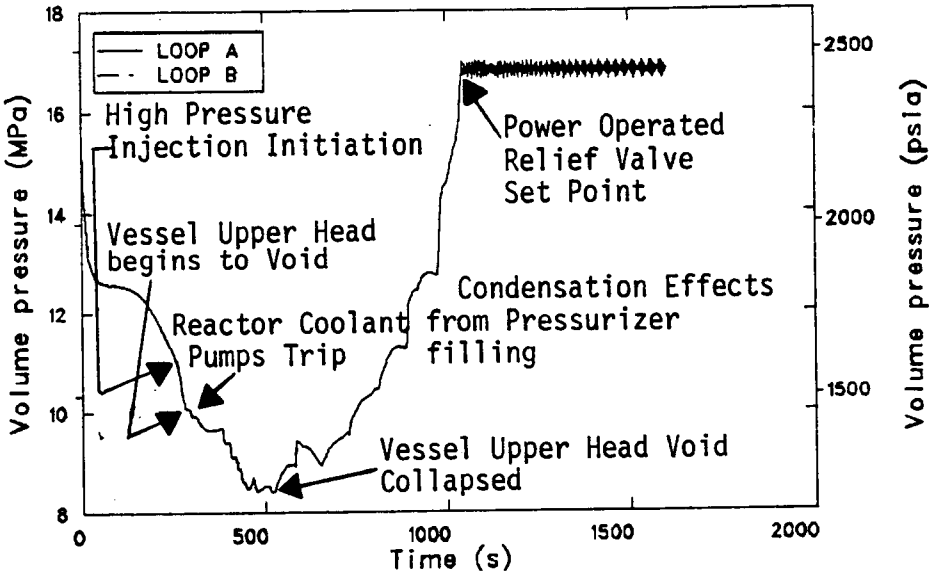

Figure 47. Maximum sustainable overfeed, hot leg pressures.

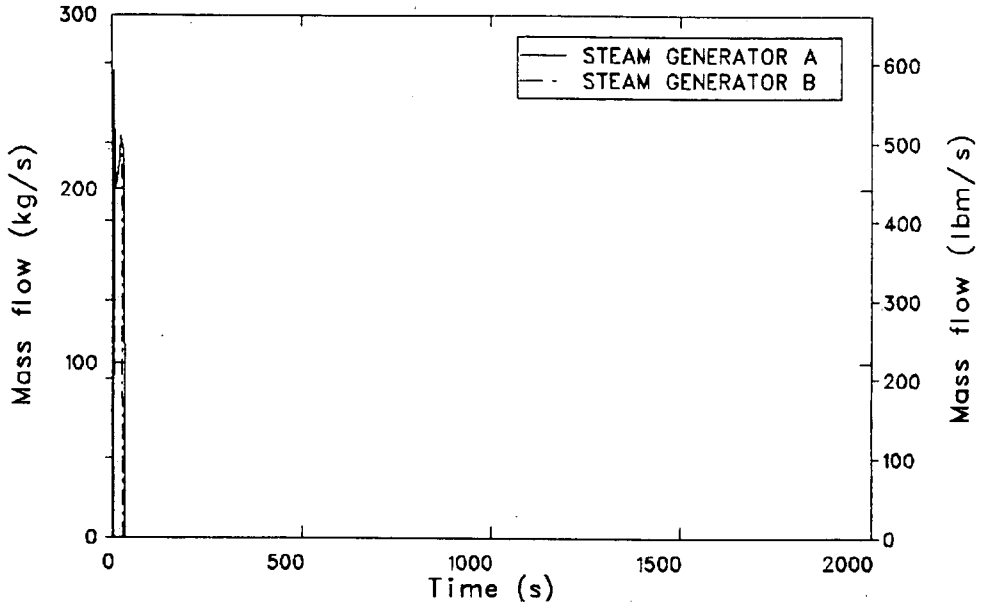

Figure 48. Maximum sustainable overfeed, SG safety relief valve flows.

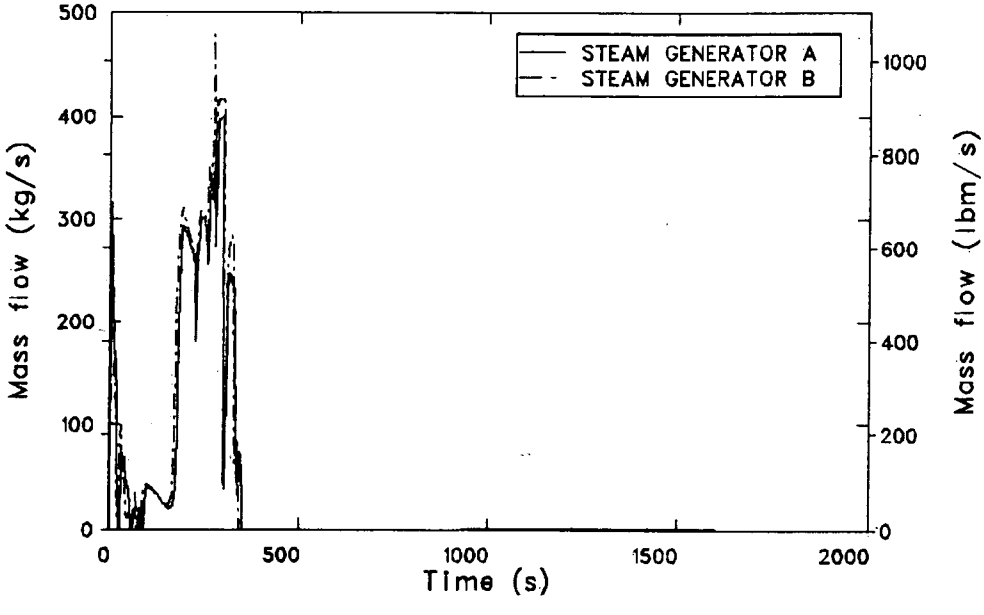

Figure 49. Maximum sustainable overfeed, turbine bypass flows.

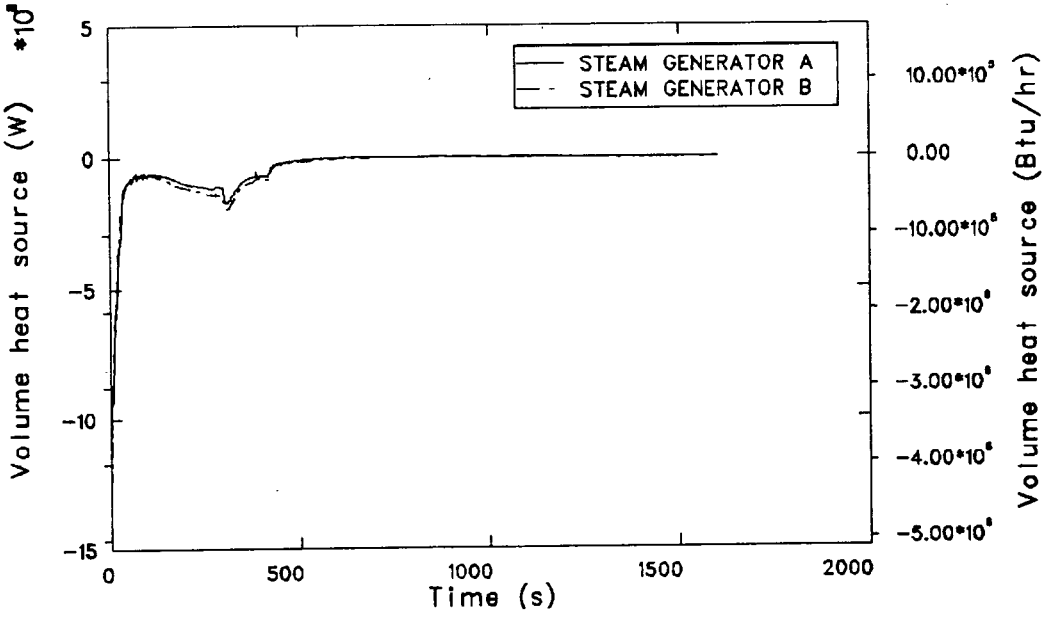

Figure 50. Maximum sustainable overfeed, SG heat removal rates.

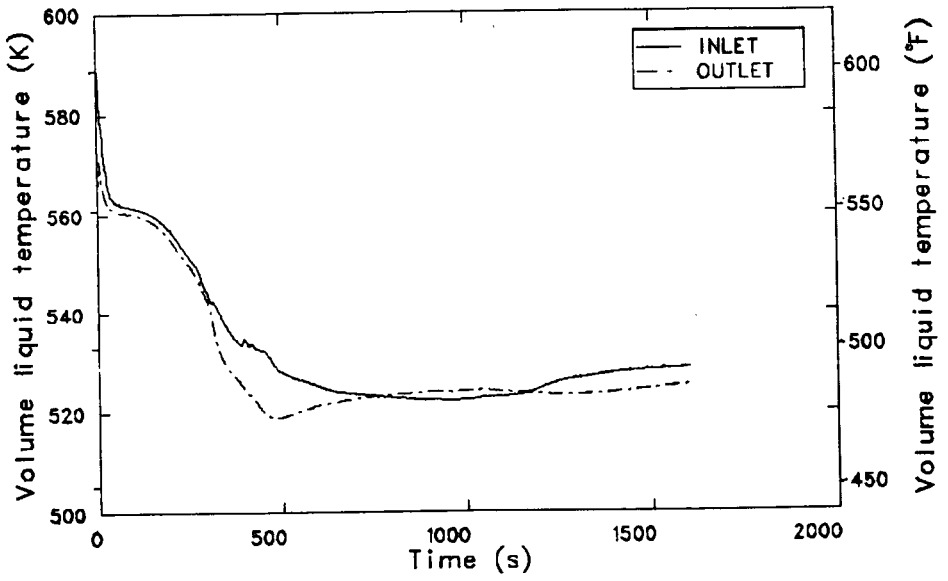

Figure 51. Maximum sustainable overfeed, SGA primary side inlet and outlet fluid temperatures.

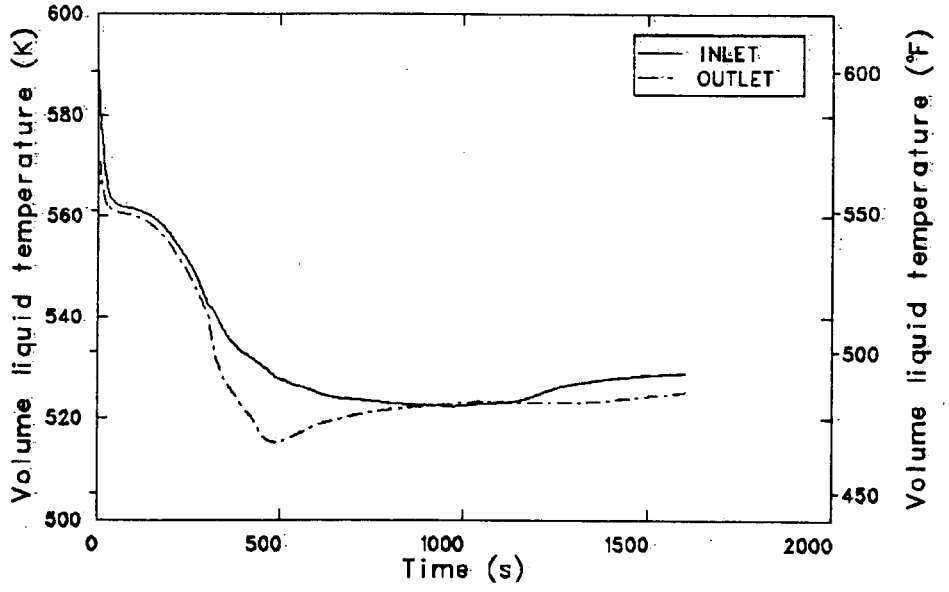

Figure 52. Maximum sustainable overfeed, SGB primary side inlet and outlet fluid temperatures.

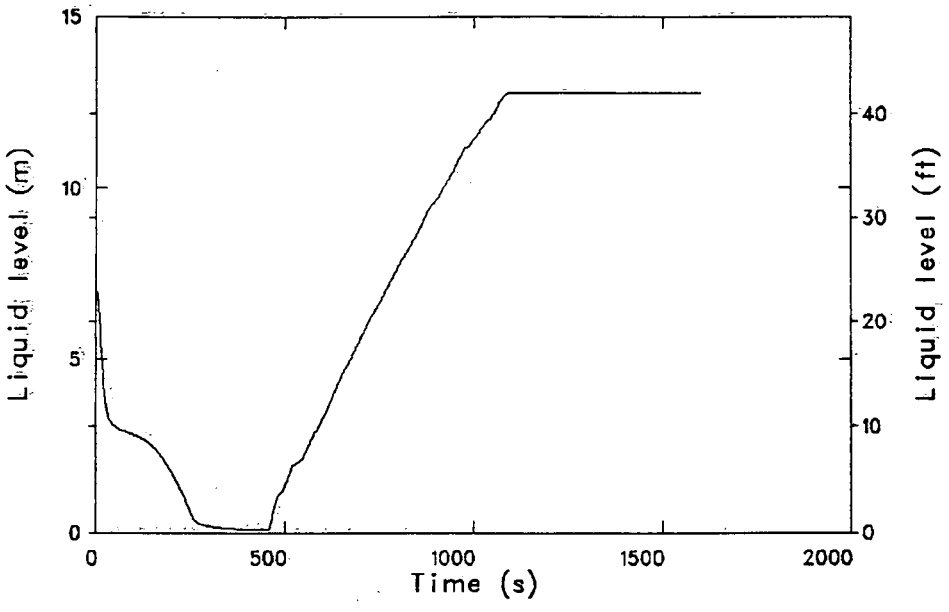

Figure 53. Maximum sustainable overfeed, pressurizer collapsed liquid level.

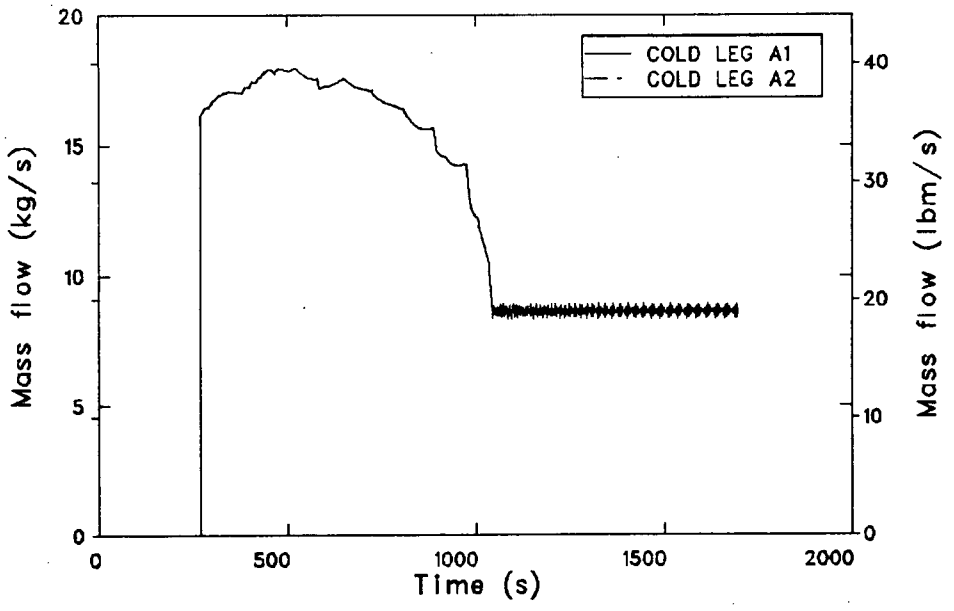

Figure 54. Maximum sustainable overfeed, loop A high pressure injection rates.

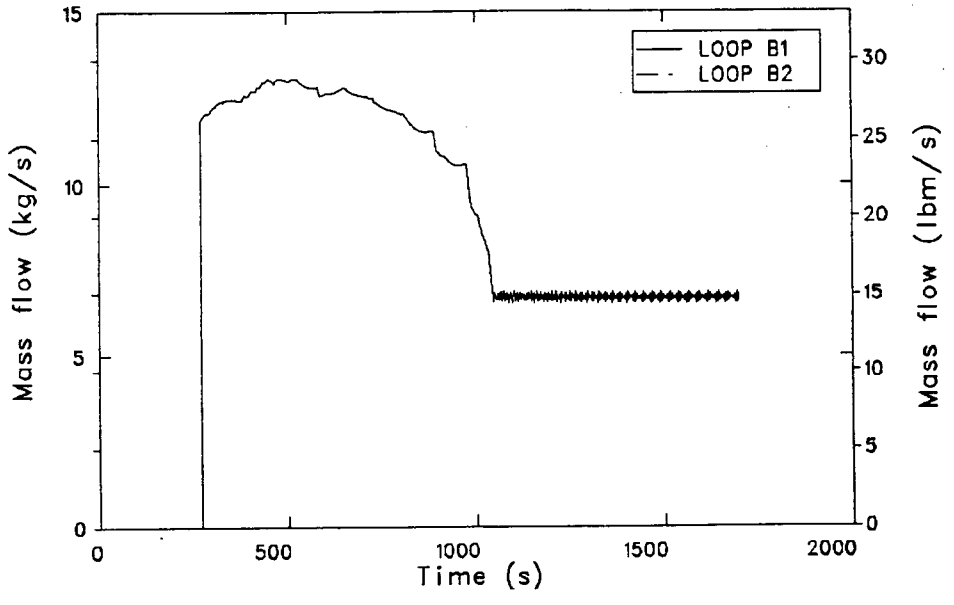

Figure 55. Maximum sustainable overfeed, loop B high pressure injection rates.

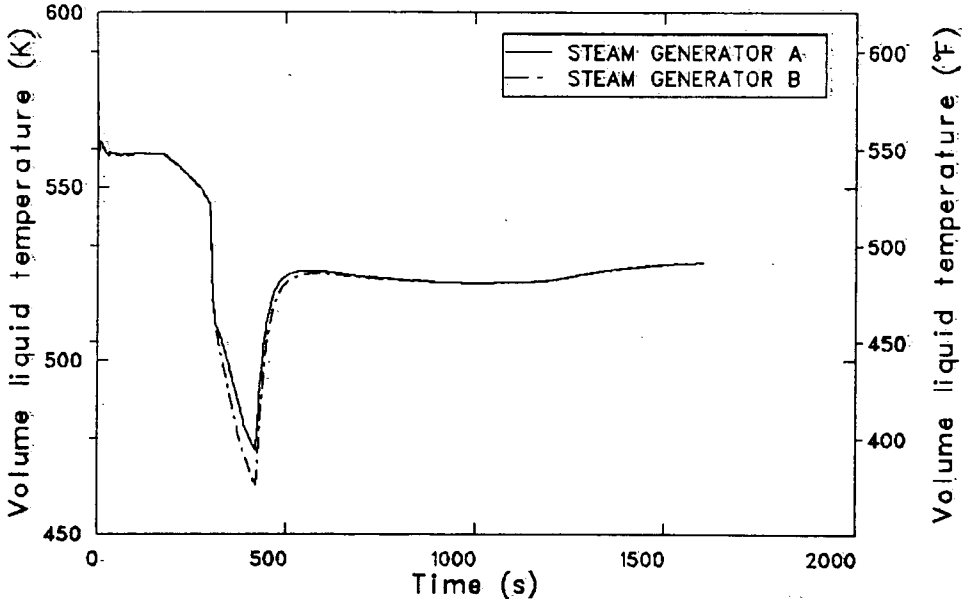

Figure 56. Maximum sustainable overfeed, liquid temperatures at top of SG boilers.

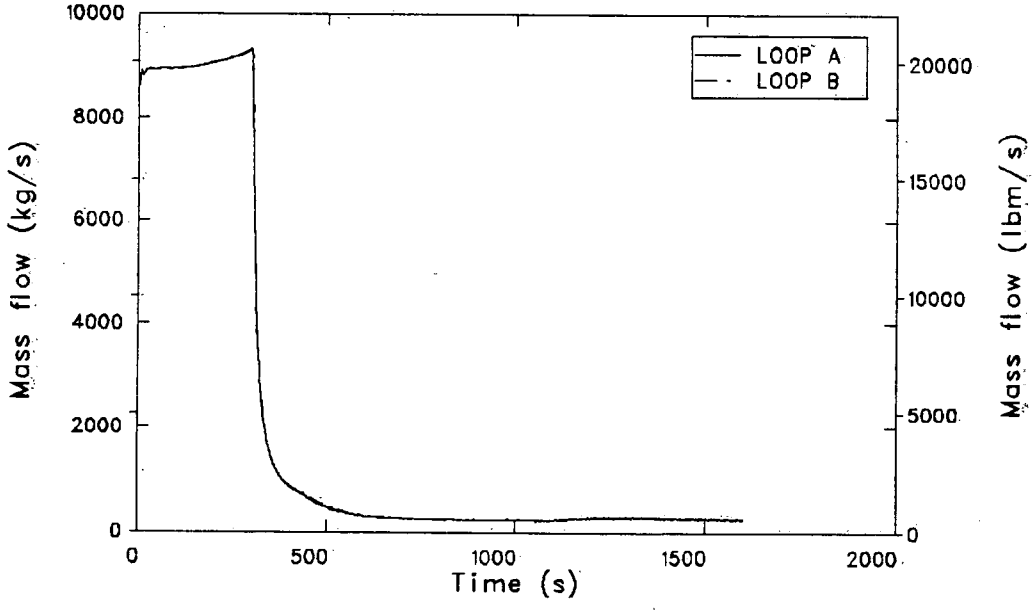

Figure 57. Maximum sustainable overfeed, hot leg mass flow rates.

At 341 and 350 s, the turbine bypass valves in steam generator B and A, respectively, had closed, because the secondary pressure had decreased below the valve setpoint. With the valves closed, the steam line rapidly filled with liquid due to the incoming feed flow. At 417 s, the B steam generator steam line had filled enough to trip the main feedwater pumps at low steam line void fraction, isolating the steam generators. The steam lines are represented by four volumes in the RELAP5 model. At the time of the main feedwater pump trip, the void fraction in the third volume of the B steam generator secondary was about 20%, while the void fraction in the A steam generator steam line was about 50%, as shown in Figures 58 and 59. Thermal expansion of the liquid in the secondary further decreased the void fraction in these volumes in the steam line volumes.

In the A steam generator steam line, the expansion of the liquid compressed the steam, which resulted in an increase in secondary pressure, as shown in Figure 46. The expansion of the liquid in the B steam generator steam line condensed the steam, which resulted in a slight pressure decrease, as shown in Figure 46. At 930 s, the pressure in the A steam generator reached the turbine bypass valve setpoint, the valves cracked open, and the pressure remained at the setpoint for the duration of the transient. It was not until 1100 s that the pressure in the B steam generator began to increase. At this time the third volume in the steam line had completely filled and the filling of the fourth volume began. Condensation ceased and the pressure increased due to steam compression. At 1424 s, the secondary pressure in the B steam generator reached the turbine bypass valve setpoint, the valves cracked open, and the pressure remained at the setpoint for the duration of the transient.

During the period of bubble formation in the RV upper head, liquid was forced out of that volume, due to the volumetric expansion of the steam generated in the upper head. At 380 s, the volumetric HPI inflow rate exceeded the volumetric shrinkage rate of the primary system liquid and the system pressure slightly increased. Also at this time, cooler liquid entered the RV upper head due to the pressure increase from HPI inflow, and the bubble size began to decrease, as shown in Figure 60. When the cooler liquid entered the upper head, the model overstated the condensation rate. The pressure in the upper head decreased locally, resulting in an increase in the mass flow rate into the upper head so that it exceeded the HPI flow rate and reversed the flow within the pressurizer surge line, as shown in Figure 61. The overpredicted condensation rate resulted in a reduction in primary system pressure, as shown in Figure 47. The incoming liquid in the upper head was heated to saturation, which stopped the condensation. Vapor generation was reestablished as shown in Figure 62. Liquid was then forced back out of the upper head and liquid flow reestablished into the pressurizer surge line, as shown in Figure 61. At 395 s, the vapor generation rate in the vessel upper head had decreased enough that liquid again flowed into the upper head and the cycle was repeated. This behavior was repeated six times before the bubble in the upper head collapsed completely.

After the bubble in the vessel upper head collapsed, all of the incoming HPI flow was directed toward the pressurizer surge line and the pressurizer. Due to the compression of the steam in the pressurizer, the primary system began to repressurize at 524 s. Again, because of the condensation and vapor generation effects as the pressurizer filled (see Figure 47), the pressure response was erratic. At 1054 s, the pressure had reached the power-operated relief valve operating setpoint (17.0 MPa, 2465 psia) and commenced cycling around that setpoint. At 1079 s, the pressurizer became liquid-full. At the termination of the calculation (1695 s), the primary system pressure was at the power-operated relief valve setpoint, and system temperatures were slowly increasing.

Conclusions

At the termination of the calculation, system behavior had stabilized so that extrapolation of the downcomer pressure, the temperature and vessel inside wall heat transfer coefficient was possible to 7200 s, as shown in Figures 63, 64, and 65. The lowest downcomer liquid temperature was 500 K (440°F). Subsequent to this minimum temperature, the maximum downcomer pressure was 17.0 MPa (2465 psia).

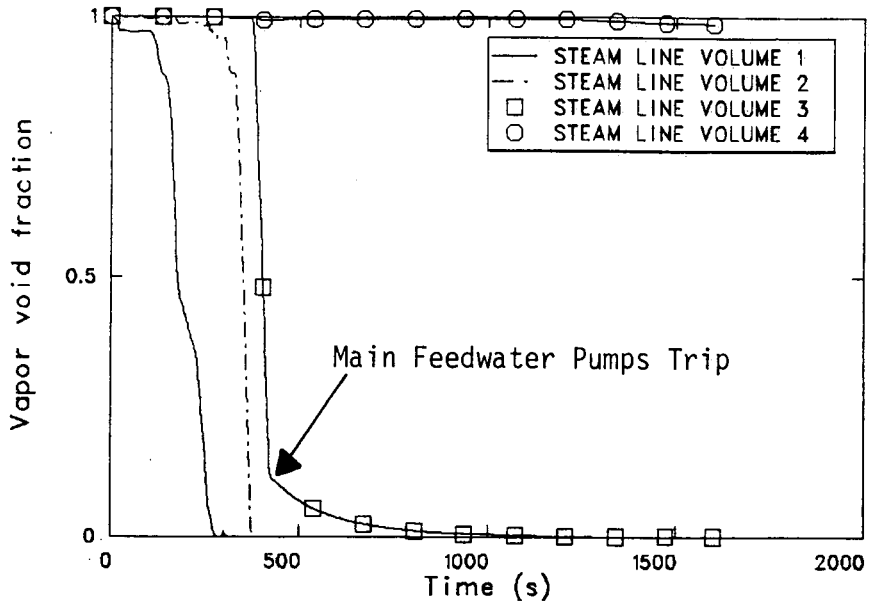

Figure 58. Maximum sustainable overfeed, steam line B void fractions.

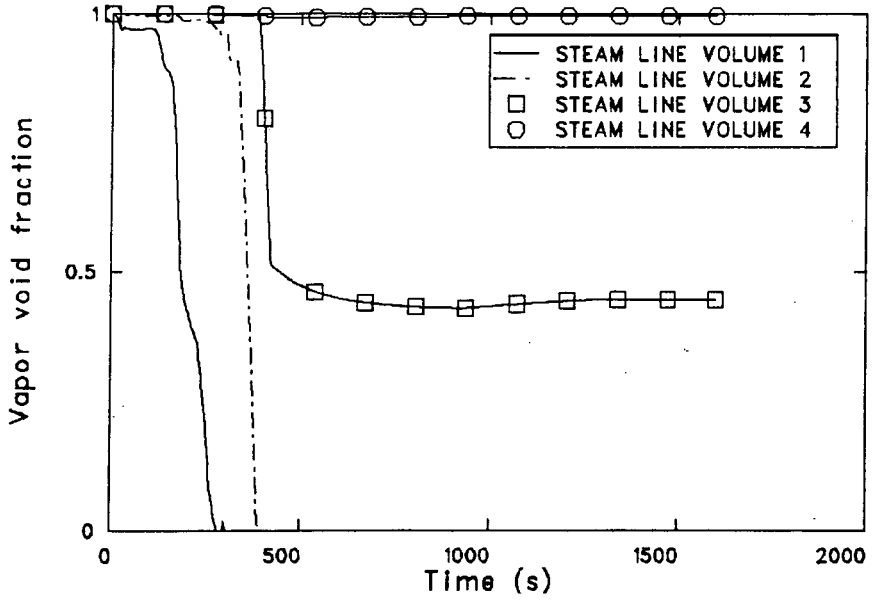

Figure 59. Maximum sustainable overfeed, steam line A void fractions.

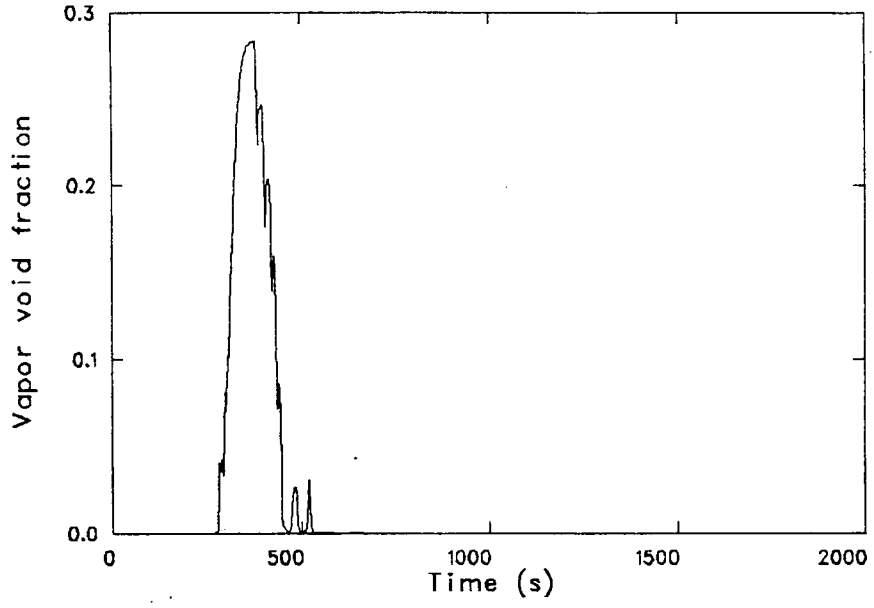

Figure 60. Maximum sustainable overfeed, RV upper head void fraction.

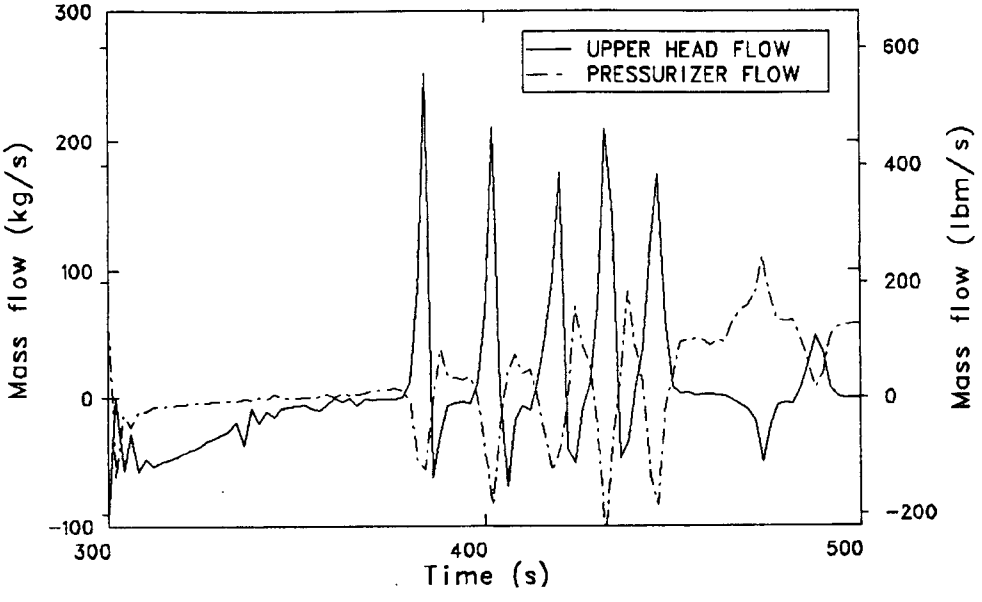

Figure 61. Maximum sustainable overfeed, mass flow rates into both RV upper head and pressurizer surge line.

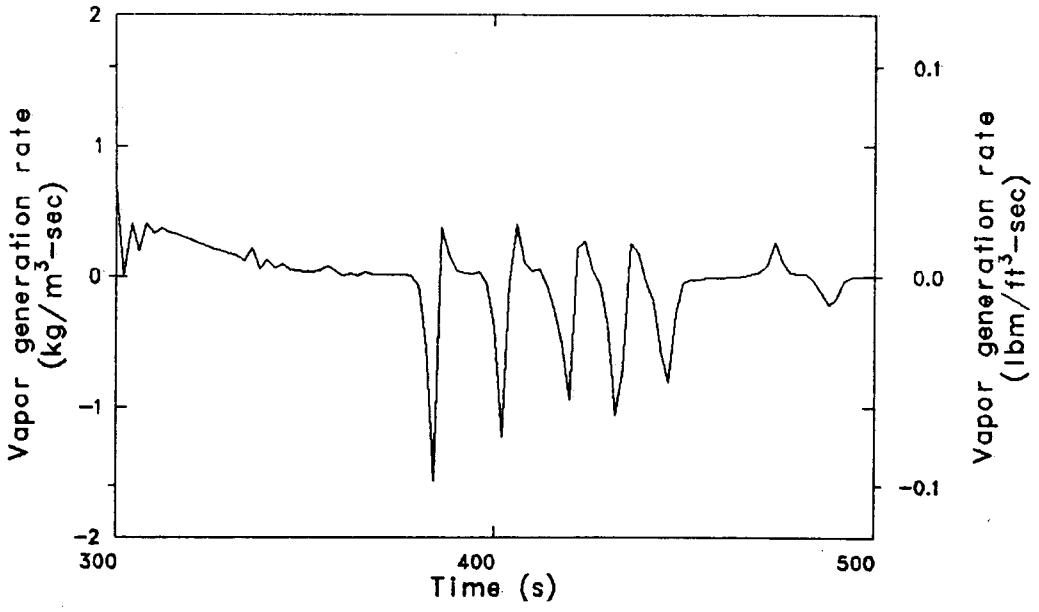

Figure 62. Maximum sustainable overfeed, vapor generation rate in RV upper head.

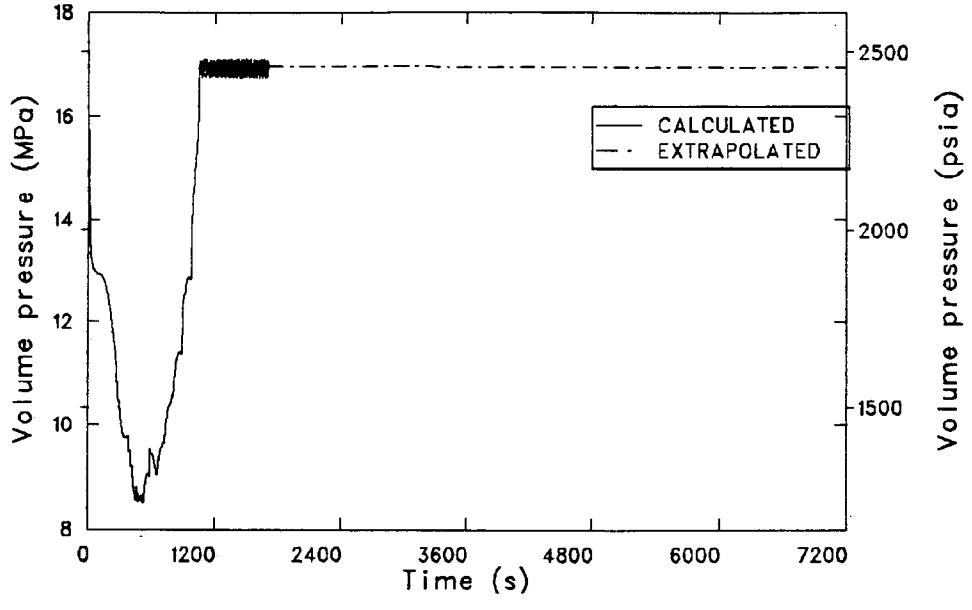

Figure 63. Maximum sustainable overfeed, RV downcomer fluid pressure.

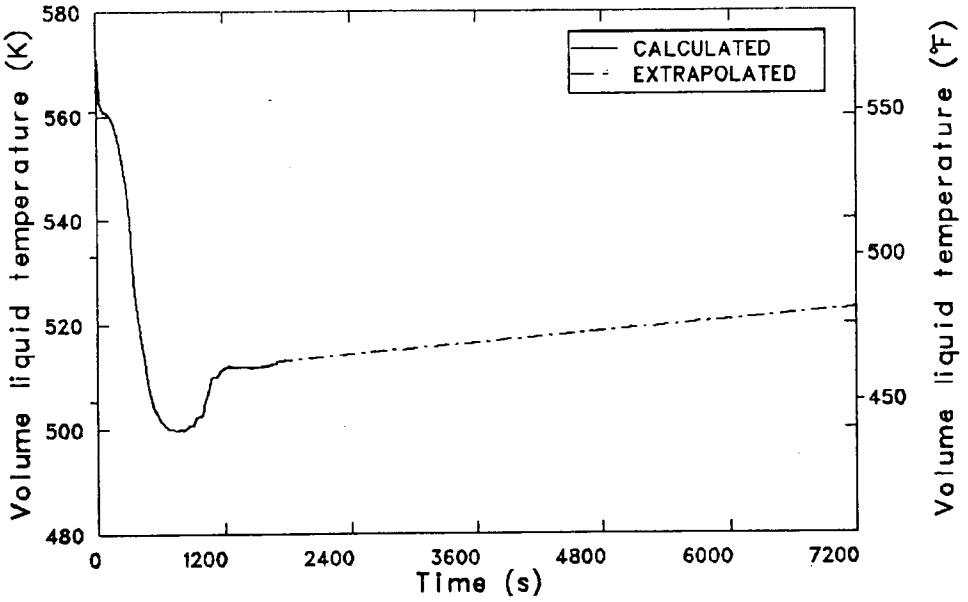

Figure 64. Maximum sustainable overfeed, RV downcomer fluid temperature.

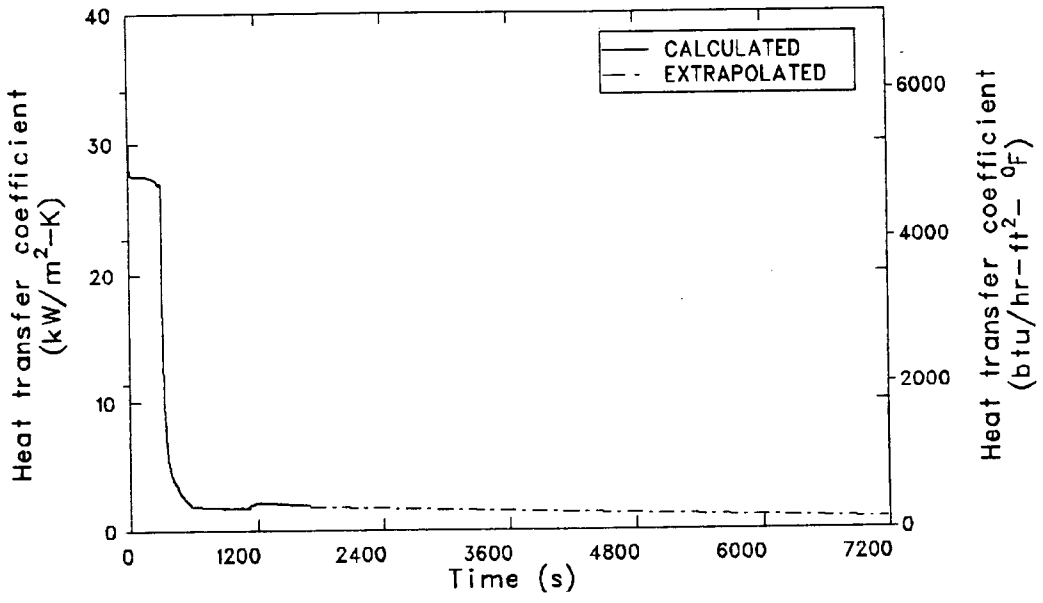

Figure 65. Maximum sustainable overfeed, heat transfer coefficient RV downcomer inside surface.

6. TURBINE BYPASS VALVE FAILURE AT REACTOR HOT STANDBY

The following subsections contain the transient scenario description, the modeling changes effected in order to perform this calculation, detailed analysis of the transient results, and conclusions drawn from the analysis.

Transient Scenario Description

A description of the transient scenario sequence appears in Table 15. This scenario was developed at Oak Ridge National Laboratory.

The transient was initiated by failing open all four turbine bypass valves with the plant at hot standby conditions. All automatic plant systems were assumed operative. Operator actions to trip off the reactor coolant pump 30 s after HPI initiation, and to close the turbine bypass valves after 10 min were modeled.

Model Changes

The RELAP5 model which was used to perform the turbine bypass valve failure at reactor hot standby calculation was described in Section 2. To perform this calculation, the basic model was modified, a RELAP5 hot standby steady state was run, and the transient calculation was initiated from the new steady state conditions. This section describes these modifications and the hot standby steady state conditions obtained.

The model nodalization used for the turbine bypass valve failure at reactor hot standby calculation was similar to that used in the other calculations described in this report, with the exception of the feed train model. The nodalization of the feed train is shown in Figures 66, 67 and 68.

The heater drain sources indicated in Figure 66, components 742, 744, 748 and 750, were deleted because the turbine is not rolled at hot standby, which means there was no steam being supplied to the feedwater heater secondaries. The deletion of these components also means that there were no heat sources for the various feedwater heater heat structures.

The components between components 752 and 763, were removed from the base model and are shown in Figure 66. This was done in order to reduce the size of the model and is justified because both feedwater pumps are controlled by the same control variable. Hence, no differences in operation between the two pumps components 754 and 760, were expected. Appropriate conditions of component 754 were doubled to account for this deletion, and the check valve, component 756/757, was removed.

The components linking the main feedwater headers with the auxiliary feedwater headers, as shown in Figures 67 and 68, were removed, as specified in the accident scenario. Additionally, the main feedwater valves, Components 770 (Figure 67) and 772 (Figure 68), were latched closed, according to hot standby operating procedure.

Operation of the startup valves, components 771 (Figure 67) and 773 (Figure 68), was controlled by the steam generator startup level errors, instead of by the plant Integrated Control System (ICS). This also represents hot standby operating procedure. The setpoint level in the steam generators was set at 0.91 m (36 inches) of indicated startup level.

The RELAP5 hot standby steady state calculation was performed with one hotwell and one condensate booster pump operating. One main feedwater pump was operating at 45% of rated speed. Manual feedwater control was assumed, with the operator controlling the startup valves based on the startup level. The level control portion of the integrated control system was deactivated. All steam exited the secondary system through the turbine bypass valves. Table 16 compares the hot standby initial conditions obtained in the RELAP5 steady state calculation to plant conditions as supplied by ORNL.

Transient Results

The results of the Turbine Bypass Valve Failure at Reactor Hot Standby calculation are presented in this section. A sequence of calculated events for this transient appears in Table 17. The transient was initiated by the opening of the four turbine bypass valves, which were modeled with a single valve component per steam generator. The calculation was run for two hours of transient time.

Table 15. Turbine bypass valve failure at reactor hot standby transient scenario

Initial Conditions:

1. Hot standby conditions:
   - T_{ave} = 551 K (532°F)
   - 14.82 MPa (2150 psia) at top of hot leg riser
   - 1 MFW pump running
   - 1 condensate booster pump running
   - 1 hotwell pump running.
2. Four RCPs are running.
3. Decay heat is 9 MW.
4. No steam is supplied to FW heaters.
5. FW is manually controlled (FW control portion of ICS deactivated).
6. FW is supplied through startup line (no flow through main line).

Sequence of Events:

1. All 4 TBVs suddenly fail full open.
2. MFW pump running at 45% speed; startup valve being controlled by steam generator level.
3. HPI initiates.
4. Operator trips all 4 RCPs, 30 s after HPI initiation.
5. Steam generator level setpoint changes to 6.1 m (240 in.)
6. FW system fails to realign with auxiliary header.
7. EFW system actuates.[a]
8. Core flood tanks inject.[a]
9. PORV, SRVs open and close at their setpoints.
10. LPI actuates [(not likely, as RCS pressure would have to fall to 1.34 MPa (195 psia)].[a]
11. Operator closes all TBV block valves at 10 min.
12. No further operator actions.

Failures:

1. Four TBVs fail open.
2. FW system fails to realign to auxiliary header.
3. Operator fails to throttle HPI and restart RCPs (procedural violation).

Basis for Transient Selection:

Determine possible system response differences as a result of transient initiation from hot standby, rather than full power, conditions (FW system alignment is different, most of ICS is deactivated, reactor temperatures/pressures are slightly different).

a. Event may or may not occur, depending on phenomena encountered.

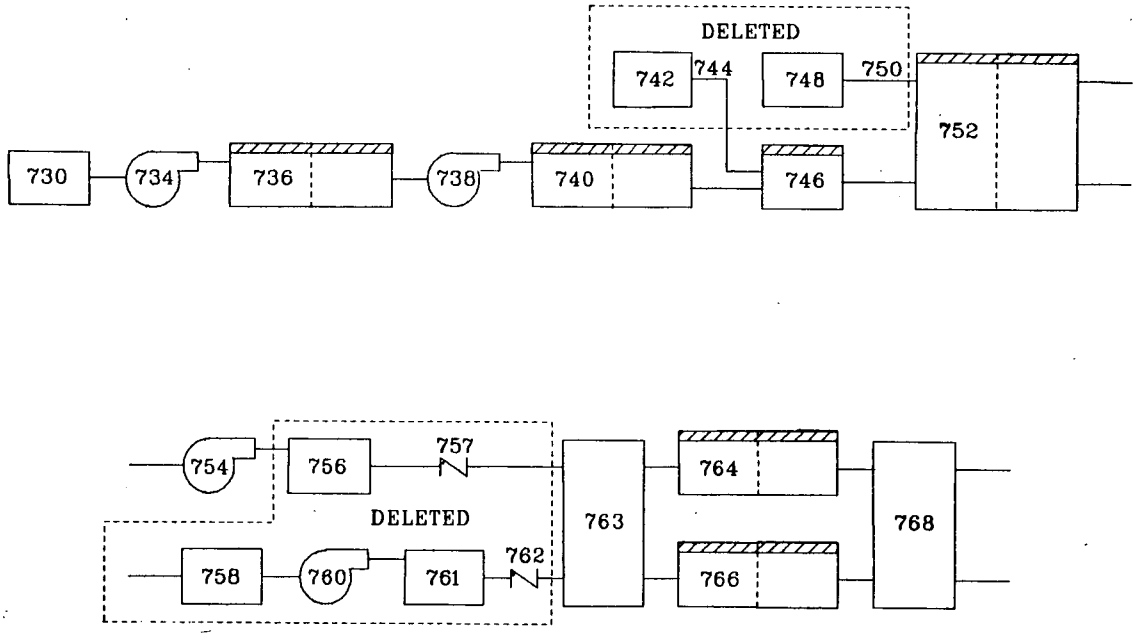

Figure 66. Hot standby model, main feedwater train.

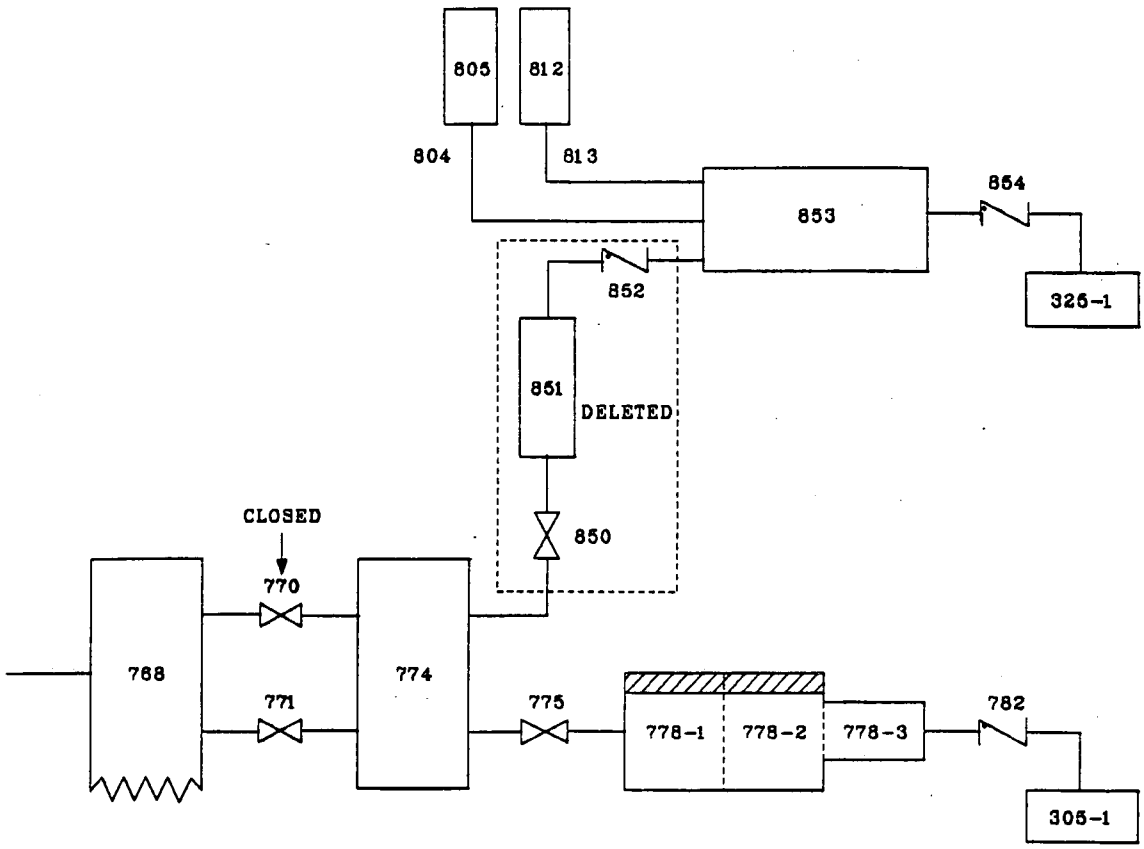

Figure 67. Hot standby model, SGA feedwater header.

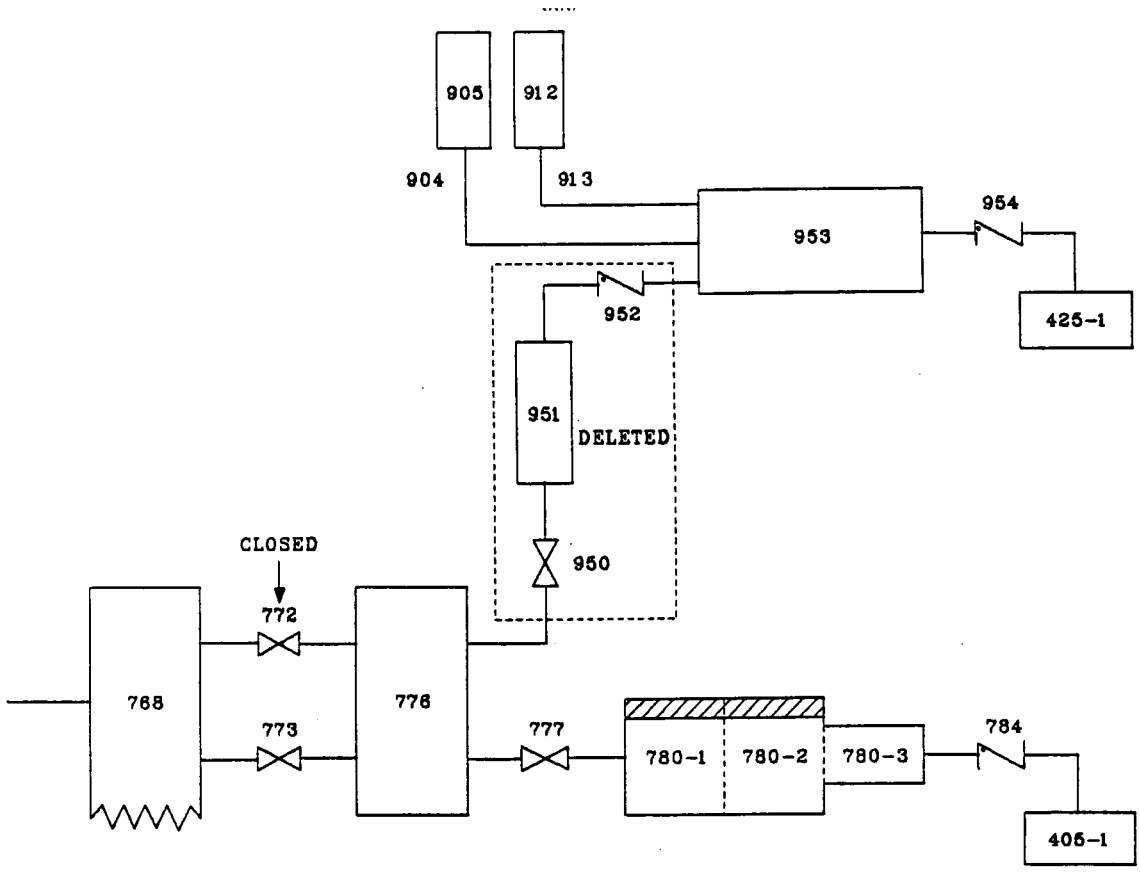

Figure 68. Hot standby model, SGB feedwater header.

Table 16. Hot standby steady state initial conditions

Parameter	Desired	RELAP5
Core power	9 MW	9 MW
RCP inlet temperature	551 K (532°F)	552 K (533.6°F)
Temperature rise across RCP	0.24 K (0.44°F)	0.23 K (0.41°F)
Hot leg pressure	14.82 MPa (2150 psia)	14.81 MPa (2148 psia)
Steam generator outlet pressure	6.21 MPa (900 psia)	6.21 MPa (900 psia)
Steam generator outlet temperature	551 K (532°F)	551 K (532°F)
Steam generator startup level	0.91 m (36 in.)	1.02 m (40 in.)
Feedwater temperature	305.4 K (90°F)	305.4 K (90°F)

Table 17. Turbine bypass valve failure at reactor hot standby transient sequence of events

Event	Time (s)
Turbine bypass valves fail open.	0.
MFW pump discharge pressure decreases to 5.27 MPa (765 psia.)	27.3
HPI begun.	125.1
RCPs trip; steam generator low level limit changes from 0.61 m (24 in.) to 6.1 m (240 in.).	155.1
EFW begun in steam generator A and steam generator B, due to change in low level setpoint.	
Condensate booster pump trips due to low suction pressure.	163.4
MFW pump trips on low suction pressure.	168.5
MFW train isolated from steam generators after feedwater flow decreases to zero.	228.6
Core flood tank injection begins.	383.5
Core flood tank injection ends.	391.6
Turbine bypass valves close.	600.0
Pressurizer liquid-solid.	900.0
PORV setpoint reached.	949.6
Steam generator operating level at 6.1 m (240 in.).	1010.2
Steam generator EFW sources trip off.	1030.4
Steam generator A operating level at 6.1 m (240 in.).	1070.5
Steam generator A EFW sources trip off.	1074.6
Primary loop B cold leg suction temperature exceeds loop B hot leg temperature.	1620.5
Primary loop A cold leg suction temperature exceeds loop A hot leg temperature.	1892.2
RV downcomer wall temperature reaches 403 K (265°F.)	4600.0
Transient terminated.	7200.0

The pressure responses of the two steam generator secondaries are shown in Figures 69 and 70. The steam generator secondaries behaved similarly, as expected. At transient initiation, the secondary system pressures decreased from 6.21 MPa (900 psia) to approximately 0.41 MPa (60 psia) in 1100 s. The pressures then increased to 0.48 MPa (70 psia) by 1300 s. Pressures gradually decreased for the remainder of the calculation and were 0.29 MPa (42 psia) and 0.32 MPa (47 psia) at the end of the transient in steam generators A and B, respectively.

The pressure response and feedwater flow rates of steam generator A (SGA) and B (SGB) secondaries for the first 600 s are shown in Figures 71 and 72. The oscillating pressure behavior calculated over the first 250 s was due to changing feedwater demands caused by the calculated startup (SU) level indication. The feedwater flow demand was controlled by the deviation of calculated SU level from the desired setpoint level of 0.91 m (3 ft). When the turbine bypass (TBP) valves opened, the indicated levels began decreasing, causing a corresponding increase in feedwater demand. The increased injection of 305 K (90°F) feedwater resulted in an accelerated depressurization in the steam generator secondaries, which continued until the setpoint SU levels were reestablished. The feedwater flow demand decreased as the SU levels became greater than the desired setpoint; the secondaries then pressurized, due to the heat transfer from the primary and choked flow at the TBP valves. These oscillations continued until the main feedwater source decreased to 0 kg/s at 190 s, the decrease being due to excessive depressurization of the main feedwater train.

The depressurization of the main feedwater train was caused by the loss of pressure in the steam generator secondaries, coupled with the operation of the SU valves and the tripping of the reactor coolant pumps (RCPs).

Operation of the SU valves in response to steam generator SU level demand resulted in depressurization of the main feedwater train. This depressurization was halted when the SU levels were recovered and the SU valves reclosed (closure of the SU valves enabled the repressurization of the feed train by the feed train pumps). This cyclic depressurization and repressurization in response to SU valve operation is shown in Figure 73, which depicts the feedwater train pressures upstream of the condensate booster pump and main feedwater pump and the SU valve area demands. Tripping of the RCPs at 155 s changed the steam generator low level setpoint from 0.91 m (3 ft) to 6.1 m (20 ft). The new low level setpoint resulted in a sustained maximum SU valve area demand, with a consequential large feedwater train depressurization. The condensate booster pump suction pressure trip setpoint of 0.21 MPa (30.7 psia) was reached 3 s later (158 s) and was sustained for the requisite 5 s, resulting in a trip of the condensate booster pump at 163 s. Loss of the condensate booster pump resulted in an accelerated depressurization of the feedwater train downstream of the pump, causing a main feedwater pump trip on low suction pressure at 168 s. The feedwater train was removed from the calculation at 228 s, when it was determined that additional feedwater could not be delivered to the secondaries.

The SGA and SGB pressures continued to steadily decrease over the next 1300 s, with three exceptions, as shown in Figures 74 and 75.

The first exception involved core flood tank injection into the reactor vessel downcomer from 383 to 392 s, which resulted in a temporary decrease in primary-to-secondary heat transfer, as the primary steam generator tube bundle flow reversed direction. This decrease in heat transfer resulted in a slight increase in the temperature-induced rate of depressurization of the secondaries.

The temperature of primary coolant in the hot legs and reactor vessel continued to increase during this period of flow reversal and accompanying stagnation. Consequently, the resumption of a positive-direction coolant flow resulted in a temporary increase of the primary-to-secondary heat transfer rate, due to the hotter primary coolant entering the tube bundle regions, and a subsequent temperature/pressure increase in the steam generator secondaries. This increase ended as a result of continued emergency feedwater (EFW) injection and resumption of the primary system cooldown.

The second delay in the secondary system depressurization occurred when the TBP valves were closed at 600 s. The resulting increase in pressure was overcome by the continued injection of EFW into the upper boiler section; however, the rate of secondary depressurization decreased due to the TBP valve closure.

The third delay in the secondary system depressurization occurred around 1620 s in SGA

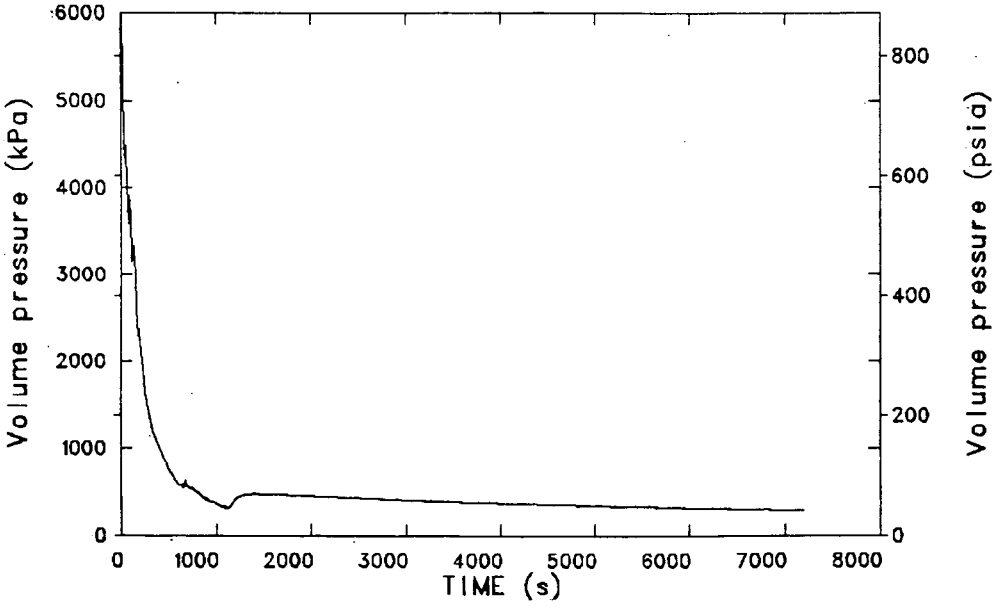

Figure 69. TBV failure at HSB, SGA secondary pressure.

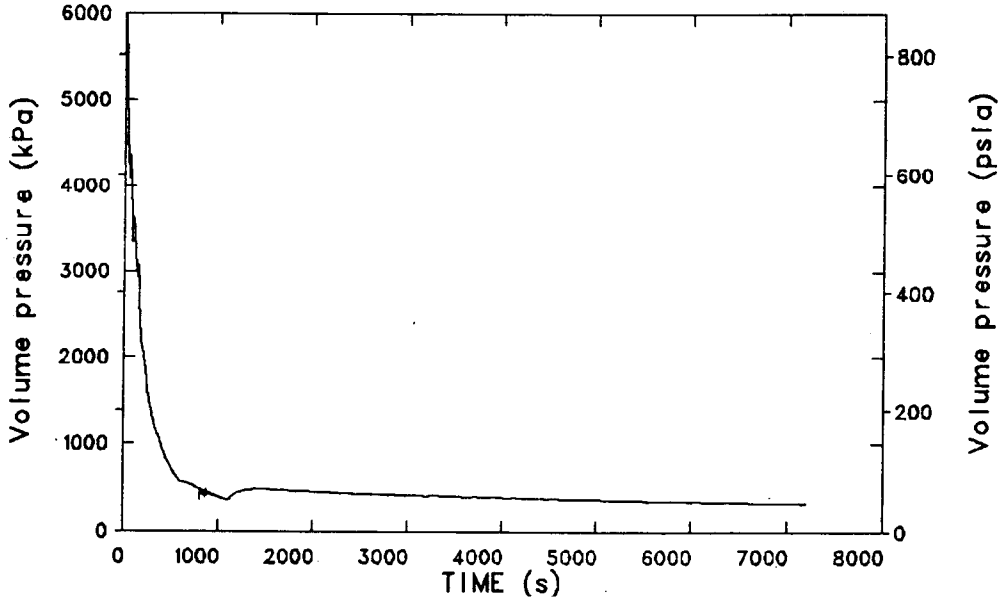

Figure 70. TBV failure at HSB, SGB secondary pressure.

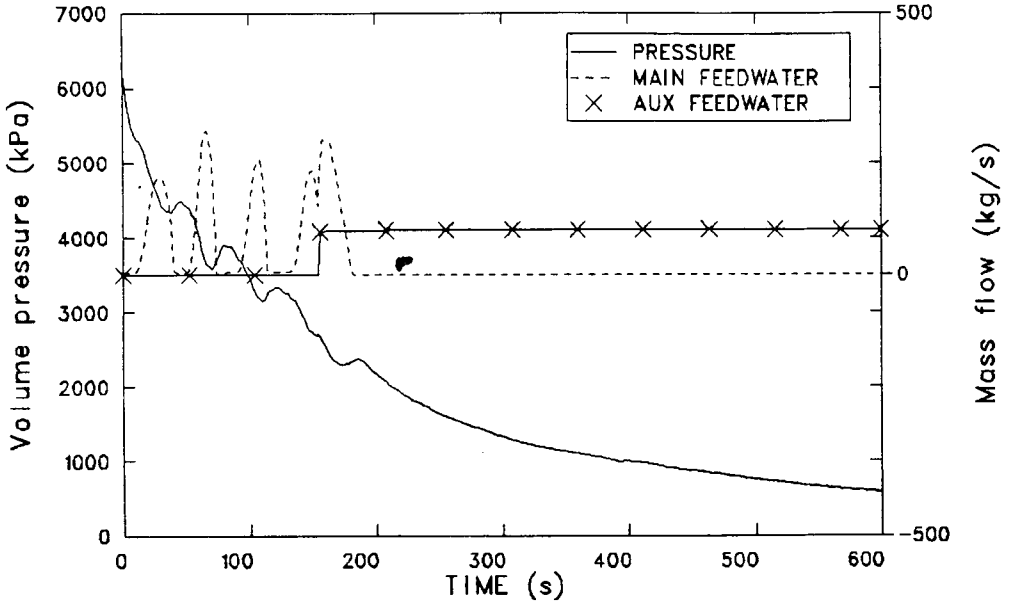

Figure 71. TBV failure at HSB, SGA secondary pressure and feedwater flow rates.

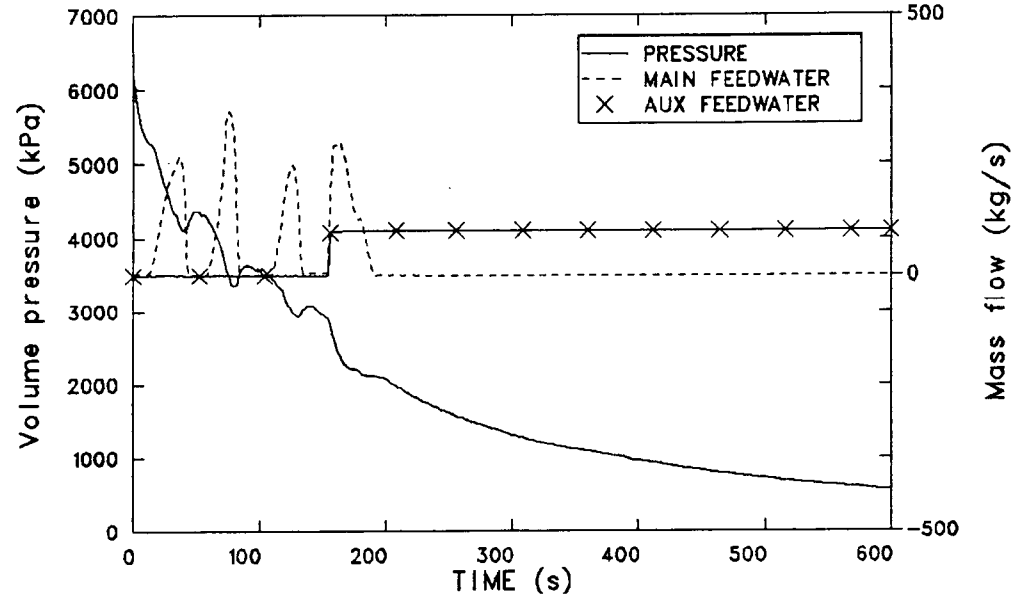

Figure 72. TBV failure at HSB, SGB secondary pressure and feedwater flow rates.

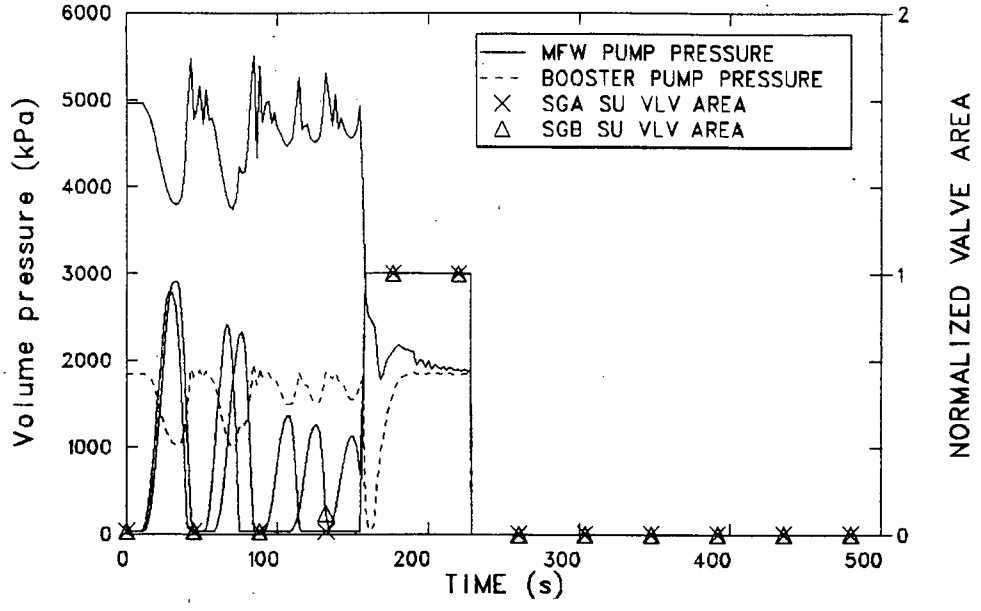

Figure 73. TBV failure at HSB, feed train pressures and normalized start-up valve areas.

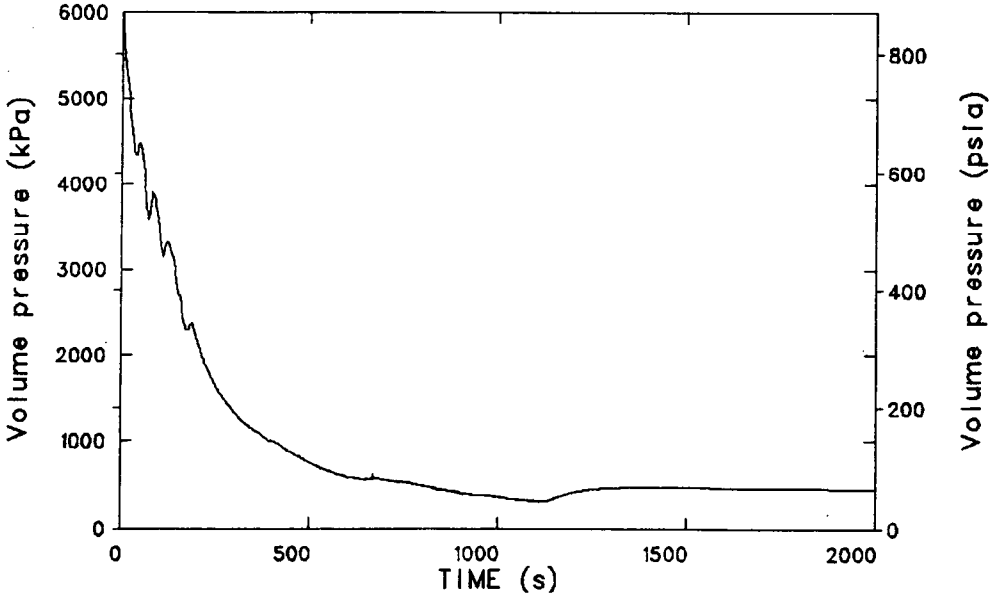

Figure 74. TBV failure at HSB, SGA secondary pressure 0-1500 s.

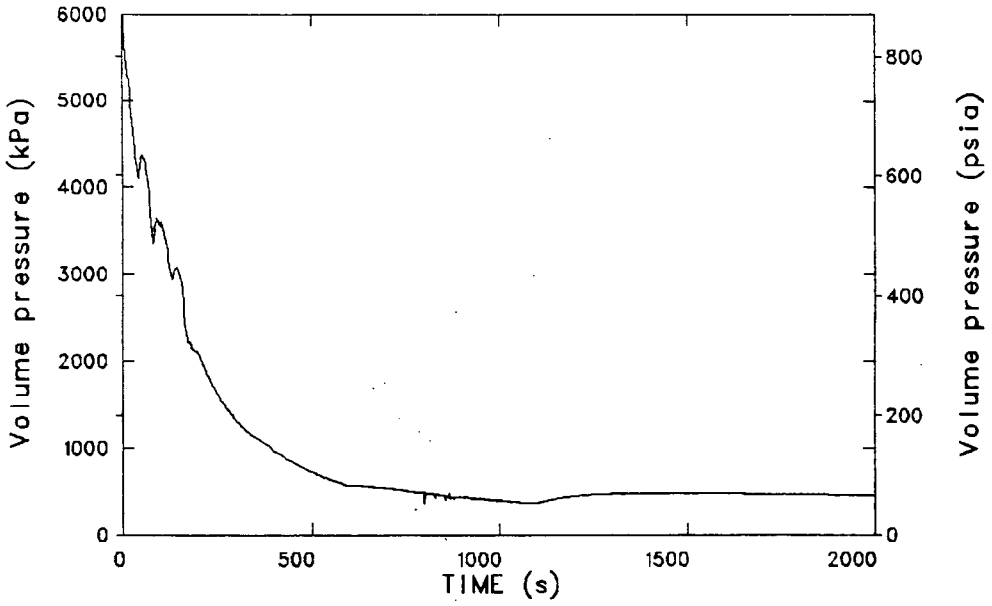

Figure 75. TBV failure at HSB, SGB secondary pressure 0-1500 s.

and 1580 s in SGB. The EFW sources to the steam generators were controlled, based upon the low level setpoint of 6.1 m (20 ft), so that EFW would be terminated when the calculated level exceeded the setpoint level. Termination of the EFW resulted in a partial loss of secondary heat removal capability. The primary-to-secondary heat transfer rate was still positive, and the secondaries began to heat up, which resulted in slight repressurizations. These increases in pressure ended as the secondary temperatures approached those on the primary side and consequently decreased the heat transfer rates to 0 MW at 120 s.

The temperature responses of the SGA and B SGB primary loops are shown in Figures 76 and 77, respectively. The same parameters are plotted in Figures 78 and 79, with an expanded time scale to better show detail at the beginning of the transient. The temperature responses of the two cold legs in a given coolant loop were identical, thus obviating a separate discussion of the calculated behavior in all four cold leg sections.

The temperatures in the hot and cold legs were essentially identical for the first 200 s of the transient. They began to diverge as the steam generator secondaries continued depressurizing and the primary-to-secondary heat transfer rates increased, due to emergency feedwater injection into the steam generator upper boiler sections. A reactor coolant pump trip at 155 s resulted in reduced primary loop flow, consequently decreasing the rate of cooldown in the hot legs and increasing the HPI-induced cooldown rate in the cold legs. The hot leg temperatures in both loops began increasing as the reactor vessel upper head began voiding, thereby contributing additional energy to the hot legs. The upper head was completely voided by 340 s, and the hot leg temperatures resumed their cooldown.

The hot leg temperature in the A loop increased at 383 s, due to core flood tank injection accompanied by temporary reverse flow. The core flood tank injection was initiated by an overprediction of condensation in the reactor vessel upper head, which resulted in a rapid depressurization of the primary system. The reverse flow caused a brief period of flow stagnation, with an accompanying increase in primary temperatures in the hot legs and vessel. The associated decrease in cold leg temperatures was due to the effects of high pressure injection, the loop flow stagnation, and core flood tank injection. The reactor vessel upper head refilled by about 392 s, and positive loop flow was reestablished. The effect of the core flood tank injection may be seen in the temperature response of the cold legs in relationship to their corresponding hot leg temperature responses. The loop A cold leg pump suction temperatures exceeded the hot leg temperature about 100 s after core flood tank injection. This time delay corresponds well with the loop transit time. A similar effect is seen in the B loop temperature response.

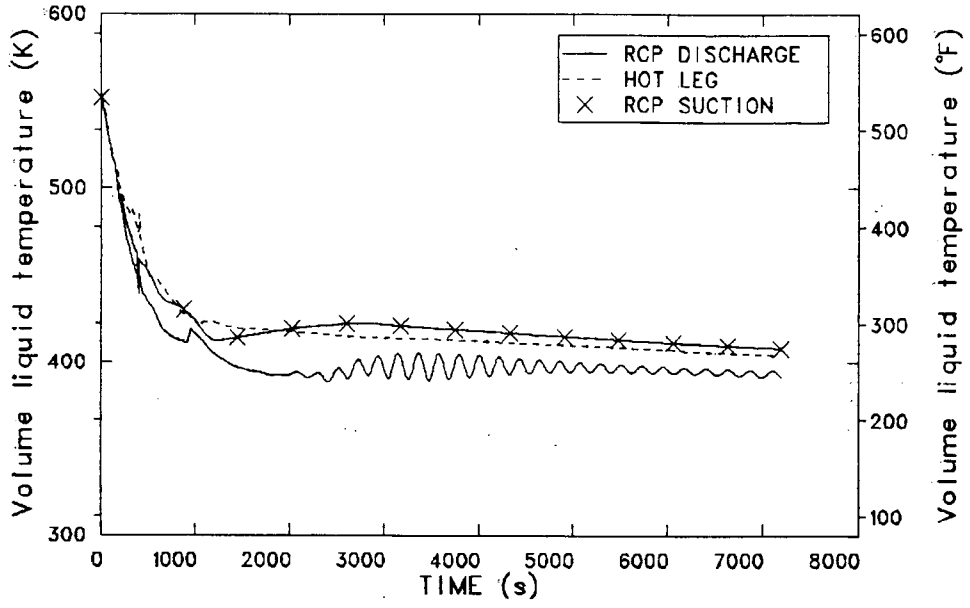

Figure 76. TBV failure at HSB, loop A fluid temperatures.

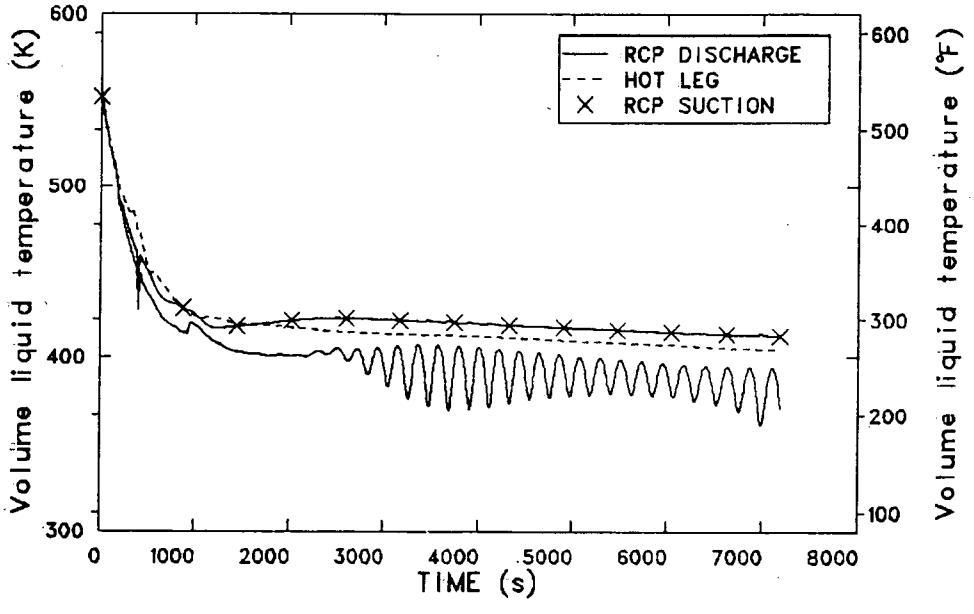

Figure 77. TBV failure at HSB, loop B fluid temperatures.

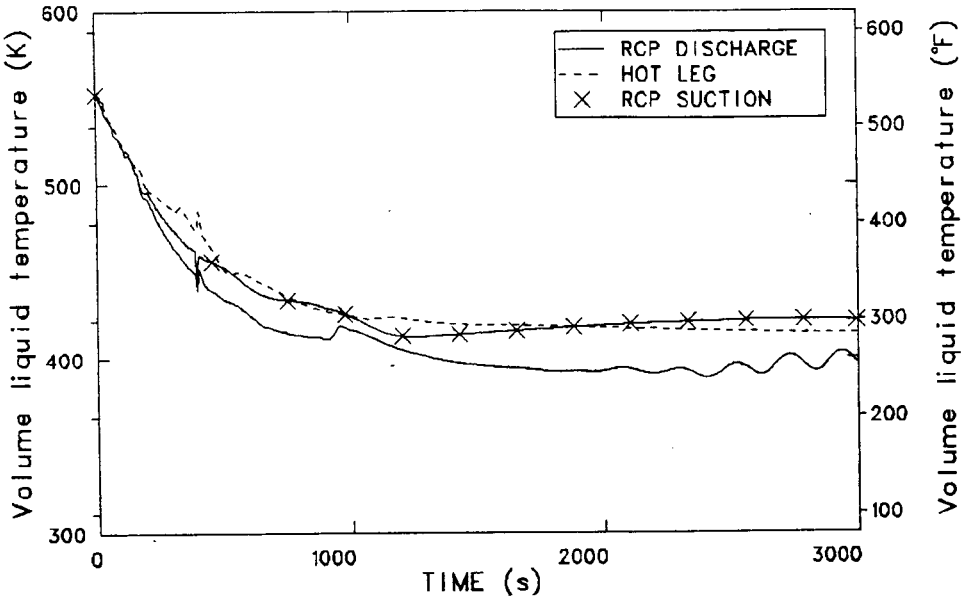

Figure 78. TBV failure at HSB, loop A fluid temperatures, 0-2500 s.

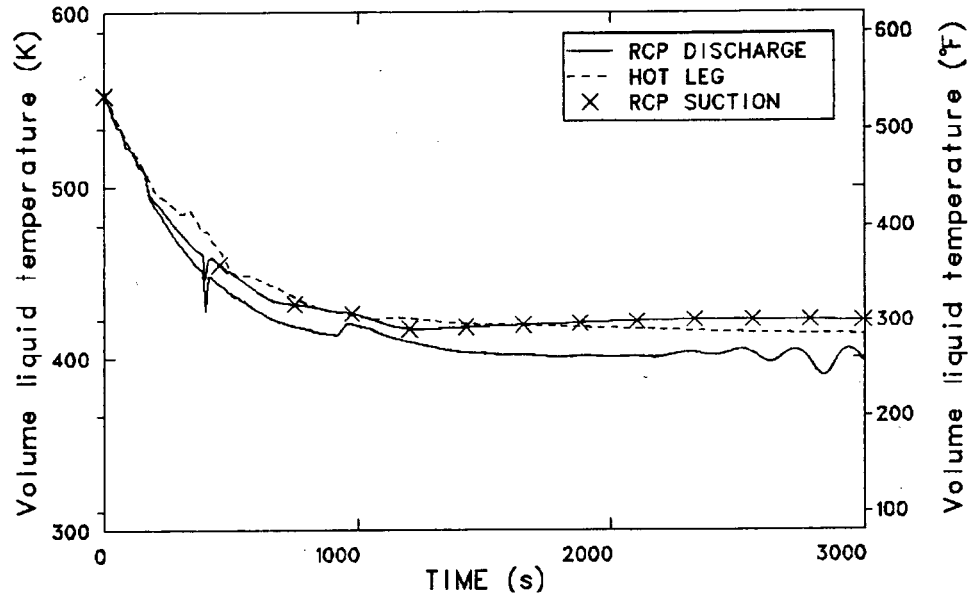

Figure 79. TBV failure at HSB, loop B fluid temperatures, 0-2500 s.

The hot leg and cold leg pump suction temperatures remained approximately the same between loops A and B, until about 1000 s. The temperatures diverged as the HPI and core flood tank inventory cooled the pump suction legs. The hot leg temperatures continued to decrease, and finally became cooler than their corresponding cold leg suction temperatures as the net heat transfer from primary to secondary became negative. The apparent heatup of the cold leg discharge sections occurred when the pressurizer became water-solid at 911 s. The resulting increase in primary pressure caused a reduction in HPI flow rates until, at 952 s, the primary pressure reached the PORV setpoint of 17.0 MPa (2465 psia). The HPI flow rates were essentially constant at 8.8 kg/s (19.51 lbm/s) in the A loop and 6.8 kg/s (15.1 lbm/s) in the B loop for the remainder of the calculation.

The reduction in HPI flow rate, in conjunction with the pump discharge leg temperature increases, resulted in two distinct temperature zones in the primary loops. The first zone consisted of the coolant that was not heated during the initial 200 s of the HPI flow rate reduction; the second zone consisted of the coolant that was heated during the same period. The effect of these two zones on the temperature response of the primary, in conjunction with the secondary-to-primary heat transfer, caused the oscillating temperature responses at the cold leg pump discharges. The mass flow rate in the vessel downcomer was driven by the density head of the inlet coolant. As the cooler zone of water entered the top of the downcomer, the density head increased, which resulted in an increased mass flow rate down the downcomer, and subsequently throughout the rest of the primary. The increased flow rate through the core resulted in a cooler core exit temperature.

The density of the warmer zone of water was responsible for the flow rate reduction through the primary. As this water entered the vessel downcomer, the density head decreased and caused a decrease in the loop flow rate. The decreased primary flow rate resulted in a greater temperature increase across the vessel. The temperature oscillations were damped out in the lower volumes of the two steam generators, which maintained primary-to-secondary heat transfer throughout the transient. However, the effect of constant HPI flow rate, coupled with the oscillating primary mass flow rate, continued to dominate the flow response of the primary for the remainder of the transient, as seen in Figures 80 and 81.

The effect of the HPI flow rate on the A and B loop temperature responses may be seen in Figure 82, which depicts the temperature responses of the A and B loop cold leg pump discharge volumes at the points of HPI injection. The larger temperature oscillations in B loop were due to the lower HPI injection flow rates. The HPI tended to damp out the A loop oscillations, but it was not of sufficient magnitude in the B loop to significantly affect the overall loop temperatures. The response of the B loop suggests that the B loop controlled the total primary temperature response; however, the net result is not significant, in that the temperatures did not vary markedly during this period.

The pressure response in the reactor vessel downcomer, at the location of the first circumferential weld below the cold legs, is shown in Figure 83, overlaid with an estimate of uncertainty due to sensitivities. The primary pressure decreased at the initiation of the transient as a result of the rapid depressurization of the steam generator secondaries, the initiation of HPI, and the tripping of the reactor coolant pumps. The first decrease in the rate of primary depressurization occurred at about 170 s, as the pressurizer emptied. Further changes in the rate of primary depressurization occurred at about 800 s, when the vessel upper head began to void. The depressurization at about 900 s was due to condensation effects in the vessel upper head. This depressurization ended when the core flood tank injection setpoint was reached and the upper head refilled. The combination of HPI and core flood tank injection resulted in the refilling of the pressurizer, with a corresponding increase in primary pressure from about 900 s until 911 s, at which time the uppermost pressurizer volume filled. By 952 s, the pressure in the pressurizer upper head increased from 6.5 MPa (943 psia) to 17.0 MPa (2465 psia). The PORV maintained primary pressure at this point and for the remainder of the transient.

The response of the reactor vessel heat transfer coefficient (HTC) in the vessel downcomer, at the same weld location, is shown in Figure 84. The HTC decreased from 29300 W/m^2-K (1.43 Btu/s-ft^2-°F) to 27000 W/m^2-K (1.32 Btu/s-ft^2-°F) by 155 s, when the reactor coolant pumps tripped. The subsequent reduction in vessel downcomer coolant velocity caused a significant reduction in the HTC to values around 1700 W/m^2-K (0.08 Btu/s-ft^2-°F) at 400 s. The depressurization caused by the upper head condensation and subsequent core flood tank

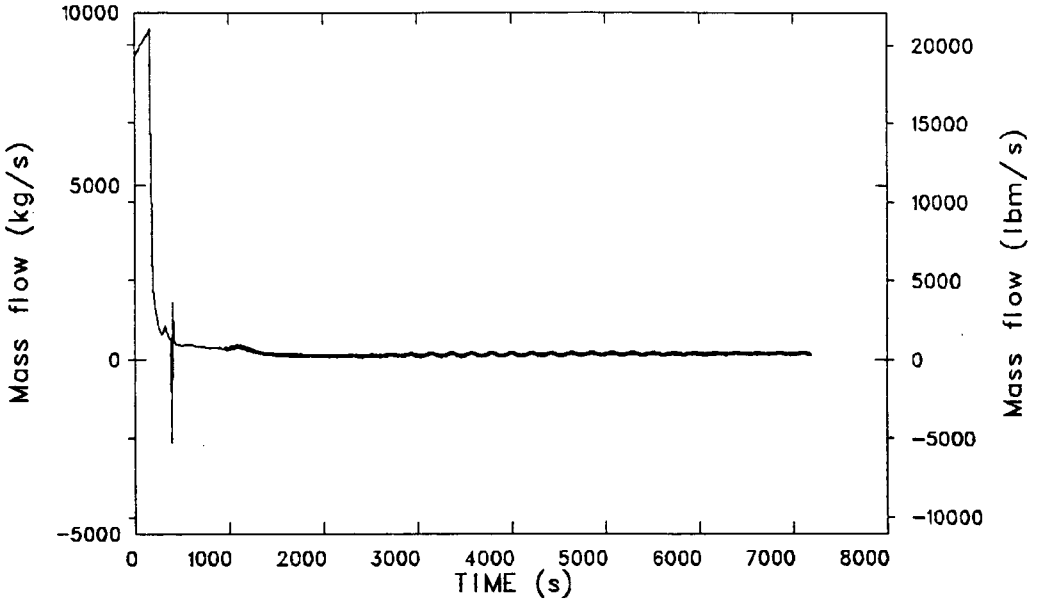

Figure 80. TBV failure at HSB, loop A hot leg mass flow rate.

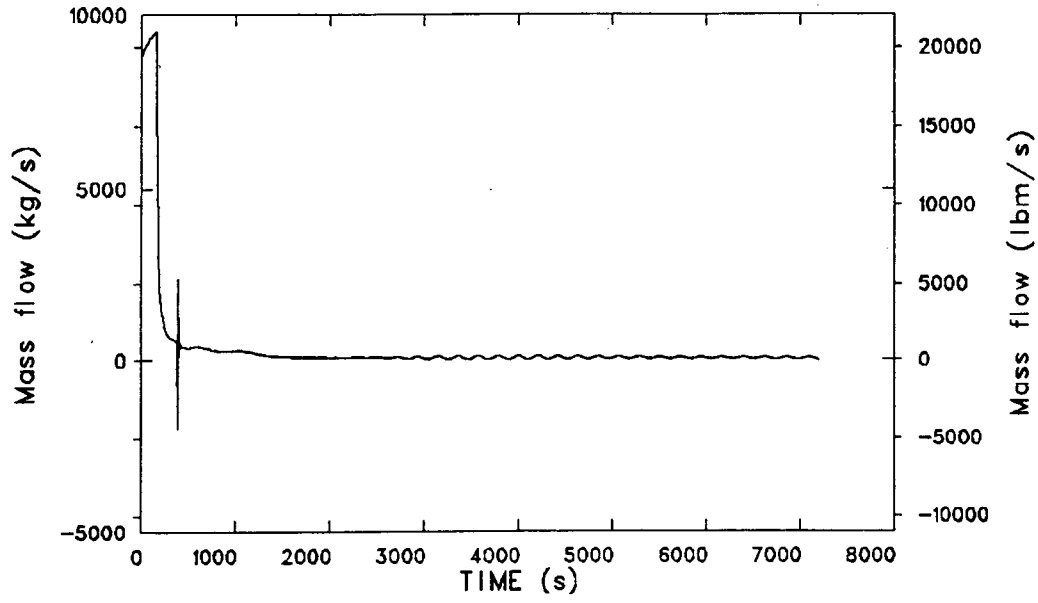

Figure 81. TBV failure at HSB, loop B hot leg mass flow rate.

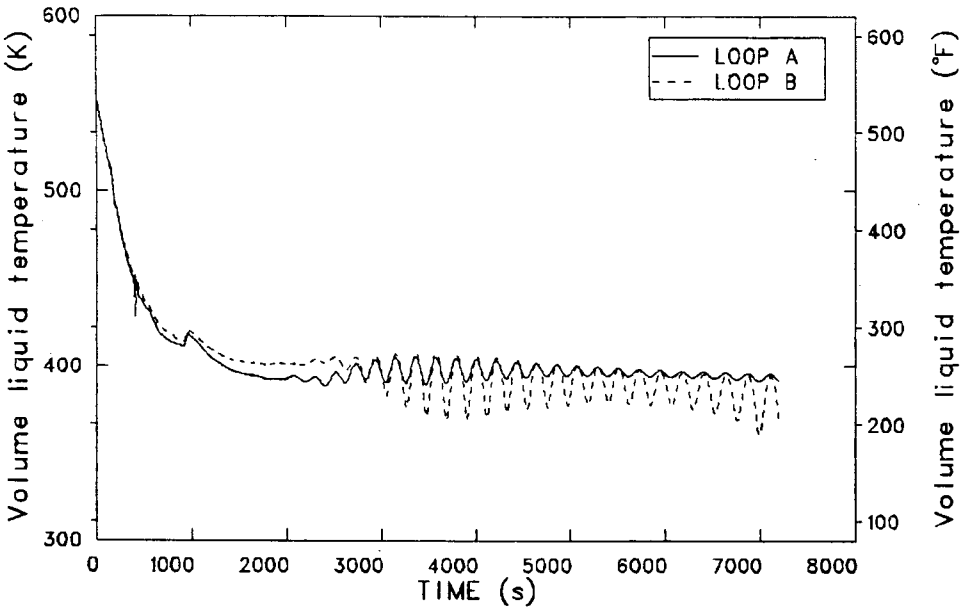

Figure 82. TBV failure at HSB, loop A and B cold leg discharge fluid temperatures.

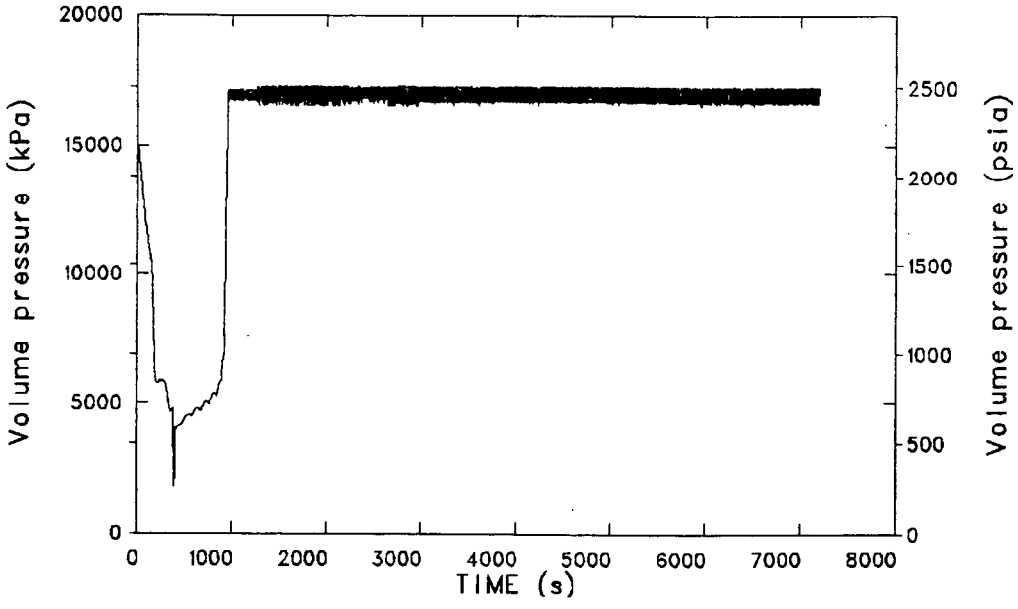

Figure 83. TBV failure at HSB, RV downcomer fluid discharge.

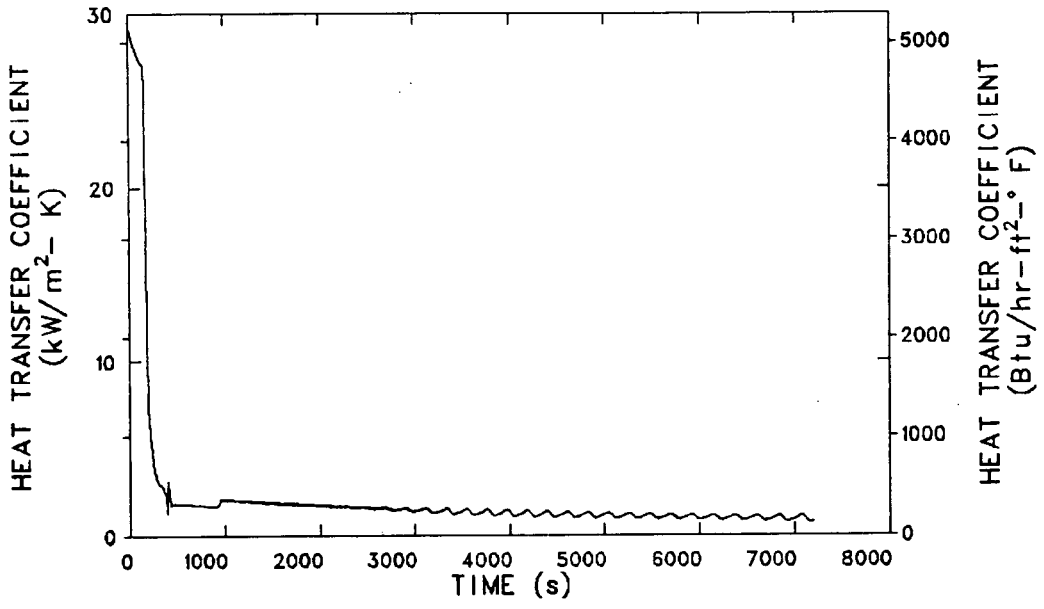

Figure 84. TBV failure at HSB, heat transfer coefficient of RV inside surface.

injection is seen at 400 s, when the HTC initially decreased due to flow stagnation and then increased as the core flood tank injection mixed with the coolant in the downcomer region. The minor increase in the HTC at 900 s was due to the reduction of HPI flow, induced by the high primary system pressure after the pressurizer filled. The reduction in HPI flow resulted in a reduction in the percentage of cold leg fluid contributed by the 283 K (50°F) HPI source. The oscillations beginning at about 2600 s are the result of the temperature and velocity oscillations previously discussed in this section. The decrease in downcomer temperature, which was coincident with the density-induced increase in velocity, resulted in an increase in the HTC.

Parameters or occurrences which may have significantly affected the calculation of the downcomer temperature are: (a) the operation of the startup valves, (b) the condensation depressurization that occurred at approximately 880 s, and (c) the calculation of the steam generator low level setpoints. The calculated downcomer temperature response, overlaid with an estimate of uncertainty due to sensitivities, is shown in Figure 85.

Operation of the feedwater startup valves determined the rate of feed train depressurization. A faster-than-normal valve closure rate would allow the feed train to repressurize in the early phases of the calculation. As described previously, closure of the startup valves prior to sufficient feed train depressurization during the early phase of the transient resulted in a recovery of the feed train pressure, due to continued operation of the condensate booster pump and the main feedwater pump. Had the startup valves remained open, the feed train would have depressurized to the condensate booster pump suction pressure trip setpoint. The amount of depressurization required was about 0.69 MPa (100 psi), which occurred during the first 20 s of the transient. Had the condensate booster pump tripped, the main feedwater pump would have tripped, due to the loss of pump suction pressure. Loss of the booster and main feedwater pumps would have reduced the amount of feedwater flow into the steam generators. The loss of the main feedwater source would have resulted in a low-level actuation of the emergency feedwater system, which would have resulted in feedwater injection into the upper tube bundle region. A sensitivity calculation was performed in order to determine the effect of initiating emergency feedwater injection at the start of the transient. The calculation was stopped when the pressurizer became liquid-filled, since no further system perturbations occurred after this event.

The difference in downcomer temperatures, between the sensitivity calculation and the transient calculation at 1100 s, was about 2 K (3.6°F). If the model startup valve opening time had been too fast, the feed train would still have depressurized at the time calculated in the transient. Due to the reactor coolant pump trip, the feed train depressurized to

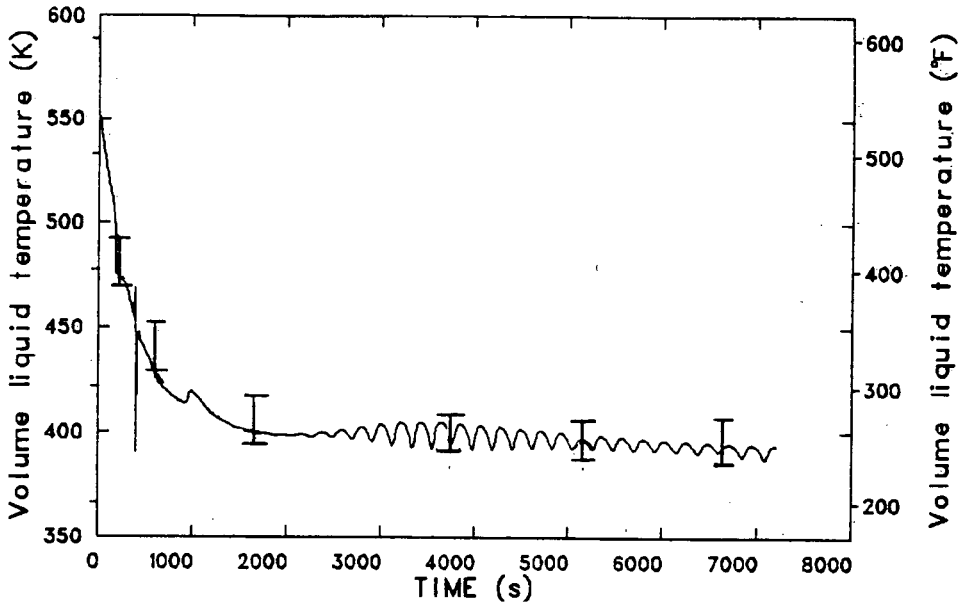

Figure 85. TBV failure at HSB, RV downcomer fluid temperature.

the condensate booster pump trip setpoint when the steam generator low level setpoint was changed from 0.91 m (3 ft) to 6.1 m (20 ft). The change in low level setpoint caused the startup valves to completely open, and remain open until feed train isolation. The rate of valve stem movement was modeled as requiring 2 s from full closure to full open. Had the valve been allowed to open instantaneously, the maximum difference in times for the full open condition would have been 2 s. The rate of pressure decrease in the feed train during this period of time was 0.48 MPa/s (70 psi/s); therefore, the time of the condensate booster pump trip would have been approximately 1 s earlier, which is insignificant.

It is concluded that early depressurization of the main feed train due to (a) a slower-than-normal startup valve response time, or (b) a faster-than-normal valve opening rate would not significantly affect the downcomer temperature response.

An overprediction of reactor vessel upper head condensation occurred at 880 s. The resulting depressurization of the primary system caused core flood tank injection of 305 K (90°F) water into the vessel downcomer. The initial effect of the depressurization was a brief period of reverse flow in the hot legs, in the pressurizer surge line and tank, and in the B loop cold legs. A flow rate decrease was also observed in the A loop cold legs. These flow perturbations resulted in a hot leg temperature increase of 11 K (20°F), due both to the essentially constant primary heat sources (9 MW reactor core decay heat and contributions from the primary coolant piping) and to the decreased heat transfer to the steam generator secondaries. The initiation of core flood tank injection resulted in a temperature decrease of 8 K (14°F). The net effect was a temporary temperature gain of 3 K (5°F), which was subsequently reversed by the steam generator secondaries. It is therefore concluded that the inadvertent depressurization of the primary system, and the subsequent core flood tank injection, did not significantly affect the final results.

The steam generator low-level conditions were calculated, using level tap locations corresponding to the startup level taps for the 0.91 m (3 ft) setpoint, and the operating taps for the 6.1 m (20 ft) setpoint. It was later determined that the startup taps are always used for determination of steam generator low-level conditions. Additionally, the startup level calculation incorporated a density head compensation term (which is not done in the prototype generators) and modeled the lower startup tap location upstream of the downcomer orifice plate. The combined effect of the above three model discrepancies was a 300 s delay in tripping off the emergency feedwater sources. This corresponds to an additional 10,200 kg (22,500 lbm) of liquid inventory in each steam generator. The excess heat transfer capability resulted in an estimated 15 K (27.5°F) underprediction of the final vessel downcomer temperature.

Conclusions

The calculation was carried out to 2 h of transient time, the entire period of interest for pressurized thermal shock. The minimum calculated reactor vessel downcomer fluid temperature was 387 K (237°F) near the end of the transient. The maximum calculated reactor vessel downcomer pressure was 16.99 MPa (2465 psia), the opening setpoint pressure for the power-operated relief valve.

The uncertainty in the calculated downcomer fluid temperature, due to startup valve operation, code-calculated condensation effects, and low-level limit determination method, was assessed. The uncertainty was found to be minor, with the conclusion that the calculated temperature represents the lower temperature limit of the uncertainty band.

7. PRESSURIZER SURGE LINE SMALL BREAK TRANSIENT

The following subsections contain the transient scenario description for the pressurizer surge line small break transient, modeling changes effected in order to perform this calculation, detailed analysis of the transient results, and conclusions drawn from the analysis.

Transient Scenario Description

A description of the scenario analyzed is presented in Table 18. This scenario was developed at Oak Ridge National Laboratory. The transient was initiated by a 0.0508-m (2-in.) diameter break in the horizontal section of the pressurizer surge line, with the reactor at full power conditions. Operator action was assumed to trip off power to the reactor coolant pumps (RCPs) 30 s after initiation of high pressure injection (HPI). This scenario was similar to that of the hot leg small break transient presented in Section 3, except that the break was larger and had been relocated from the PORV to the surge line. Operator action to trip RCPs was assumed.

Model Changes

The thermal-hydraulic model used for this transient was the same as that described in Section 2, with one exception. The transient description specified that the break should be midway between the hot leg riser and the pressurizer. Therefore, pipe Component 600 (see Figure 3), which represented the pressurizer surge line, was split and the break was inserted between the two sections. The break had an area of 0.00203 m^2 (0.02182 ft^2), which corresponds to a diameter of 0.0508 m (0.167 ft).

The transient was initiated from normal steady state conditions with the core at full power. Reactor power was set to trip off when the primary system pressure dropped below the pressure determined by the following relationship:

$$P_{TRIP} = 13.26\ T_{HOT} - 5989$$

where

P_{TRIP} =pressure at which scram occurs, psig, and

T_{HOT} =hot leg temperature, loop A, °F.

This scram relationship was obtained from the Oconee-1 FSAR and, on cooldown transients, was typically encountered before the low pressure scram setpoint was reached. After scram, the decay heat was assumed to be at the ANS standard rate. The reactor coolant pumps were set to run at a constant speed of 1226 rpm, until they were tripped 30 s after HPI began.

The secondary system was controlled as follows:

1. Steam flow control valves were set to close on reactor scram (to simulate closing of turbine stop valves).

2. Heater drains into feedwater system were set to ramp closed within 5 s after reactor scram.

3. ICS was allowed to control feedwater to both steam generators throughout transient.

4. Feedflow was diverted from the main feedline into the emergency feedwater header when the reactor coolant pumps (RCP) tripped.

5. At the time of RCP trip, the low level limit in the steam generators changed from 0.61 m (2.0 ft) to 6.10 m (20.0 ft).

6. Minimum speed of the main feedwater pumps, prior to pump trip, was set to 4270 rpm.

7. Hotwell and booster pumps were set to run at constant speeds of 1180 rpm and 3581 rpm, respectively.

Transient Results

This section chronologically describes the events, and their causes, which occurred during the transient calculation. A sequence of calculated events is also presented in Table 19. The calculation covered 6200 s of transient time. The responses of both steam generators were essentially the same throughout the transient; therefore, any reference to the steam generators will apply equally to both.

Table 18. Pressurizer surge line break transient scenario

Initial Conditions:

1. Reactor at full power.
2. Temperatures/pressures are nominal.
3. PZR spray and heaters operate as designed.
4. Decay heat is ANS standard.

Sequence of Events:

1. 0.167-m (2-in.) diameter hole opens midway between pressurizer and the riser portion of the candy cane of the "A" steam generator.
2. Reactor trips; turbine trips; TSVs close.
3. HPI actuates at setpoint.
4. Operator trips RCPs 30 s after HPI actuation.
5. TBVs/SRVs in secondary function as designed.
6. MFW and EFW systems function as designed.
7. Core flood tanks dump; LPI system actuates.[a]
8. No further operator actions, i.e. no throttling of HPI.[b]

Failures Assumed:

1. SBLOCA
2. Violation of procedures (Event number 8)

Basis for Transient Selection:

Determine cooldown experienced during "stagnant" SBLOCA. RCS pressure will probably stabilize below PORV/SRV setpoints. Addresses the importance of vent valve flow in the B&W design.

---

a. Event may or may not occur, depending on phenomena encountered.

b. Calculation restart point: on attainment of 42 K (75°F) subcooling in least-subcooled coolant loop, operator throttles HPI sufficiently to maintain 42 ± 14 K (75 ± 25°F) subcooling. Note: In calculating subcooling with RCPs off, pressure for each loop is taken from top of hot leg riser, and temperature is taken from core outlet.

Table 19. Pressurizer surge line break transient sequence of events

Event	Time (s)
Break initiated in pressurizer surge line.	0.0
Reactor scrams on P, T relationship; turbine stop valves close; heater drains to feedtrain and begins to close; MFW pumps begin to run back.	45.2
TBV opens due to high steam generator pressure.	47.0
SRV opens due to high steam generator pressure.	50.0
Pressurizer heaters turn off due to low pressurizer liquid level.	55.3
SRV close as steam generator pressure falls.	69.0
MFW pumps trip on high pump discharge pressure.	70.0
HPI injection begins on low primary pressure.	78.5
Upper head begins to void.	86.0
RCP trip 30 s after HPI initiation; realign main feedwater to emergency feedheaders; emergency feed begins due to low steam generator level.	108.5
TBV closes as steam generator pressure falls.	117.0
Upper head volume completely drained of liquid; top volume of downcomer begins to void.	~300.0
Feed to steam generator B stops as low liqunid level limit is exceeded	500.0
Emergency feed to steam generator A stops as low liquid level limit is exceeded.	503.0
Vent valves open.	554.0
Bubble forms in tubes of steam generator A and starts to move to top of candy cane.	768.0
Flow stagnates in loop A as bubble fills top of candy cane.	815.0
Circular flow between cold legs of loop A exists.	872.0
Bubble forms in tubes of steam generator B and starts to move to top of candy cane.	892.0
Flow stagnates in loop B as bubble fills top of candy cane.	1020.0
Bubble in top volume of downcomer collapses.	1383.0
Partial collapse of bubble in upper head. Liquid drawn up is heated and vaporized by hot metal; primary pressure momentarily increases.	1400.0

Table 19. (continued)

Event	Time (s)
Bubble in upper head collapses; volume refills with liquid; large flows throughout primary system as liquid moves toward upper head.	1488.0
Core flood tank begins injection due to low primary pressure.	2215.0
Circular flow between cold legs of loop B starts.	2378.0
Circular flow between cold legs of loop B reverses direction.	2443.0
Pressurizer begins to refill with liquid.	5064.0
LPIS injection begins due to low primary pressure.	5124.0
Calculation terminated.	6200.0

The mass flow rate out the break is shown in Figure 86. The transient was begun by opening the break in the pressurizer surge line. The primary system pressure and the liquid level in the pressurizer decreased as mass was lost from the primary system (see Figure 87). Almost all other conditions in the plant, both primary and secondary, remained essentially unchanged until 45 s, at which time the primary system pressure had decreased to the point where reactor power was tripped. The steam flow valves on both steam generators closed, thereby increasing secondary system pressure and temperature.

Figure 88 shows secondary system pressures. At 46 s, the turbine bypass valves opened; at 47 s, the secondary relief valves opened, and both generators started to dump steam to the condenser and atmosphere. Figure 89 shows that the SG liquid levels dropped as the mass inventory in the generators was depleted. This resulted in a rapid cooldown of the fluid in the steam generators and, as shown in Figures 90 through 93, a cooldown of the primary system fluid. As the primary system fluid cooled, it shrank, decreasing the pressurizer level even faster, thereby increasing the rate of primary system depressurization.

As reactor power decreased after scram, the ICS calculated a reduced feedwater demand, ran back the main feedwater pumps to their minimum speed, and began to close the main feedwater (MFW) and startup valves, sharply decreasing feedwater flow to the generators. The MFW valves closed faster than the startup valves and were closed by 50 s. The startup valves began to close at about 67 s. As the startup valves began to close, the pressure downstream of the MFW pumps increased. At 70 s, the outlet pressure of the MFW pumps exceeded the high discharge pressure trip set point, and the MFW pumps were tripped. After the pump trip, the ICS began to reopen the startup valves and, by 74 s, they were full open again.

By 69 s, the energy removal rate from the steam generators had decreased the secondary system fluid temperatures to a point at which the saturation pressure in the steam generators was below the relief valve setpoint. These valves closed, which stopped the cooldown in the secondary system. The turbine bypass valves continued to release just enough steam to hold the secondary pressure near the turbine bypass system opening pressure setpoint.

The fluid in the upper head of the reactor vessel, as modeled, was outside the normal reactor vessel circulation flow path and remained fairly stagnant. Therefore, as the rest of the primary fluid cooled, this fluid stayed near the initial, steady state hot leg temperature. At about 86 s, primary system pressure had decreased to the saturation pressure of this fluid, and it began to flash, as shown in Figure 94. This flashing slowed the primary depressurization rate significantly.

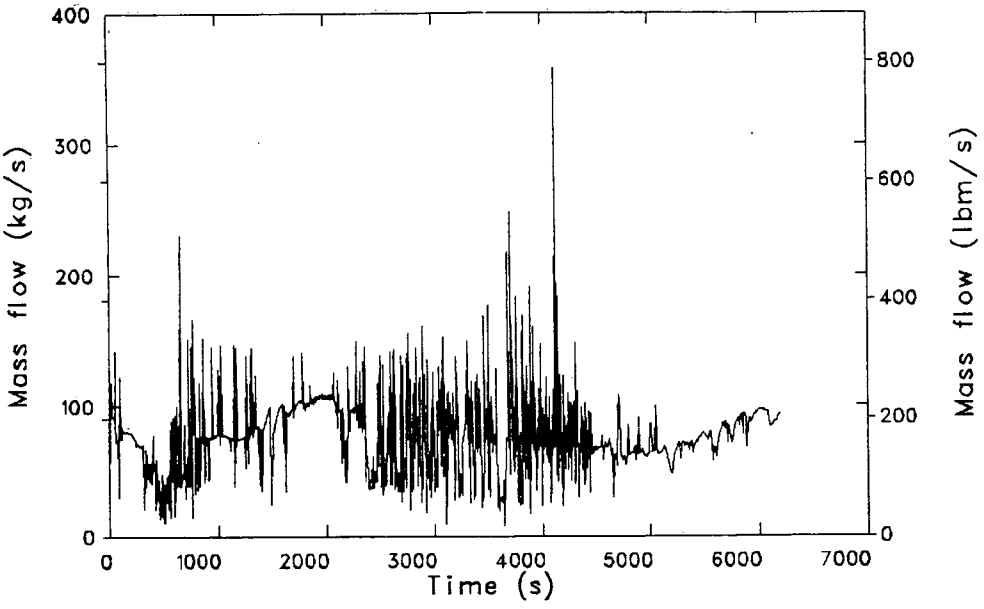

Figure 86. Pressurizer surge line break, break mass flow rate.

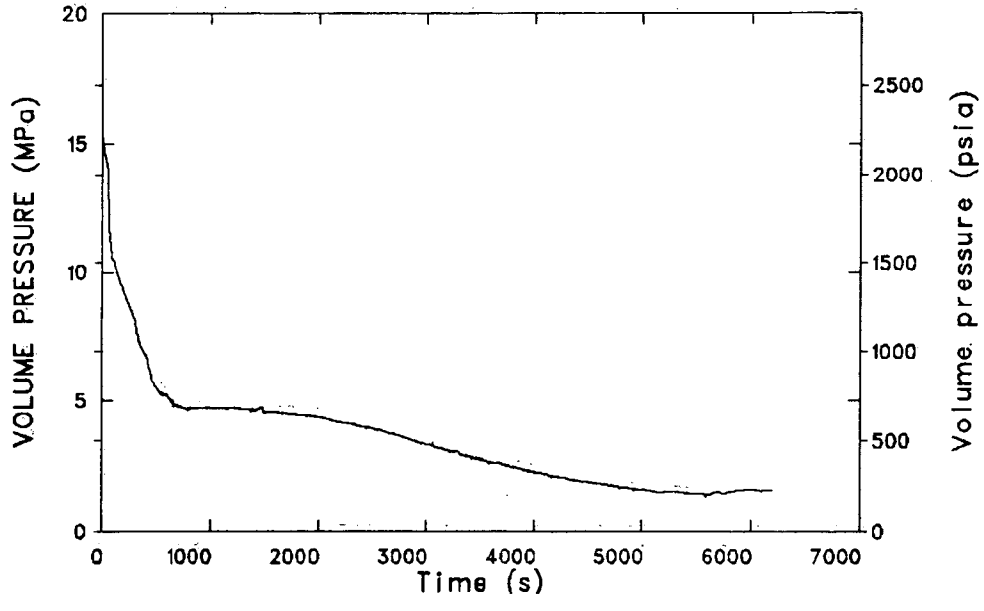

Figure 87. Pressurizer surge line break, hot leg pressure.

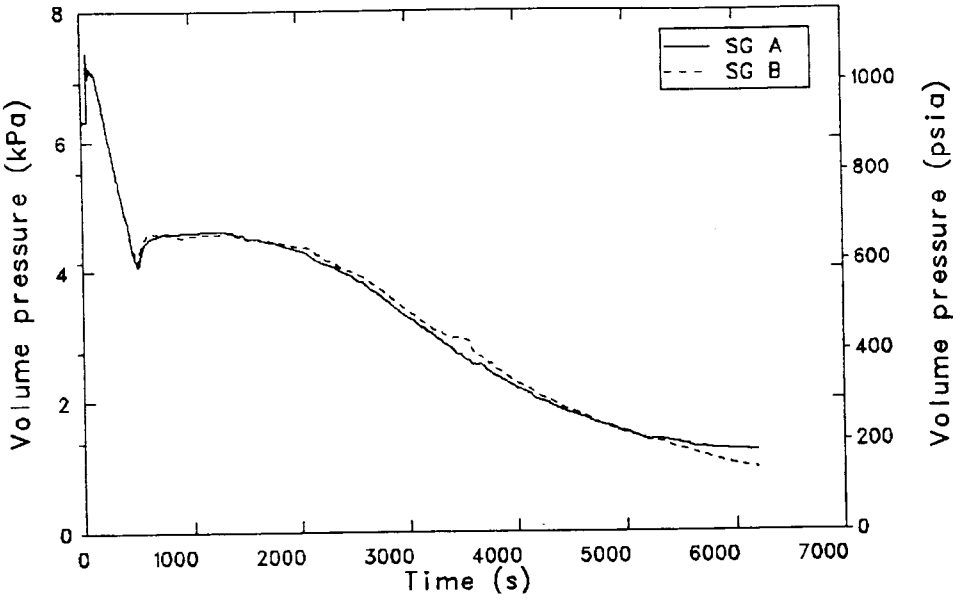

Figure 88. Pressurizer surge line break, SG secondary pressures.

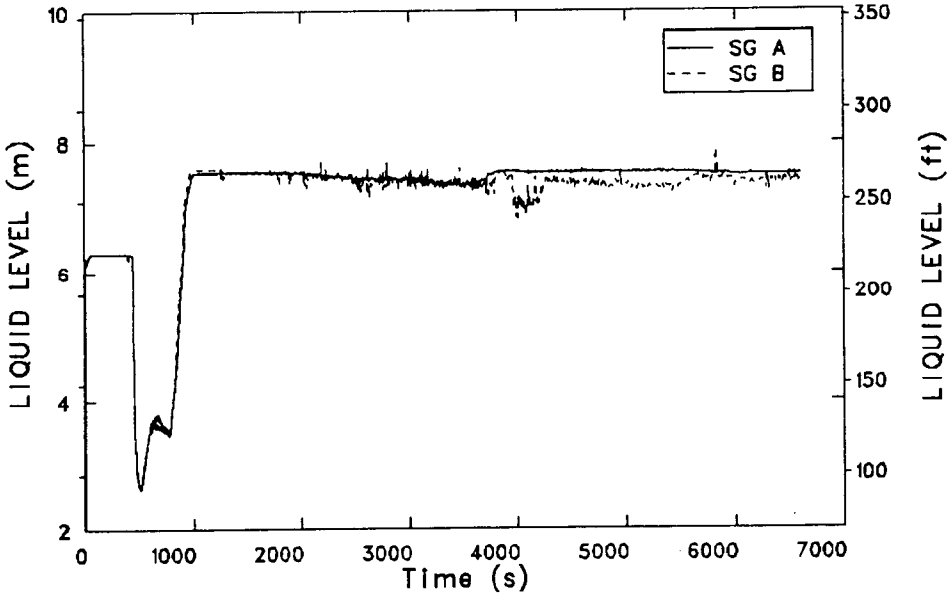

Figure 89. Pressurizer surge line break, SG start-up levels.

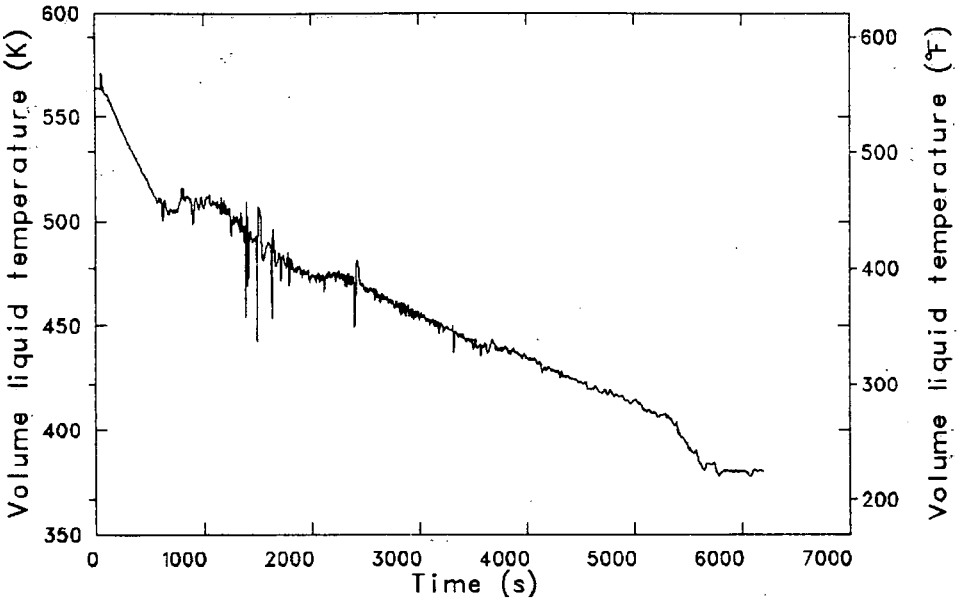

Figure 90. Pressurizer surge line break, RV downcomer fluid temperature.

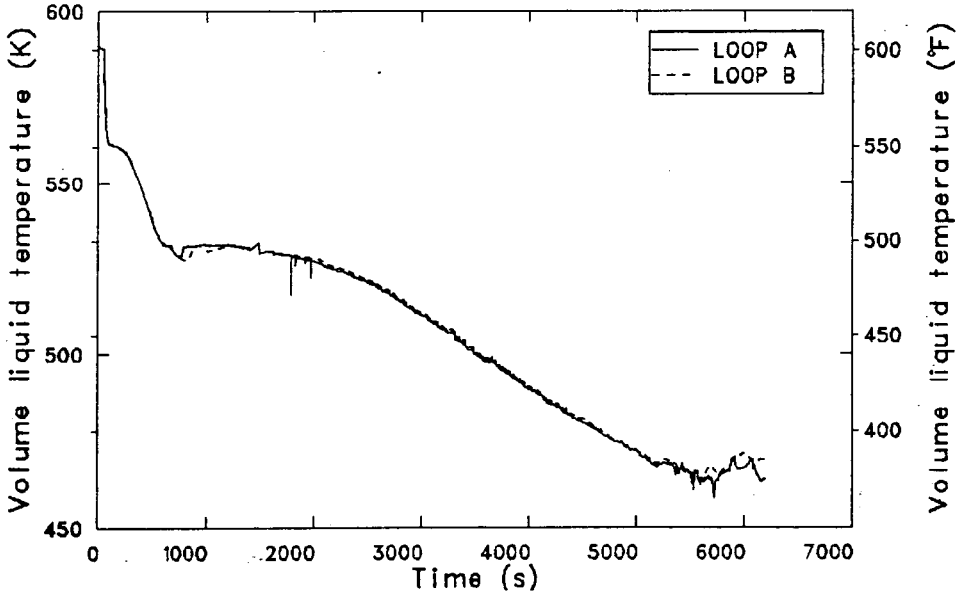

Figure 91. Pressurizer surge line break, hot leg fluid temperatures.

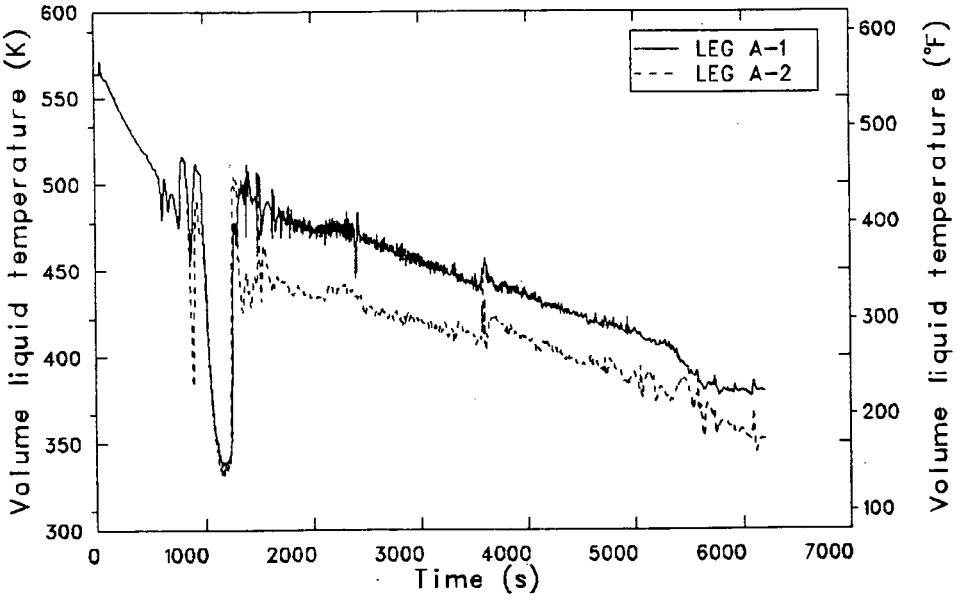

Figure 92. Pressurizer surge line break, loop A cold leg fluid temperatures.

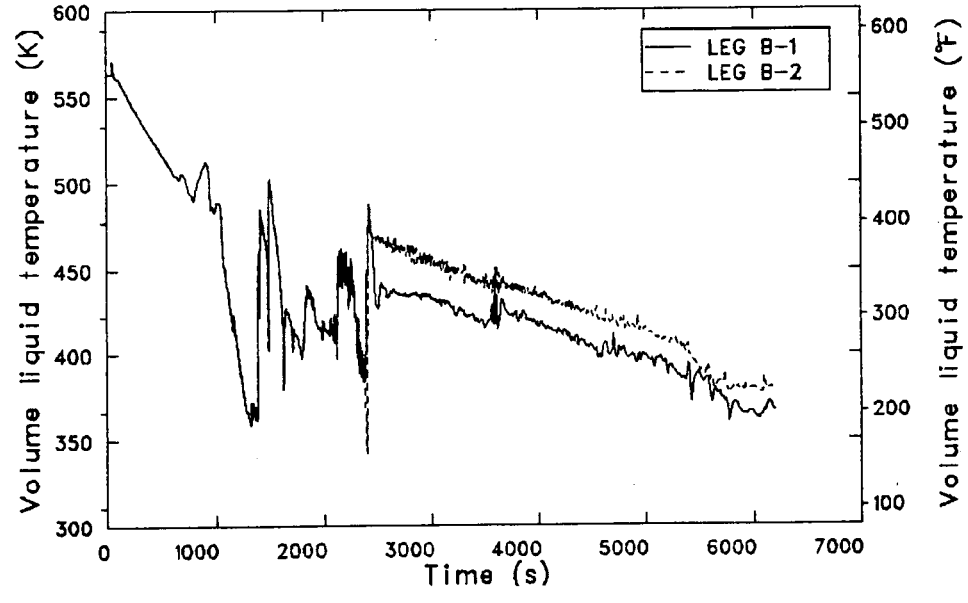

Figure 93. Pressurizer surge line break, loop B cold leg fluid temperatures.

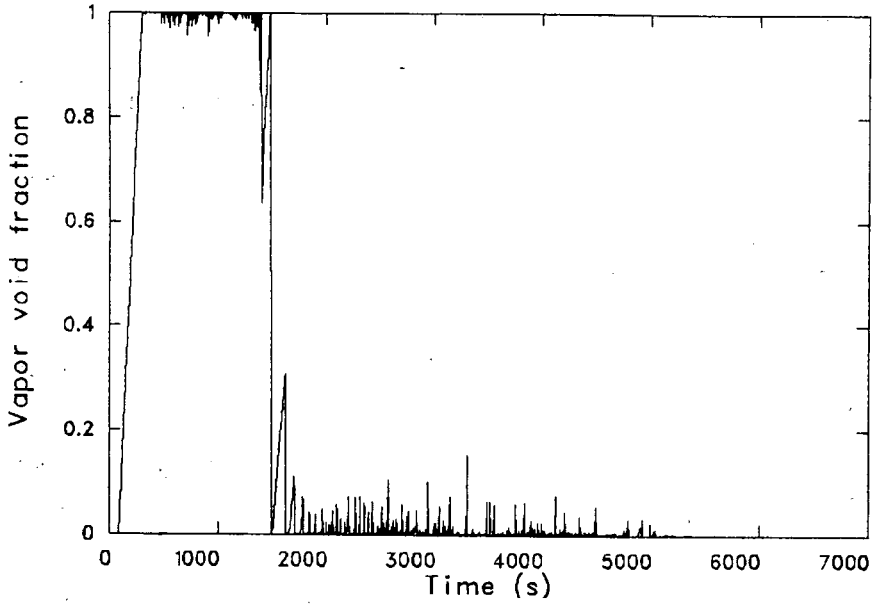

Figure 94. Pressurizer surge line break, void fraction in RV upper head.

Primary system pressure reached the HPI setpoint of 10.45 MPa (1515 psia) at 78 s, and the HPI system began injecting cold water into all four cold legs. At 108 s, 30 s after HPI initiation, the primary coolant pumps were tripped. At that time, the main feedwater train was realigned to the emergency feedwater header. Also, because the steam generator liquid levels were below the new low level limit of 6.10 m (20.0 ft), emergency feedwater was initiated to both steam generators. Total feedwater flow to the generators is shown in Figure 95. This cold flow into the top of the steam generators depressurized them somewhat, which in turn closed the turbine bypass valves. The liquid injected into the top of the generators fell to the bottom and began to fill the generators from the bottom up.

After the primary coolant pumps coasted down, natural circulation kept some flow moving around both loops. Natural circulation was maintained because significant energy was removed from the primary system into the steam generators due to the cold emergency feedwater being injected into the steam generators. This energy removal from the primary system also caused a smooth cooldown in primary system fluid temperatures between 109 and 500 s, as seen in Figure 90.

At about 300 s, the upper head of the reactor vessel had completely drained of liquid, and as a result, primary system pressure began to decrease more rapidly. However, relatively hot fluid was present in the top volume of the downcomer. The primary system pressure reached this fluid's saturation pressure, and as shown in Figure 96, it began to flash and slow the primary depressurization. The effect of this flashing and draining can be seen as ripples in the primary system pressure response, shown in Figure 87.

Even though the MFW pumps had been tripped earlier, the condensate booster pump in the MFW train was still running against a closed check valve and delivered no flow. At 416 s, the pressure in the steam generator secondaries had decreased to the point where the head produced by the condensate booster pump exceeded the pressure in the steam generators. Feedwater began to flow from the MFW train into the steam generators via the emergency feedwater headers. By 500 s, the combination of main and emergency feedwater flow had filled the steam generators to above the low-level limit, and the emergency feedwater flow was shut off. The ICS also began to close the startup feedwater valves, and by 621 s, main feed to the generators had also been terminated.

The natural circulation flow rates dropped as the emergency feedwater was terminated. The temperature of the fluid in the steam generators increased and approached the temperature of the primary system hot leg fluid. At 554 s, the natural circulation flow decreased to the point where the reactor vessel vent valves opened, allowing flow between the upper plenum and the top of the

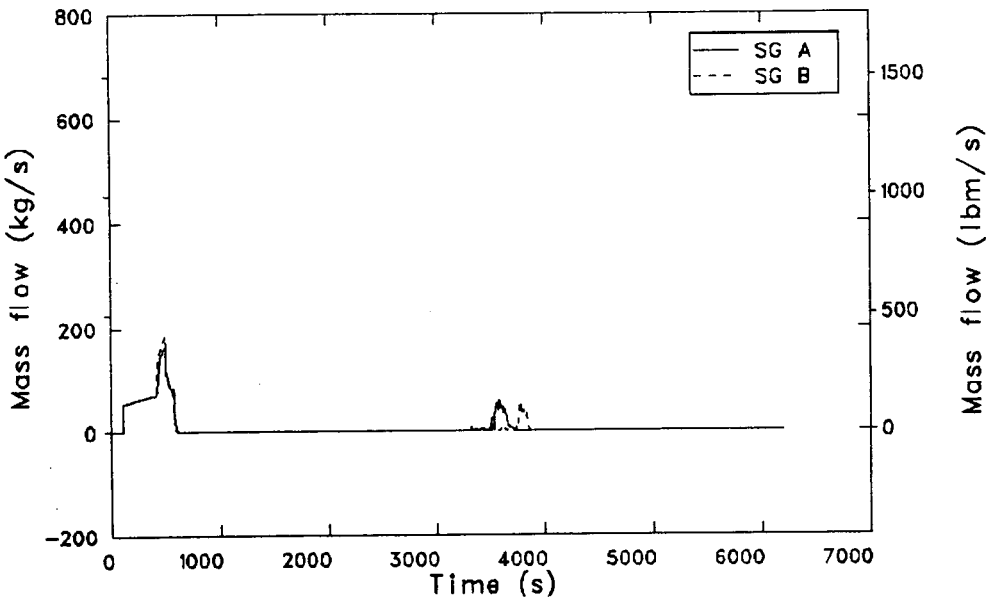

Figure 95. Pressurizer surge line break, total feedwater flow rates.

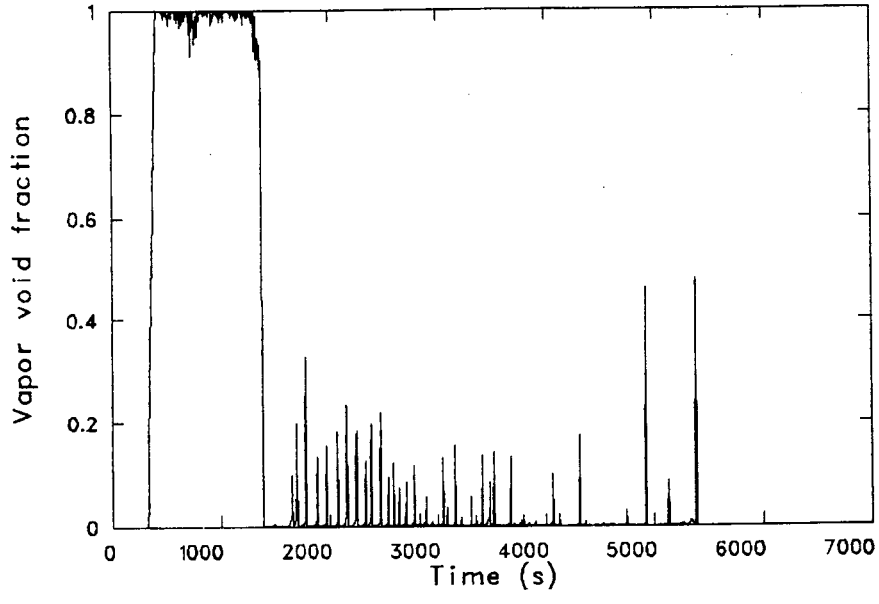

Figure 96. Pressurizer surge line break, void fraction in top of RV downcomer annulus.

downcomer in the reactor vessel. This mixed a significant amount of warm fluid from the upper plenum with the fluid in the downcomer and slowed the cooldown rate in the downcomer, as shown in Figure 90. By about 675 s, the temperature of the primary system hot leg fluid decreased below the temperature of the fluid in the steam generator secondaries, and the steam generators became heat sources to the primary system.

The primary system pressure, having continually dropped throughout this cooldown period, had, by 768 s, dropped to the saturation pressure of the fluid in the primary side of the tubes of steam generator A. This primary fluid then began to flash and create voids inside the tubes. Figure 97 gives the mass flow rates in both cold legs of loop A, which show a large surge of flow moving in the reverse direction, starting at 770 s. At that time, the bubble in the primary side of steam generator A had grown to the point where the buoyant force on the bubble exceeded the momentum force of the fluid trying to push the bubble in the positive direction around the loop, and the bubble began to rise up the tubes of the generator. This resulted in the large reverse flow throughout the A loop as the bubble pushed liquid ahead of it down the hot leg, and pulled liquid behind it though both cold legs. By 815 s, the bubble had collected at the top of the candy cane, and flow through the A loop stopped.

The flows which were encountered when the bubble moved to the top of the candy cane also served to redistribute mass around the primary system. Temperatures in the reactor vessel downcomer rose when reverse flows pulled fluid from the core region into the downcomer. The primary system depressurization virtually stopped when the fluid in the hot leg of loop A began to flash. Bubbles began to form in the tubes of steam generator B at about 890 s, and by 1020 s, enough voids had collected at the top of the loop B candy cane to cut off loop flow (see Figure 98). The primary system then began a smooth, gradual depressurization as the energy removed through the break exceeded the energy added from decay heat.

From about 1000 s to the end of the transient, the fluid in the reactor vessel experienced a gradual but irregular cooldown. Two primary factors controlled the temperature of the fluid in the downcomer: (a) the mass flow rates, and (b) the temperatures of the fluids flowing through the vent valves and from the four cold legs. Three phenomena which prevented cold leg flows from stagnating completely occurred in this portion of the transient. The cold HPI water therefore mixed with the warm primary fluid before it flowed into the downcomer.

The first of these phenomena was a manometer-type oscillation between liquid levels in the upflow and downflow legs of the candy canes. After the bubble had formed at the top of each candy cane, there was distinct liquid level in the riser portion. This level was balanced hydrostatically by the liquid level inside the steam generator tubes. As shown in Figures 92 and 93, when the loop flow stagnated, the cold HPI fluid, injected into the cold legs, quickly decreased the temperature of the fluid moving from the cold legs to the downcomer. As a result, the downcomer fluid became cooler. Since the fluid was cooler, and therefore more dense, it exerted a slightly higher hydrostatic pressure. To balance this higher pressure on the cold leg side, fluid flowed up the hot leg and increased the liquid level in the riser portion of the candy cane. However, as the fluid in the downcomer cooled, the differential pressure across the vent valves increased, tending to cause them to open further. The increased flow of warm fluid through the vent valves warmed the fluid in the downcomer, thereby decreasing the hydrostatic head imposed by the downcomer liquid. Fluid then flowed in the reverse direction down the hot leg and decreased the liquid level in the riser, again balancing the fluid in the downcomer and inside the tubes of the steam generator. Warming the fluid in the downcomer also decreased the differential pressure across the vent valves. The valves closed somewhat, decreasing the vent valve flow. The downcomer started to cool again, and the whole cycle was repeated. The overall result of this phenomenon was that the hot and cold leg flows oscillated slowly, mixing the fluid injected from the HPI with warmer primary fluid before it flowed to the downcomer.

Starting at 872 s in the A loop and at 2378 s in the B loop, another mixing phenomenon, which completely overshadowed the mixing encountered from the above manometer oscillation effect, occurred. Figure 97 shows that at 872 s, flow began to move within the two cold legs of the A loop. The flow moved in the positive direction from the steam generator lower plenum down cold leg A-2 to the downcomer of the reactor vessel. It then flowed in the reverse direction up cold leg A-1 back to the steam generator lower plenum. In the A loop this internal circulation lasted until 952 s. It then stopped but started again at 1230 s and continued

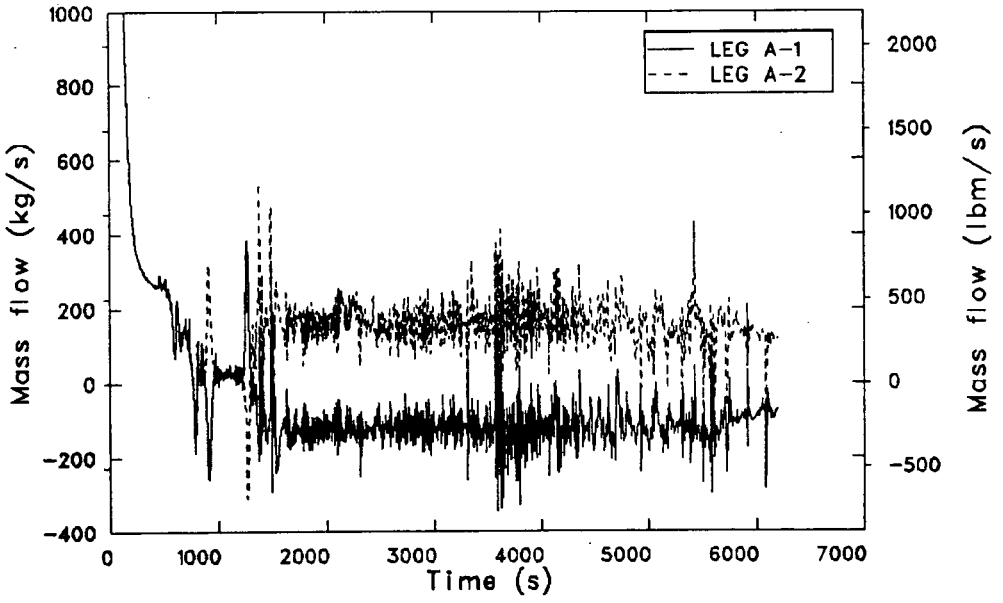

Figure 97. Pressurizer surge line break, loop A cold leg flow rates.

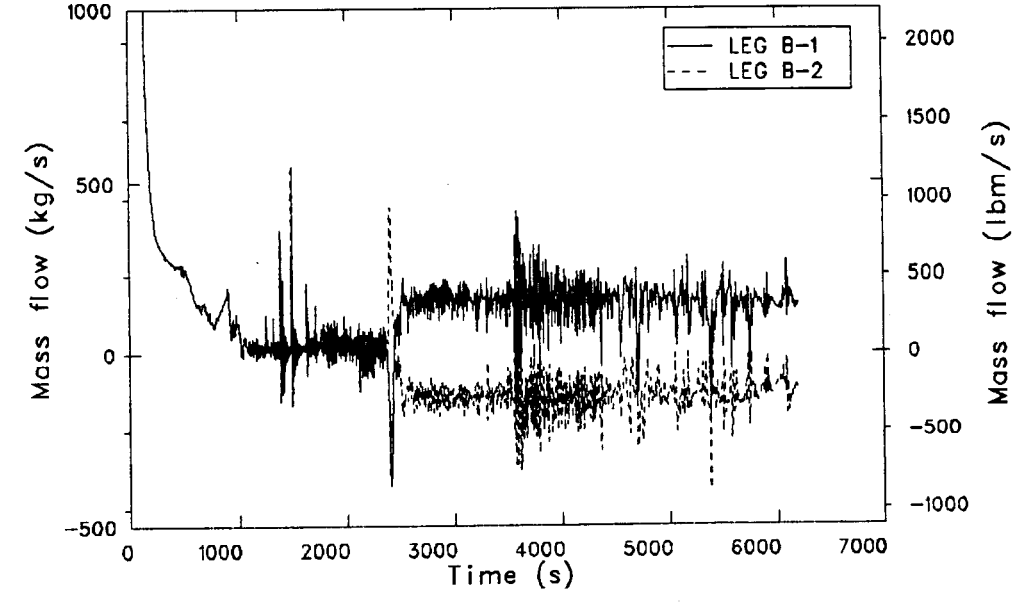

Figure 98. Pressurizer surge line break, loop B cold leg flow rates.

until the end of the transient. Figure 98 shows that, in the B loop, the circulation flow started at 2378 s, reversed directions at 2443 s, then continued to the end of the transient.

The driving force for this flow was a difference in the temperatures between the fluids in the pipes connecting the steam generator outlet plenum to the two primary coolant pumps on the same loop. There is an elevation change of about 5.2 m (17 ft) in this piping. When the flow was circulating, the cold HPI water injected into one of the cold legs swept up the pipe toward the steam generator and down the vertical section of pipe into the pump suction. The flow then moved through the outlet plenum of the steam generator and up the other cold leg. However, the steam generator outlet plenum is large, and was filled with relatively warm fluid, so when the flow moved through it and mixed with the fluid in the outlet plenum, its temperature increased 8.3 K (15°F). As a result, the colder, more dense fluid in one of the pump suction pipes exerted a greater static pressure than the warmer column of fluid in the other pump suction pipe. This difference in the static pressure exerted by the two columns of fluid pushed fluid around the loop formed by the two cold legs.

A hand calculation verified that the differential pressure due to the static heads of the two columns of fluid was sufficient to force the fluid around the cold legs at the velocities encountered in the calculation, about 0.3 m/s (1 ft/s). It is not understood what initiated this flow. From a geometric standpoint, the cold legs in any given loop were identical. One theory is that the oscillating-manometer-effect mixing of the HPI flow in the cold legs moved some of the cold HPI water backward up the cold legs and into the pump suction piping. Due to stochastic differences in the oscillating flows, the fluid in one pump suction leg became colder than that in the other, thus starting the internal flow.

The third phenomenon which affected the downcomer fluid temperature was the rapid condensation of steam bubbles in the primary system. Figures 94 and 96 show the void fractions in the upper head of the reactor vessel and in the top volume of the downcomer. At 1400 s, the bubble in the upper head began to collapse, drawing liquid into the upper head. This liquid contacted the hot metal structures in the upper plenum and immediately began to boil, producing vapor, forcing the remaining liquid out of the volume, thereby increasing the primary pressure. At 1483 s, another surge of water entered the upper head. It did not boil to steam but began to condense the steam already there. As the steam condensed, its volume shrank, drawing even more liquid from the upper plenum. The additional liquid condensed even more steam, and the condensation essentially fed itself. The upper head steam bubble completely collapsed and filled with liquid in about 3 s. This unrealistically high condensation rate caused very large flow rate surges throughout the primary system, as liquid rushed toward the upper head to fill the volume removed by condensation. These large flow rates redistributed warmer fluid into the region of the downcomer and temporarily raised fluid temperatures there. The large flow rates due to the condensing steam bubbles warmed the fluid in the downcomer to approximately the same temperature as that of the fluid in the core. As a result, the differential pressure at the elevation of the vent valves could not keep the valves open.

With the vent valves closed, the colder water in the cold legs flowed into the downcomer, causing temperatures there to decrease. The cooler temperatures in the downcomer caused an increase in the differential pressure at the vent valves, at which time the valves reopened. Because of the relatively large flows encountered when the vent valves opened, this cooler fluid was flushed out of the downcomer, and temperatures returned to the point they were prior to the bubble collapse. This effect is seen (in Figure 90) as sharp spikes in the downcomer temperature between 1200 and 1700 s. After 1700 s, smaller bubbles formed and collapsed many times in both the upper head and the top of the downcomer. However, the flow rates induced when these bubbles collapsed were not large enough to greatly perturb the downcomer temperature.

Between 1700 and 5100 s, as more energy escaped through the break than was added by decay heat, the primary system gradually cooled and depressurized. The mass flow from the break was only slightly greater than that input from the HPI, so the primary system lost mass very slowly. At 2215 s, primary pressure dropped below the core flood tank setpoint pressure, and some flow was delivered by the core flood tank. The mass flow rate from the core flood tank is shown in Figure 99. The mass added by the core flood tank shifted the mass balance so that slightly more mass was being added to the primary system than was being lost through the break. However, the core flood tank flow rates were never large enough to significantly affect either the primary system pressure or the downcomer temperature.

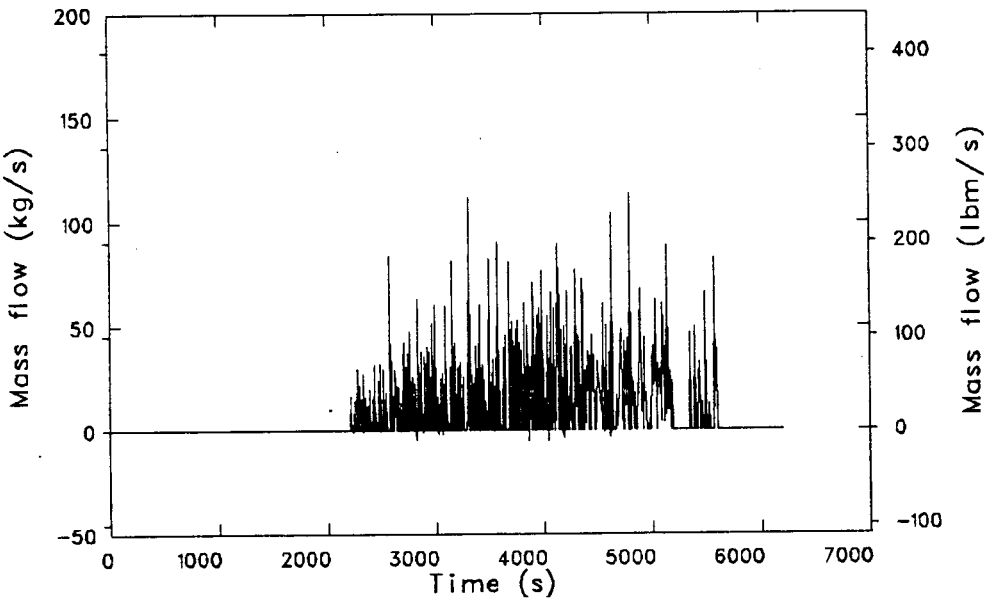

Figure 99. Pressurizer surge line break, core flood tank injection rate.

At 5124 s, the primary system pressure decreased below 1.34 MPa (195 psia), and the LPI system began to inject fluid into the reactor vessel downcomer. The mass flow delivered by the LPI is shown in Figure 100. The initial LPI flow rate was sufficiently large to cause a more rapid cooldown in the downcomer fluid, but these large flow rates also increased the primary pressure, which in turn reduced the LPI flow rate. By the end of the transient, at 6200 s, a quasi-steady state was reached. Enough flow was obtained from the LPI to keep the primary pressure very close to the shutoff head for the LPI, 1.48 MPa (214 psia). Not enough fluid was added to cause a cooldown of the downcomer fluid any greater than that seen just prior to LPI initiation.

Based on the cooldown rates experienced just prior to LPI initiation, downcomer temperatures would decrease to 355 to 361 K (180 to 190°F), if extrapolated to 7200 s. Because of the action of the LPI system, primary system pressure would stay close to the LPI shutoff head of 1.48 MPa (214 psia), out to 7200 s.

The temperature of the fluid in the downcomer of the reactor vessel depended on the cold leg mass flow rates and fluid temperatures and on the vent valve mass flow rate and fluid temperature. The following paragraphs identify, and assign uncertainties to, those phenomena predicted by RELAP5 which could affect the downcomer liquid temperature and which might have been insufficiently characterized in the calculation. Two such phenomena have been identified: (a) the unrealistically high condensation rates in the reactor vessel upper head and downcomer, and (b) the internal cold leg flows, which started at 872 and 2378 s in the A and B loop cold legs, respectively.

When large condensation rates caused the steam bubble in the reactor vessel head to collapse, a spike occurred in the downcomer temperature. The reasons for this spiking were discussed earlier. Had condensation occurred at a more reasonable rate, the large flow rates calculated around the primary system would not have occurred, and vent valve operation would not have been as severely perturbed. As a result, the spikes in the downcomer temperature between 1200 and 1700 s would not have occurred. However, the absence of the spikes would not have affected the temperature of the fluid in the downcomer after the condensation-induced effects were over (after 1700 s). The downcomer fluid temperatures would have continued the gradual cooldown, with no significant change from the calculated result. It is concluded that condensation effects in the reactor vessel upper head had little effect on the final downcomer fluid temperature.

The internal cold leg flows caused mixing of the fluid within the cold legs, instead of allowing them to remain stagnant. Because the fluid in the cold legs was mixed, warmer fluid was delivered to the downcomer volume, thereby maintaining higher downcomer fluid temperatures. In order to determine how cold the downcomer fluid would have become had no mixing been allowed between the fluid injected by HPI and the fluid in the cold legs, a sensitivity calculation was performed. In this calculation, the fluid injected by the HPI system was mixed directly with the fluid flowing into the downcomer from the vent valves, and a mixture temperature was determined. The calculated mixture temperature is shown in Figure 101, along with the RELAP5-calculated downcomer temperature. The downcomer did not become significantly colder in the sensitivity calculation because the temperature of the fluid passing through the vent valves was the primary controller of the downcomer fluid temperature. This was because the vent valve flow rate, shown in Figure 102, was much greater than the flow injected by the HPI system, shown in Figure 103. Although the temperature of the downcomer did not decrease significantly when no mixing occurred, the temperature of the fluid in the cold legs flowing into the downcomer decreased to the temperature of the fluid being injected by the HPI system, 283 K (50°F).

Figures 104, 105, and 106 show the downcomer pressure, fluid temperature, and heat transfer coefficient, extrapolated to 7200 s.

As shown in Figures 104 and 105, uncertainty bars have been added to the RELAP5-calculated reactor vessel downcomer fluid pressure and temperature curves. A comprehensive study of the uncertainties in the calculation is beyond the scope of this work. However, the fracture mechanics analysts required an estimate of the uncertainty in the calculation for use as boundary conditions for further analyses. Therefore, a limited-uncertainty estimate has been made, based primarily on information gained from the comparison of the TRAC and RELAP5 calculations, presented in Appendix C.

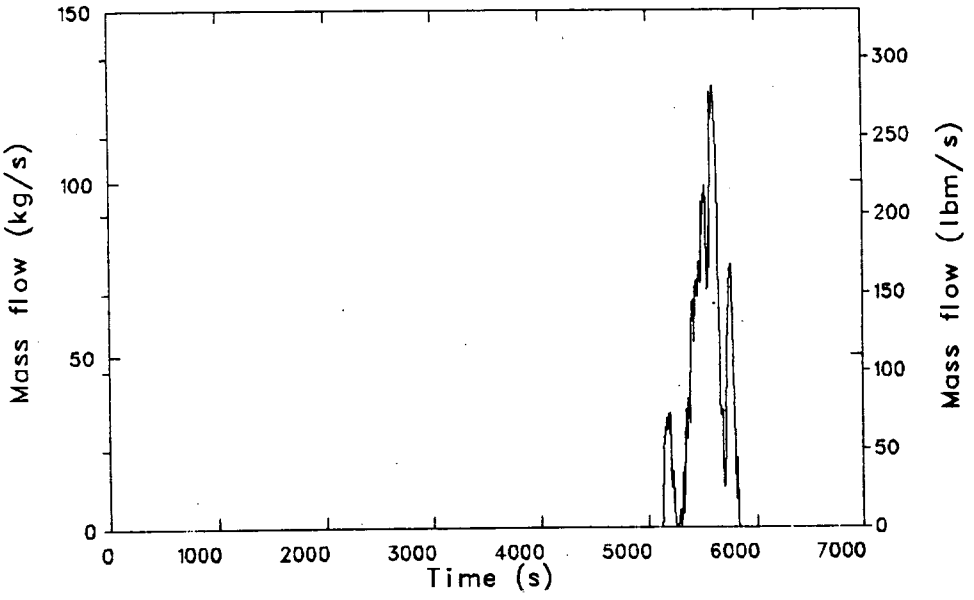

Figure 100. Pressurizer surge line break, LPI rate.

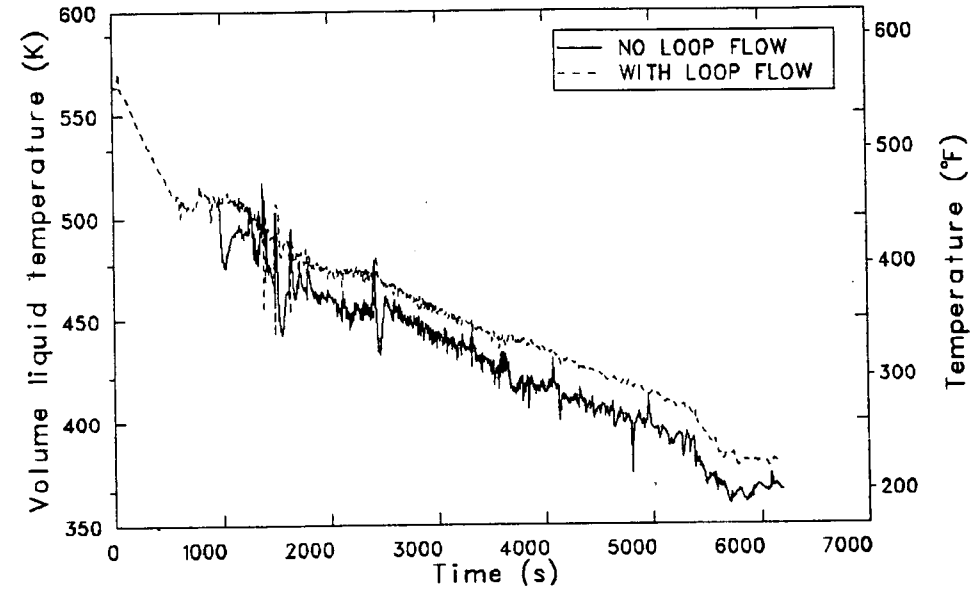

Figure 101. Pressurizer surge line break, RV downcomer fluid temperature, with and without cold leg circulation

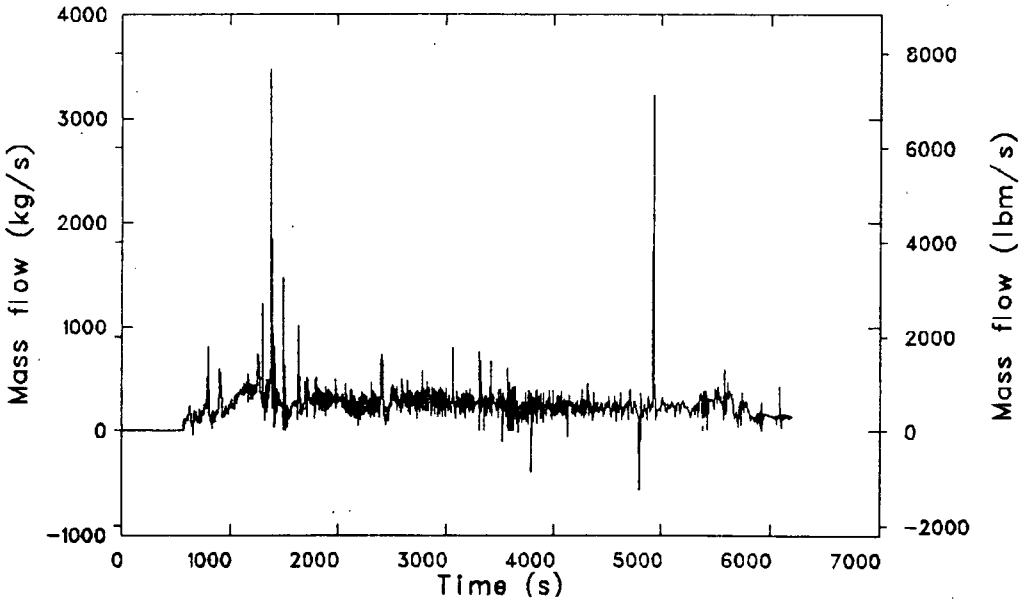

Figure 102. Pressurizer surge line break, vent valve mass flow rate.

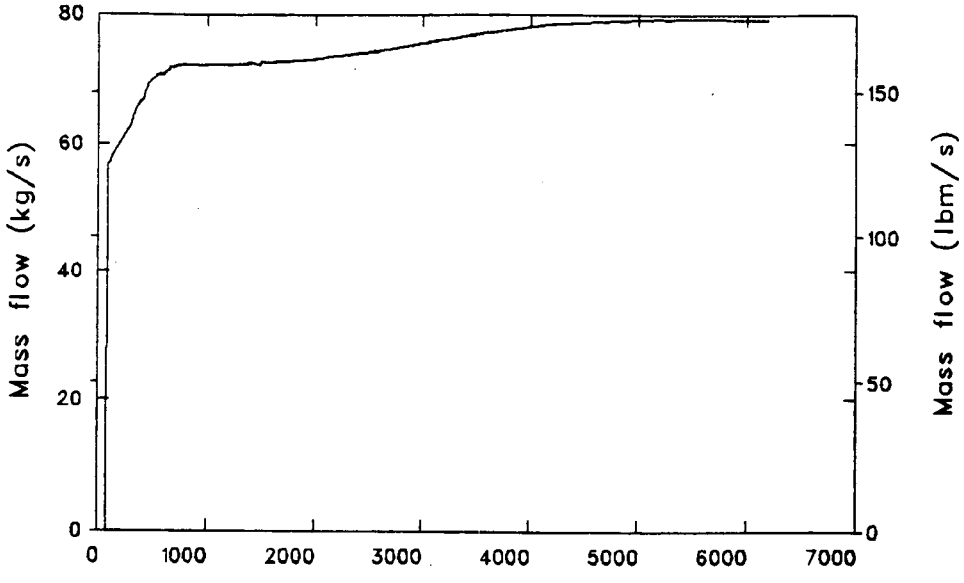

Figure 103. Pressurizer surge line break, total HPI mass flow rate.

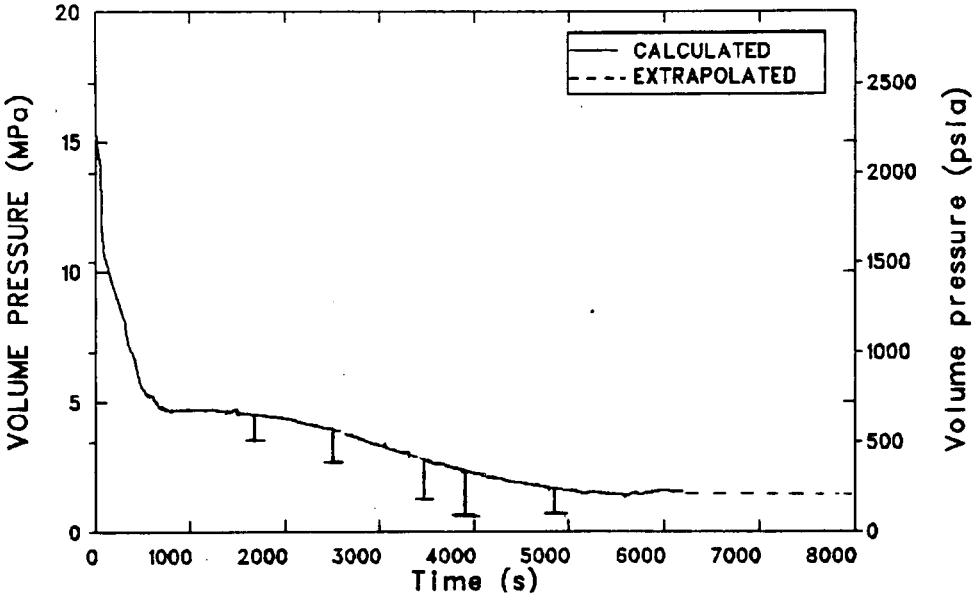

Figure 104. Pressurizer surge line break, extrapolated RV downcomer pressure.

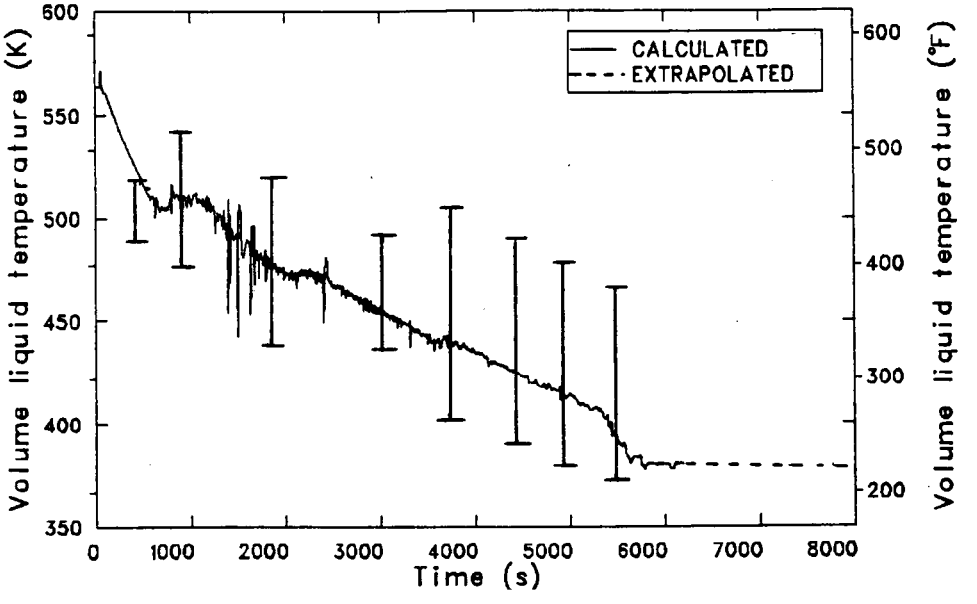

Figure 105. Pressurizer surge line break, extrapolated RV downcomer fluid temperature.

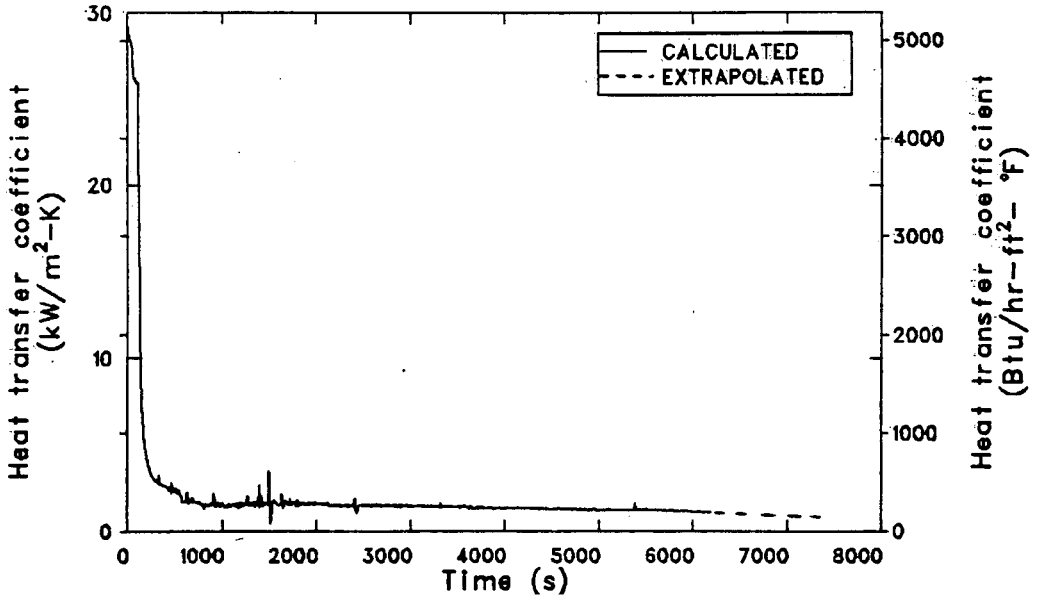

Figure 106. Pressurizer surge line break, extrapolated heat transfer coefficient for RV downcomer inside surface.

The uncertainty bars were constructed by accounting for three effects: (a) break energy removal differences, (b) cold leg circulation uncertainty, and (c) main feedwater pump trip uncertainty. These uncertainties are addressed separately.

As discussed in Appendix C, a difference between the TRAC and RELAP5 break energy removal was observed. This difference was due to greater availability of liquid at the break with RELAP5 than with TRAC. As a result, the break energy removal was higher with TRAC, resulting in a higher rate of primary system depressurization. Since this difference was unresolved, it represents an uncertainty in the primary system depressurization and cooldown rates. The lower end of the uncertainty bars were determined by assuming the higher TRAC depressurization and cooldown rates.

Figure 101 shows the effect the cessation of RELAP5-calculated cold leg circulation has on the downcomer fluid temperature. An average -20 K (-36°F) shift in reactor vessel downcomer fluid temperature was used in constructing the lower end of the uncertainty bars. This uncertainty does not significantly affect the primary system pressure.

The effect of uncertainty in main feedwater pump trip, discussed in Appendix C, was estimated to be a +40 K (+72°F) change in reactor vessel downcomer fluid temperature. This assessment was made using Figure C-2 as a guide. It is estimated that this uncertainty does not significantly affect the primary system pressure.

Conclusions

The minimum downcomer fluid temperature that was calculated was 380 K (225°F) and occurred at the end of the calculation, 6200 s. By extrapolating trends evident near the end of the calculation, the downcomer temperature would decrease to 355 K (180°F) by 7200 s. The minimum cold leg temperature calculated (adjacent to the reactor vessel) was 333 K (140°F). This occurred at 1130 s, when the primary system pressure was 6.1 MPa (740 psia). At the end of the calculation, the primary system pressure was at the LPI shutoff head, 1.48 MPa (214 psia). Since LPI injection held primary pressure at this point, it would be expected to stay close to that pressure through 7200 s.

8. REACTOR COOLANT PUMP SUCTION SMALL BREAK TRANSIENT

The following subsections present the transient scenario description, modeling changes effected in order to perform this calculation, detailed analysis of the transient results, and conclusions drawn from the analysis.

Transient Scenario Description

The transient was initiated from full-power steady state conditions. The pressurizer heaters and spray operate as designed. The transient began with a break downstream of a valve in the letdown line connected to the bottom of the A-1 pump suction leg. Following reactor scram, the decay heat was assumed to be at the ANS standard rate. The turbine stop valves closed, and it was assumed that the integrated control system operated as designed. After the core flood tanks emptied, the break was isolated; high pressure injection flow was throttled when 28 K (50°F) subcooling was attained after the primary system repressurized to the power-operated relief valve (PORV) setpoint. A transient scenario is provided in Table 20.

Model Changes

The primary change made to the steady state model (presented in Section 2) was adding a pipe and valve component to the A-1 pump suction leg. As stated above, the break was in the letdown line, which is a 0.0635 m (2-1/2 in.) diameter line. The break was assumed to occur downstream of a motor valve which could be closed. The distance from the primary piping to the valve in the line was approximately 15.24 m (50 ft). This line was modeled with three volumes. The valve throat was assumed to have the same inside diameter as that of the pipe.

Transient Results

This section presents the results of the RELAP5 pump suction leg small break calculation. Table 21 presents the sequence of events of the calculation.

A break in the letdown line downstream of an isolatable valve initiated this transient. The letdown

Table 20. Pump suction break transient scenario

1. Break in letdown line (connected to the A-1 pump suction leg) occurs downstream of an isolatable valve.
2. Reactor scrams; turbine trips; turbine stop valves close; heater drains close; the integrated control system operates as designed.
3. Turbine bypass valves and safety relief valves on steam generator secondary operate as designed.
4. Main and emergency feedwater systems function as designed.
5. High pressure injection initiates at setpoint.
6. Operator trips reactor coolant pumps 30 s after high pressure injection actuation; main feedwater is realigned to EFW headers.
7. Core flood tanks dump; low pressure injection system actuates.
8. Break isolated after core flood tanks empty.
9. High pressure injection throttled when 28 K (50°F) subcooling occurs but after the primary system repressurizes to the power operated relief valve setpoint.[a]
10. Maintain 28 K (50°F) subcooling.

a. In calculating subcooling with the reactor coolant pumps off, pressure for each loop is taken from the top of the hot leg riser, and temperature is taken from the core outlet.

Table 21. Pump suction break transient sequence of events

Event	Time (s)
Break in loop A-1 pump suction leg occurs.	0.0
Reactor scrams (P, T relationship); turbine stop valves close; heater drains begin to close; turbine bypass and steam generator secondary safety valves operate as designed.	48.60
Pressurizer heaters latch off due to low level in pressurizer.	60.92
Main feedwater pumps trip due to high discharge pressure.	75.88
Primary pressure drops below high pressure injection setpoint and injection begins.	94.32
Upper head begins to void.	100.0
Reactor coolant pumps trip 30 s after high pressure injection initiation; main feedwater flow realigned to the EFW headers.	124.32
Motor and turbine driven emergency feedwater systems initiated due to low level limit in the steam generator secondaries.	124.36
Steam generator A and B turbine bypass valves close.	135.0
Upper head completely voided.	424.0
Steam generator B secondary pressure drops below the booster pump head in the main feedline; main feedwater begins to flow into B generator secondary via the startup valves and crossover.	500.0
Steam generator A secondary pressure drops below the booster pump head in the main feedline; main feedwater begins to flow into A generator secondary via the startup valves and crossover.	545.0
Steam generator B emergency feedwater flow stops due to liquid level above the low level signal.	573.71
High level limit signal in steam generator B is reached, due to flow through startup valves.	596.97
Loop natural circulation established.	600.0
Steam generator A emergency feedwater flow stops due to liquid level above the low level signal.	631.90
High pressure injection volumetric flow rate exceeds the break volumetric flow rate, and primary system depressurization essentially stops.	650.0
High level limit signal in steam generator A is reached, due to flow through startup valve.	660.80
ICS causes B startup valve to close, isolating steam generator B secondary.	675.0

Table 21. (continued)

Event	Time (s)
Vent valve flow commences.	680.0
Level in pressurizer begins to recover; void in upper head begins to collapse.	700.0
ICS causes A startup valve to close, isolating steam generator A secondary.	731.0
Primary mass lost through the break is regained by high pressure injection mass.	900.0
Upper head becomes liquid-full; primary system begins to repressurize.	1350.0
Natural circulation lost in loop B.	2000.0
Primary pressure turned over; volumetric break flow exceeds volumetric HPI flow.	2200.0
Flow in loop B reversed.	2380.0
Flow reversal in loop B recovered.	2800.0
Series of flow reversals in loop B mixes cold HPI water with warm primary liquid in the loop B cold legs.	2800.0 to 4900.0
Transient terminated. Pattern established in transient to enable extrapolation of downcomer pressure and temperature to 7200 s. Downcomer pressure and temperature at termination of transient were 6.0 MPa (870 psia) and 470 K (386°F), respectively.	4900.0
Extrapolated downcomer pressure and fluid temperature are 5.1 MPa (740 psia) and 446 K (343°F), respectively.	7200.0

line was connected to the A-1 pump suction leg. The primary system rapidly depressurized, as shown in Figure 107, resulting in a reactor scram at 48.6 s. This was due to violation of the pressure, temperature relationship scram criteria of the Oconee-1 plant. At the time of reactor scram, the turbine stop valves closed, which produced a rapid increase in the steam generator secondary pressure, shown in Figure 108. The turbine bypass and safety valves operated as designed and arrested the secondary pressure increase. Also, the feedwater heater drains were closed over a 5 s period starting at the time of scram. At 60.9 s, primary mass inventory had decreased enough that the pressurizer heaters were turned off, due to low liquid level in the pressurizer.

At 75.9 s, the main feedwater pumps were tripped due to high discharge pressure. At reactor scram, the integrated control system (ICS) ran back the main feedwater (MFW) pumps to their minimum value of 447 rad/s (4270 rpm). The MFW and startup valves, also controlled by the ICS, began to close. The closing response time for the MFW valves was faster than that for the startup valves, so the MFW valves were closed at 62 s, as shown in Figure 109. It was not until 74 s that the ICS began closing the startup valves as shown in Figure 110. When the startup valves began to close, the pressure upstream of the valves began to increase, due to the head produced by the MFW pumps. By 75.88 s, the pressure upstream of the valves increased above the MFW pump high

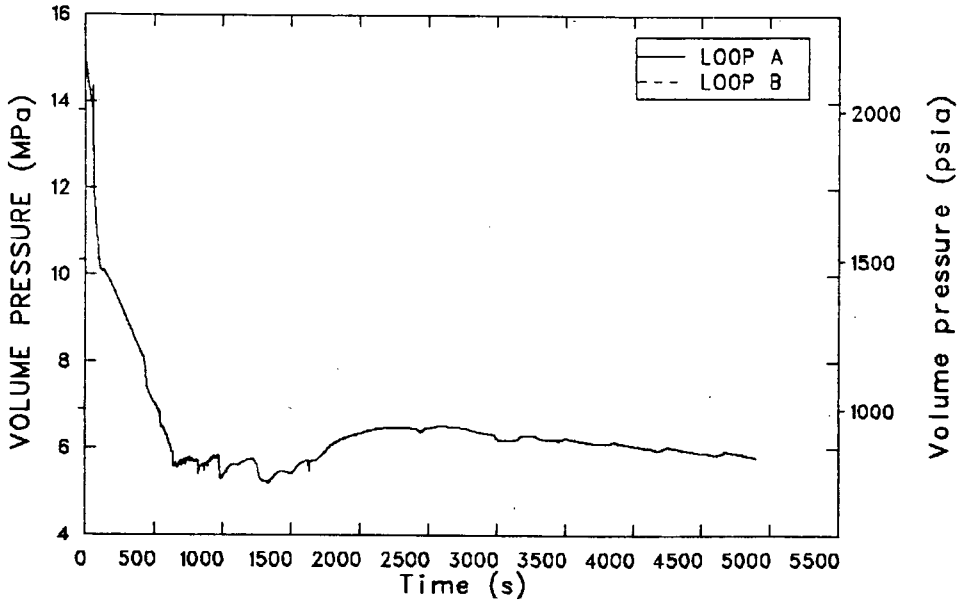

Figure 107. Pump suction break, hot leg pressures.

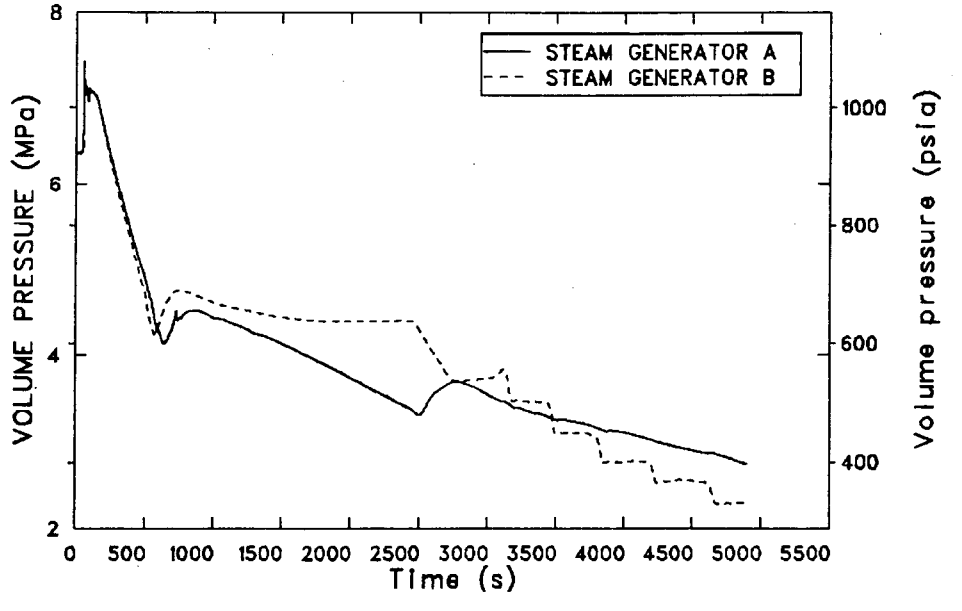

Figure 108. Pump suction break, SG secondary pressures.

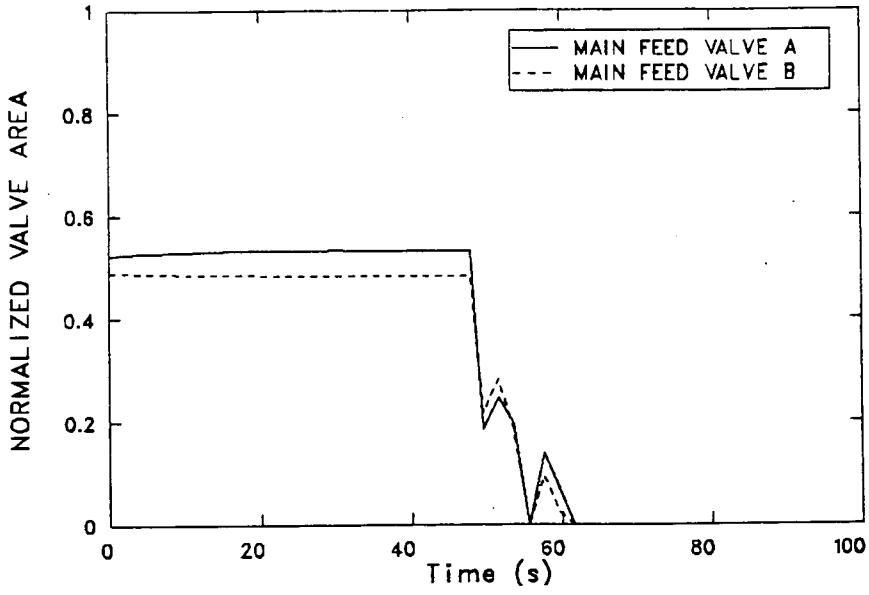

Figure 109. Pump suction break, normalized main feedwater valve area.

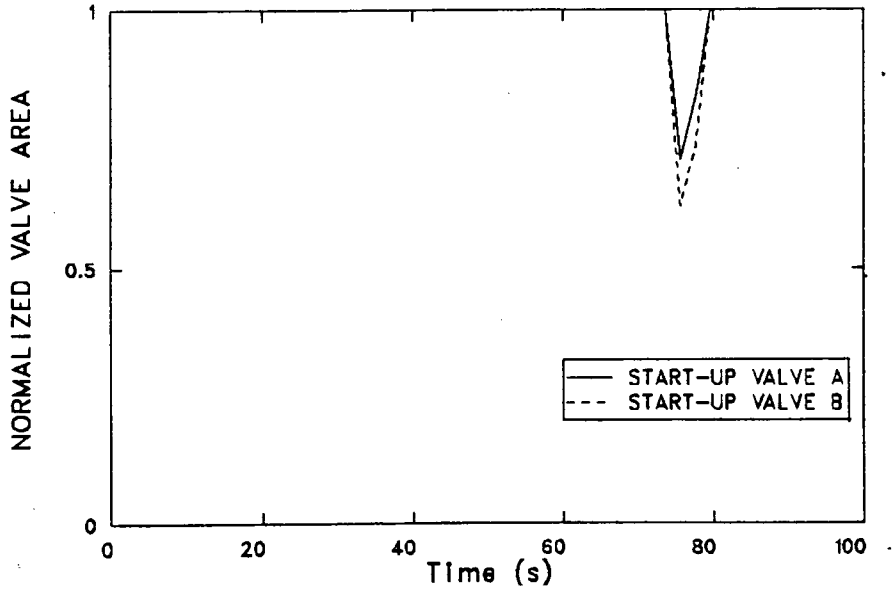

Figure 110. Pump suction break, normalized startup valve area.

discharge pressure setpoint, and the MFW pumps tripped. When the pumps tripped, the ICS began to open the MFW and startup valves. The opening response time for the startup valves was faster than that of the MFW valves; therefore, the startup valves opened almost immediately after the pump trip, as shown in Figure 110. The MFW valves remained closed because a sufficient signal from the ICS was needed to open them.

Due to volumetric liquid shrinkage, the primary system depressurization rate increased. Primary pressure dropped below the high pressure injection (HPI) setpoint at 94 s. At 100 s, the primary pressure dropped below the saturation temperature in the reactor vessel upper head, liquid flashed to steam, and the upper head began to void, as shown in Figure 111. The production of steam in the upper head momentarily stopped the depressurization and, as the upper head voided, resulted in a decrease in the depressurization rate, as shown in Figure 107. The trip of the reactor coolant pumps, 30 s after HPI initiation, also contributed to the decrease in the depressurization rate.

Coincidentally with the reactor coolant pump trip at 124 s, the main feedwater realigned to the emergency feedwater headers, and the steam generator secondary low level signal increased from 0.61 m (24 in.) to 6.1 m (240 in.). At this time the level in both generators was below the new low level signal, and emergency feedwater was initiated to both steam generators, as shown in Figure 112. As a result of the injection of cold emergency feedwater into the secondary system, the secondary system depressurization rate increased, as shown in Figure 108. At 135 s, the turbine bypass valves closed, as shown in Figure 113.

At 424 s the upper head was completely voided, and the depressurization rate increased until the pressure reached the saturation condition of the fluid in the top of the reactor vessel downcomer. The fluid in this volume flashed, slowing the depressurization rate. By 550 s, this volume was essentially voided and the depressurization rate again increased until the pressure reached the saturation condition of the fluid in the next lower volume.

At 500 and 545 s, respectively, the pressure in the steam generators A and B secondaries decreased below the pressure in the main feedline, the latter being primarily determined by the condensate booster pump head. Main feedline fluid began to flow into the steam generator secondaries via the startup valves and the emergency feedwater headers, as shown in Figure 112. The secondary liquid level rose above the low level setpoint, terminating emergency feedwater at 573 and 631 s for steam generators B and A, respectively. At termination of emergency feedwater, the temperature of the fluid entering the secondary via the emergency feedwater connection increased, thus decreasing the subcooling of the liquid entering secondaries. This resulted in an increase in secondary pressure, shown in Figure 108. Flow from the main feedline to the steam generators continued at a decreased rate because of the repressurization of the secondary systems. At 597 s, the B steam generator reached its high level limit, sending a signal to the ICS to close the B startup valve. At 675 s, the B startup valve had closed, isolating the B steam generator. Similarly, the A steam generator secondary reached its high level limit by 661 s, and the A startup valve had closed by 731 s, thus isolating the A steam generator. Shortly after the isolation of the secondaries, the steam generators became heat sources to the primary system. Secondary side pressures decreased, as shown in Figure 108, due to cooling of the secondary as heat was removed from the secondary to primary system.

Natural circulation was established in the primary loops by 600 s, as shown in Figures 114 and 115. After the steam generators became heat sources to the primary fluid, the temperature of the primary fluid exiting the steam generators was warmer than the fluid entering the generators, as shown in Figures 116 and 117. A density gradient was established in the loops so that the fluid densities entering the steam generator and in the cold legs were higher than the fluid density leaving the steam generator (see Figures 118 and 119). The low density fluid between the two high density fluids tended to slow the loop mass flow rate, as shown in Figures 114 and 115.

At 650 s, the volumetric HPI flow rate exceeded the volumetric break flow rate, as shown in Figure 120. The pressurizer level began to increase, as shown in Figure 121, and the primary system depressurization stopped, as shown in Figure 107. Also, liquid began entering the upper head, resulting in condensation effects which caused the primary system pressure oscillations shown in Figure 107, the pressurizer liquid level oscillations shown in Figure 121 and the upper head void fraction oscillations shown in Figure 111. By 1350 s, the void fraction in the upper head had collapsed; the

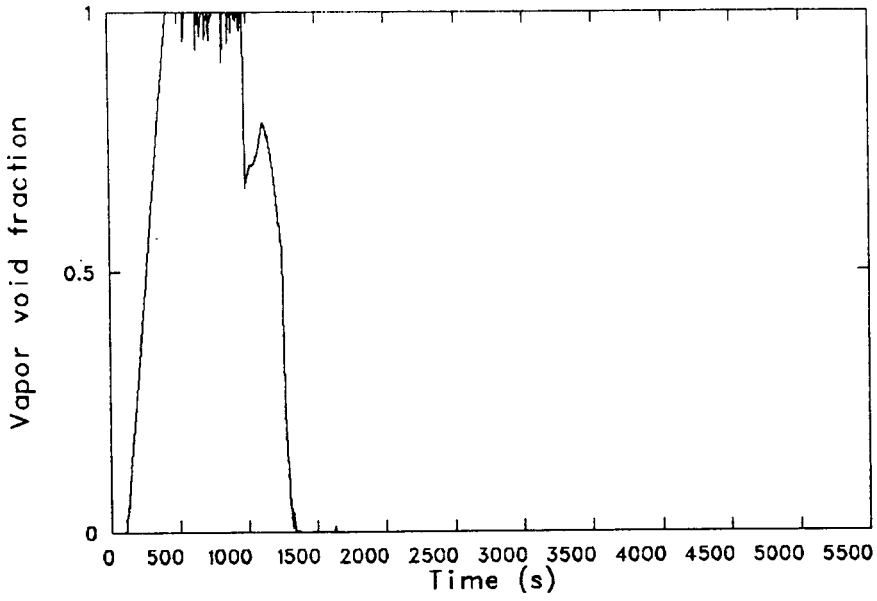

Figure 111. Pump suction break, RV upper head void fraction.

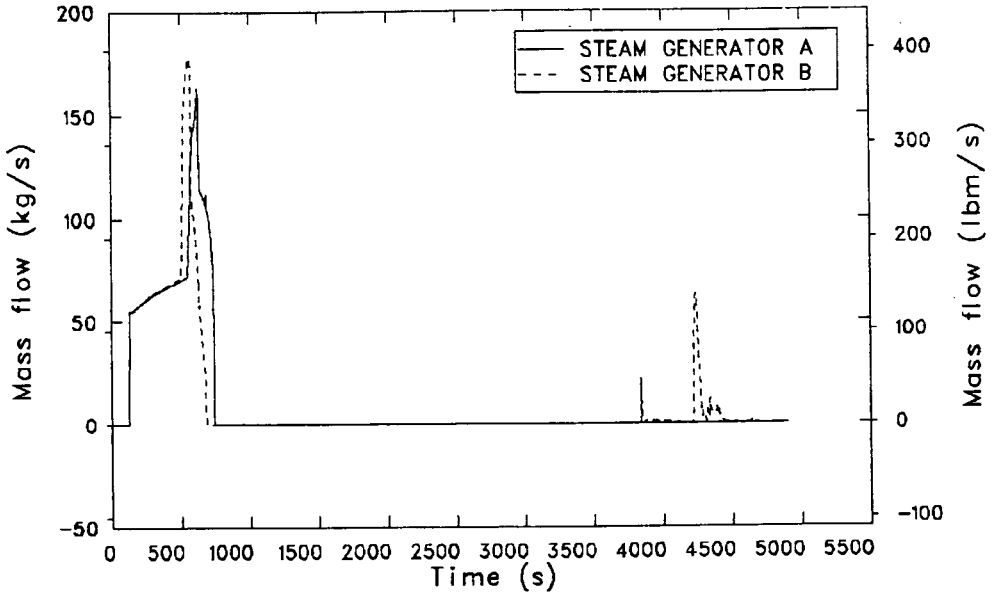

Figure 112. Pump suction break, EFW flow rates.

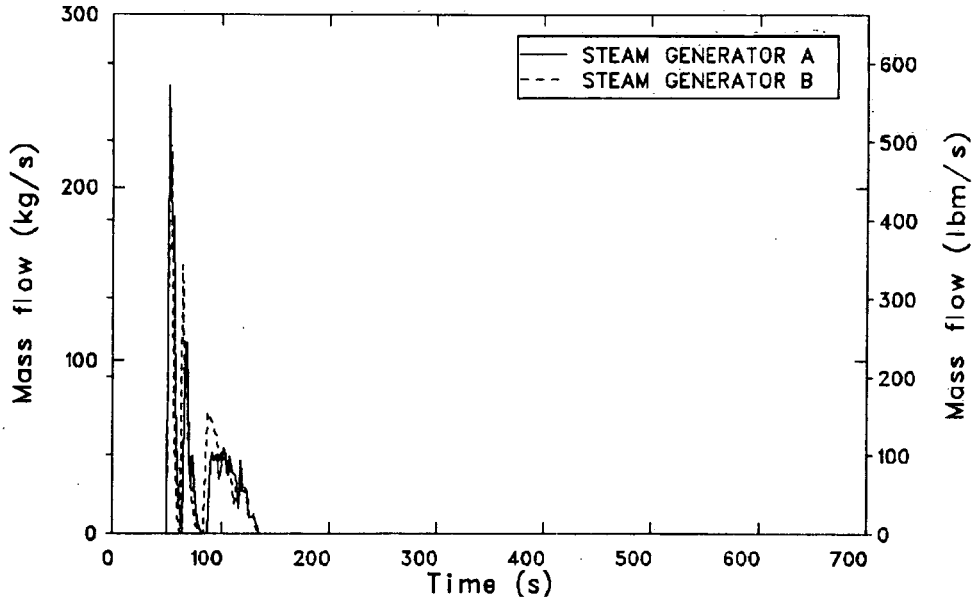

Figure 113. Pump suction break, turbine bypass flow rates.

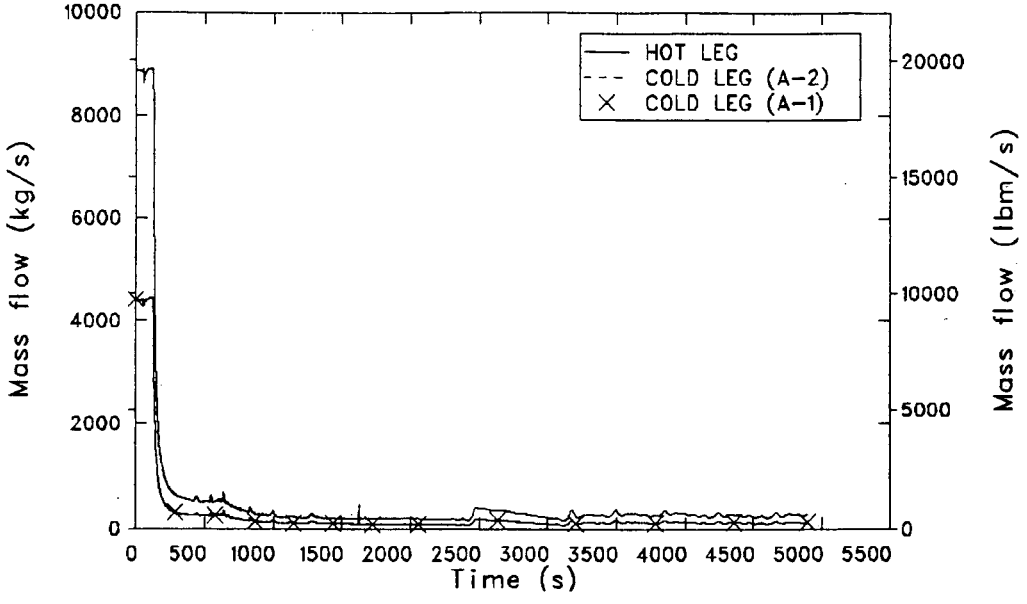

Figure 114. Pump suction break, loop A hot and cold leg mass flow rates.

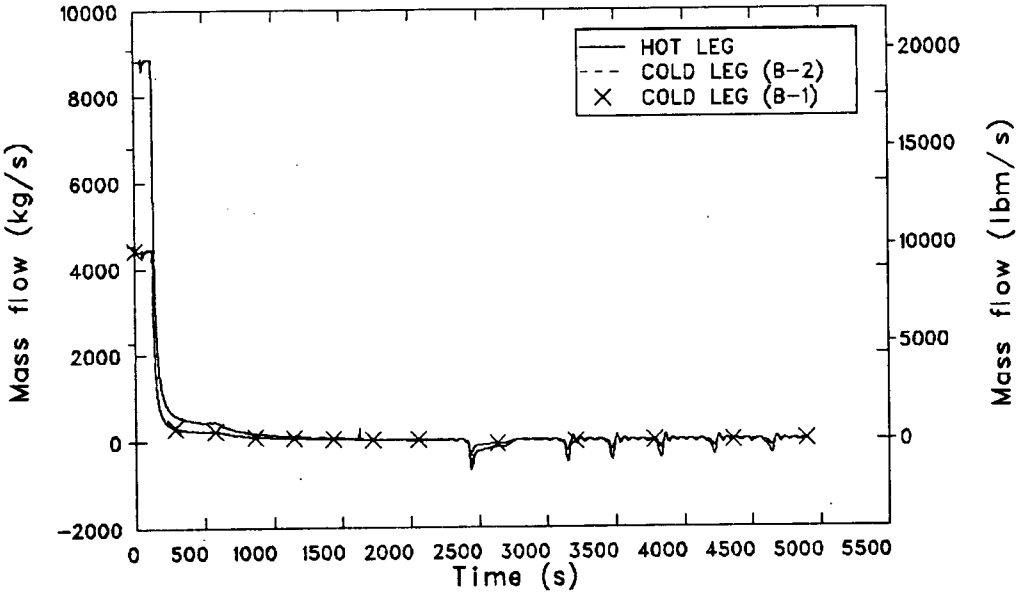

Figure 115. Pump suction break, loop B hot and cold leg mass flow rates.

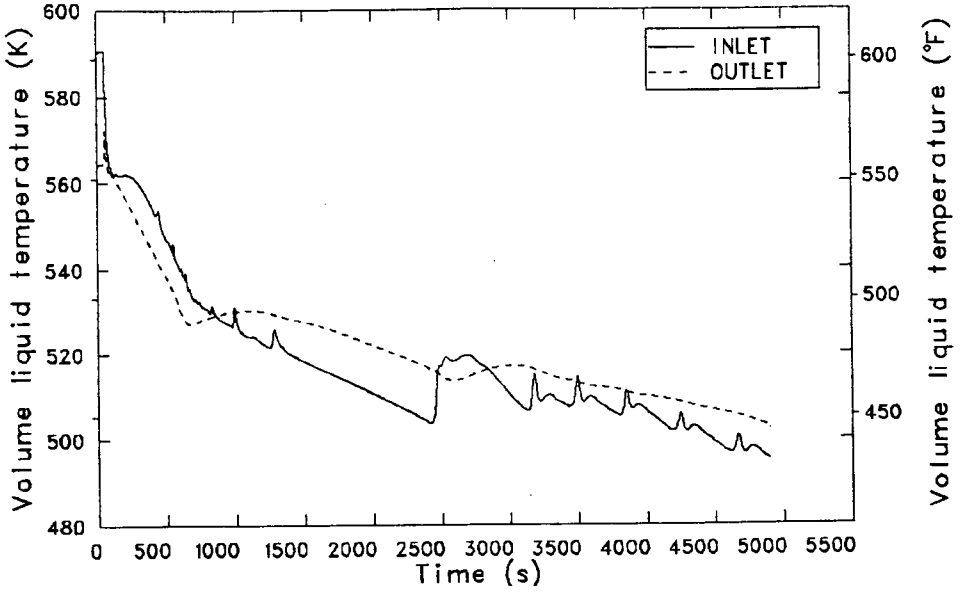

Figure 116. Pump suction break, loop A SG primary inlet and outlet fluid temperatures.

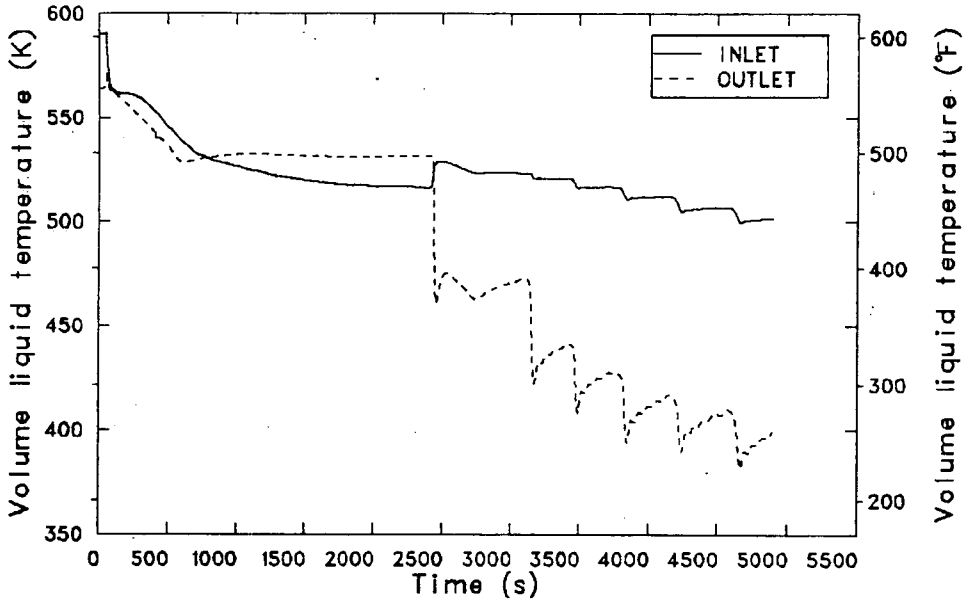

Figure 117. Pump suction break, loop B SG primary inlet and outlet fluid temperatures.

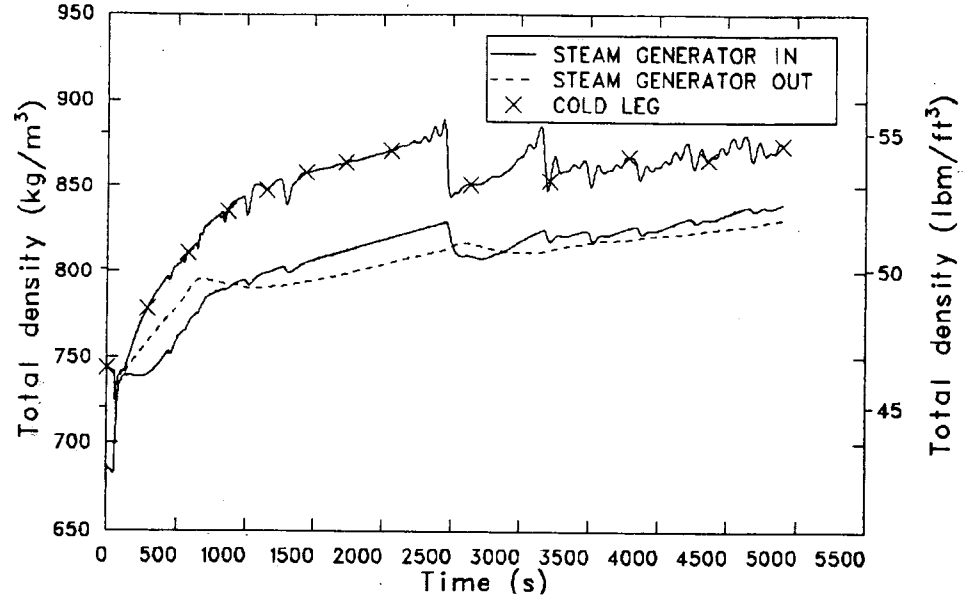

Figure 118. Pump suction break, loop A SG primary inlet and outlet fluid densities.

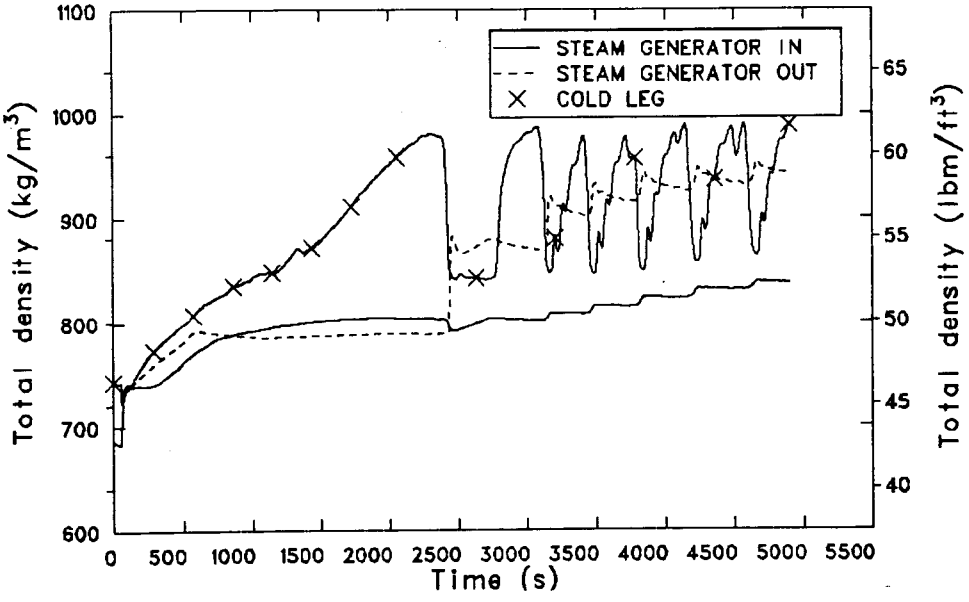

Figure 119. Pump suction break, loop B SG primary inlet and outlet fluid densities.

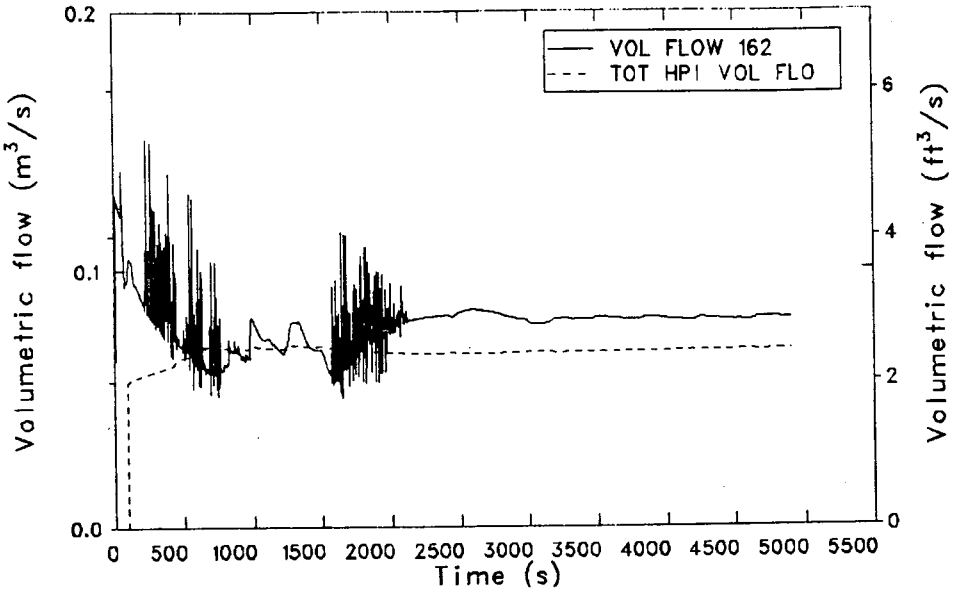

Figure 120. Pump suction break, HPI and break volumetric flow rates.

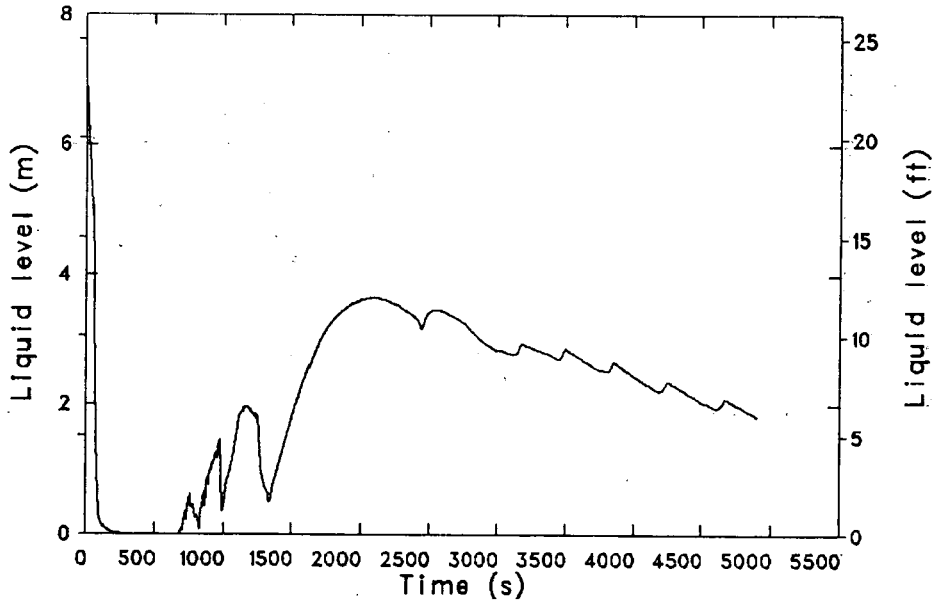

Figure 121. Pump suction break, pressurizer collapsed liquid level.

pressurizer level had rapidly increased, and the primary system had repressurized. At approximately this time, the mass escaping from the system through the break was exceeded by the mass injected into the system by the HPI, as shown in Figure 122.

Discontinuous flashing phenomena occurring in the pipe between the pump suction and the break caused the oscillations observed in the break flow (see Figure 120). Because of the near-saturation, or saturation, fluid temperature in the break pipe during primary system depressurization and repressurization, the fluid exiting the break oscillated between single- and two-phase conditions. This resulted in oscillations in the mixture density, which were used to calculate the break flow rate. As the primary system repressurized, the fluid exiting the break became single-phase, subcooled, and the oscillations damped out. At 2200 s the break mass flow rate became steady at a rate near the HPI mass flow rate, as shown in Figure 123. The primary system pressure, however, began decreasing because the volumetric break flow exceeded the volumetric HPI flow, as shown in Figure 120, and the primary system slowly depressurized.

By 1800 s the primary system was water-filled except for the top of the pressurizer. The break and HPI acted as heat sinks to remove decay heat, thereby continuing natural circulation in loop A. When the steam generator in the B loop changed from a heat sink to a heat source, natural circulation essentially stopped. Loop flow oscillations, which may have been established due to asymmetric flows and density gradients between the loops and the vent valve flow, further perturbed the B loop flow rate, as shown in Figure 124. Cold fluid from the HPI began to pool in the B loop cold legs, further decreasing the loop flow rate until the HPI inflow exceeded the cold leg flow into the reactor vessel. HPI flowed back into the cold leg toward the reactor coolant pump. This back flow occurred at 2250 s and resulted in an increase in the fluid density of the volumes upstream of the HPI connection point. The back flow lasted 20 s, as observed in Figure 124.

A similar back flow, occurring at 2320 s and lasting about 30 s, further increased the density of the fluid in the cold leg upstream of the HPI connection. Finally, at about 2390 s, a third reversal resulted in a density gradient between the pump suction leg and the steam generator tubes (see Figure 125) so that a complete flow reversal in the B loop occurred, as shown in Figure 18. As a result of the B loop flow reversal, the A loop mass flow rate increased, as shown in Figure 114. The flow reversal lasted 445 s, during which time the cold fluid in the B loop cold leg traveled through the pump and pump suction leg and into the steam generator tubes, while warm fluid from the reactor vessel downcomer entered the cold legs. At 3165 s, the density difference between the fluid in the steam generator tubes and that in the cold legs was such that the flow reversal stopped and normal

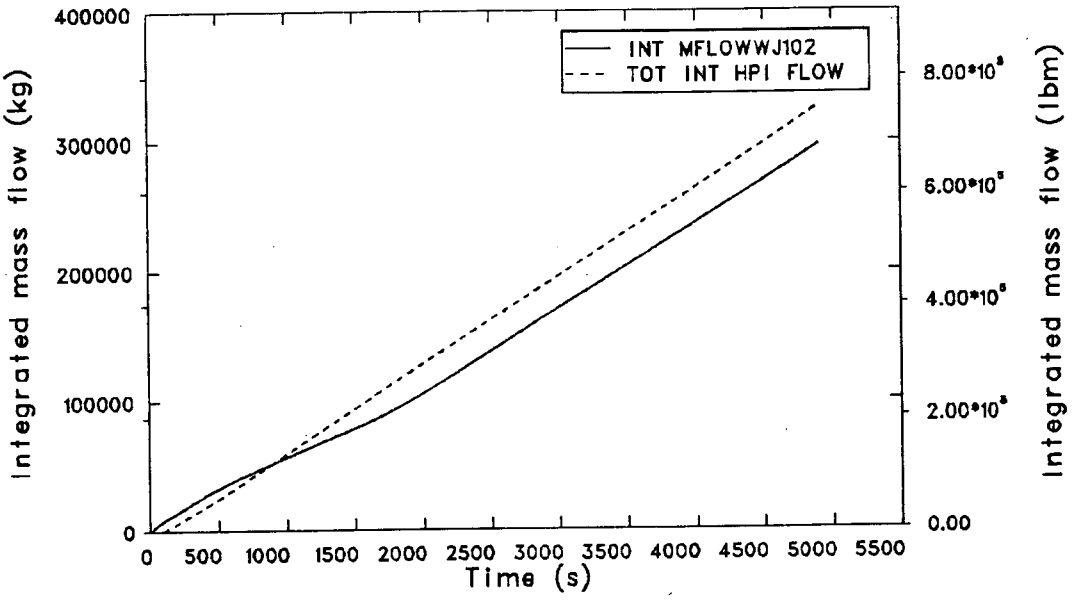

Figure 122. Pump suction break, break and HPI integrated mass flow rates.

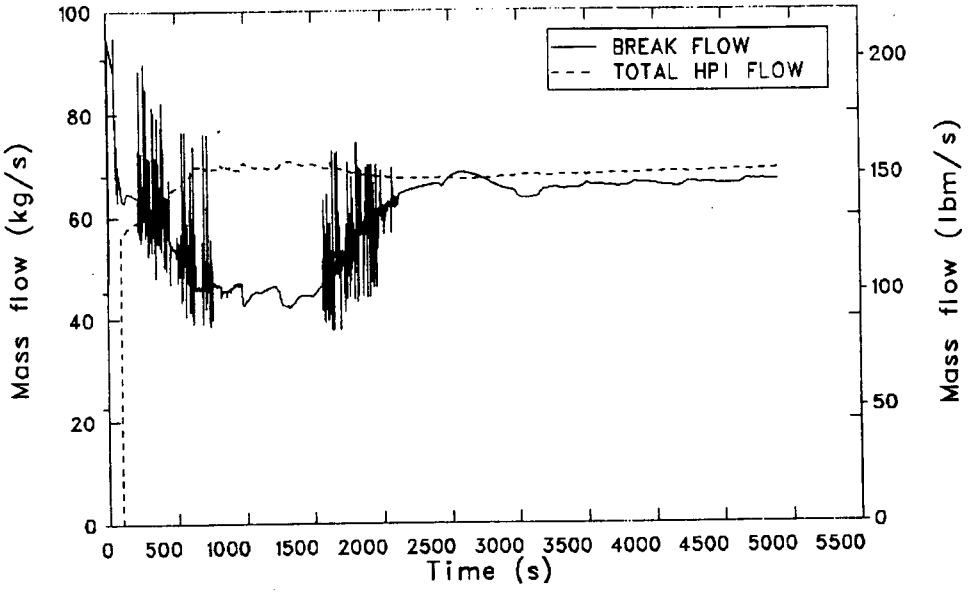

Figure 123. Pump suction break, break and HPI mass flow rates.

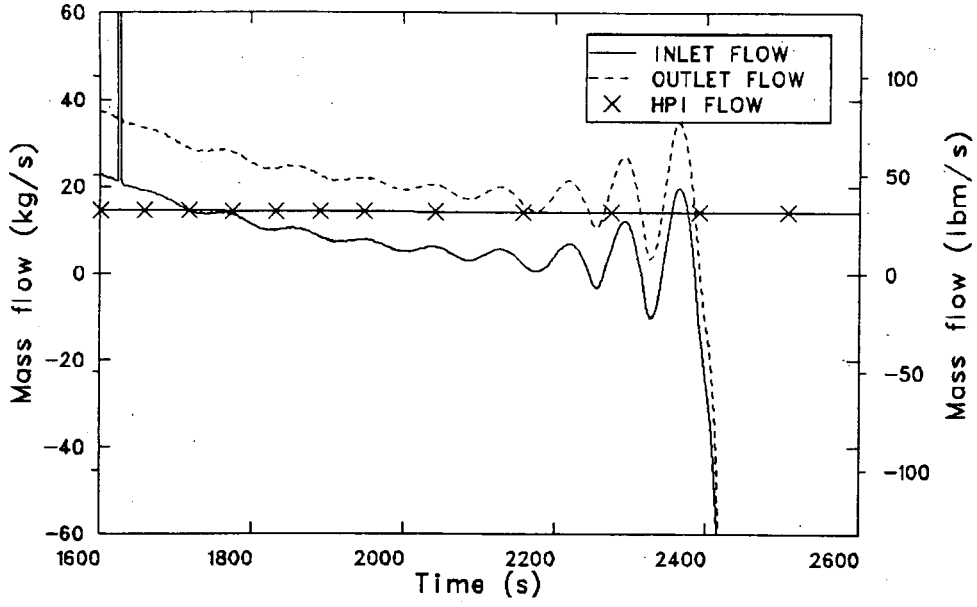

Figure 124. Pump suction break, cold leg B-2 mass flow rates in the region of the HPI injection site.

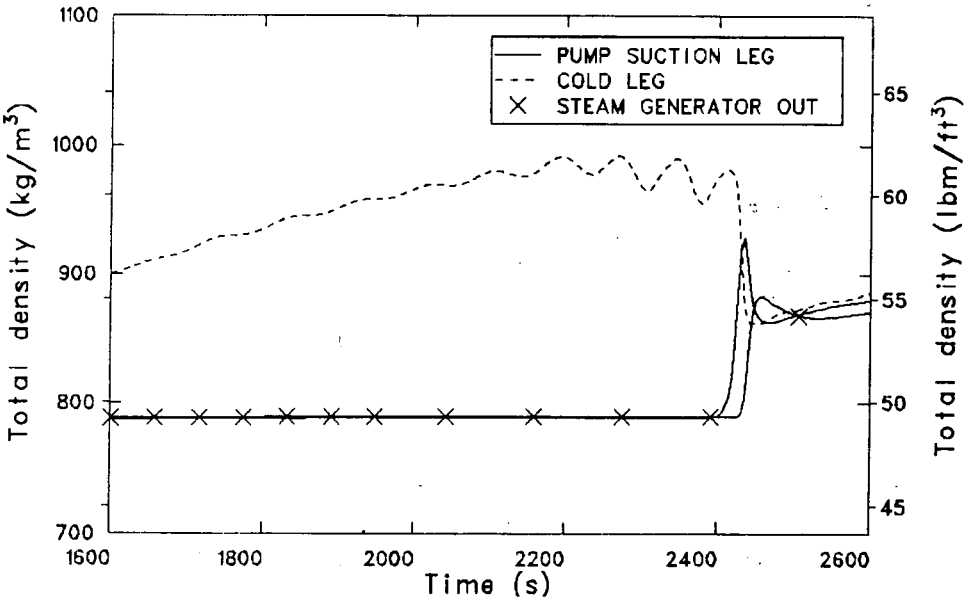

Figure 125. Pump suction break, fluid densities in loop B cold leg pump suction and SG outlet regions.

loop flow was reestablished. Similar flow reversals occurred throughout the remainder of the transient. The magnitude of the reversals decreased with time, as shown in Figure 115.

The flow reversals in the B loop, which began at 2390 s, effectively increased the downcomer fluid temperature by mixing the cold HPI fluid with the warm downcomer fluid (see Figure 126). Had the flow reversals continued, the effective temperature at 7200 s was extrapolated to be 446 K (343°F). The corresponding vessel downcomer pressure, shown in Figure 127, at 7200 s would have been 5.1 MPa (740 psia). Had the flow reversals in the B loop not occurred, cold HPI liquid from the B loop would have entered the vessel downcomer at the B loop HPI injection rate. This cold liquid would have mixed with the vent valve flow and the flow from the A loop cold leg. The overall result would have made the vessel downcomer temperature colder than that calculated with RELAP5. Uncertainty bars have been included in Figure 126 in order to represent the uncertainty in the liquid downcomer temperature history had the flow reversals not occurred. The coldest downcomer fluid temperature which would have been achieved, had the flow

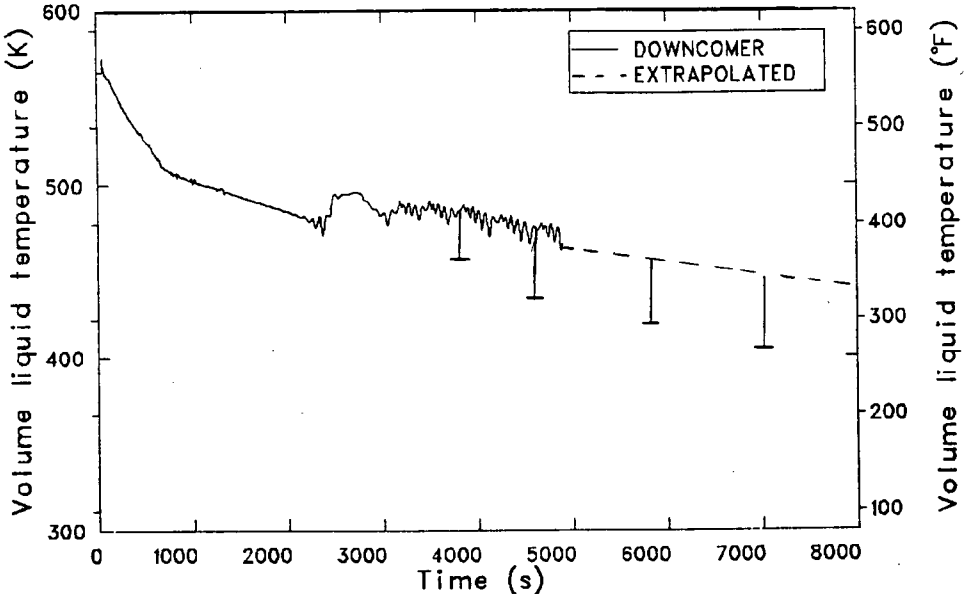

Figure 126. Pump suction break, RV downcomer fluid temperature.

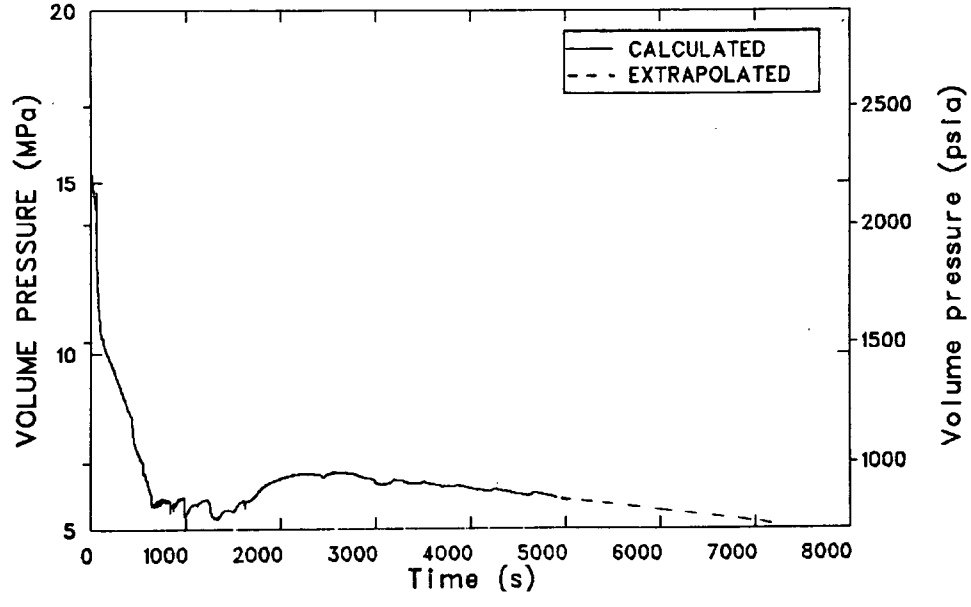

Figure 127. Pump suction break, RV downcomer fluid pressure.

reversals not occurred. The coldest downcomer fluid temperature which would have been achieved, had the flow reversals not occurred, was 390 K (242°F). The primary system pressure history would not be affected by the presence or absence of the flow reversals. In order to aid in future fracture mechanics calculations, Figure 128 shows the heat transfer coefficient of the reactor vessel wall inside surface.

The transient was terminated at 4900 s, after a pattern in the system pressure and temperature had been established. The primary system experienced a continuous cooldown, which was expected to continue. The depressurization of the primary system was not large enough to reach the core flood tanks injection pressure. Thus, core flood tanks flow was not established, and the break was not isolated. After HPI initiation, the HPI volumetric flow exceeded the volumetric break flow, and the primary system repressurized. At 2200 s, an equilibrium between the break mass flow rate and the HPI mass flow rate was established; however, the volumetric break flow rate exceeded the volumetric HPI flow rate, and the primary system slowly depressurized. Had the calculation been continued, an equilibrium between the volumetric break and HPI flows would have been established, and the primary system pressure would have stabilized.

Conclusions

At the end of the reactor coolant pump suction break sequence calculation, the downcomer fluid temperature was 470 K (386°F). The transient was extrapolated to 7200 s (2 h) and, at that time, the downcomer temperature was estimated to be 446 K (343°F) at a pressure of 5.1 MPa (740 psia).

The major uncertainty in the calculation is related to the existence of loop flow oscillations. Had these oscillations not been present in the calculation, the estimated downcomer fluid temperature at 2 h would have been 390 K (242°F).

The sequence requirement to isolate the break by closing the motor block valve in the letdown line, was not encountered, because core flood tank injection did not occur. Had this isolation occurred, the subsequent maximum primary pressure would have been ∿17.0 MPa (2465 psia), the opening pressure setpoint of the power-operated relief valve.

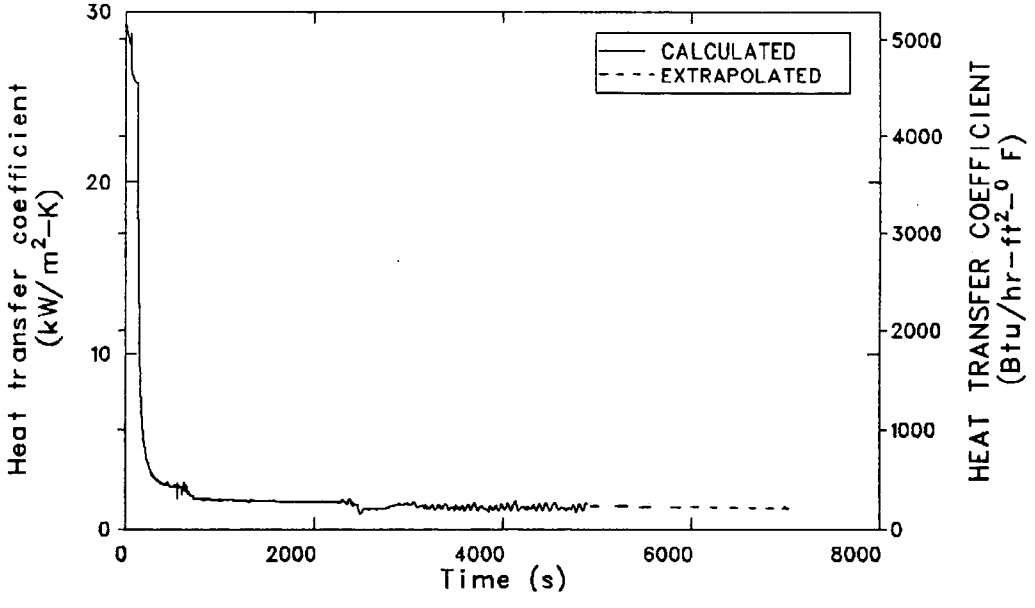

Figure 128. Pump suction break, heat transfer coefficient of RV downcomer inside surface.

9. STEAM GENERATOR TUBE RUPTURE TRANSIENT

The following subsections contain the transient scenario description, modeling changes effected in order to perform this calculation, detailed analysis of the transient results, and conclusions drawn from the analysis.

Transient Scenario Description

The transient was initiated from full-power, steady state conditions (nominal temperature and pressure). The pressurizer heaters and spray operated as designed. The transient began with a rupture of a single steam generator tube (double ended break) in the A loop steam generator. It was assumed that the ICS operated as designed. The reactor scrammed and the turbine stop valves closed. Emergency feedwater started at low level limit signal, and secondary safety relief and turbine bypass valves operated as designed. At 20 minutes, the operator used the PORV to reduce the reactor coolant system pressure to 7.17 MPa (1039 psia). The operator also isolated the affected steam generator, based either on time or hot leg temperature criteria. In order to maintain 90 K (50°F) subcooling after steam generator isolation, the operator throttled the HPI and started one reactor coolant pump per loop. A transient scenario is provided in Table 22.

Model Changes

To incorporate the tube rupture, the following changes were made to the steady state model:

Table 22. Steam generator tube rupture transient scenario

1.	Steam generator A tube ruptures (double-ended break).
2.	Reactor trips; turbine trips; turbine stop valves close; heater drains close.
3.	HPI actuates on low primary pressure.
4.	Operator trips the reactor coolant pumps 30 s after HPI initiation.
5.	ICS controls main feedwater, based on steam generator level signals.
6.	Main feedwater pump protection system operates as designed.
7.	Main feedwater pumps trip on high steam generator A level.[a]
8.	Emergency feedwater pumps start on low main feedwater pump discharge pressure.[a]
9.	Emergency feedwater flow is controlled by steam generator level.[a]
10.	Secondary safety relief and turbine bypass valves function as designed.
11.	At 20 min, operator uses PORV to reduce primary pressure to 7.17 MPa (1040 psia).[a]
12.	Operator isolates affected steam generator at 20 min, or when hot leg temperature <558 K (545°F), whichever is later.
13.	Following isolation of affected steam generator, operator throttles HPI to maintain 28 K (50°F) subcooling and restarts one reactor coolant pump per loop.

a. Event is dependent upon phenomena encountered.

- The rupture was assumed to be a double-ended break occurring at the top tube sheet in the A steam generator.

- The tube side of the break was modeled using a four-volume pipe component; the broken end of the tube was connected to the upper volume of the secondary (Cell 32501 in Figure 5) by means of a junction.

- The tube sheet side of the break was connected, by means of a junction, to the same secondary volume.

- Two time-dependent volumes and junctions were incorporated into the primary system to represent the letdown and makeup systems.

The makeup system flow was controlled by the pressurizer liquid level in such a way that, if the pressurizer level dropped below 5.588 m (18.333 in.), the makeup flow would increase by a factor of three. The letdown flow remained constant until the time of HPI initiation, when both the letdown and makeup systems were isolated.

Transient Results

This section presents the result of the steam generator tube rupture calculation. A sequence of events of the transient is presented in Table 23.

The initiating event was the tube rupture, which occurred in the A steam generator. The secondary pressure in the A steam generator increased as a result of primary fluid flashing upon entering the secondary side. The pressure increase propagated up the main feed line to the A main feed valve, reducing the differential pressure across the valve, and therefore reducing the flow into the steam generator. To maintain the desired flow, the feed flow mismatch controller opened the valve, and the main feedwater pump speed increased to maintain the differential pressure across the valve. At the same time, the main feed valve for the B steam generator closed, because of the higher flow from the increased main feedwater pump speed. The valves oscillated until a new steady state value was achieved by the ICS.

As a result of the tube rupture, as shown in Figure 129, the primary system pressure decreased. Pressurizer heaters were turned on as the pressure decreased. By 180 s, all the heaters were on and the primary system pressure momentarily increased, resulting in a slight increase in the break mass flow rate through the tube side of the break, as shown in Figure 130. The increase in break mass flow rate was enough to reverse the primary system repressurization; at 220 s, primary depressurization began again.

At 319 s, the reactor tripped due to violation of the pressure, temperature relationship. This resulted in a turbine trip, closure of the turbine stop valves and closure of the feedwater heater drains. Also, the ICS ran back the main feedwater pump to its minimum speed and closed the main feedwater valves. Upon closure of the turbine stop valves, the secondary pressure, shown in Figure 131, increased to the turbine bypass setpoint and, momentarily, to the secondary safety valve setpoint, shown in Figures 132 and 133, respectively. Primary system pressure increased as a result of the increase in secondary system pressure and a decrease in primary-to-secondary heat transfer. However, due to increased steam cooling when the turbine bypass and safety valves opened, the primary system pressure rapidly decreased, as shown in Figure 129. As the primary system pressure decayed, the break mass flow from the tube side also decayed, as shown in Figure 130. However, the break mass flow from the tube sheet side increased, as shown in Figure 134. The mechanism used to increase the flow appears to be related to flow choking and to a decrease in the primary liquid temperature, which resulted in a higher liquid density. At 400 s, as the conditions at the break oscillated between choked and unchoked conditions, the tube sheet side break mass flow oscillated. This behavior persisted for 600 s. It has been occasionally observed that the RELAP5 code has difficulty in calculating break flows and in determining choked or unchoked conditions. It should be noted that the effect of the choking and unchoking on the overall results of the transient was minor, as will be explained later.

As a result of primary system depressurization, the level in the pressurizer decreased due to system shrinkage, as shown in Figure 135. At 325 s, the level in the pressurizer decreased below the setpoint level for increasing system makeup flow (220 in.), and the makeup flow increased from 1.4 kg/s (3.1 lbm/s) to 7.6 kg/s (16.8 lbm/s). At 336 s, the pressurizer level decreased below 127 in., and the pressurizer heaters turned off.

Table 23. Steam generator tube rupture transient sequence of events

Event	Time (s)
Steam generator tube rupture in steam generator A occurs. ICS adjusts MFW valves to compensate for perturbation in steam generator A secondary system.	0.0
Reactor scram (P, T relationship) turbine trip; turbine stop valve closes; heater drains close over 5 s period; ICS runs back MFW pumps and MFW valves.	319.2
Pressurizer heaters come on, due to low primary pressure.	321.6
Pressurizer level drops below 5.6 m (220 in.) and makeup flow increases.	325.4
Pressurizer level drops below 3.2 m (127.6 in.), tripping the pressurizer heater power.	336.3
Main feedwater pumps trip on high discharge pressure, due to ICS running back the startup valves.	349.0
Primary pressure increased, due to reduction in primary-to-secondary heat transfer.	650.0
Level in steam generator B secondary oscillates around low level setpoint, allowing periodic flow of emergency feedwater into secondary system; periodic flow of emergency feedwater enhances primary-to-secondary heat transfer; primary pressure turns over.	775.0
Primary pressure drops below HPI setpoint; HPI flow initiated; makeup and letdown flow stops.	942.4
RCPs trip 30 s after HPI initiation; steam generator low level setpoint increases and motor- and turbine-driven emergency feedwater systems turned on; increased primary to secondary heat transfer enhances primary fluid cooldown.	972.4
Liquid in the main feedline begins to flow into steam generator B through the start-up valve and crossover due to the decrease of the secondary pressure below the booster pump head.	1280.0
Liquid in the main feedline begins to flow into steam generator A through the start-up valve and crossover, due to the decrease of the secondary pressure below the booster pump head.	1300.0
Liquid level in steam generator A increases above the low level limit setpoint, and EFW into the secondary was terminated.	1396.6
Liquid level in steam generator B increases above the low level limit setpoint, and EFW into the secondary is terminated.	1415.5
Liquid level in steam generator A rises above the high level limit setpoint, and ICS closes the startup valve, isolating steam generator A.	1426.0
Liquid level in steam generator B rises above the high level limit setpoint, and ICS closes startup valve, isolating Steam Generator B.	1437.6
Steam generators become heat sources; primary temperatures begin to increase.	1600.0
Primary pressure reaches PORV setpoint; the valves oscillate around the setpoint.	2200.0
Pressurizer becomes liquid-full.	2450.0
Transient terminated; vessel downcomer liquid temperature at 517 K (471°F) and increasing; pressure at the PORV setpoint (17.0 MPa, 2465 psia).	2800.0

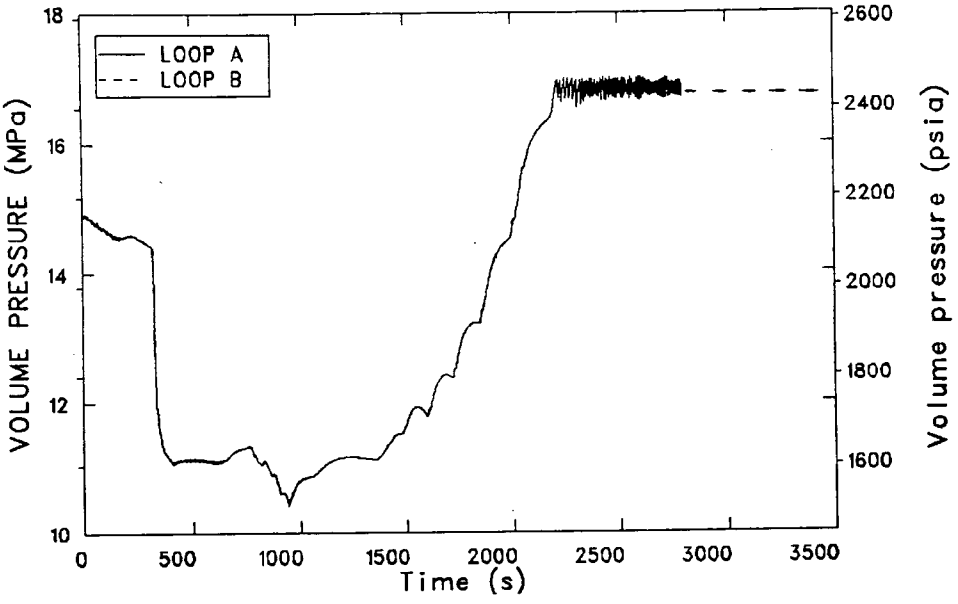

Figure 129. SG tube rupture, hot leg pressures.

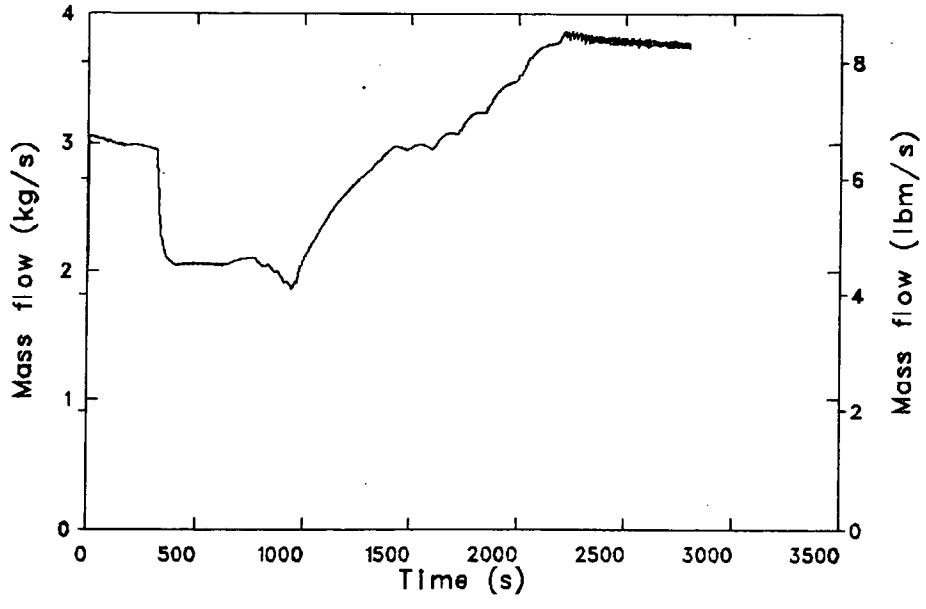

Figure 130. SG tube rupture, tube side break mass flow rate.

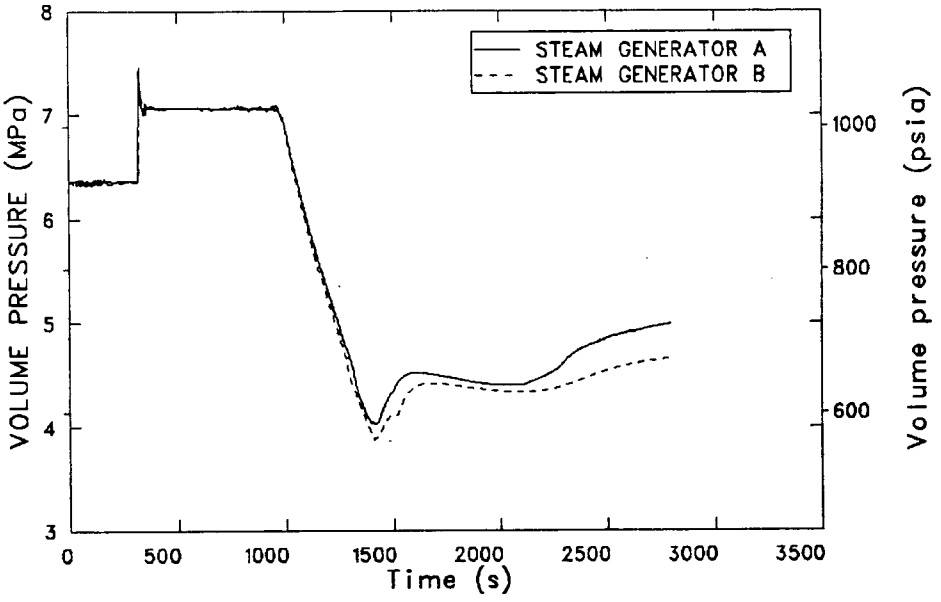

Figure 131. SG tube rupture, SG secondary pressures.

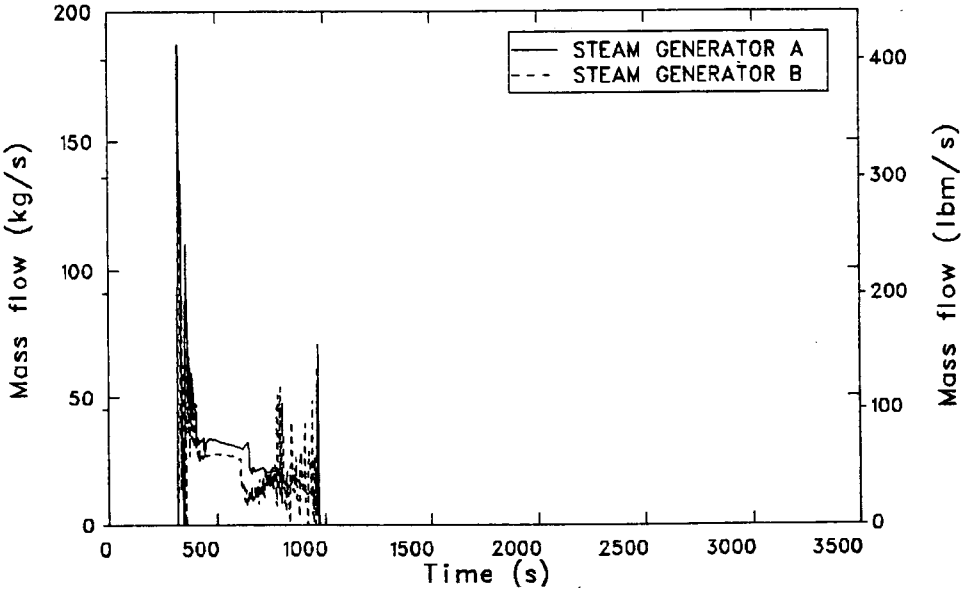

Figure 132. SG tube rupture, turbine bypass mass flow rates.

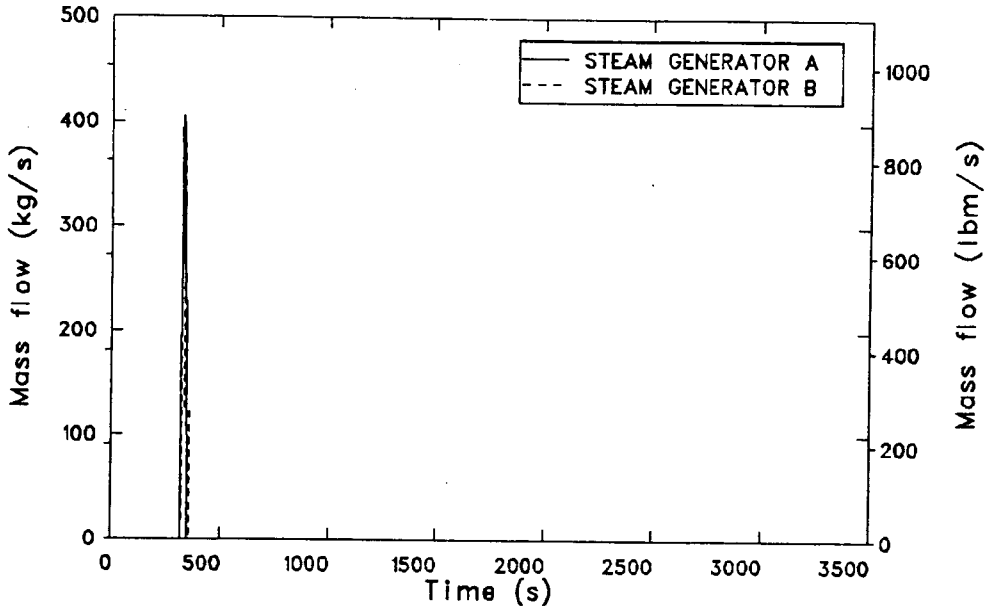

Figure 133. SG tube rupture, SG relief valve mass flow rates.

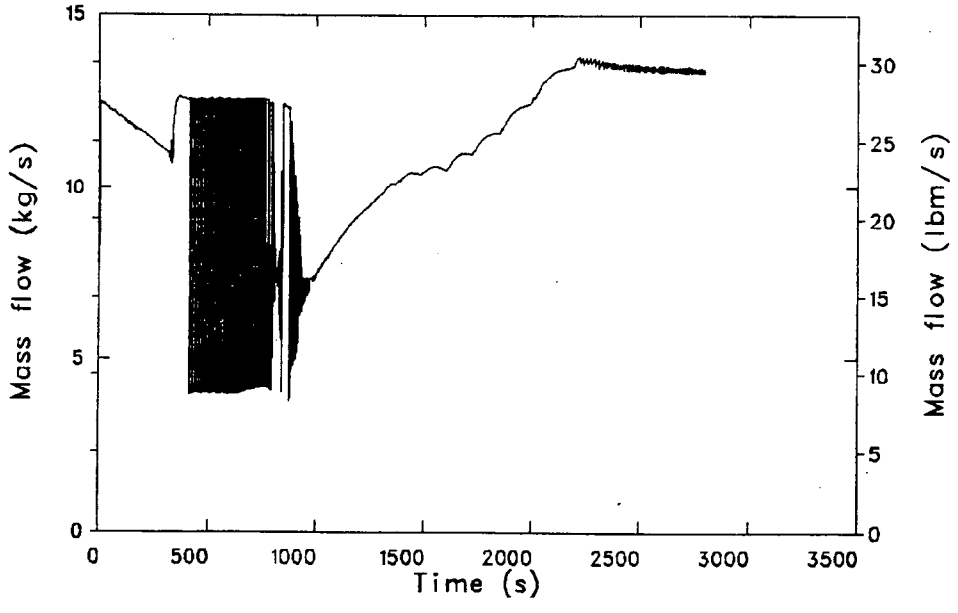

Figure 134. SG tube rupture, tube sheet side break mass flow rate.

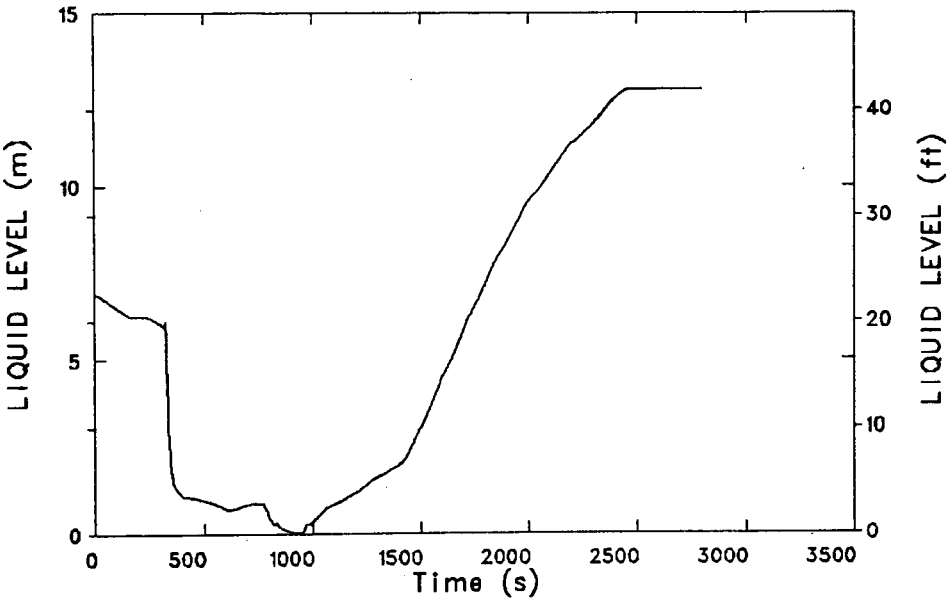

Figure 135. SG tube rupture, pressurizer collapsed liquid level.

The secondary liquid level rapidly decreased, due to the opening of the turbine bypass and safety valves at reactor scram, as shown in Figures 136 and 137. As a result of the decrease in liquid level, the heat transfer between the primary and secondary decreased, as shown in Figure 138. Also affecting the reduction in primary-to-secondary system heat transfer was the tripping of main feedwater pumps, due to high discharge pressure when the ICS began closing the startup valves at 349 s. After the pumps were tripped the startup valves opened because of the feed-flow mismatch controller. At 650 s, the primary-to-secondary heat transfer rate further decreased, due to a corresponding decrease in secondary liquid level. This resulted in an increase in the primary system pressure, as shown in Figure 129. The pressure continued to increase until 775 s, when: (a) the level in the B steam generator decreased below the 24-in. low level set point, and (b) the emergency feedwater system for the B steam generator was started in order to maintain the 24-in. level, as shown in Figure 139. The introduction of cold emergency feedwater flow into the steam generator secondary system enhanced the primary-to-secondary heat transfer so that the primary system pressure began to decrease once again.

The primary system pressure continued to decrease until 942 s, at which time the pressure reached the HPI setpoint, initiating HPI flow. As shown in Figure 140, the HPI flow overwhelmed the total break flow, and, with the primary system liquid-full, the HPI inflow began filling the pressurizer, as shown in Figure 135. This repressurized the primary system, as shown in Figure 129, and resulted in an increase in break mass flow rate, shown in Figure 140. Thirty seconds after HPI initiation the reactor coolant pumps were tripped, and loop flow decreased to natural circulation rates, shown in Figures 141 and 142.

When the reactor coolant pumps tripped, the secondary side low level setpoint signal increased to 240 in., and full emergency feedwater flow was initiated to each steam generator, as shown in Figure 139. The cold emergency feedwater entering the secondary system resulted in a rapid depressurization of the secondary, shown in Figure 131, and in termination of turbine bypass flow shown in Figure 132. At 1280 and 1300 s, the pressure in both B and A steam generators, respectively, fell below the condensate booster pump head. Flow from the main feed line began into the steam generators via the startup valves and emergency feedwater headers. At 1396 and 1415 s, the level in steam generators A and B, respectively, increased to the low level set point, and emergency feedwater was terminated. However, flow from the main feedline continued until 1426 and 1437 s for steam generators A and B, respectively. At that time the level had increased to the high level setpoint, and the ICS closed the startup valves, isolating the steam generator secondaries. With the cooling mechanism removed from the secondary side, the pressure began to increase, as shown in Figure 131.

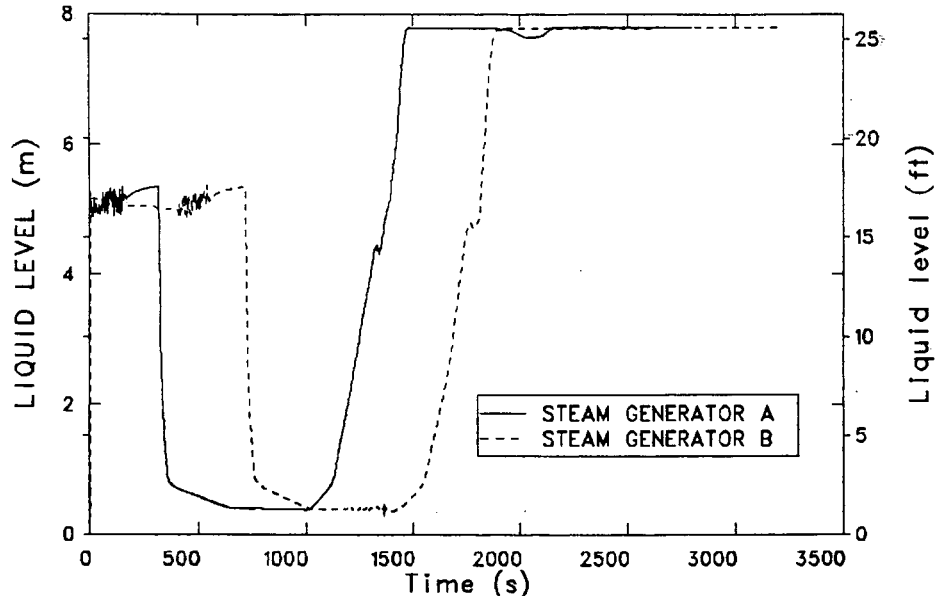

Figure 136. SG tube rupture, SG operating levels.

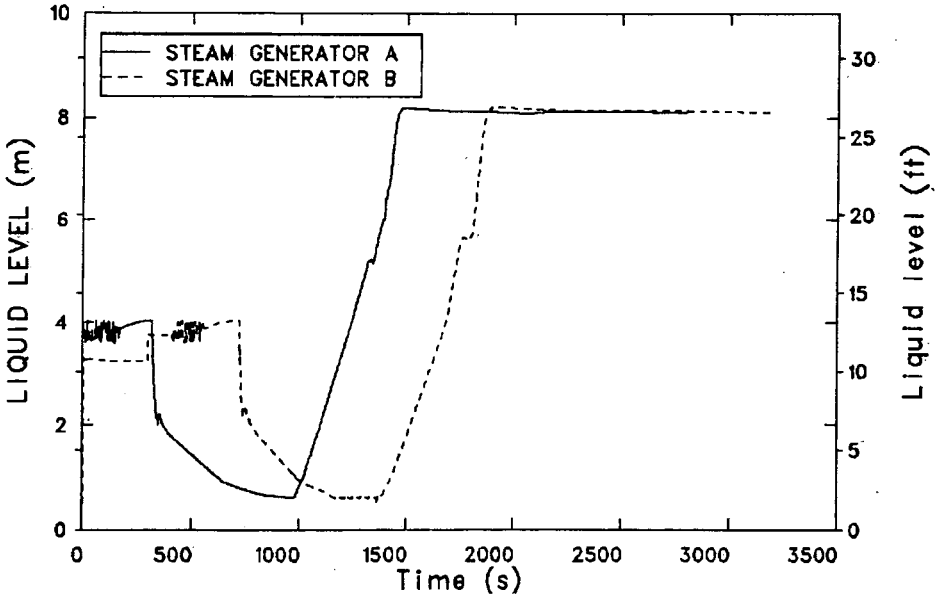

Figure 137. SG tube rupture, SG start-up levels.

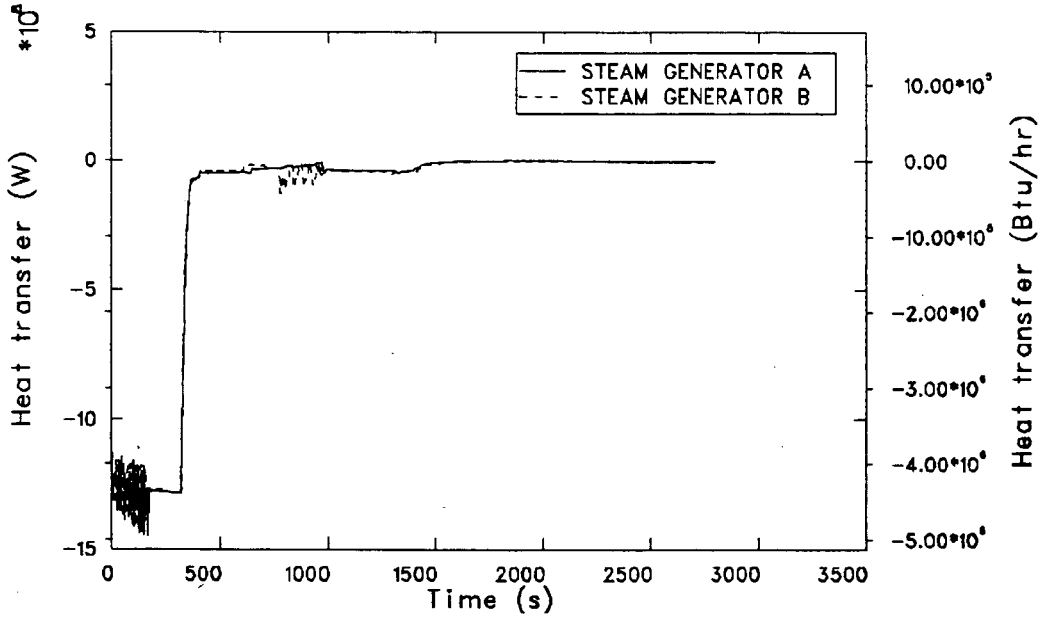

Figure 138. SG tube rupture, SG heat removal rates.

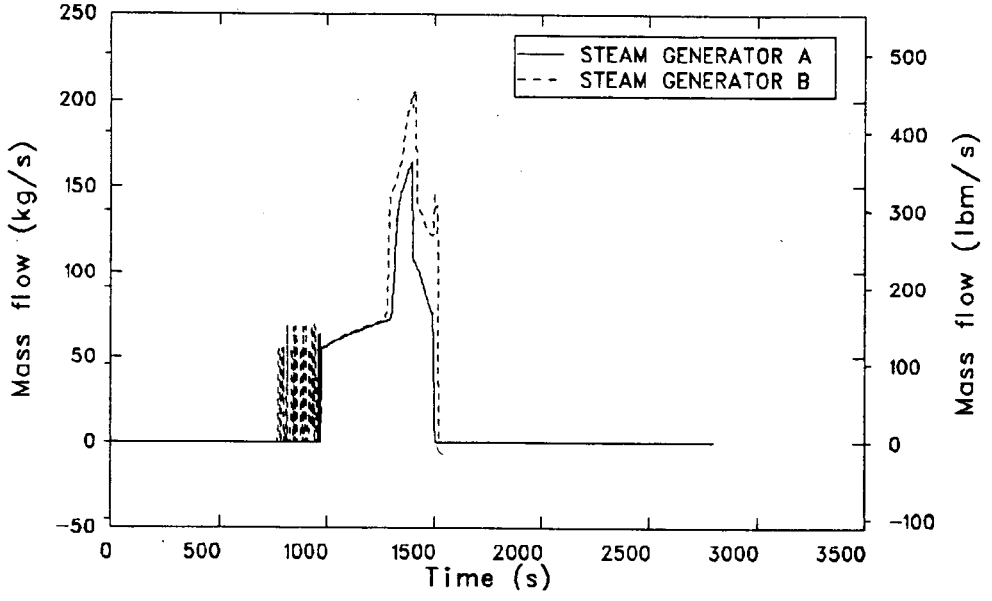

Figure 139. SG tube rupture, EFW header mass flow rates (sum of EFW and MFW delivered at the EFW header).

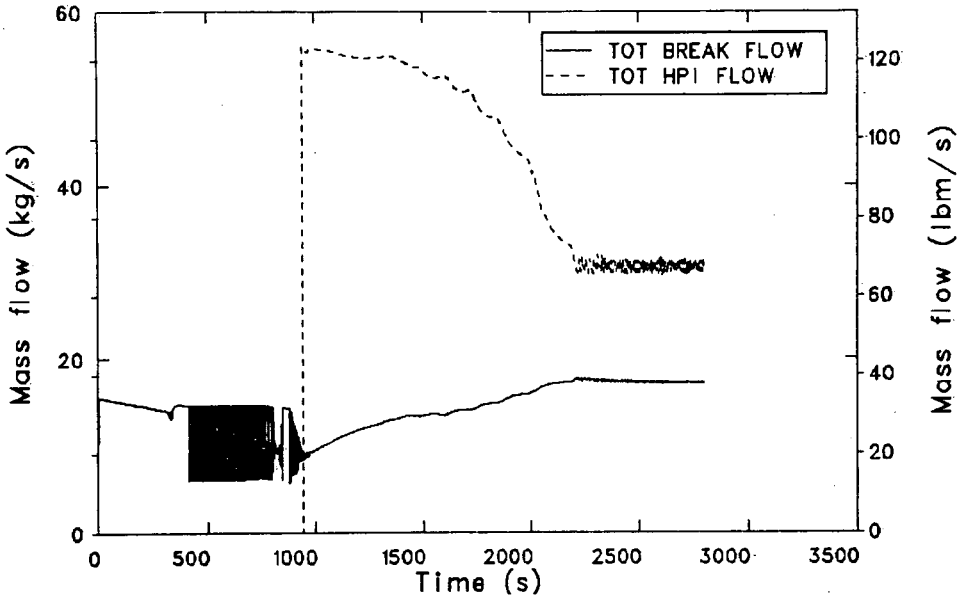

Figure 140. SG tube rupture, total break and total HPI mass flow rates.

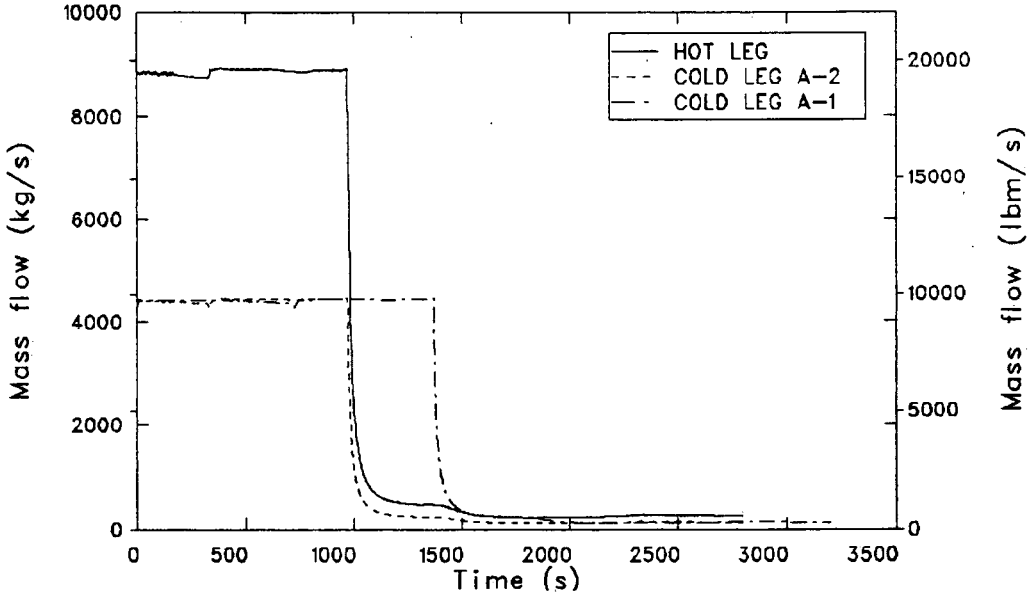

Figure 141. SG tube rupture, loop A hot and cold leg mass flow rates

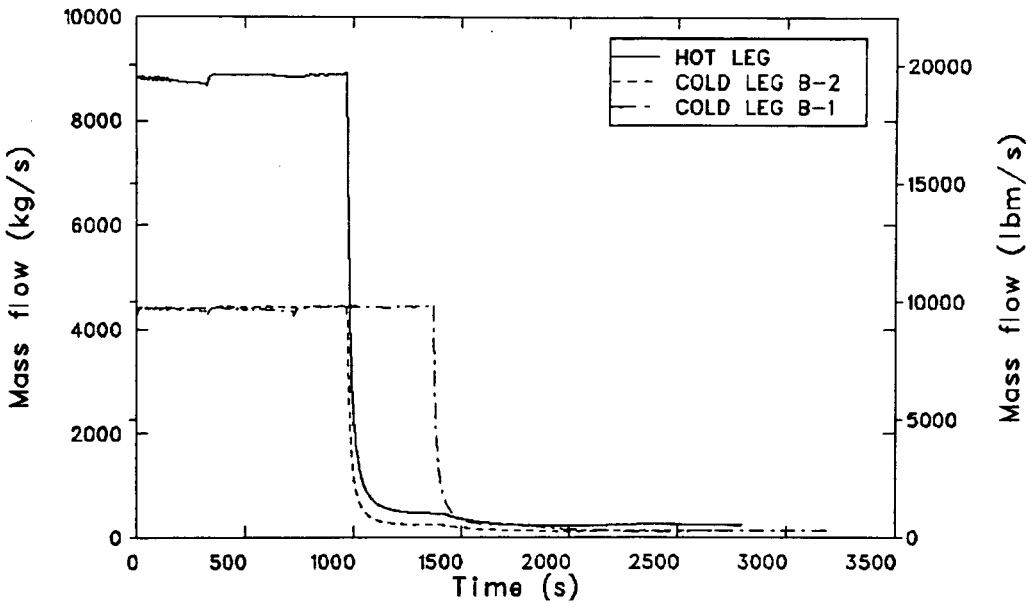

Figure 142. SG tube rupture, loop B hot and cold leg mass flow rates.

Primary system coolant temperatures decreased upon initiation of HPI, as shown in Figures 143 and 144. At 1600 s, the secondary liquid temperature became warmer than the primary temperature, so that the overall primary-to-secondary heat transfer reversed and the steam generators became heat sources to the primary system. As shown in Figure 131, secondary pressures decreased as a result of the heat given up by the secondaries. Primary system liquid temperatures increased, as shown in Figures 143 and 144. The lowest primary system liquid temperatures were calculated at this time.

At 2200 s, the primary pressure reached the PORV setpoint and oscillated around the setpoint, as shown in Figure 129. Throughout the duration of the transient the PORV held the pressure at its opening setpoint. Also, the primary liquid temperature had increased enough that the net primary-to-secondary heat transfer was nearly zero, with the generators acting as slight heat sinks. At 2450 s, the pressurizer became liquid-full. The transient was terminated at 2800 s, at which time trends in the pressure and temperatures in the primary system had been established, allowing extrapolations to 7200 s.

Conclusions

At the termination of the transient, the primary system pressure was oscillating around the PORV setpoint pressure of 17.0 MPa (2465 psia). The reactor vessel downcomer liquid temperature, which is of PTS concern, was at 517 K (470°F) and increasing slightly. The response of the vessel downcomer pressure, liquid temperatures, and heat transfer coefficient are shown in Figures 145, 146, and 147, respectively, with extrapolations to 7200 s. As shown, the extrapolated values of pressure and temperature to 7200 s are 17.0 MPa (2465 psia) and 544 K (520°F), respectively. The lowest vessel downcomer liquid temperature was 505 K (450°F), which occurred at 1700 s. The heat transfer coefficient is provided for use in future fracture mechanics calculations.

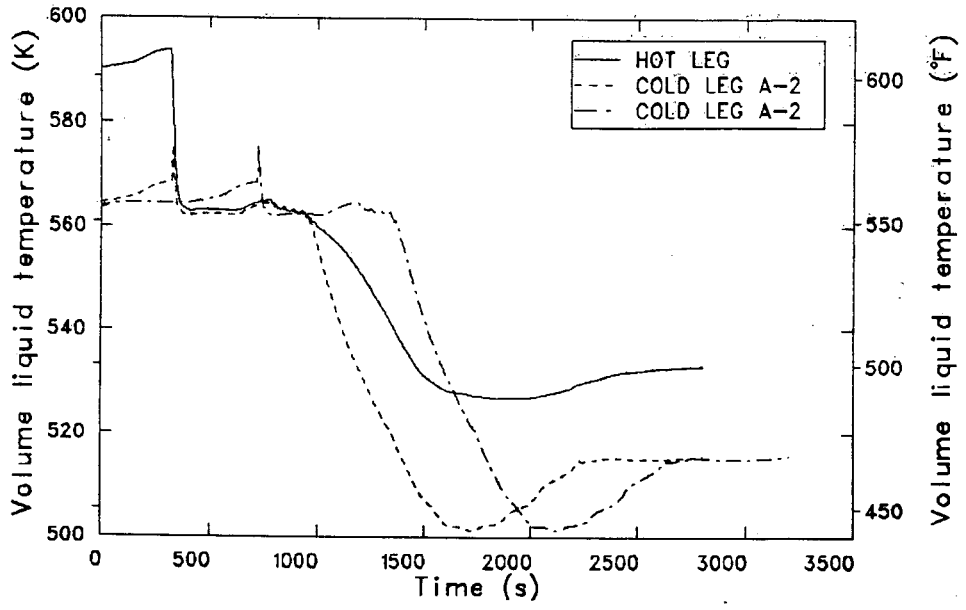

Figure 143. SG tube rupture, loop A hot and cold leg fluid temperatures.

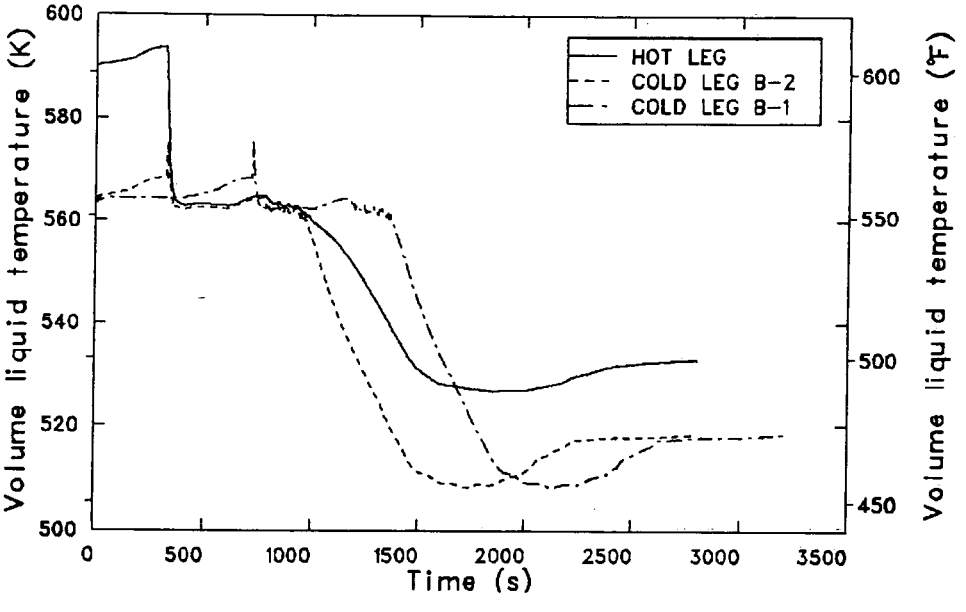

Figure 144. SG tube rupture, loop B hot and cold leg fluid temperatures.

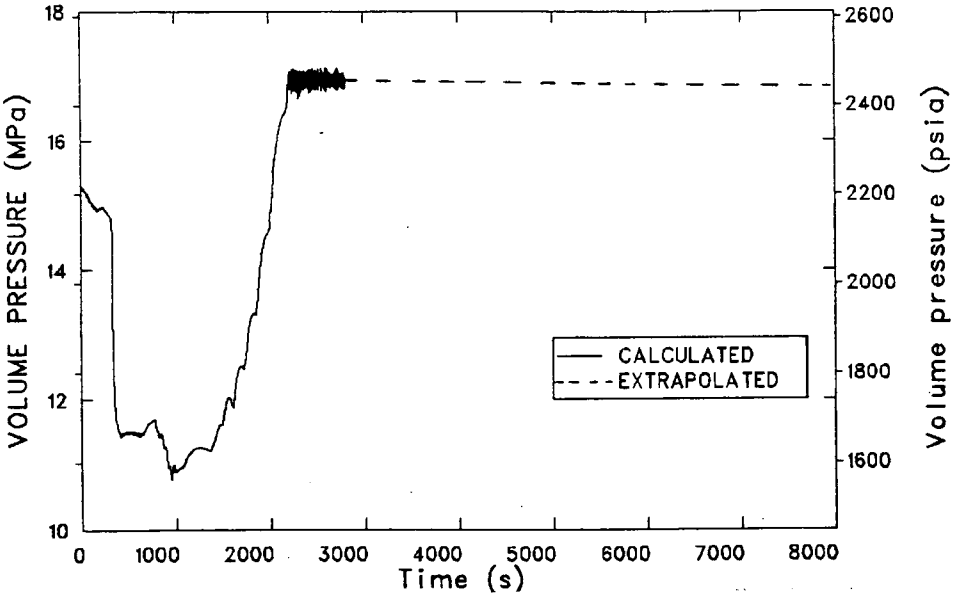

Figure 145. SG tube rupture, extrapolated RV downcomer fluid pressure.

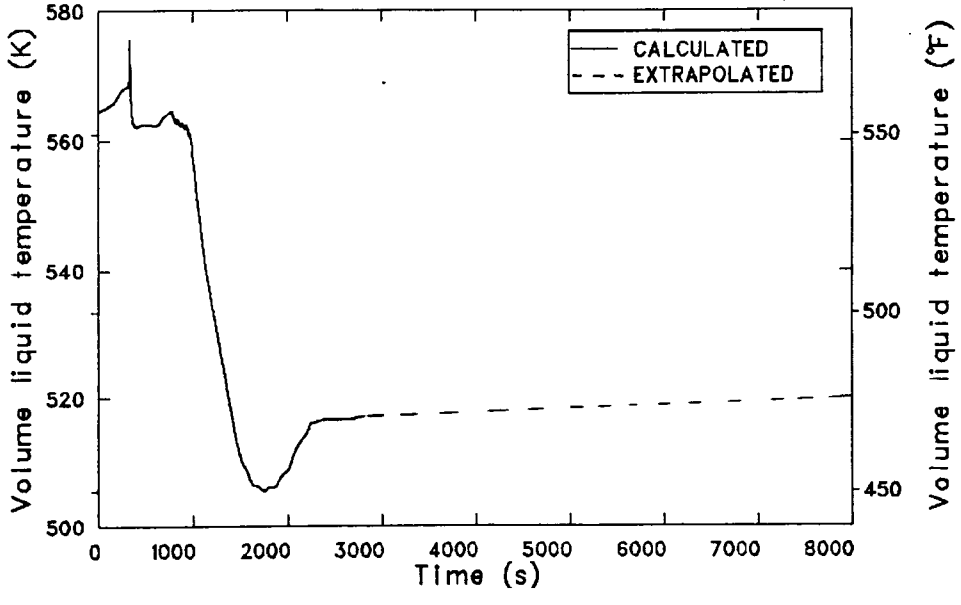

Figure 146. SG tube rupture, extrapolated RV downcomer fluid temperature.

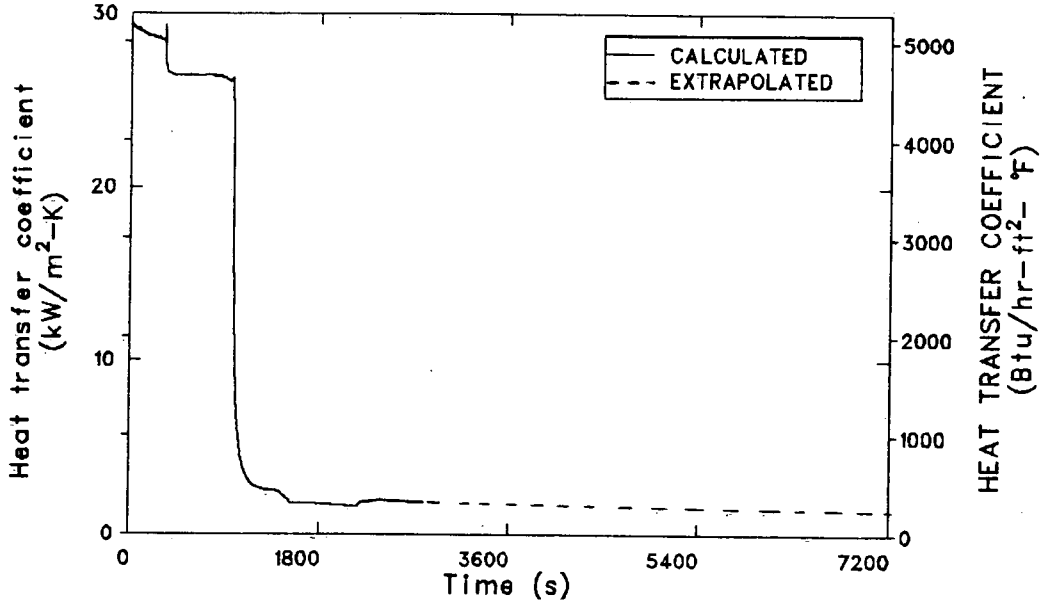

Figure 147. SG tube rupture, extrapolated heat transfer coefficient of RV downcomer inside surface.

10. OVERVIEW AND CONCLUSIONS

This report has presented analyses of the results of ten RELAP5 calculations pertinent to the study of pressurized thermal shock (PTS) in the Oconee-1 pressurized water reactor (PWR). One of these calculations simulated a turbine-trip transient which occurred in the Oconee-3 PWR. A comparison of code-calculated and measured data indicated generally good agreement, thus providing an informal and limited, but useful, qualification of the model. The remaining nine calculations simulated hypothetical rapid cooldown sequences with potential for primary system repressurization.

Table 24 presents a summary of minimum fluid temperatures and maximum subsequent fluid pressures in the reactor vessel downcomer for each of the nine sequences. The pressures and temperatures were calculated at the elevation of the first reactor vessel circumferential weld below the cold leg nozzles. Note that the pressures and temperatures shown are generally not coincident. The temperatures shown represent the lowest calculated or, in the event of calculations terminated before the end of the PTS 2-h period, the lowest extrapolated temperatures within the 2-h period. Uncertainty analyses were performed for calculations with the most severe outcomes. The effects of these uncertainties on the minimum downcomer fluid temperatures are also shown in Table 24.

Table 24. Summary tabulation of Oconee-1 PTS RELAP5 calculation results

Sequence	Reference Section in This Report	Minimum RV Downcomer Fluid Temperature		Maximum Subsequent RV Downcomer Fluid Pressure	
		K	°F	MPa	psia
Main steam line break					
RC pumps restarted 10 min after subcooling attained	3.1	481 403[b]	407 266[b]	17.0 17.34[a]	2465 2515[a]
RC pumps restarted at time subcooling attained	4.0	494 415[c]	429 287[c]	17.0 17.34[a]	2465 2515[a]
Steam generator overfeed					
MFW pumps tripped on low suction pressure	3.2	505	450	17.0 17.34[a]	2465 2515[a]
Maximum sustainable without tripping MFW pumps	5.0	500	440	17.0 17.34[a]	2465 2515[a]
Failure open of 4 TBP valves at reactor hot standby	6.0	387	237	17.0	2465
Small break LOCA					
Stuck-open PORV, RC pumps not tripped	3.3	545	521	11.38	1650
Two-inch diameter pressurizer surge line break	7.0	355 305[d]	180 90[d]	1.48	214
Two and one-half inch diameter RC pump suction break	8.0	446[e] 390[h]	343[e] 242[h]	5.10[f] 17.34[a]	740[f] 2515[g]

Table 24. (continued)

Sequence	Reference Section in This Report	Minimum RV Downcomer Fluid Temperature		Maximum Subsequent RV Downcomer Fluid Pressure	
		K	°F	MPa	psia
Steam generator tube rupture	9.0	505	450	17.0 17.34[a]	2465 2515[a]

a. Calculation was extrapolated to 2 h, this pressure assumes code safety valve is demanded.

b. Includes maximum effects of uncertainty presented in Reference 1.

c. Includes maximum effects of uncertainty summarized in Section 4.

d. Includes maximum effects of uncertainty described in Section 7.

e. Minimum temperature extrapolated to occur at 2 h, see Section 8.

f. Extrapolated pressure at 2 h, see Section 8.

g. Includes uncertainty due to operator closing letdown line block valve.

h. Includes uncertainty due to flow oscillations, see Section 8.

11. REFERENCES

1. M. A. Bolander et al., *RELAP5 Analysis of Oconee-1 PWR Transients for Pressurized Thermal Shock Integration Study (Proprietary)*, EG&G Idaho EGG-NTAP-6190, March 1983.

2. *Internals Vent Valve Evaluation (Proprietary)*, topical report BAW-10005, Babcock & Wilcox Company, July 1969.

3. R. A. Hedrick, "First Pass Feedwater Train Model for Oconee-1," letter, SAI-Oak Ridge, May 11, 1982.

4. J. M. Keeton, "Oconee 1 Control System Model," letter, SAI-Oak Ridge, October 13, 1982.

5. "Instruction Book 620-0003, Duke Power Company, Oconee Nuclear Plant, Unit No. 1," Bailey (Babcock & Wilcox) Company, March 15, 1977.

6. J. A. Dearien, "Estimation of Uncertainty in a RELAP5 Calculation of a Main Steam Line Break in Oconee-1 PWR," letter JAD-114-82, EG&G Idaho, Inc., November 4, 1982.

7. B. Bassett et al., *TRAC Analyses of Severe Overcooling Transients for the Oconee-1 PWR,* draft report, Los Alamos National Laboratory, March 1983.

8. N. G. Trikourous et al., *RETRAN Analysis of Rapid Cooldown Transient, Three Mile Island Unit 2,* GPU Service Corp., August 1978.

APPENDIX A

COMPUTER RUN TIME STATISTICS

APPENDIX A

COMPUTER RUN TIME STATISTICS

Table A-1 presents a timing survey of the final six RELAP5 Oconee-1 PTS calculations and contains geometric and timing information. Figures A-1 through A-6 show differentiated CPU time versus time for the six calculations. The CDC 176 computer at the Idaho National Engineering Laboratory was used to perform the calculations. The calculations used the RELAP5/MOD1.5 computer codes. Timing statistics for the initial four calculations appear in Appendix A of Reference 1.

Table A-1. Timing statistics

Calculation Parameter	Revised Main Steam Line Break	Maximum Sustainable Steam Generator Overfeed	Hot Standby TBP Valve Failure	Pressurizer Surge Line Small Break	RC Pump Suction Small Break	Steam Generator Tube Rupture
Total number volumes (#C)	220	218	218	220	222	226
Total number heat structures	208	208	208	208	208	211
Transient time seconds (RT)	2697	1695	7200	6200	4900	2800
Total CPU seconds used	19305	11435	14008	40971	25180	14889
Total number of time steps (#DT)	65442	35934	54859	142765	80597	48316
CPU/real time	7.16	6.75	1.95	6.61	5.14	5.32
$\frac{CPU \times 10^2}{RT \times \#C}$	3.25	3.09	0.893	3.00	2.31	2.35
$\frac{CPU \times 10^6}{RT \times \#C \times \#DT}$	0.497	0.861	0.163	0.210	0.287	0.487
$\frac{CPU \times 10^3}{\#C \times \#DT}$	1.34	1.46	1.17	1.30	1.41	1.36

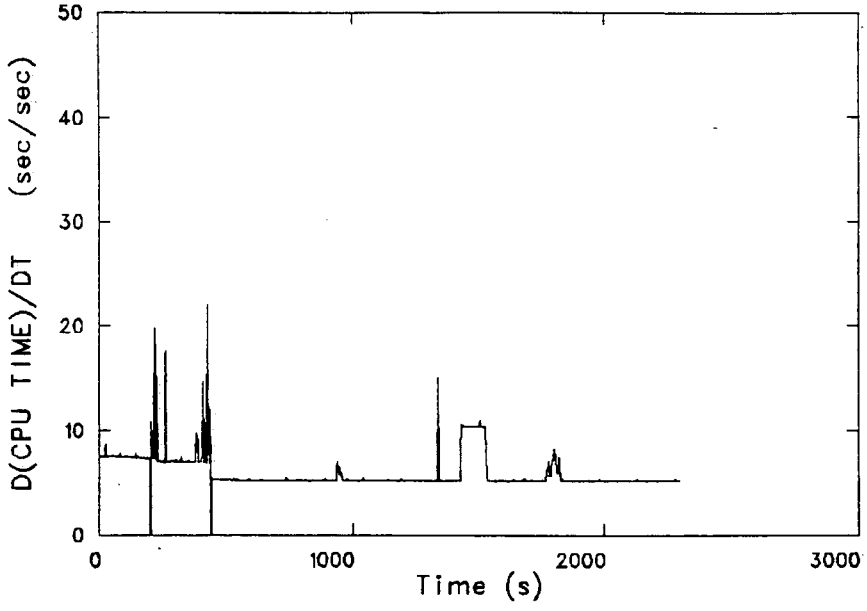

Figure A-1. Differentiated computer run time, revised MSLB.

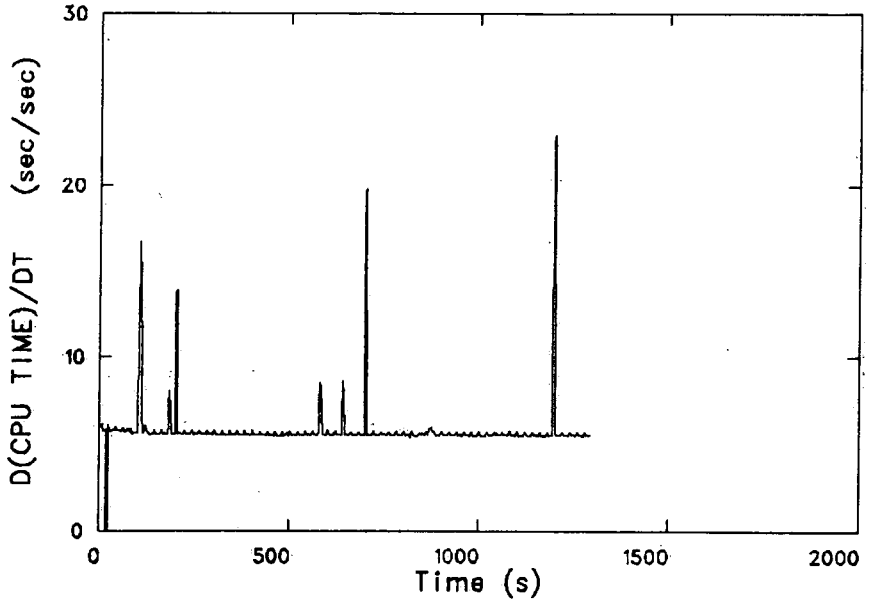

Figure A-2. Differentiated computer run time, maximum sustainable overfeed.

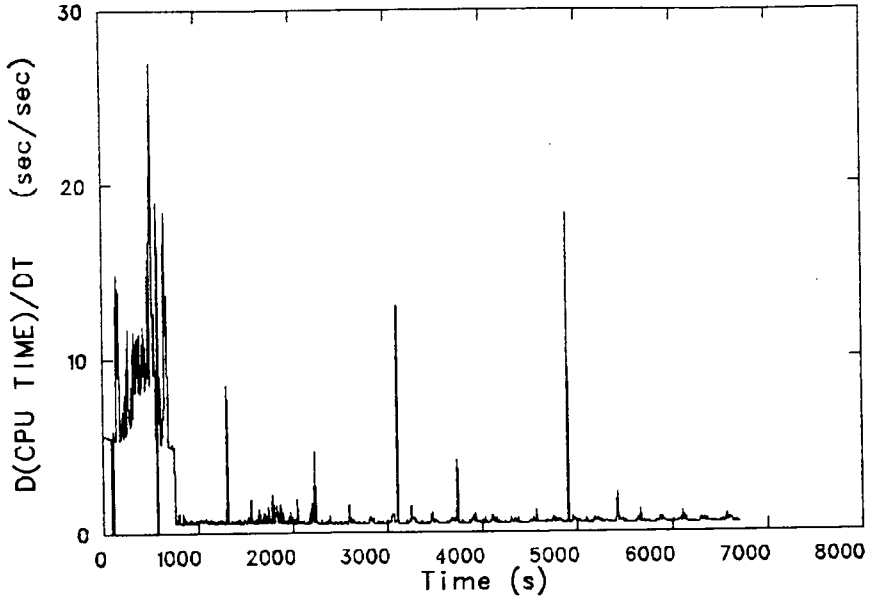

Figure A-3. Differentiated computer run time, TBP failure at hot standby.

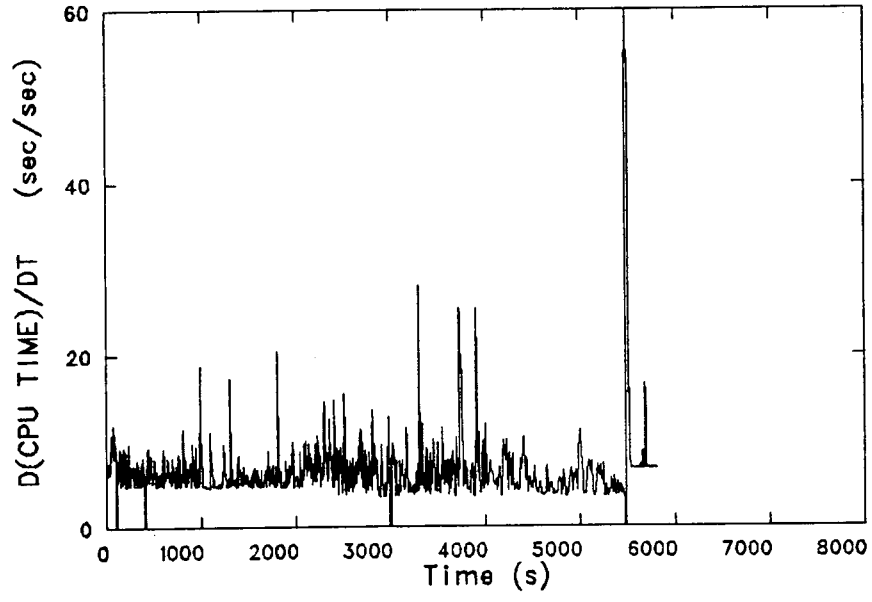

Figure A-4. Differentiated computer run time, pressurizer surge line break.

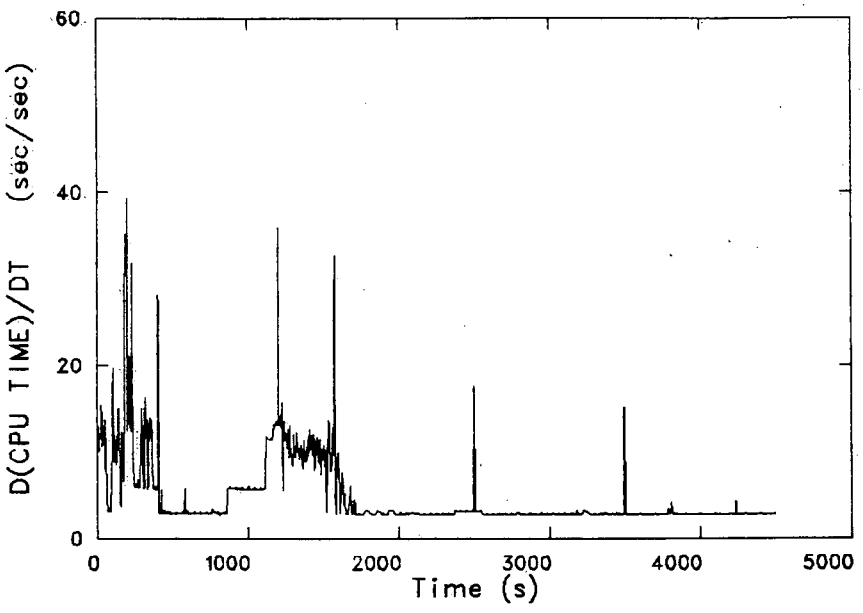

Figure A-5. Differentiated computer run time, pump suction break.

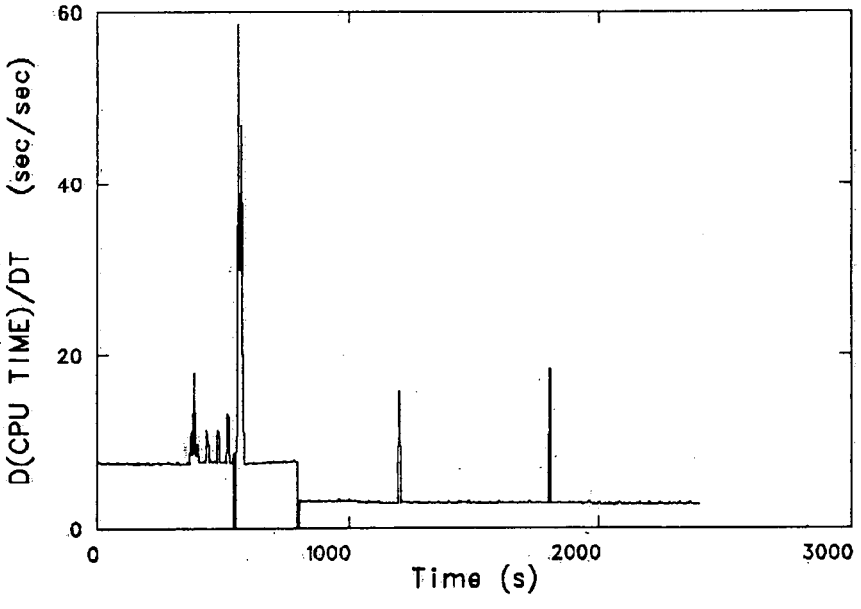

Figure A-6. Differentiated computer run time, SG tube rupture.

APPENDIX B

MAIN STEAM LINE BREAK REVISED TRANSIENT, COMPARISON OF COUNTERPART TRAC AND RELAP5 CALCULATIONS

APPENDIX B

MAIN STEAM LINE BREAK REVISED TRANSIENT, COMPARISON OF COUNTERPART TRAC AND RELAP5 CALCULATIONS

This Appendix presents a comparison between counterpart calculations of the revised main steam line break sequence performed at Los Alamos National Laboratory (LANL), using the TRAC-PF1 computer code, and those made at the Idaho National Engineering Laboratory (INEL), using the RELAP5/MOD1.5 computer code. A detailed description of the sequence and analysis of the results of the RELAP5 calculation appear in Section 4. A detailed analysis of the TRAC calculation may be found in Reference 7.

A comparison of initial, steady state conditions indicates no significant differences between the starting points for the TRAC and RELAP5 calculations. For the TRAC calculation, these conditions may be found in Tables II.D-I and II.D-II of Reference 7. For the RELAP5 calculation, these conditions are shown in Table 1 of this report.

Figure B-1 shows a comparison of hot leg pressures for the two calculations. TRAC output data were available only for the first 900 s of the calculation; therefore comparisons are shown for only that period. This is not a significant limitation since most events of interest occur during the initial portions of the sequence in both calculations. As shown in Figure B-1, the primary system initially depressurized faster in the RELAP5 calculation, but the depressurization progressed further in the TRAC calculation. Figure B-2 shows that the reactor vessel downcomer fluid temperature was lower in the TRAC calculation. The primary purpose of this Appendix is to explain the differences in primary pressure and downcomer fluid temperature between the two calculations.

Table B-1 compares the timing of events between the calculations noting significant differences. The following discussions examine these differences. For purposes of discussion, the sequence is separated into four phases: (a) transient initiation to time of reactor coolant pump trip, (b) time of RCP trip to time of RCP restart, (c) time of RCP restart to time of feedwater termination, and (d) time after feedwater termination.

Table B-2 shows how the timing of the four phases of the sequence differed in the two calculations. Specifically, the times dividing Phases 1 from 2 and 2 from 3 are different. The differences in the timing of the sequence phases will be discussed first, followed by a discussion of differences between phenomena occurring during each of the phases.

Phase 1 ends and Phase 2 begins at the time of RCP trip. This trip is scheduled 30 s after HPI initiation, which occurs when the hot leg pressure is reduced to 10.44 MPa (1515 psia). The RCP trip occurred at 35.3 s with RELAP5 and 51.2 s with TRAC. As shown in Figure B-1, the primary pressure declined more quickly to the HPI initiation setpoint with RELAP5 than it did with TRAC. This difference appears to be caused by a greater heat removel rate in the affected steam generator with RELAP5, as shown in Figure B-3. This in turn was caused by the higher RELAP5 break mass flow rate, shown in Figure B-4. A complete explanation of the differences between TRAC and RELAP5 initial secondary blowdown behavior would require a detailed evaluation of mass distribution, heat transfer processes, and break flow during the blowdown and is beyond the scope of this comparison. The differences in heat removal rate, shown in Figure B-3, explain why sequence Phase 1 ended sooner in the RELAP5 calculation than in the TRAC calculation.

Phase 2 ends and Phase 3 begins at the time of RCP restart. One RCP per loop was to be restarted only after 42 K (75°F) subcooling was attained in all hot legs and cold legs. This criterion was met at 300 s in the RELAP5 calculation and 526 s in the TRAC calculation. The reason for this difference is that, in the RELAP5 calculation, natural circulation flow continued in both loops, while in the TRAC calculation, the unaffected loop stagnated, as shown in Figures B-5 and B-6, during the time period from about 100 s to 300 s. Loop B flow was terminated in the TRAC calculation when the fluid at the top of the loop B hot leg flashed and formed a large steam bubble, as shown in Figure B-7. This flashing occurred in the TRAC calculation, but

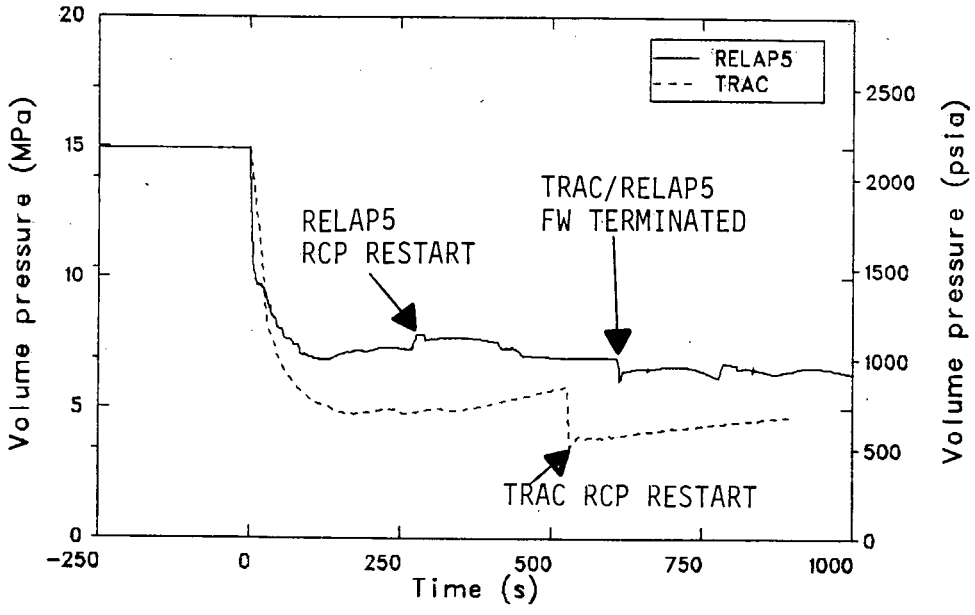

Figure B-1. TRAC and RELAP5 comparison, revised MSLB, hot leg pressures.

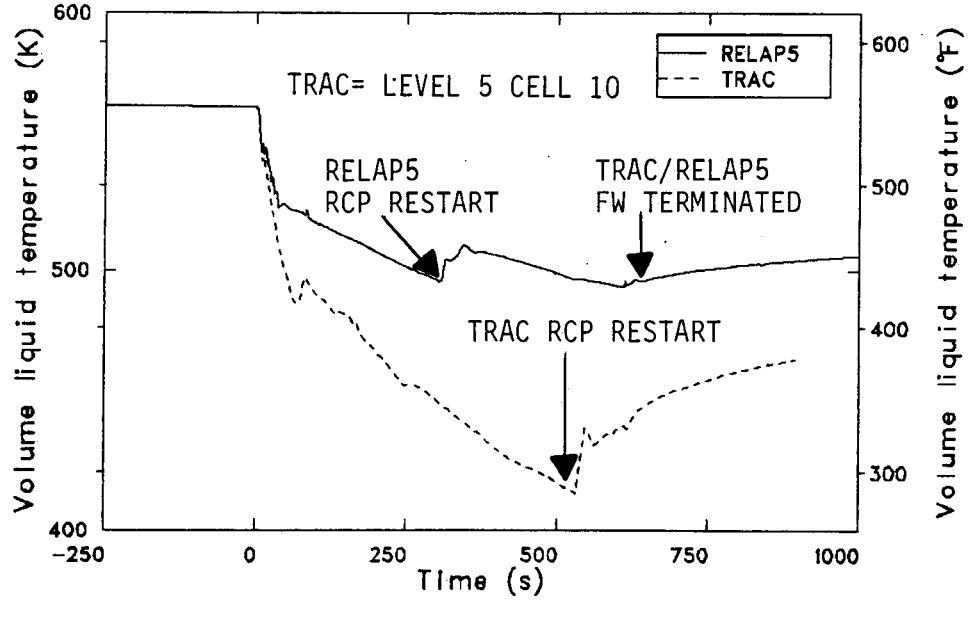

Figure B-2. TRAC and RELAP5 comparison, revised MSLB, RV downcomer fluid temperature.

Table B-1. Comparison of TRAC and RELAP5 sequences of events, main steam line break revised transient

Event	Time of Event (s)		Notes (T = TRAC, R = RELAP5)
	TRAC	RELAP5	
Break opens	0.0	0.0	
MFW pumps trip due to high level indication in SGA	Not calculated	0.3	T—trip occurs later (47.8 s) due to low suction pressure
Reactor trip	0.5	0.09	R—one timestep plus 0.05 s
Turbine trip	0.5	0.5	
Feedwater heater power and drain flows trip	1.0	1.0	
Lose condenser feed from turbine	1.5	Not calculated	
SGB turbine bypass opened	5.0	2.0	T—low pressure safety not challenged; TBP cycled twice
SGB safety opened	Not calculated	3.0	
SGB safety closed	Not calculated	12.0	R—safety and TBP challenged and cycled once each
SGB turbine bypass closed	39.9	13.0	
HPI initiated due to low hot leg pressure	21.2	5.3	
EFW initiated to SGA	29.4	4.4	
MFW pumps trip due to low suction pressure	47.8	Not calculated	R—trip occurred at 0.35 due to high SGA level indication
EFW initiated to SGB	48.7	4.4	
RCPs trip, MFW realigned to EFW header	51.2	35.3	
Condensate booster pump trip due to low section pressure	53.9	Not calculated	
SGB level recovered, EFW throttled	346.7	320	

Table B-1. (continued)

Event	Time of Event (s) TRAC	Time of Event (s) RELAP5	Notes (T = TRAC, R = RELAP5)
42K subcooling attained in hot legs, A-1 and B-1 RCPs restarted and HPI throttled	526	300	
Motor-driven EFW terminated to both SG	Not calculated	5.3	
Core flood tanks inject	530.9 - 537.9	Not calculated	
All EFW, MFW, and TBP isolated to both SG	600	600	
SGB TBP and EFW restored	900	900	
PORV setpoint pressure reached	4678	2432	
Calculation terminated	7200	2697	R—data for 2697—7200 s was extrapolated

Table B-2. TRAC and RELAP5 sequence phase timing

Sequence Phase Number	TRAC (s) From	TRAC (s) To	RELAP5 (s) From	RELAP5 (s) To
1. Initiation to RCP trip	0	51.2	0	35.3
2. RCP trip to RCP restart	51.2	526	35.3	300
3. RCP restart to FW termination	526	600	300	600
4. After FW termination	600	7200	600	7200

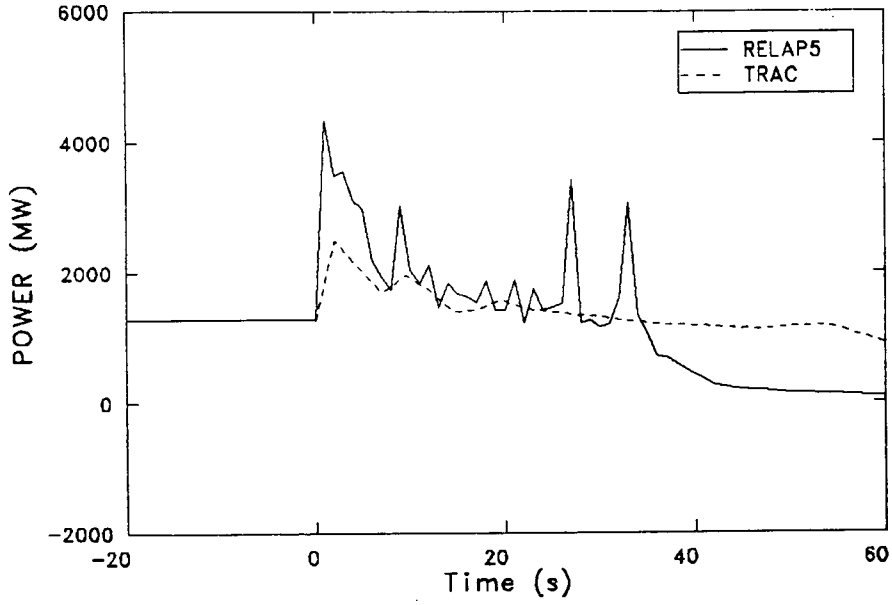

Figure B-3. TRAC and RELAP5 comparison, revised MSLB, affected SG heat removal rates.

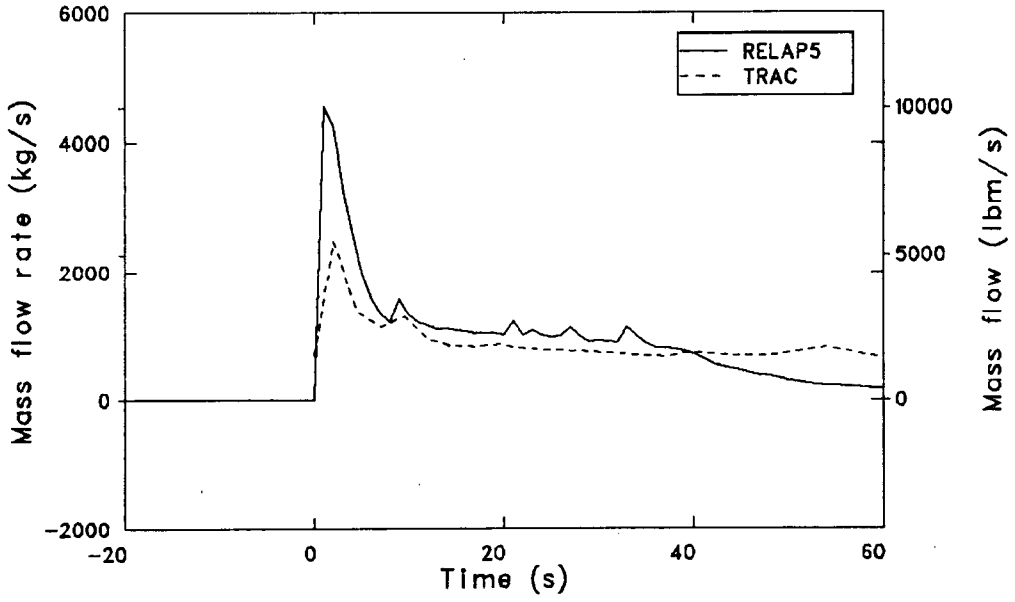

Figure B-4. TRAC and RELAP5 comparison, revised MSLB, break mass flow rates.

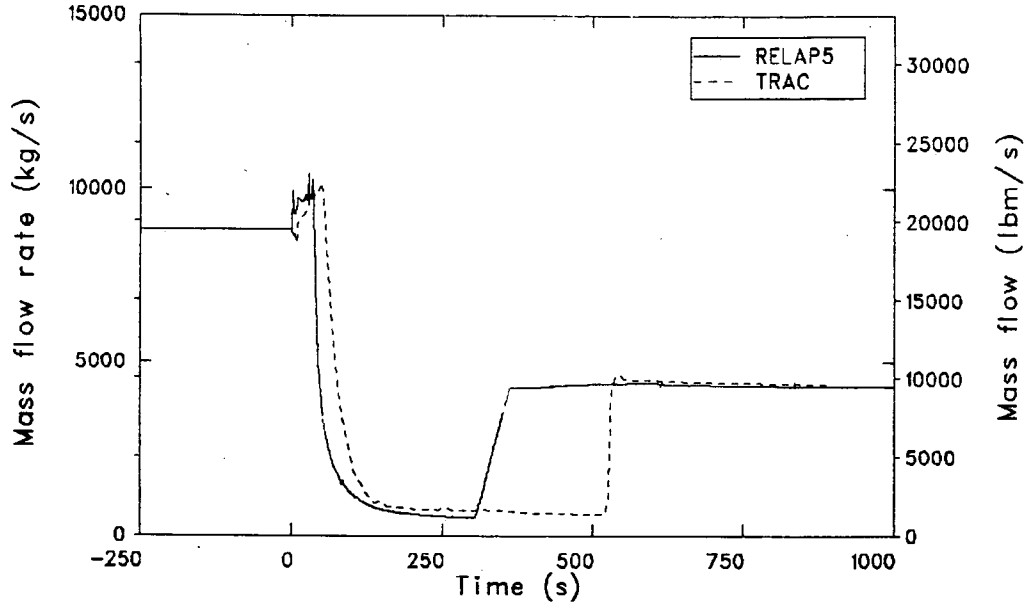

Figure B-5. TRAC and RELAP5 comparison, revised MSLB, loop A hot leg mass flow rates.

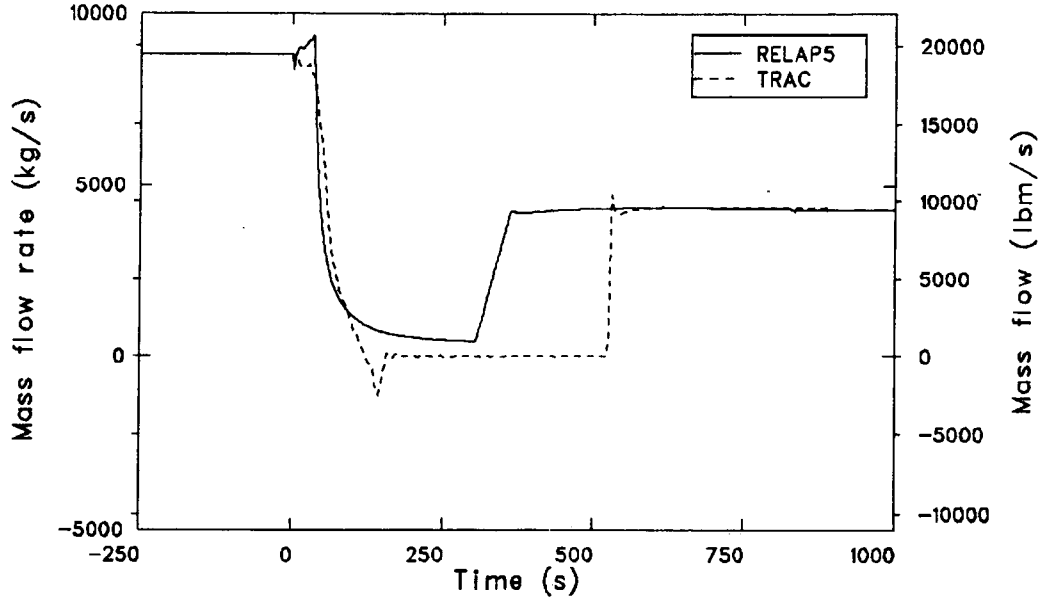

Figure B-6. TRAC and RELAP5 comparison, revised MSLB, loop B hot leg mass flow rates.

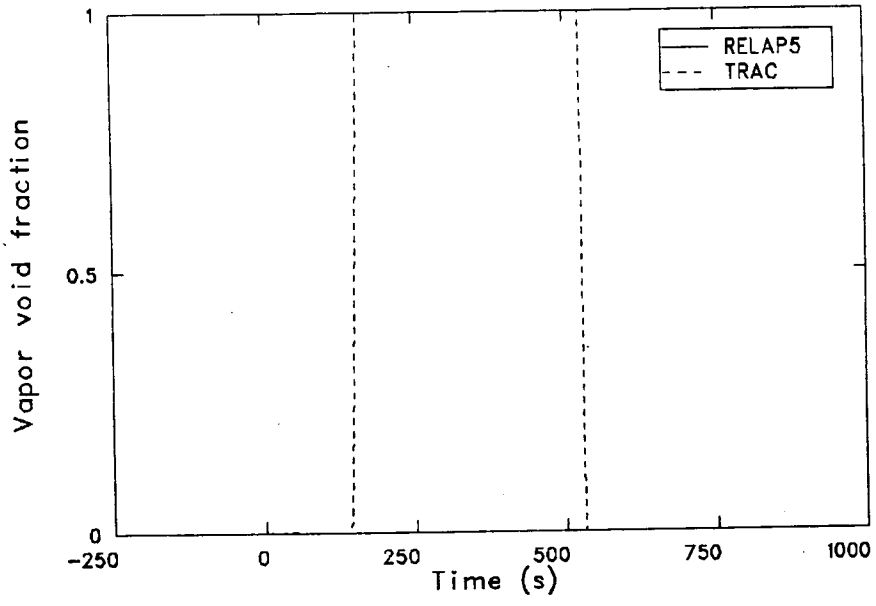

Figure B-7. TRAC and RELAP5 comparison, revised MSLB, void fractions at top of loop B hot legs.

not in the RELAP5 calculation, because the loop B hot leg fluid temperature was higher with TRAC than with RELAP5, as shown in Figure B-8.

Figure B-9 shows that the opposite was true in loop A. When Figures B-8 and B-9 are compared, one observes that the RELAP5 loop A and B hot leg fluid temperatures are identical, while the TRAC loop A temperatures are below, and the loop B temperatures are above, the corresponding RELAP5 temperatures. These differences are caused by the one-dimensional nature of the RELAP5 reactor vessel model as compared to the three-dimensional nature of the TRAC reactor vessel model. The two hot leg temperatures shown for RELAP5 are identical, because the same reactor vessel cell feeds both hot legs. The temperatures are different with TRAC because different reactor vessel cells feed the hot legs, and these cells contain different temperature fluids.

The high TRAC loop B hot leg temperature caused the hot leg to flash and cut off the natural circulation in loop B. With loop flow stopped, the subcooling margin necessary for restarting the RCPs was not attained until 526 s in the TRAC calculation, at which time HPI volume addition had repressurized the primary system and sufficiently raised the saturation temperature. Because of the lower RELAP5 loop B hot leg temperature, loop B hot leg flashing was not calculated. The loop flow continued, and the subcooling margin was attained much sooner, at 300 s.

As shown in Figure B-2, the RCP restart had a significant effect on the reactor vessel downcomer temperatures in both calculations. TRAC and RELAP5 calculated different RCP restart times, primarily due to multi-dimensional behavior within the TRAC reactor vessel model which the RELAP5 model did not address. Specifically, in the TRAC calculation, the fluid entering the affected loop hot leg was colder than that entering the unaffected loop hot leg, because the affected cold legs were colder than the unaffected loop cold legs. The asymmetric fluid temperature distribution around the reactor vessel downcomer inlet caused the upper plenum fluid temperature distribution to also be asymmetric. The one-dimensional RELAP5 reactor vessel model, however, perfectly mixed the flow from all cold legs and apportioned the same temperature fluid to each hot leg. The extent of this asymmetry in the prototype plant will be a function of the geometry of the flow paths from the downcomer inlet annulus to the upper plenum, and of the velocities of fluid through the paths. For a fast flow and complicated geometry, symmetric behavior could be expected.

The true extent of asymmetry expected for the Oconee-1 plant, at the flow rates calculated by the computer codes, is not known. Existing test data from a subscale facility, with different reactor design, indicates that a degree of asymmetry is to be expected. Due to proprietary considerations, this data is not available here. No attempt has been made to compare the magnitude of the TRAC-calculated asymmetry with the test data. However,

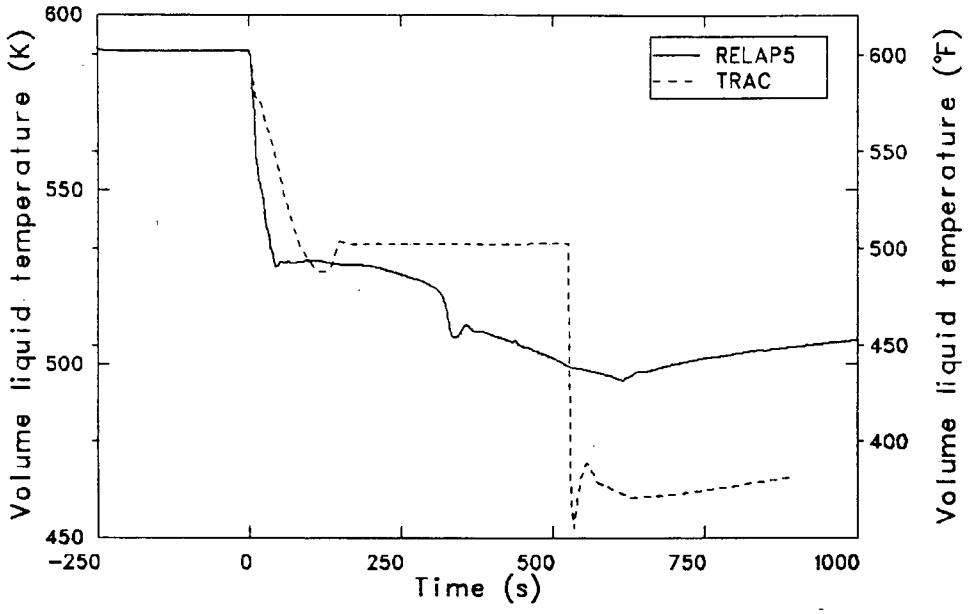

Figure B-8. TRAC and RELAP5 comparison, revised MSLB, loop B hot leg liquid temperatures.

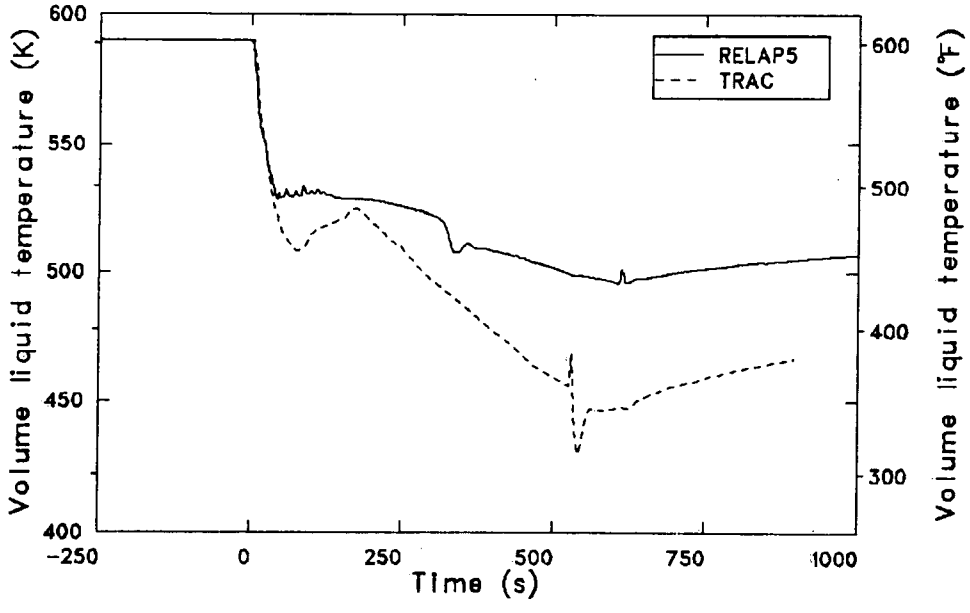

Figure B-9. TRAC and RELAP5 comparison, revised MSLB, loop A hot leg liquid temperatures.

it is likely that, for the main steam line break sequence (which includes highly asymmetric steam generator secondary behavior), the TRAC-calculated asymmetric hot leg conditions are more reasonable than the RELAP5-calculated symmetric hot leg conditions. Thus the RCP restart (and the end of sequence Phase 2) calculated with TRAC at 526 s is probably more reasonable than that calculated with RELAP5 at 300 s.

Differences between the TRAC and RELAP5 calculations during sequence Phase 1 are discussed next. Phase 1 extends from transient initiation to time of RCP trip, 51.2 s with TRAC and 35.3 s with RELAP5.

As discussed in Section 2 (Secondary System subheading), in the RELAP5 calculation, the secondary level indication was determined in a prototypical manner using differential pressures and a reference density. The TRAC calculation used a nonprototypical downcomer collapsed level indication. As discussed in Section 4 (Transient Results subheading) the main feedwater (MFW) pumps were tripped at 0.3 s in the RELAP5 calculation, as a result of high level indication in the affected steam generator. This trip did not occur until 47.8 s in the TRAC calculation, when the MFW pump trip occurred due to low suction pressure. The early MFW pump trip calculated with RELAP5 better represents the behavior expected during a main steam line break than does the late MFW pump trip calculated with TRAC.

The first effect of the discrepancy in MFW pump trip time was a difference in the initiation of emergency feedwater (EFW). With TRAC, EFW was initiated to steam generator A at 29.4 s and to steam generator B at 48.7 s. With RELAP5, EFW was initiated at 4.4 s to both steam generators. As discussed in Section 4 (Transient Results subheading) with RELAP5, EFW initiation should have been delayed by 4 s for steam generator A and 11 s for steam generator B. Since initiation of EFW requires a low MFW pump discharge signal and a low secondary level signal, and since continued MFW pump operation delays receipt of both of these signals, EFW initiation occurred later with TRAC than with RELAP5. The break mass flow discrepancy, from about 10 to 35 s in Figure B-4, was due to EFW injection with RELAP5 (but not with TRAC) during this period.

A comparison of affected steam generator secondary pressures is shown in Figure B-10. The figure shows excellent agreement between TRAC and RELAP5 until 5 s, at which time EFW was initiated with RELAP5 but not with TRAC. After 5 s, the pressures diverged, with the RELAP5 pressure about 0.6 MPa (87 psi) below that of TRAC. The RELAP5 pressure was lower due to the depressurizing effect of injecting cold EFW liquid. With a colder affected steam generator secondary, heat removal was enhanced. This explains the slightly higher affected steam generator heat removal rate with RELAP5, from about 10 to 35 s, shown in Figure B-3.

A second effect of the discrepancy in MFW pump trip time was the different affected steam generator MFW injection behavior, shown in Figure B-11. The flow rates shown in this figure diverged over approximately the first 10 s, due to opposite MFW valve response induced by the different secondary level indications. In the TRAC calculation, the MFW valve initially opened wider, due to the low level indication, while in the RELAP5 calculation the valve closed, due to the high level indication. After about 10 s, the RELAP5 indicated level also fell to the low level setpoint, and the MFW valves opened. Between 10 and 35 s, compensating differences are noted between the calculations. During this period with TRAC the MFW pumps were running; with RELAP5 they were not. However, as just discussed, during this period with RELAP5, the secondary pressure was significantly lower than it was with TRAC, resulting in a higher RELAP5 affected steam generator MFW flow.

The final difference between the calculations observed during sequence Phase 1 concerns reactor vessel upper head voiding. Figure B-12 compares the RELAP5 upper head void fraction with that of a representative cell in the TRAC model. As shown, about 65% of the RELAP5 upper head voided during the first few seconds of the transient, while a very minor void fraction was calculated using TRAC. The reason for this difference is related to the modeling in this part of the vessel. The TRAC model considers the entire upper head region as being in a flow path between the core outlet and the hot legs. The RELAP5 model considers the uppermost 1.74 m (5.7 ft) of the upper head to be a stagnant region, removed from this flow path. As a result of this modeling difference, the RELAP5 upper head fluid remained at its initial temperature and flashed considerably as the primary system depressurized; the TRAC upper head fluid was cooled by flow during the depressurization and did not flash significantly. This difference is important,

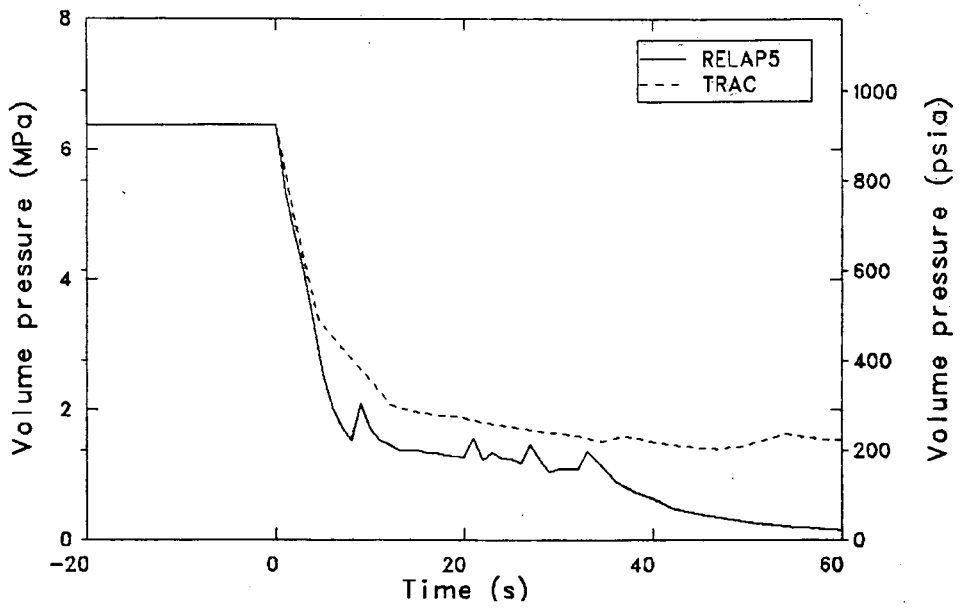

Figure B-10. TRAC and RELAP5 comparison, revised MSLB, affected SG secondary pressures.

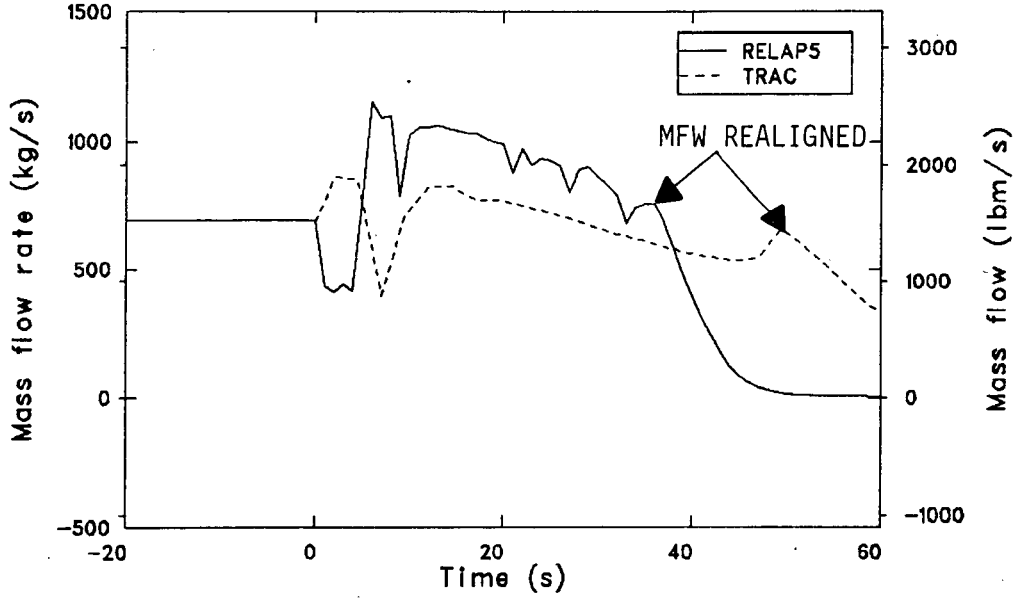

Figure B-11. TRAC and RELAP5 comparison, revised MSLB, affected SG main feed header mass flow rates.

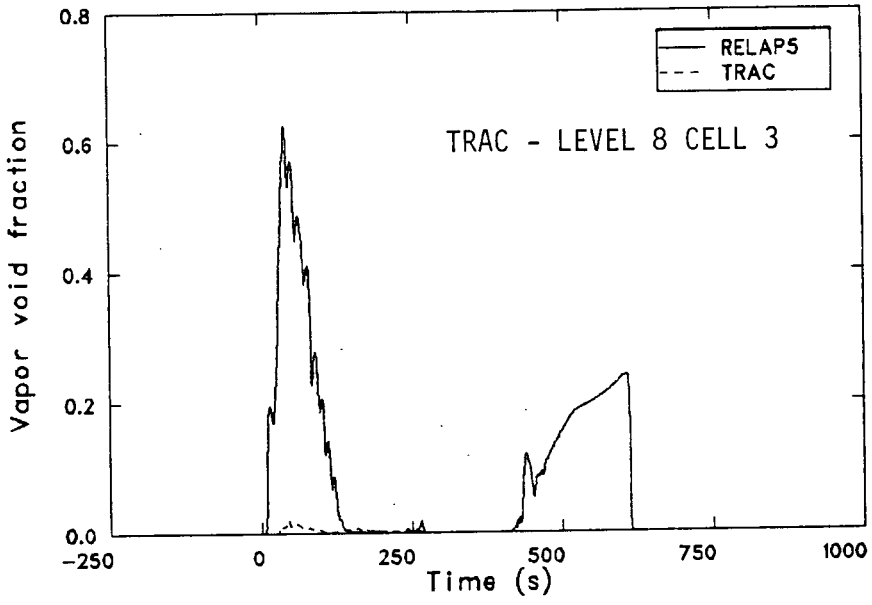

Figure B-12. TRAC and RELAP5 comparison, revised MSLB, RV upper head void fractions.

in that either the upper head or a hot leg may be expected to flash, and that the location of flashing was different in the two calculations. As explained earlier, the hot leg flashing calculated by TRAC delayed the RCP restart and was caused by asymmetric hot leg fluid temperatures. The upper head behavior represents an additional reason why the hot leg flashed with TRAC but not with RELAP5. The two models represent the extremes of flashing potential, with the TRAC model ensuring virtually no flashing and the RELAP5 model significant flashing.

Reference 8 investigated a cooldown transient which occurred in the Three Mile Island, Unit 2 plant during 30% power operation. The conclusion of this report was that, for a primary system cooldown rate of 0.37 K/s (0.70 F/s), the plant experienced partial flashing of upper head fluid. The amount of fluid flashed is sensitive to the cooldown rate. The main steam line break cooldown rate is about 5 times that for the plant transient examined in the reference. Therefore, significant upper head flashing is likely during the main steam line break sequence.

Differences between the TRAC and RELAP5 calculations during sequence Phase 2 are discussed next. Phase 2 extends from the time of RCP trip (51.2 s with TRAC, 35.3 s with RELAP5) to time of RCP restart (526 s with TRAC, 300 s with RELAP5).

During Phase 2 of the sequence, main feedwater (MFW) was realigned to the emergency feedwater (EFW) header. Flows from the MFW and EFW systems were mixed before injection near the top of the steam generator boiler region. To flow downward into the lower portions of the boiler, the feedwater must penetrate tube support plates which restrict the flow area to 43% of the area in the tube bundle itself. Countercurrent flow limiting phenomena at the uppermost tube support plate are discussed in Reference 7 for the TRAC calculation and in Section 4 of this document for the RELAP5 calculation.

The first difference between the calculations during sequence Phase 2 was the tripping of the condensate booster pump. This pump was to be tripped if its suction pressure decreased to (0.21 MPa) 30 psia for a period longer than 5 s. The pump was tripped off with TRAC but not with RELAP5. This difference was probably caused by an earlier MFW realignment to the EFW header with RELAP5. After realignment, MFW was delivered only through the small flow area of the startup control valves, thus limiting further depressurization of the upstream MFW train (including the condensate booster pump suction region). With the condensate booster pump on, more flow was delivered through the MFW train to the EFW header of the affected steam generator. This explains the higher RELAP5 EFW header flow, as shown in Figure B-13.

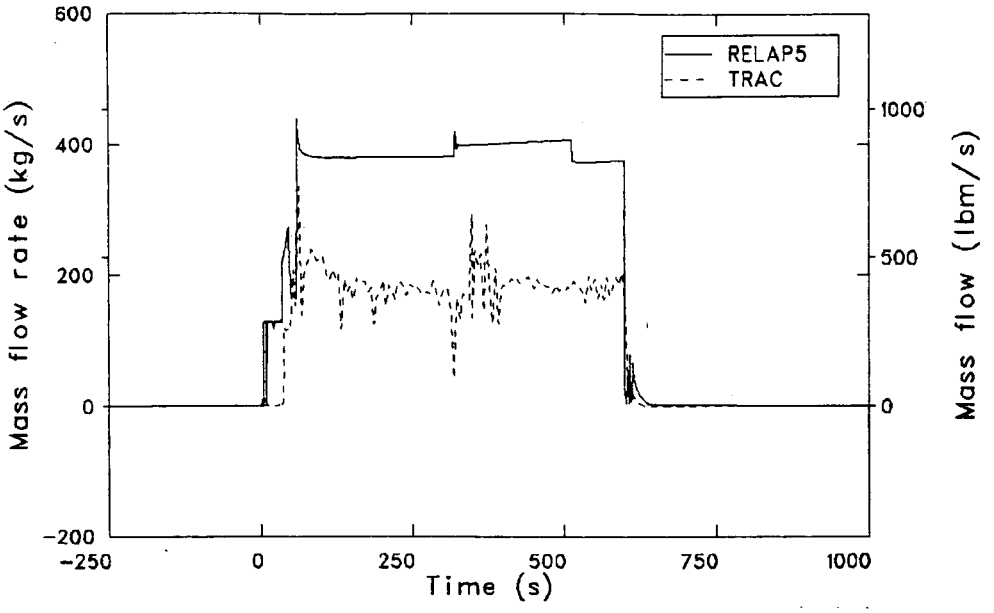

Figure B-13. TRAC and RELAP5 comparison, revised MSLB, affected SG emergency feedwater header flow rates.

During the injection of EFW and MFW through the EFW header, the flow entered the boiler section and was flashed, due to the much lower pressure in the boiler section than in the EFW line. Figure B-14 compares the void fractions calculated at the top of the boiler in the affected steam generator. During the period from about 50 to 350 s, the void fractions calculated by the two codes are in excellent agreement. Note that at the low pressures involved here, a 98% void fraction corresponds to about a 10% mixture quality. The divergence which began at 350 s was caused when the TRAC-affected steam generator EFW flow increased because of unaffected steam generator EFW throttling.

After entering the affected steam generator boiler section, most of the EFW flow was bypassed to the break in both calculations. However, a portion of liquid penetrated downward into the lower boiler section and was vaporized there. This produced a vapor upflow that limited further penetration of liquid. Figure B-15 compares the liquid volumetric flow rates at the upper tube support plate of the affected steam generator. The rates compare favorably with the TRAC liquid penetration rate, which was generally 10% more than that of RELAP5.

Figure B-16 compares the affected steam generator heat removal rates of the two calculations. For the period from about 50 to 300 s, the heat removal rate with TRAC was shown to be much higher than that with RELAP5. Only a small part of this difference was accounted for by the slightly higher TRAC liquid penetration just discussed. Another small part was found to be caused by a RELAP5 calculational problem which was discovered as a result of this comparison.

Figures B-17 and B-18, respectively, compare the liquid and vapor temperatures at the top of the affected steam generator secondary. The RELAP5 liquid temperatures are below, and the RELAP5 vapor temperatures are above, the corresponding TRAC temperatures. The rate of heat removal from the primary was proportional to the differential between the primary liquid, and secondary vapor and liquid temperatures. The vapor superheat calculated with RELAP5 from 50 to about 500 s, was excessive. The problem was caused by an understatement of the interphase mass transfer area and by the fact that the liquid phase must remain at the saturation temperature. The interphase mass transfer was based on the Saha correlation and the difficulty was encountered only in situations combining low pressure and low quality.

The RELAP5 calculational problem was not determined to contribute significantly to the differences between the TRAC and RELAP5 heat removal rates shown in Figure B-16. This was determined by comparing the original main steam line break calculation (which was not affected by the vapor superheat problem) with the revised calculation. Had the superheat problem not been encountered, the RELAP5 heat removal rate would have increased by only 10 MW. The primary difference

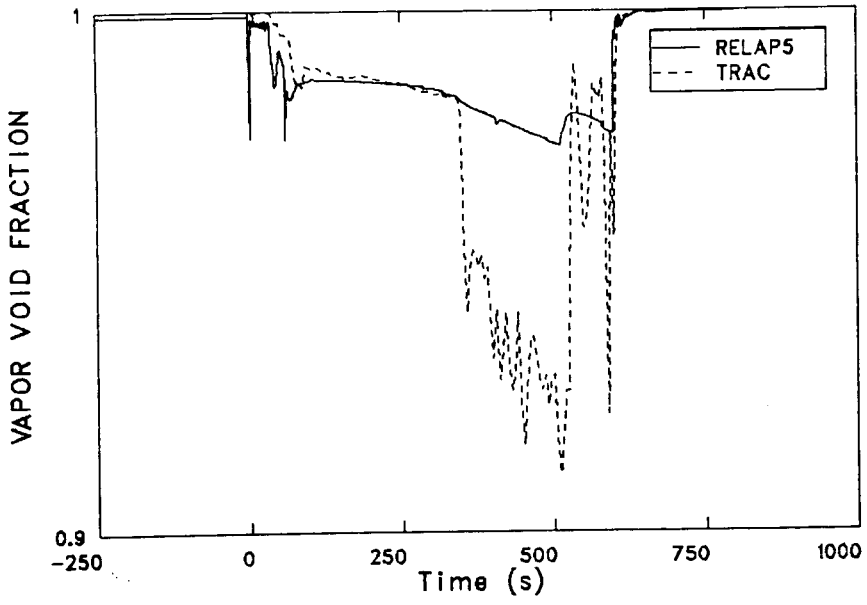

Figure B-14. TRAC and RELAP5 comparison, revised MSLB, void fractions at top of affected SG boiler.

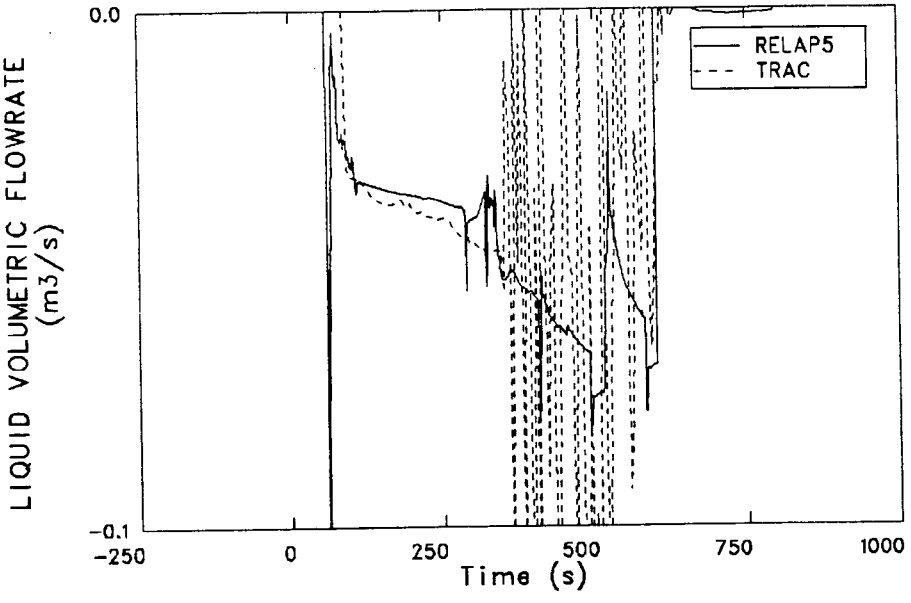

Figure B-15. TRAC and RELAP5 comparison, revised MSLB, volumetric flow rate of liquid at upper tube support plate of affected SG.

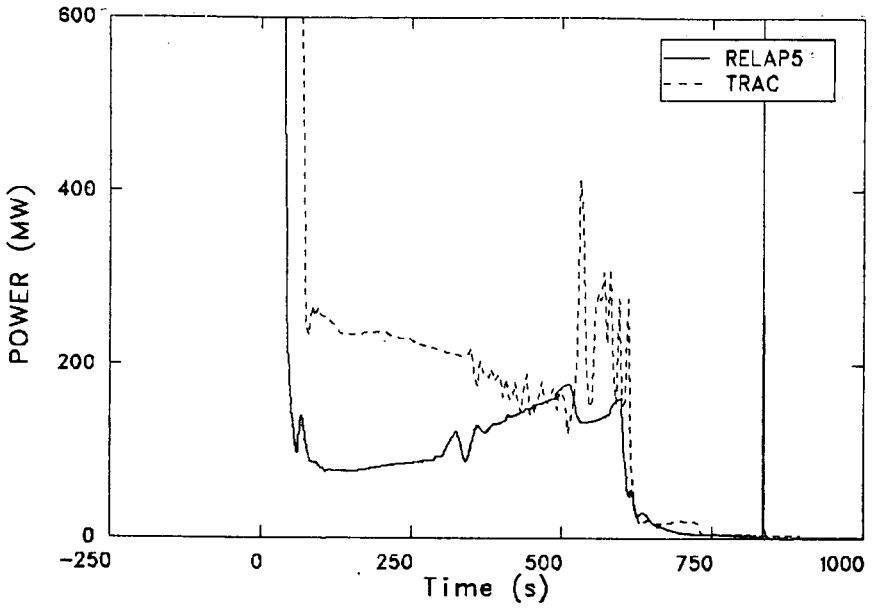

Figure B-16. TRAC and RELAP5 comparison, revised MSLB, affected SG heat removal rate, 0-1000 s.

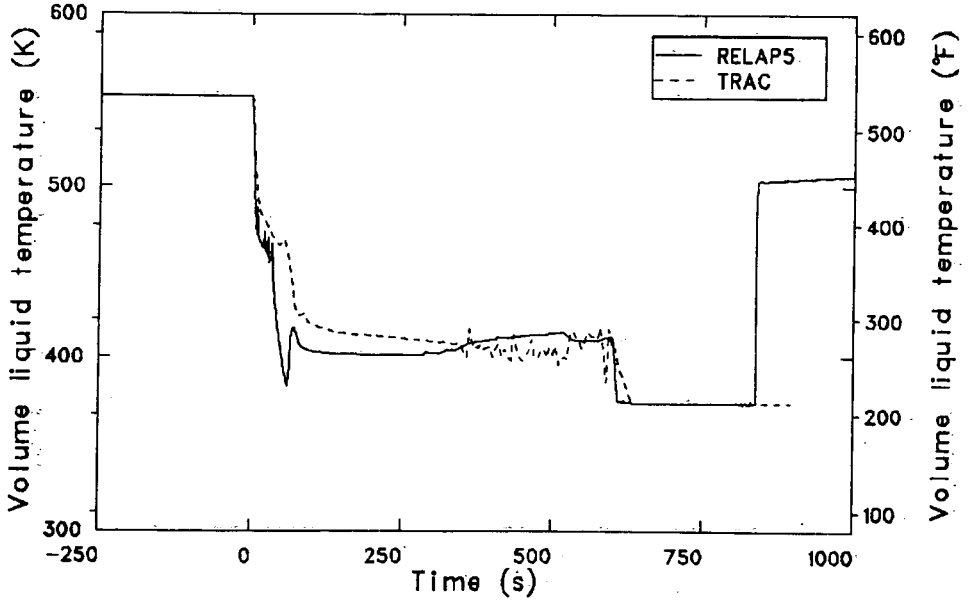

Figure B-17. TRAC and RELAP5 comparison, revised MSLB, liquid temperature at top of affected SG boiler.

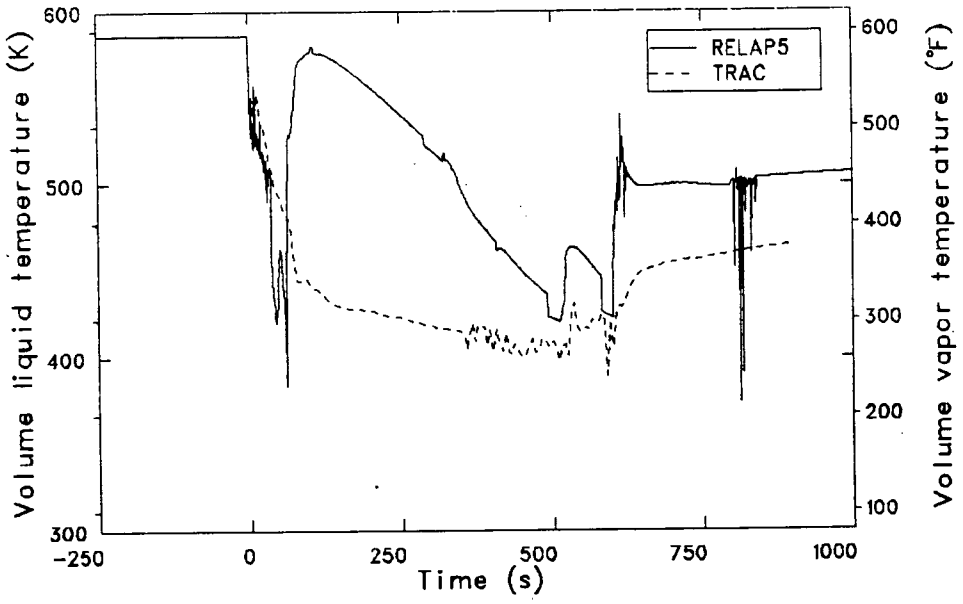

Figure B-18. TRAC and RELAP5 comparison, revised MSLB, vapor temperature at the top of affected SG boiler.

between the TRAC- and RELAP5-calculated heat removal rates during the period from 50 to 300 s is believed to be the steam generator tube outside surface heat transfer coefficients in the top calculational cells of the steam generator secondaries. These coefficients are determined by the code heat transfer packages and are based on the flow regimes and wall temperatures present. With TRAC this coefficient is believed to be larger than with RELAP5, causing a higher TRAC heat removal rate. This finding is supported by observing the different heat removal responses when the RCPs were restarted (526 s with TRAC and 300 s with RELAP in Figure B-16). The TRAC heat removal dramatically increased when RCPs were restarted; with RELAP5 it did not. This indicates that, in TRAC, heat removal is being limited by the tube inside surface coefficient and in RELAP5, by the outside surface coefficient. A direct comparison of heat transfer coefficients in the two calculations was not possible because noncomparable heat transfer data is stored on the calculation output tapes. An undetermined fraction of the TRAC heat transfer coefficient was due to the lower-than-actual hydraulic diameter used in the TRAC model to achieve steady state conditions.

A further consideration in determining the heat removal rate above the upper tube support is the size of the upper calculational cell in the models of the secondary boiler sections. This is important for, even if either code perfectly modeled the heat transfer processes on the outside of the tubes, it is the size of the cell which determines the effective heat transfer area over which it applies. In both the TRAC and RELAP5 models, this area is overstated, because the uppermost calculational cell is taller than the length from the uppermost tube support plate to the bottom of the upper tubesheet. With the TRAC model, the heat transfer area apportioned to the region between the plate and tube sheet is overstated by about 50% and with RELAP5 by about 100%; both represent a conservatism in that heat removal is overstated. The affected steam generator heat removal rate difference shown in Figure B-16 caused the different cooldown rates shown in Figure B-2. It is uncertain, however, whether the TRAC- or RELAP5-calculated heat removal rate better represents the phenomena.

Finally, differences between the TRAC and RELAP5 calculations during sequence Phase 3 are discussed. Phase 3 extends from the time of RCP restart (526 s with TRAC, 300 s with RELAP5) to 600 s, at which time all feedwater was terminated, by definition of the sequence.

When the RCPs were restarted, a decrease in primary pressure was calculated with TRAC. This pressure decrease caused a momentary core flood tank injection which was not of significance to the reactor vessel downcomer temperature and is shown in Figure B-2. The rapid drop in primary pressure with TRAC was due to the spike in heat removal to the secondaries, as indicated on Figure B-16. With RELAP5, the pressure decrease was less

severe, due to the lower affected steam generator heat removal rate. This difference was caused by the fact that the heat removal rate to the affected secondary was limited by the steam generator tube inside surface heat transfer coefficient with TRAC, but by the outside surface heat transfer coefficient with RELAP5. Thus, when the RCPs restarted, the TRAC heat transfer rate responded dramatically to the increased heat transfer coefficient on the inside surface of the steam generator tubes; the effect on the RELAP5 rate was much smaller. With both codes, restarting RCPs is shown in Figures B-9 and B-2 to be a time when the primary system cooldown was reversed or moderated. Therefore, the differences between TRAC and RELAP5 noted for sequence Phase 3 are not significant to the overall results of the study.

For the sequence Phase 4, which extends from 10 min to 2 h, no differences between the TRAC and RELAP5 calculations which might be significant to the overall results of the study were observed.

In summary, a comparison of the TRAC and RELAP5 calculations has been performed and significant differences examined. These differences are: (a) a difference in primary system heat removal rate during the first 10 s of the transient, (b) different main feedwater pump trip behavior, (c) different reactor coolant pump restart times resulting from asymmetric hot leg behavior, (d) different flashing behavior in the reactor vessel upper head, and (e) different affected steam generator heat removal rates during periods of emergency feedwater header injection.

The insights gained while performing this comparison were used in the evaluation of uncertainty in the RELAP5 calculation presented in Section 4.

APPENDIX C

PRESSURIZER SURGE LINE BREAK, COMPARISON OF COUNTERPART TRAC AND RELAP5 CALCULATIONS

APPENDIX C

PRESSURIZER SURGE LINE BREAK, COMPARISON OF COUNTERPART TRAC AND RELAP5 CALCULATIONS

This appendix presents a comparison between counterpart calculations of the revised main steam line break sequence performed at Los Alamos National Laboratory (LANL), using the TRAC-PF1 computer code, and those done at the Idaho National Engineering Laboratory (INEL), using the RELAP5/MOD1.5 computer code. A detailed description of the sequence, and analysis of the results of the RELAP5 calculation, appears in Section 7. A detailed analysis of the TRAC calculation may be found in Reference 7.

A comparison of initial, steady state conditions indicates no significant differences between the starting points for the TRAC and RELAP5 calculations. For the TRAC calculation, these conditions may be found in Tables II.D-1 and II.D-II of Reference 7. For the RELAP5 calculation these conditions are shown in Table 1 of this report.

Table C-1 presents a comparison of sequence of events timing between the two calculations. Note the difference in reactor trip time. In the TRAC calculation, reactor trip was modeled to occur at 0.5 s, while in the RELAP5 calculation, the reactor trip did not occur until a pressure-temperature reactor trip occurred at 45 s. The RELAP5 reactor trip model is prototypical of actual plant behavior, yet the difference in time of reactor trip did not materially affect the overall results of the calculation. However, the difference did cause an offset in the timing of primary system pressure and temperature changes during the first 120 s of the transient, as shown in Figures C-1 and C-2.

Due to high MFW pump discharge pressure, the main feedwater (MFW) pumps were tripped at 70 s in the RELAP5 calculation but not until 788 s in the TRAC calculation. MFW pump discharge pressure is sensitive to MFW pump speed and MFW control valve flow area, both of which are controlled by the integrated control system (ICS). As a result of input received from the Btu-limit calculator and MFW control valve differential pressure indication, MFW pump speed during the initial portion of this sequence was expected to be run back to the minimum speed. Because of the Btu-limit calculator, main and startup valves were expected to close during the initial portion of this sequence. Both of these effects increased MFW pump discharge pressure, which caused a MFW pump trip. It has not been resolved why the MFW pump was tripped earlier with RELAP5 than with TRAC. We suspect that the two calculations used different minimum allowed main feedwater pump speeds, or that the startup or main feedwater control valves were closed at different times.

The reason the MFW pump continued to run with TRAC, but not with RELAP5, was that the steam generators were fed with a mixture of MFW and emergency feedwater (EFW) in the TRAC calculation but only with the colder EFW in the RELAP5 calculation. This caused the RELAP5 steam generator secondary pressures to be far below those with TRAC, as indicated by the steam generator A pressures shown in Figure C-3.

The primary system depressurization, shown in Figure C-1, continued with RELAP5 until it was stabilized by the flashing of the reactor vessel upper head and hot legs, as shown in Figures C-4 and C-5. The upper head flashing was more complete with RELAP5, causing more liquid to be present at the break with RELAP5 than with TRAC, as shown in Figure C-6. The generally higher TRAC primary system pressure from about 500 to 1500 s caused the TRAC break mass flow rate to exceed that of RELAP5, as shown in Figure C-7. The depressurization response comparison was thus related to many effects: pressurizer level at time of reactor trip, hot leg and upper head flashing behavior, and critical flow models. A discussion of upper head flashing appears as part of the main steam line break comparison in Appendix B.

Loop natural circulation flow continued longer with RELAP5 than with TRAC, as shown in Figure C-8. This may have been caused by the different MFW pump trip behavior discussed earlier. With TRAC, the secondary feed was performed with a combination of EFW and MFW, while with RELAP5 the feed was only with EFW and was colder. The colder feed may have caused the extended RELAP5 natural circulation.

Table C-1. Comparison of TRAC and RELAP5 sequences of events, pressurizer surge line break transient

Event	Time of Event (s) TRAC	RELAP5	Notes (T = TRAC, R = RELAP5)
Break opens	0.0	0.0	
Reactor and turbine trips	0.5	45	T—scram at 0.5 s transient time R—scram on violation of P, T relationship
Turbine bypass opens (both loops)	4.2	47	
HPI initiation	42.8	78.5	
Turbine bypass closes (both loops)	93	117	
RCP trip, MFW realigned	72.8	108.5	R&T—by sequence definition 30 s after RCP trip
EFW trips on	72.9	108.5	
Vent valves open	100	554	
"Candy canes" voided	600	815 (Loop A) 1020 (Loop B)	
Main FW pump trip	788	70	R&T—trip on MFW pump high discharge P
Core flood tank flow initiated	Not calculated	2215	
LPI initiation	Not calculated	5124	
Calculation terminated	1800	6200	

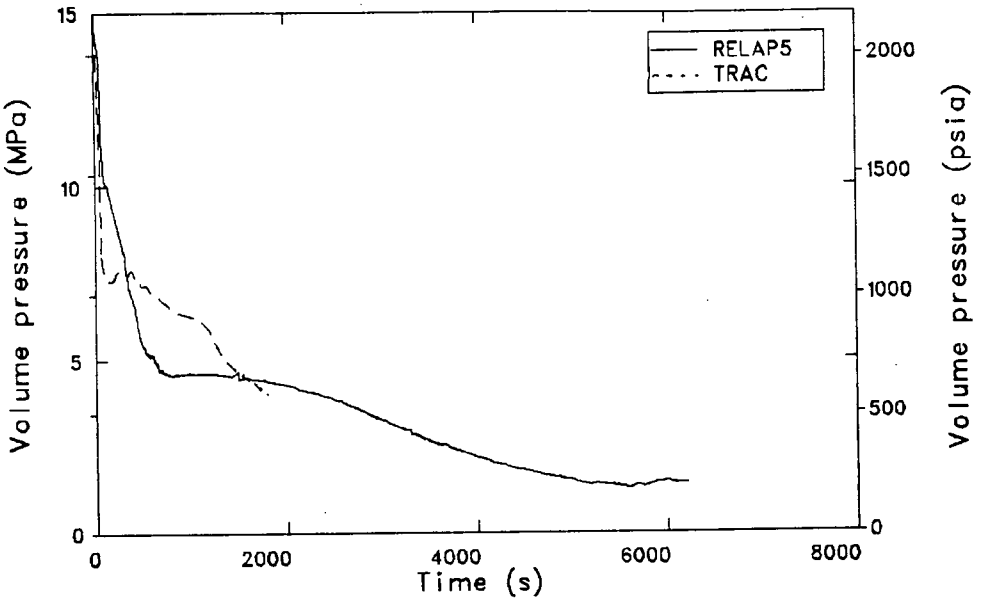

Figure C-1. TRAC and RELAP5 comparison, pressurizer surge line break, hot leg pressures.

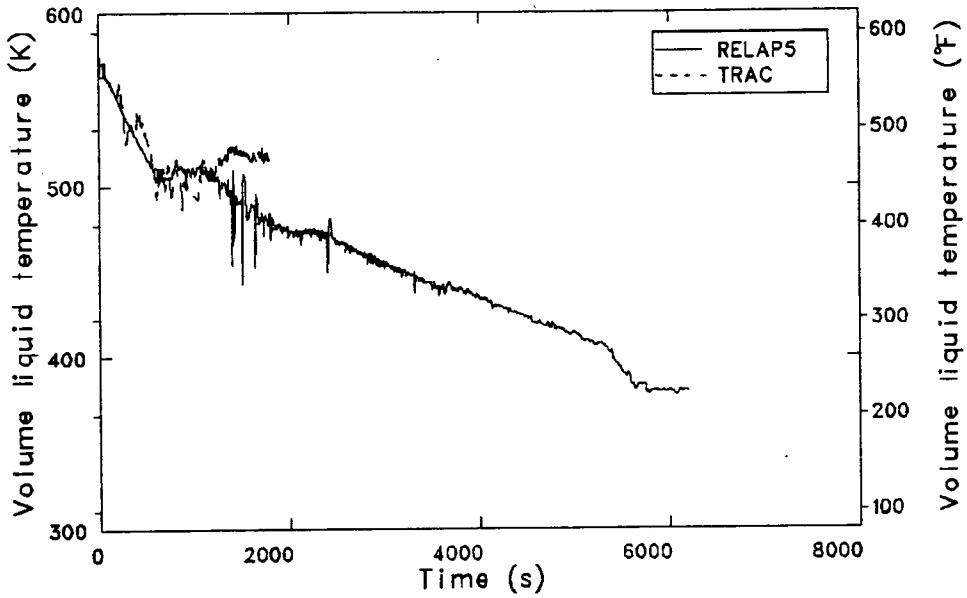

Figure C-2. TRAC and RELAP5 comparison, pressurizer surge line break, RV downcomer fluid temperature.

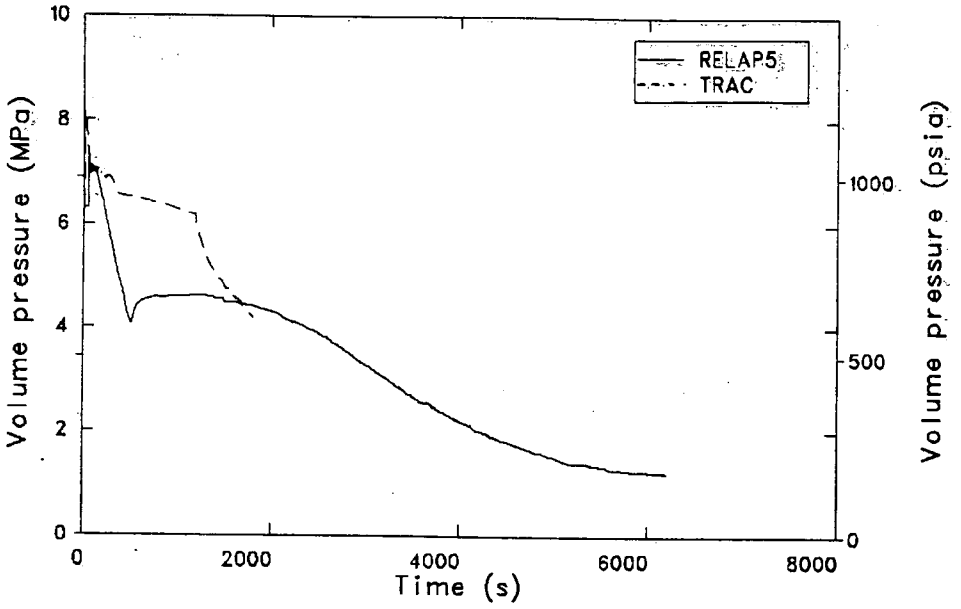

Figure C-3. TRAC and RELAP5 comparison, pressurizer surge line break, SGA secondary pressures.

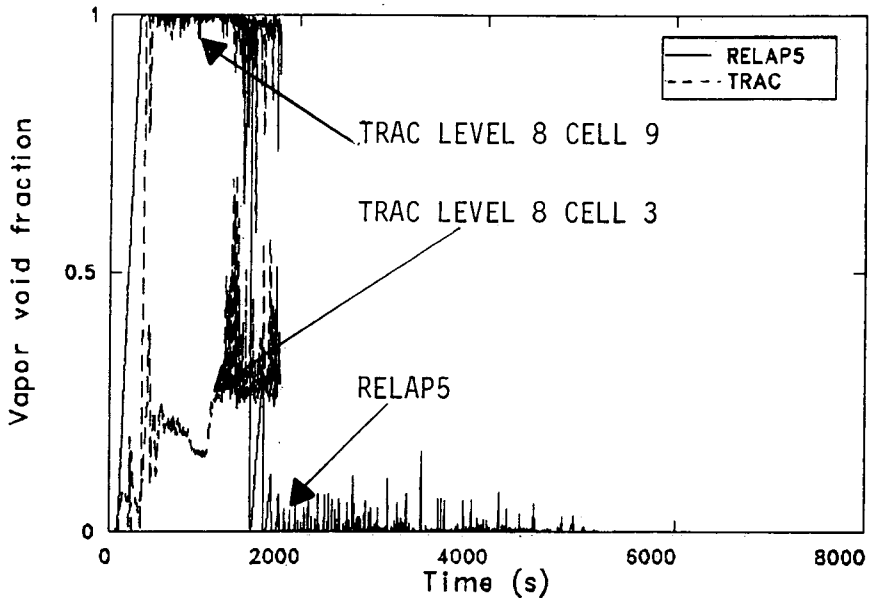

Figure C-4. TRAC and RELAP5 comparison, pressurizer surge line break, R-V upper head void fractions.

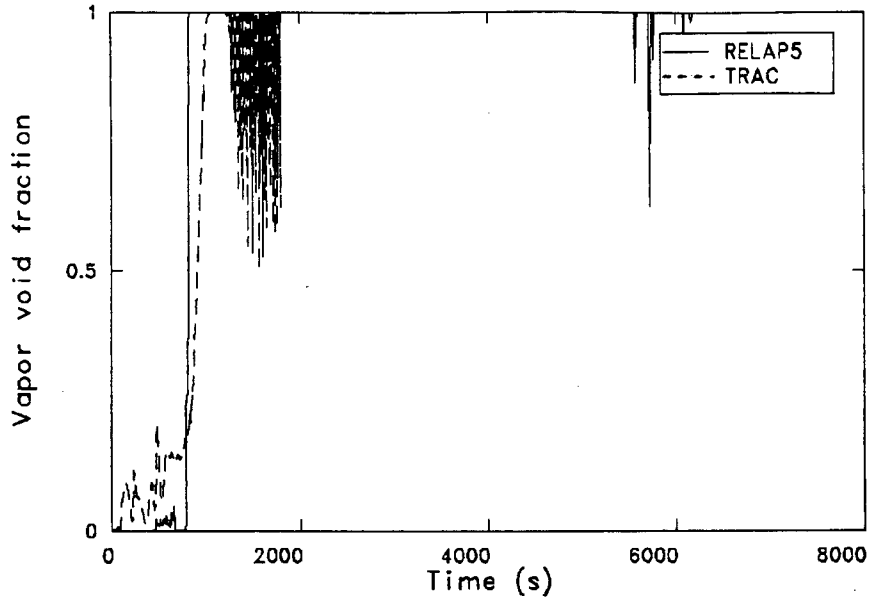

Figure C-5. TRAC and RELAP5 comparison, pressurizer surge line break, void fractions at top of loop A hot leg.

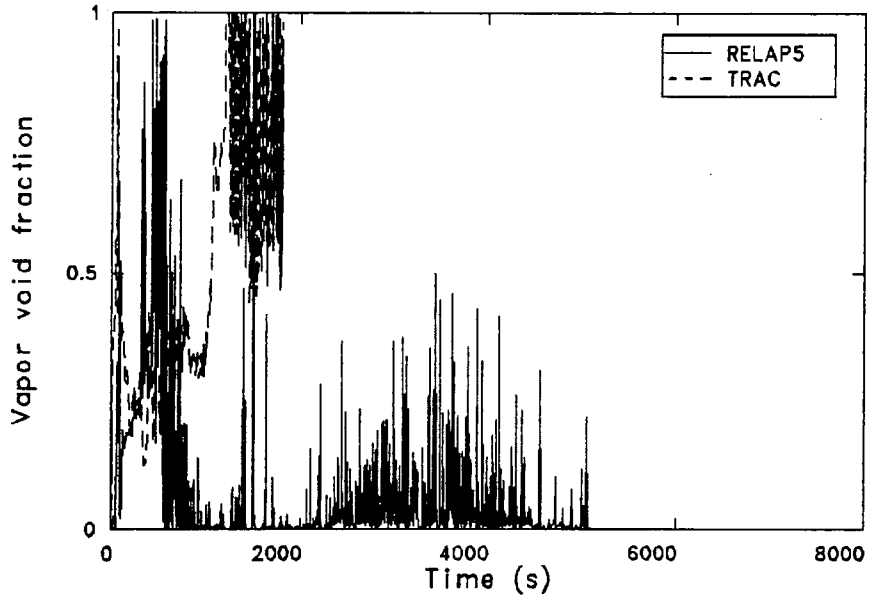

Figure C-6. TRAC and RELAP5 comparison, pressurizer surge line break, void fractions in cells upstream of break.

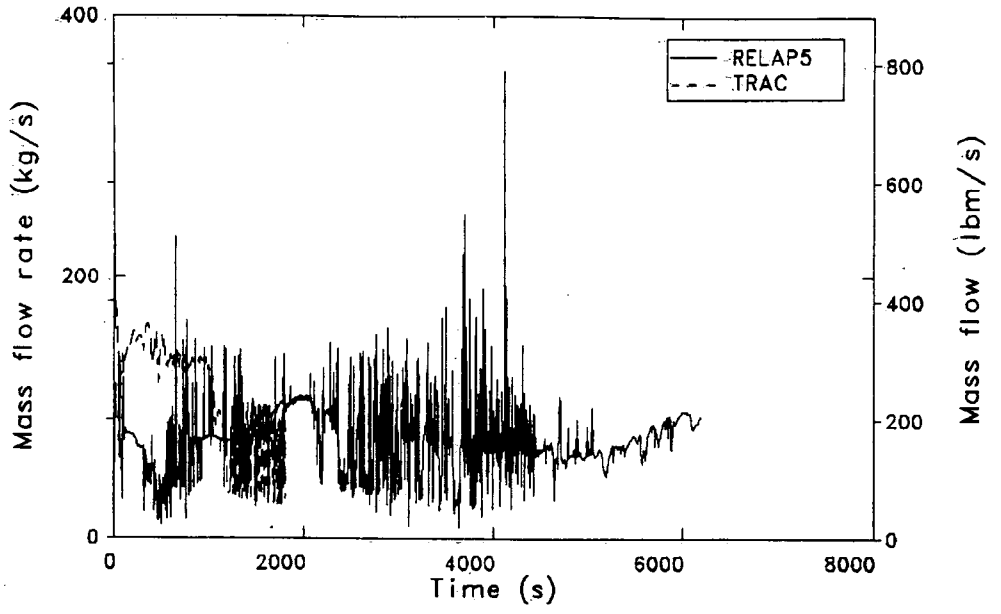

Figure C-7. TRAC and RELAP5 comparison, pressurizer surge line break, break mass flow rates.

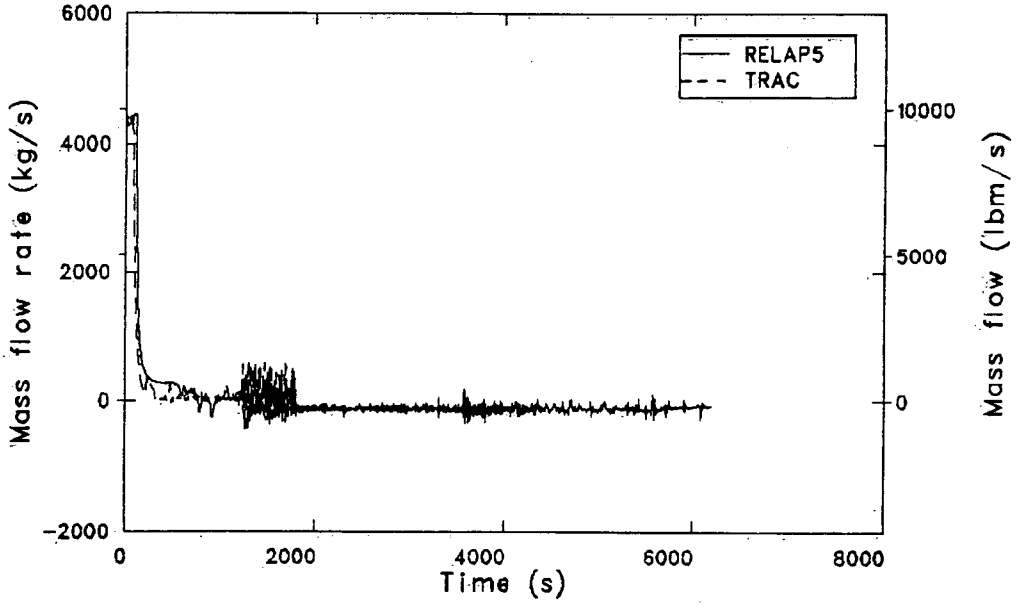

Figure C-8. TRAC and RELAP5 comparison, pressurizer surge line break, cold leg A-2 mass flow rates at RV.

The earlier termination of natural circulation with TRAC caused the cold leg temperatures at the vessel to decrease rapidly, as shown in Figure C-9 for the A-2 cold leg. With RELAP5 the decrease occurred later. The loop A hot leg liquid temperatures, shown in Figure C-10, indicate that the TRAC hot leg fluid temperature exceeded that of RELAP5, up to about 1500 s. Because of a higher TRAC total vent valve mass flow rate (Figure C-11), the TRAC hot leg temperature was higher even though the cold leg temperature was lower. The higher TRAC vent valve flow rate was consistent with the lower TRAC loop flow rate.

The TRAC calculation was carried out to 1800 s and the RELAP5 calculation to 6200 s. The figures showing comparisons between the two calculations used an abscissa of 8000 s, primarily to highlight the similarities between the calculations. While different TRAC and RELAP5 short-term behavior has been discussed, the plant conditions and trends at 1800 s, the end of the TRAC calculation, were similar. The primary system pressures, shown in Figure C-1, were in good agreement and the trends were converging, with the TRAC depressurization rate slowing and that of RELAP5 increasing. The same similarity was present in the secondary system pressures, shown in Figure C-3. Loop flow had been essentially stagnated in both calculations at 1800 s, as shown in Figure C-8. However, different minor flows have been established. With TRAC, a manometer-type oscillation was observed between hot leg and steam generator tubes; with RELAP5, a steady circulation was observed between cold legs on the same loop. Details of the RELAP5 circulation appear in Section 7 (Transient Results subheading). At 1800 s, hot and cold leg temperatures and trends of the two calculations were approximately the same, as shown in Figures C-9 and C-10. The TRAC reactor vessel downcomer fluid temperature, shown in Figure C-2, was about 25 K (45°F) higher than that of RELAP5 at 1800 s because of the higher vent valve flow, shown in Figure C-11. A difference was noted in the break void fraction comparison at 1800 s, as shown in Figure C-6. The TRAC void fraction remained above that of RELAP5, indicating more liquid at the break with RELAP5 than with TRAC. The nodalizations of the two models were compared, and modeling of the break location was found to be consistent. The difference in break void fraction appeared to be caused by the manometer oscillation in the TRAC calculation which allows vapor to enter the pressurizer surge line. The hot leg surge line nozzle remained essentially liquid covered in the RELAP5 calculation. The higher break void fraction at 1800 s with TRAC was the cause of the slightly higher TRAC depressurization rate at that time.

In summary, the two calculations had inconsistencies during the first 1800 s of the transient, the time period for which the TRAC calculation was run. Plant conditions and trends at 1800 s however were similar, indicating that, had the TRAC calculation been carried further, TRAC and RELAP5 results would apparenty have been similar over an extended period. There was an uncertainty, however, in the expected depressurization rate from 1800 to 7200 s. The TRAC depressurization rate during this period was extrapolated higher than that calculated with RELAP5. This was due to a higher average break void fraction with TRAC and appeared to be caused by minor differences in hot leg flow behavior.

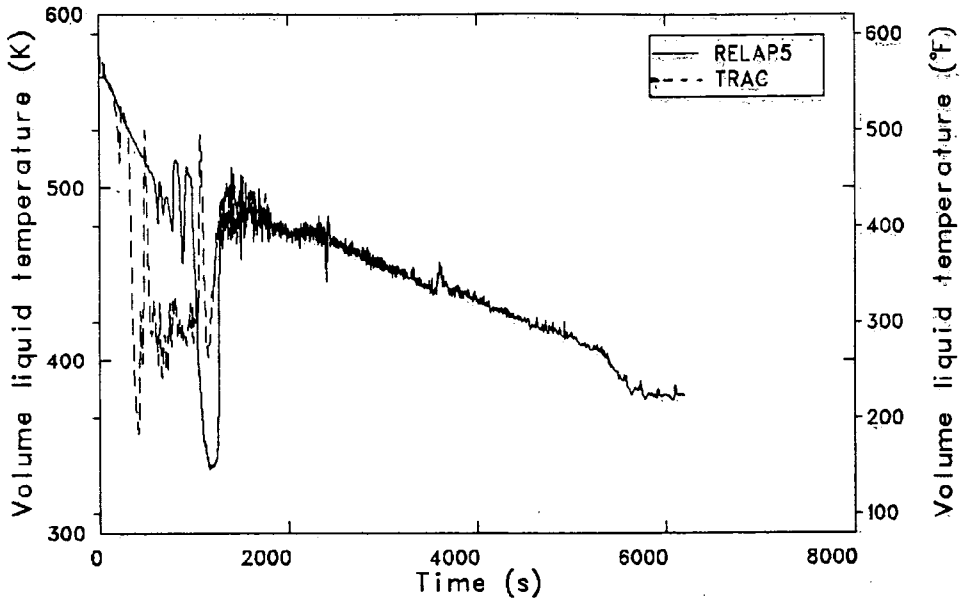

Figure C-9. TRAC and RELAP5 comparison, pressurizer surge line break, cold leg A-2 liquid temperature at RV.

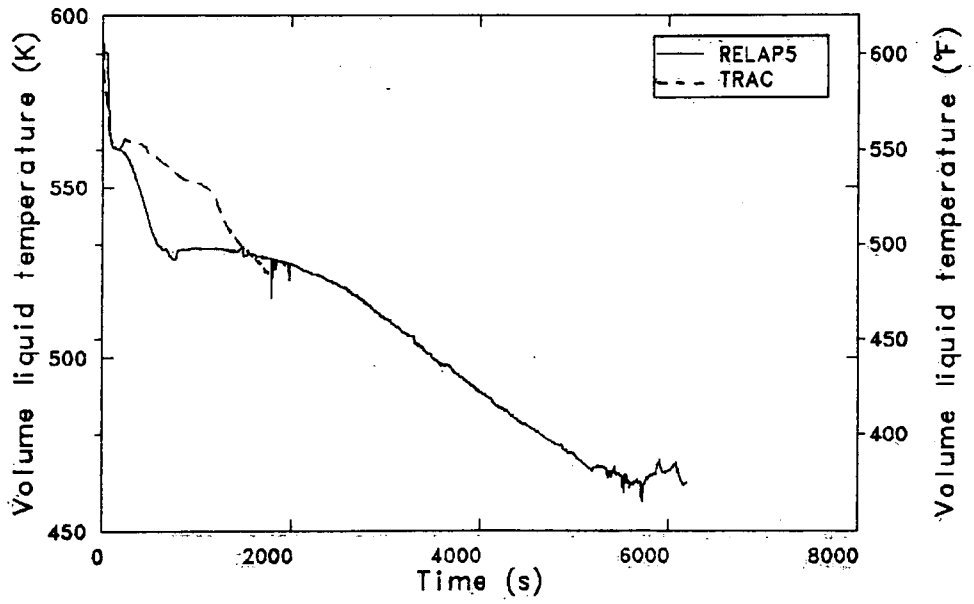

Figure C-10. TRAC and RELAP5 comparison, pressurizer surge line break, loop A hot leg liquid temperatures.

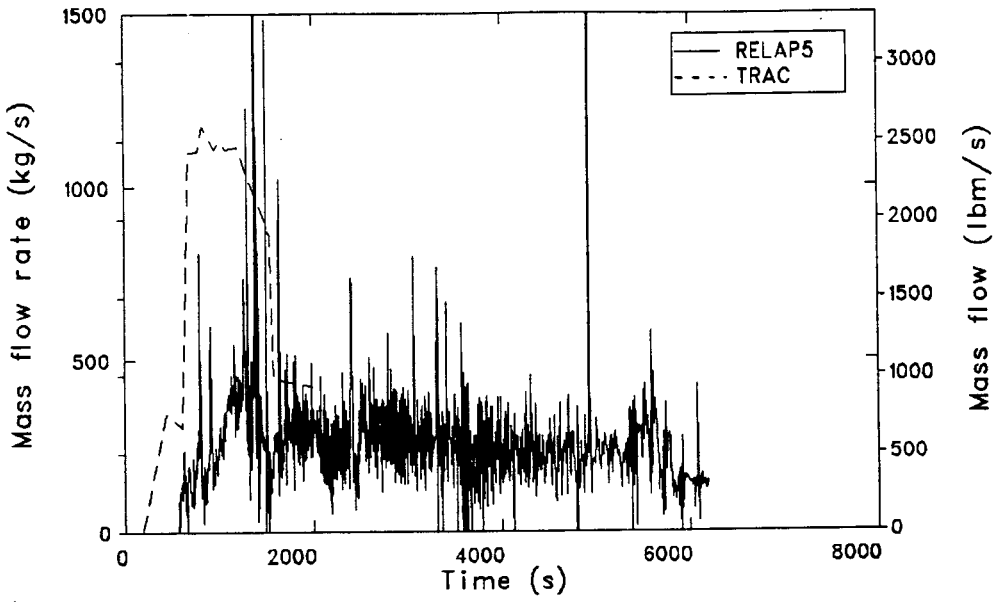

Figure C-11. TRAC and RELAP5 comparison, pressurizer surge line break, total vent valve mass flow rates.

A2310

EG&G Idaho, Inc.
P.O. Box 1625
Idaho Falls, Idaho 83415